University of Southampton

Faculty of Medicine

TASK-5, a potential mitochondrial channel characterised by planar patch-clamp electrophysiology

Eleni Georgiades

Thesis submitted for the degree of Doctor of Philosophy

July 2018

Abstract

Since its first identification 17 years ago, TWIK-related acid-sensitive K^+ channel 5 (TASK-5) was described as a “non-functional” two-pore domain acid-sensitive potassium (K^+) channel family member as, researchers failed to identify K^+ currents on the plasma membrane of transfected cells or oocytes. Evidence that TASK-5 protein shows a putative expression within the inner mitochondrial membrane (IMM) was provided by members of the O’Kelly group in 2012; where *in vitro* binding assays and immunocytochemistry demonstrated that the channel bound mitochondrial resident proteins and showed co-localisation with mitochondrial markers. The work within this thesis tests the hypothesis that TASK-5 preferentially shows intracellular localisation and may elicit K^+ currents in mitochondria. An assumption that was further endorsed by immunocytochemistry followed by co-localisation analyses where transfected cells (with a GFP-tagged TASK-5 DNA construct) were stained with either Mitotracker red or IMM protein complexes.

To achieve electrophysiological characterisation of IMM resident TASK-5, an experimental strategy was designed consisting of isolating mitochondria from cells transfected with a GFP-tagged channel DNA construct. Organelles expressing the channel were subsequently sorted by flow cytometry to ensure that mitochondria are selected over cell debris. The IMM was then accessed by an incubation in hypotonic conditions to strip off their outer mitochondrial membrane (OMM) and expose the IMM (mitoplasts). The extent of mitochondrial matrix swell induction and OMM rupture was also investigated by transmission electron microscopy (TEM). Last, planar patch-clamping was performed on mitoplasts over-expressing TASK-5 to investigate whether the channel can elicit K^+ currents. This was achieved by administrating a cocktail of channel blockers to mitoplasts and comparing residual current amplitudes between non- and transfected organelles. To determine if the channel of interest was acid-sensitive, transfected mitoplasts were bathed in low pH solution and currents were compared to mitoplasts that did not over-express TASK-5.

This study demonstrates that over-expression of TASK-5 may be linked to K^+ current differences observed during pharmacological assays performed on mitochondrial membranes, explaining why previous published studies were unable to detect K^+ currents on plasma membranes. The planar patch-clamp method provides the potential to gain electrophysiological understanding, not only for future mitochondrial ion channel studies, but also for broader range of pharmacological and functional intracellular compartment research.

Table of Contents

List of figures

List of tables

Research Thesis: Declaration of Authorship

Print name:	Eleni Georgiades

Title of thesis:	TASK-5, a potential mitochondrial channel characterised by planar patch-clamp electrophysiology.

I declare that this thesis and the work presented in it are my own and has been generated by me as the result of my own original research.

I confirm that:

1. This work was done wholly or mainly while in candidature for a research degree at this University;
2. Where any part of this thesis has previously been submitted for a degree or any other qualification at this University or any other institution, this has been clearly stated;
3. Where I have consulted the published work of others, this is always clearly attributed;
4. Where I have quoted from the work of others, the source is always given. With the exception of such quotations, this thesis is entirely my own work;
5. I have acknowledged all main sources of help;
6. Where the thesis is based on work done by myself jointly with others, I have made clear exactly what was done by others and what I have contributed myself;
7. None of this work has been published before submission

Signature:		Date:	30/11/2018

Acknowledgements

First and foremost, I wish to express my sincerest appreciation and gratitude to my academic supervisors Peter Smith, Maurits de Planque and Ita O'Kelly for the continuous support, guidance and motivation to complete my PhD study. I am grateful for all the advice, insightful discussions and suggestions, and could not have imagined having better advisors.

Besides my supervisors, my gratitude is extended to the FACS facility manager Richard Jewell, the Biomedical imaging manager Anton Page and Mark Willet who in many occasions lent a helping hand in a number of experimental trials but answered many questions that assisted me to widen my research from various perspectives.

Lastly, no words can describe how thankful I am to my family and Theo for the unconditional support through this venture over the last few months; you accepted nothing less than excellence from me.

Abbreviations

4-AP: 4-aminopyridine

ADP: Adenosine diphosphate

ANT: Adenine nucleotide translocator

ATP: Adenosine triphosphate

cIII-sub1: Cytochrome bc1 complex subunit 1

Ca^{2+}: Calcium

ChTx: Charybdotoxin

Cl^- : Chloride

Cm: membrane capacitance

COX II: Cyclooxygenase II

ER: Endoplasmic reticulum

F: Fluoride

GFP: Green fluorescence protein

GHK: Goldman–Hodgkin–Katz

hERG: Human *Ether-à-go-go*-Related Gene

HVACCs: High voltage-activated Ca^{2+} channels

IMAC: Inner membrane anion channel

IMM: Inner mitochondrial membrane

IMS: Intra-mitochondrial space

IPC: Ischemic preconditioning

I-V: Current to voltage

K^+: Potassium

K2P: Two-pore domain

K_{Ca} : Calcium-gated potassium channel

$K_{Ch:}$ Potassium channel

KF: Potassium fluoride

K_{ir} : Inward rectifier

K_{v} : Voltage-gated potassium channel

LIN: Linolenic acid

LPC: Lysophosphatidylcholine

MCU: Mitochondrial Ca^{2+} uniporter

MAC: Mitochondrial apoptosis–induced channel

MAM: Mitochondria-associated membrane

MCC: Mander's coefficient correlation

Mg^{2+}: Magnesium

mitoATPase-β : Mitochondrial ATPase subunit beta

mitoBKCa: Big conductance potassium channel Ca^{2+} sensitive

mitoIKCa: Intermediate conductance potassium channel Ca^{2+} sensitive

mPTP: Mitochondrial permeability transition pore

mRYR: mitochondrial ryanodine receptor

Na^{+}: Sodium

NO: Nitric oxide

OMM: Outer mitochondrial membrane

OXPHOS: Oxidative phosphorylation

P: Pore domain

PCC: Pearson's coefficient correlation

pH_i : Intracellular pH

pH_o : Extracellular pH

Pi: Phosphate

PUFAs: Polyunsaturated fatty acids

RAM: Rapid mode of mitochondrial Ca^{2+} uptake

PKC: Protein kinase C

R: Resistance

R_a: Acces resistance

R_m: Membrane resistance

R_s: Series resistance

R(obs): Pearson's coefficient observed

(R(rand): Pearson's coefficient random

ROI: Region of interest

ROS: Reactive oxygen species

RR: Ruthenium red

SNP: Single nucleotide polymorphism

siRNA: Small interference ribonucleic acid

TALK : TWIK-related alkaline-sensitive K^+ channel

TASK : TWIK-related acid-sensitive K^+ channel

TEA : Tetraethyl ammonium

TEM: Transmission electron microscopy

THIK : Tandem pore domain halotane-inhibited K^+ channel

TIM : Translocase of the inner membrane of mitochondria

TMS : Transmembrane segment

TOM : Translocase of the outer membrane of mitochondria

TRAAK : TWIK-Related Arachidonic Acid-stimulated K^+ channel-mechano-sensitive

TREK : TWIK for Two P-domain in a weakly inward rectifying K^+channel,

TRESK: TWIK-related spinal cord K^+ channel-Ca^{2+} activated

TWIK: Tandem of P-domains in a weak inwardly rectifying K^+ channel

UCP: Uncoupling protein

VDAC: Voltage- dependent anion channel

V_c: Command voltage

V_m: Membrane voltage

V_{rev} : Reversal potential

$\Delta\Psi_m$: Voltage difference across the mitochondrial membrane

Chapter 1

Overview

1.1 Motivation

The research work presented within this thesis was based on the hypothesis that TASK-5 is an intracellular potassium channel preferentially expressed in the IMM. Electrophysiological and pharmacological characterisation of TASK-5 will determine if it is an active mitochondrial channel. Successful demonstration of TASK-5 activity will contribute to future studies focusing on the functional, biophysical, patho- and physiological role of the channel in the organelles.

1.2 Aims and objectives

This project aims to deepen knowledge on the electrophysiological activity of the two-pore domain potassium (K2P) channel TASK-5. Inability to show that TASK-5 elicits potassium currents on the plasma membrane since 2001 demonstrates how problematic it is to characterise the particular channel (Ashmole, Goodwin et al. 2001, Kim and Gnatenco 2001). Based on data provided by previous lab members of the O'Kelly group, evidence that TASK-5 is a mitochondrial channel allowed to set up an experimental strategy with the purpose of identifying if the channel elicits potassium currents within organelles.

The strategic approach involved the following six experimental steps:

1. Transient transfection of COS-7 or HeLa cells with a in frame GFP-tagged TASK-5 DNA construct;
2. Mitochondrial staining with Mitotracker red fluorescent probe;
3. Mitochondrial isolation from transfected and stained cells;
4. Sorting of double fluorescent mitochondria by flow cytometry;
5. Mitochondrial matrix swelling in hypotonic conditions followed by OMM rupture;
6. Organelle K^+ current recording post-application of mitochondrial channel blockers or pH modification of the external recording solution.

Establishment of the aforementioned strategy allowed the following objectives:

(a) To identify current differences between mitochondria and mitoplasts (stripped of their outer membrane);

(b) To compare currents between isolated non-transfected and transfected organelles and determine electrical activity differences between endogenous and over-expressed conditions;

(c) To show that K^+ currents recorded from transfected mitoplasts tend to be more sensitive to a commonly used TASK blocker or increased $[H^+]$ during pharmacological studies.

Chapter 2

Introduction

2.1 Ion channels

Ion channels are pore-forming transmembrane proteins which open and close under specific stimuli and mediate rapid or delayed selective ion transport through the membrane in excitable and non-excitable cells (Hille 2001). Several examples of such stimuli are the electrochemical gradient difference across the membrane, intracellular or extracellular ligands, acidic or basic pH, temperature and mechanical pressures applied to cells which control the opening or closing state of ion channels (Hille 2001). When an ion channel is open, ions move into or out of the membrane in single-file fashion i.e, the rate of passage is limited to one ion at a time. Exceptions to this statement are ion exchangers which interchange two ions or larger molecules at a time (Hille 2001).

Ion channels have three main physiological roles. Briefly, they contribute to setting up the resting membrane potential of almost all cells. The flow of ions across the membrane constitutes an electric current where channel opening and closing modulates the electrical signalling in excitable cells such as nerves and muscles (Hille 2001). Secondly, the flow of ions through ion channels contributes to the electrolyte movements required for volume regulation of single cells and the transport of salt across secretory and epithelial cells. Finally, entrance of ions from the extracellular medium or intracellular organelles, is the primary mechanism for translation of electrical signals into chemical signals. More precisely, this is how electrical signals in electrically excitable cells couple to hormone secretion, neurotransmitter release, muscle contraction and changes in gene expression (Hille 2001).

The ability of ion channels to accomplish these physiological functions also requires the operation of another class of membrane proteins, the transporters and pumps, to set up standing ion concentration gradients across cell membranes. Nevertheless, during the current study focus will be principally given to potassium (K^+) channels (K_{Ch}).

2.2 The 3 types of potassium channels and their membrane topology

Potassium channels are protein complexes which form the largest, most diverse family of ion channels allowing the passive transport of K^+ ions through selective pores across the membranes (Lesage and Lazdunski 2000, Wickenden 2002). K_{Ch} play a key role in the control of K^+ homeostasis and cell volume but also in physiological functions associated with modifications of the electrical membrane potential ($\Delta\psi$). Examples of such modifications include the neurotransmitter and hormone secretion or the neuronal and muscular excitability with a role in both excitable and non-excitable cells (Lesage and Lazdunski 2000, Wickenden 2002). More than 60 pore-forming subunits have been cloned in mammals which were classified into three families according to their structural, functional and biophysical properties (Gutman, Chandy et al. 2003). Figure 2.1 illustrates the structure of K^+ sub-

families such as the voltage (K_v), calcium-gated (K_{Ca}) or leak K^+ channels. K_v or K_{Ca} contain a hydrophobic core with 6 trans-membrane segments (TMS) and 1 pore (P) forming domain. The pore domain is involved in the formation of the selectivity filter that offers the specificity to transport K^+ ions. The second family is composed of pore-forming subunits with only 2TMS and 1P domain. The characterisation of these two types of cloned subunits both *in vitro* and *in vivo*, as well as the isolation of associated regulatory subunits, has allowed the reconstitution of many different types of K^+ channels such as the classic inward rectifiers (Kir2.x), G protein gated Kir (Kir3.x), K_{ATP} channels (Kir6.x/SURx), and K- transport channels (Kir1.1, Kir4.x, Kir5.1, and Kir7.1) (Lesage and Lazdunski 2000). In order to be functional, these families need to form non-covalent tetramers (4P-domains) (Lesage and Lazdunski 2000). The last group of K^+ selective pore-forming subunits corresponds to proteins with 4TMS and 2P (K2P) domains which resemble two K_{ir} pore structures associated together to form one subunit. In order to be functional K2P channels need to assemble in pairs with two subunits linking the 4P-forming domains. These channels are central in the control of the membrane potential of cells and function as background or "leak" channels by showing activity which is usually voltage and time independent (Enyedi & Czirjak, 2010;Bayliss & Barrett, 2008).

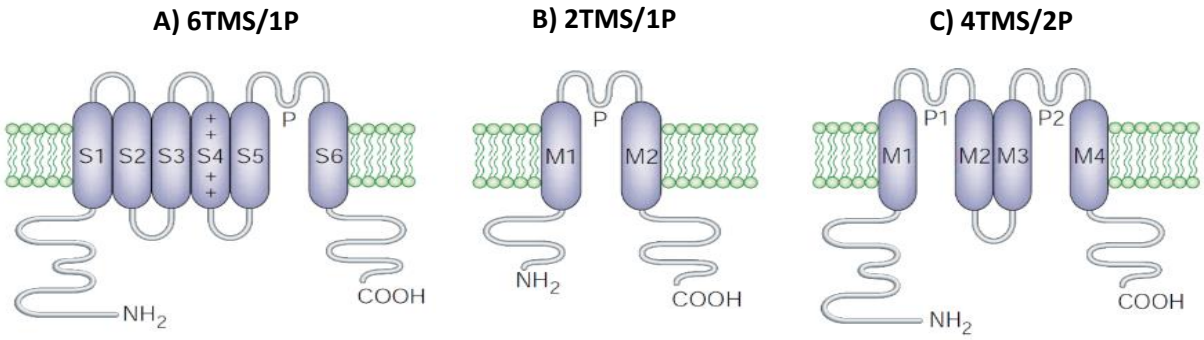

Figure 2. 1 Membrane topology of the potassium channel sub-families. A. K_v and K_{Ca} channel subunits have six transmembrane segments (6TMS) and one pore domain (1P) where the fourth cytoplasmic helix (S4) acts as a voltage sensor. **B.** K_{ir} channel subunits have two transmembrane domains and one pore domain (2TMS/1P). **C.** K2P channels have four transmembrane helices and two pore domains (4TM/2P). To form functional K2P channels 4P domains are required for a K^+ selective pore filter. Image adapted from Goldstein et al, 2001.

2.3 The two-pore domain potassium channel family

In 1996, the first human K2P channel TWIK-1 was identified and cloned by Lesage et al., which differed from previously cloned K^+ channels as it had two pore domains in tandem instead of the usual single P-domain and 2 or 6 TMS (Lesage, Guillemare et al. 1996). The name given to the channel is an acronym for tandem of P-domains in a weak inwardly rectifying K^+ channel (TWIK). TWIK-1 was the first in a family of proteins comprising 15 mammalian members that rapidly emerged in the scientific literature between 1996 and 2003

all sharing sequence similarities, functional resemblances and having 4TMS with 2P domains in tandem (Lesage, Guillemare et al. 1996). The categorisation into sub-families was undertaken as despite the relatively low number of members, the sequence variation between K2P channel sub-families proved to be almost as high as that between the families of K^+ channels. Although members of different sub-families show relatively low sequence similarities (e.g. 28% identity between TWIK-1 and TREK-1 at the protein level (Fink, Duprat et al. 1996)), all members of the background K^+ channel family are characterised by the same general molecular structure.

2.4 Members of the K2P family and their characteristics

An important element of the signature of K^+ channel function has long been attributed to the GYG sequence of the pore domain. In K2P channels, this GYG motif is conserved in the first pore domain (P1) but is replaced by GFG (TASK-1-3-5, TREK-1, and TRAAK) or GLG (TWIK-1 and TWIK-2) in the second pore (P2) domain (Salinas, Reyes et al. 1999) (Chavez, Gray et al. 1999). All members of the K2P family are summarised in Figure 2.2 where their sensitivities to multiple stimuli or activating conditions are indicated.

Except THIK1/2,TRESK and TASK-5, the rest of the K2P channels clearly respond to changes of extra- or intracellular H^+ concentrations (Lesage and Barhanin 2011). Extracellular acidification (pH ~6) inhibitsTWIK-1 with a pKa value of 6.7 but not TWIK-2 which is only inhibited by a decrease in intracellular pH (Rajan, Plant et al. 2005). This could be linked to the two *N*-glycosylation consensus sequences in the M1-P1 loop of TWIK-2 compared to the single glycosylation site at N95 of TWIK-1 (Chavez, Gray et al. 1999). Conversely, TWIK-1 and TWIK-2 are inhibited by exposure to 100% CO_2 which is expected to acidify the intracellular milieu (Chavez, Gray et al. 1999). In fact, TWIK-1 was shown to be sensitive to decreased extracellular pH when transiently expressed in CHO cells (Ma, Zhang et al. 2012). TWIK-1 is also highly expressed in hippocampus, cerebellar granule and Purkinje cells indicating an important role in the maintenance of the resting potential of neuronal cells (Lesage and Lazdunski 2000). TWIK channels have also a widespread tissue distribution in adult mice and humans such as the brain, heart, pancreas, kidneys, liver, lungs, ovaries, prostate and colon suggesting that these could be involved in the control of background K^+ conductance of multiple cell types (Lesage and Lazdunski 2000).

TREK1, TREK2 and TRAAK form a functional sub-class of K2P channels which are highly expressed in the human nervous system (hippocampus, neocortex, cerebellum, brain stem nuclei, and olfactory bulb) (Fink, Duprat et al. 1996) but also in the small intestine (TREK1), kidney (TREK1, TREK2), pancreas (TREK2) and placenta (TRAAK) (Lesage and Barhanin 2011). Intracellular H^+ activate both TREK1 and TREK2 (Maingret, Patel et al. 1999, Honore,

Maingret et al. 2002) whereas external acidification strongly inhibits TRAAK and TREK1 with a pK of 7.4 (Sandoz, Bell et al. 2011). TRAAK is activated by cytoplasmic alkalinisation from pH 7.3 (Kim, Bang et al. 2001). Moreover, these channels show complex regulatory properties as they are strongly stimulated by raised temperature, mechanical stretch of the plasma membrane and application of free polyunsaturated fatty acids (PUFAs)(Lesage and Lazdunski 2000). Hence, their denomination as mechano-sensitive channels.

TWIK-related acid-sensitive K^+ channel 1 or TASK-1 ($K_{2P}3.1$) was identified in 1997 as being sensitive only to extracellular acidic pH (pH_o) with only 10% of the maximal current being recorded at pH 6.7 and 90% at pH 7.7 (Duprat, Lesage et al. 1997). When further members similar to TASK were identified, the name TASK-1 (KCNK3 or $K_{2P}3.1$) was attributed to the first TASK channel and TASK-3 ($hK_{2P}9.1$) or TASK-5 ($K_{2P}15.1$) to the rest. TASK-3 is the second to date functional channel of the TASK sub-family (Kim, Bang et al. 2000) and is almost fully active at pH 7.4 while its current activity decreases by 96% at pH_o 6.0 (Kim, Bang et al. 2000).

TASK-2 ($K_{2P}5.1$) was discovered in 1998 (Reyes, Duprat et al. 1998) as an alkali-activated channel being half-maximally activated at pH_o 8.Together with TASK-2, TALK-1 ($K_{2P}16.1$) and TALK-2 (also called TASK-4) form the separate TALK branch of alkaline activated K2P channels as they require higher pH_o values well above conceivable physiological levels to be activated (Girard, Duprat et al. 2001). In addition to their sensitivity to extracellular pH, TASK-2 and TASK-4 open by increases in pH_i in the 7.5–10 range (Niemeyer, Cid et al. 2010). Moreover, TALK-1 and TASK-4 are strongly activated by nitric oxide species (NOS) and reactive oxygen species (ROS) suggesting that ROS and NOS could act as endogenous openers able to rise their activity at physiological pH (Duprat, Girard et al. 2005).

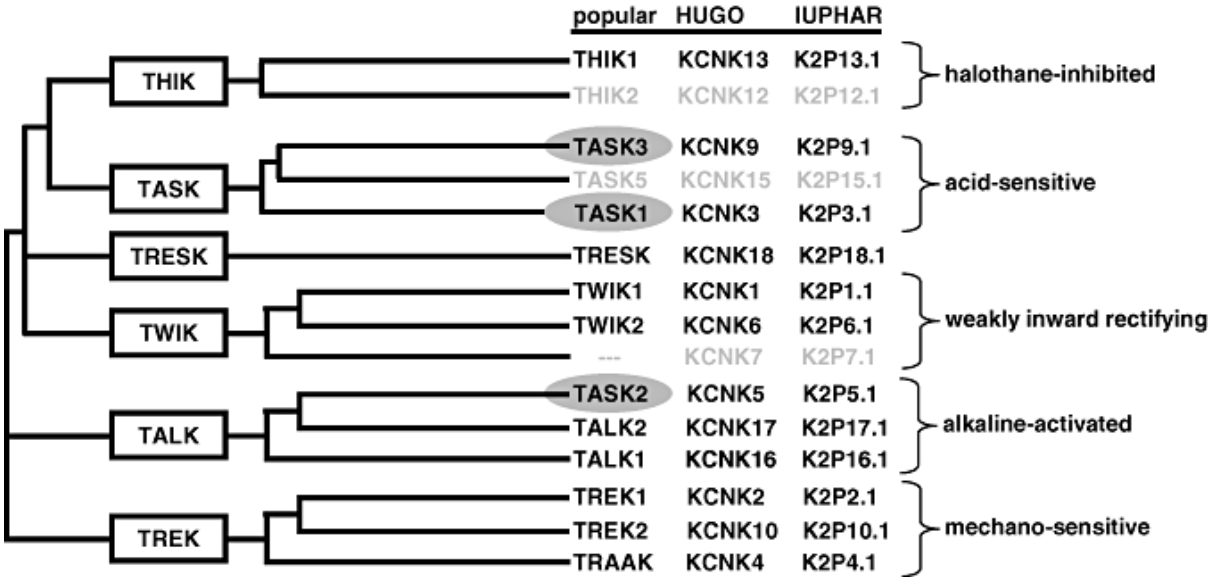

Figure 2. 2 A dendrogram showing the two-pore domain potassium channel family. The KCNK classification of the Human Genome Organization (HUGO) and the K2PX.1 nomenclature of the International Union of Pharmacology (IUPHAR) are displayed and divided into six structural and functional sub-groups. Non-functional members are displayed in grey and channels of special interest during the study are highlighted in grey in addition to TASK-5. TASK-4 is also known as TALK2 and TRESK is a Ca^{2+} activated channel. Image adapted from (Bittner, Budde et al. 2010).

K2P channels such as TASK-5, THIK2 or K2P7.1 were entitled as 'silent' subunits because of their lack of functional expression in heterologous systems or cells (Bichet, Blin et al. 2015). This raised the question whether they were non-functional isoforms or functional subunits that require unidentified activators and/or protein partners. The second possibility was strengthened by the recent demonstration that K2P12.1 (THIK2) could be turned on by overcoming two silencing mechanisms such as a retention in the endoplasmic reticulum (ER) and a low activity at the plasma membrane (Chatelain, Bichet et al. 2013). Inactivation of the ER retention signal allowed the expression of THIK2 at the plasma membrane, enabling its electrophysiological characterisation. THIK2 has electrophysiological and pharmacological properties very similar to those of THIK1 including inhibition by halothane and insensitivity to extracellular pH changes. Thus, similar approach may be successful in obtaining functional expression of the 'silent' hK2P15.1 and K2P7.1 channels in future studies.

K2P7.1 was cloned in 1999 showing 30% and 42% amino acid identity with TWIK-2 and TWIK-1 accordingly with a wide tissue distribution in the cerebral cortex, hippocampus, nucleus accumbens and spinal cord and a highest level of expression in peripheral blood leukocytes (Medhurst, Rennie et al. 2001). A unique feature of K2P7.1 was the presence of an unusual sequence in its second pore domain (Salinas, Reyes et al. 1999). In fact, a glutamic acid residue (GLE) was detected instead of the strictly conserved glycine residue (GLG). In addition, two adjacent residues, a tyrosine and a valine (Tyr^{234}-Val^{235} in TWIK-1)

which are preserved in all other members of the family were replaced by a leucine-leucine sequence (Leu^{221}-Leu^{222}) in K2P7.1. Thus, these sequence misplacements leading to a change in ionic selectivity could be an additional reason associated with its failure to show channel activity by itself. In 2008, Yost, Oh et al., generated a knockout mice by deleting the KCNK7 gene in order to examine the phenotypic consequences of KCNK7 inactivation and determine the potency of inhalational anaesthetics in these mice (Yost, Oh et al. 2008). Results indicated that deletion of the gene resulted in mice that not only had indistinguishable phenotypes from wild type or heterozygous animals but also had unaltered response to the three volatile anaesthetics tested. These findings showed that KCNK7 did not play a dominant role in the mechanism of action of volatile anaesthetics nevertheless, the possibility of compensatory changes in ion channel gene expression was not excluded and further K2P channel knockouts or conditional knockouts were suggested to fully understand their role in the mechanism of action of volatile anaesthetics (Yost, Oh et al. 2008).

2.5 Protein subunit structure and assembly

Amino acid sequences of mammalian K2P genes range between 300 and 500 residues and exhibit a similar predicted topology consisting of a short cytosolic amino terminal followed by four transmembrane domains (M1–M4) and a relatively long cytosolic carboxyl terminal as illustrated by the predicted topology of the human ortholog of TWIK-1 (Lotshaw 2007) (Figure 2.3). The 3.4 angstrom (A) crystal structure resolution of the human K2P channel TWIK-1 was studied and was observed that the linker sequences connecting M domains were longer than other K^+ channel structures which generally have short (typically 5 to 20 amino acids) linker domains (Miller and Long 2012). In fact, the sequence connecting M1 and M2 (also called extracellular cap or linker) of TWIK-1 is longer (56 amino acids) and includes the first pore domain (P1) (Doyle, Morais Cabral et al. 1998). The M1–M2 extracellular linker domain loop is a coiled–coiled domain which contains two helices (E1 and E2) from each subunit that form a structure resembling an A-frame that is positioned directly above the extracellular side of the selectivity filter. It also usually contains one or more asparagines (N) which may function in N-linked glycosylation and a cysteine residue (Cys^{69}) which is located in the turn between the E1 and E2 helices at the top of the extracellular cap. Dimerisation is attributed to a sequence within the extracellular M1–P1 linker predicted to form an amphipathic a-helix that mediates subunit interaction (Doyle, Morais Cabral et al. 1998, Lesage and Lazdunski 2000, Long, Campbell et al. 2005). Moreover, the extracellular linker restricts access to the selectivity filter allowing the passage of K^+ ions only through two side portals. The portals are funnel-shaped and their narrow ends meet above the selectivity filter (Miller and Long 2012). Sequence alignments indicate that several of the residues present on the side portals vary among K2P

channels. This may account for some of the electrophysiological differences between K2P channels (Enyedi and Czirjak 2010) and suggests that it may be possible to block the extracellular ion pathway with channel-specific drugs. The presence of the extracellular linker explains why protein toxins that block the pores of many tetrameric K^+ channels from the extracellular side are ineffective against K2P channels (Hidalgo and MacKinnon 1995, Lesage, Guillemare et al. 1996). In addition to conferring resistance to toxins, it is possible that the extracellular linker serves as a binding site for endogenous extracellular factors that modulate K2P channel activity. Noradrenaline or serotonin synthesising neurons and/or thalamocortical neurons were shown to modulate cell groups expressing TASK and TREK channels and contribute to altered states of stimulation (Sirois, Lei et al. 2000, Washburn, Sirois et al. 2002, Heurteaux, Lucas et al. 2006, Meuth, Aller et al. 2006). Finally, the second pore domain (P2) is located between the M3 and M4 domains and the cytosolic C-terminal domain has been shown to play several important roles in modulation of channel gating within specific subfamilies.

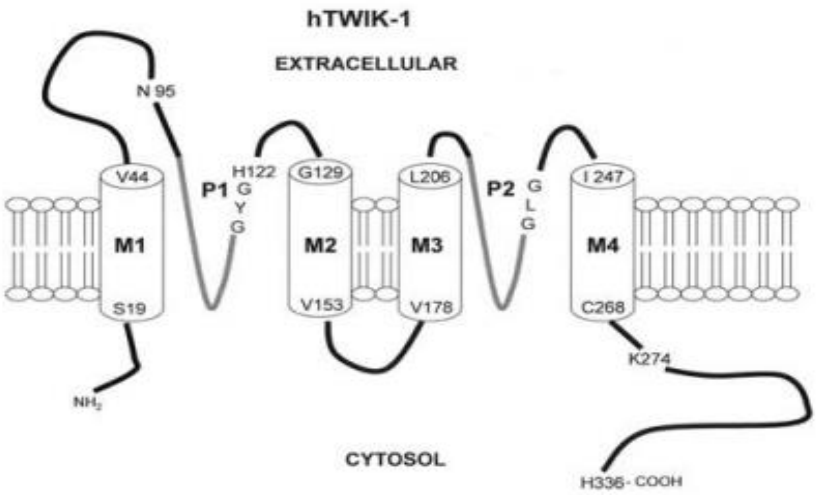

Figure 2. 3 Predicted membrane topology of TWIK-1 protein subunit. Predicted topology of K2P channels consist of a short cytosolic amino terminal followed by four transmembrane domains (M1–M4) and a relatively long cytosolic carboxyl terminal. The linking sequence connecting M1 and M2 is longer (between 80 and 90 residues) than other K^+ channels and includes the first pore domain (P1). The M1–M2 extracellular linker domain usually contains one or more asparagines and one or more cysteines. P2 is located between M3 and M4. Domain designations are based on the analysis of Lesage et al. 1996. Image adapted from (Lotshaw 2007).

2.6 Electrophysiological features of K2P channels

TWIK-1 was the first K2P channel characterised at the electrophysiological level in *Xenopus* oocytes and was shown to be open at rest, capable to drive the membrane potential towards the equilibrium potential for K^+ ions (-90 mV; E_{K+}) (Lesage, Guillemare et al. 1996). It also lacked time or voltage dependence as in open or leak channel rectification characteristics. These information were later used by Enyedi and Czirjak who assigned these current properties to K2P channels as the majority of them gave rise to background K^+ currents

which were almost instantaneous and non-inactivating over the whole range of voltage steps applied to cell membranes (Enyedi and Czirják 2010).

Therefore, it is practical to keep in mind what kind of properties an ideal background K^+ current should have if it followed the Goldman-Hodgkin-Katz (GHK) rectification. An ideal background K^+ current is voltage-independent, meaning that the opening probability (Po) of the channel is the same at all membrane potentials. Po is also independent from the K^+ concentrations on the two sides of the plasma membrane and the amplitude of this K^+ current does not instantaneously follow changes of the membrane potential (+/- mV range) (Enyedi and Czirják 2010). K2P channels are also “time independent” meaning that they do not have activation, deactivation or inactivation kinetics (Duprat, Lesage et al. 1997).

In contrast to the K2P channels, the Po of the voltage-activated channels is dependent on the membrane potential due to a relatively minimal re-arrangement of the protein configuration. Therefore, as an example, voltage-gated Kv2.1 currents have a delayed response upon a change of the membrane potential (from -20 mV to +50 mV) at the millisecond timescale (Figure 2.4A). Conversely, the membrane potential does not influence the Po of ideal background K^+ channels as changes of the membrane potential results in an “immediate” response. Thus, voltage steps in a voltage-clamp experiment generate square wave-like K^+ currents when TASK-3 is expressed in oocytes (Figure 2.4B).

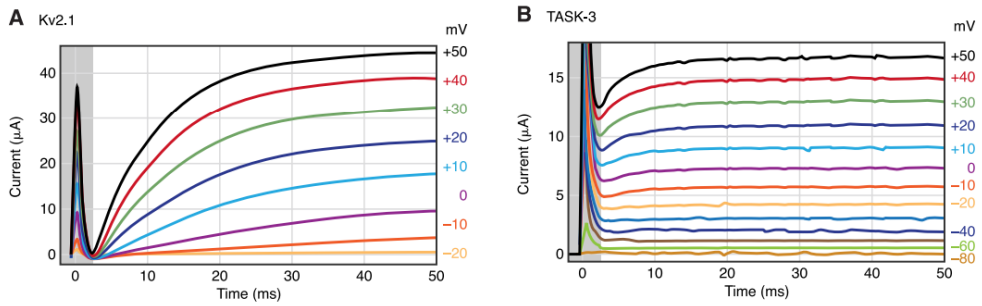

Figure 2. 4 Representative current traces of voltage-gated and background potassium channels. A. Kv2.1 voltage-gated or **B.** TASK-3 background K^+ channels were over-expressed in *Xenopus* oocytes. Currents were elicited by voltage steps applied from −80 or -20 mV to +50 mV in 10 mV increments with a holding potential of −80 mV in a solution containing 2 mM [K^+]. Kv2.1 channels were only active 2.5 ms post-stimulation whereas TASK-3 were always at their open state. Image adapted from (Enyedi and Czirják 2010).

Moreover, an ideal background channel does not rectify as opposite driving forces (electrochemical potential of ions) of equal amplitudes induce opposite currents of equal amplitudes (Enyedi and Czirják 2010). This means that the apparent rectification in external physiological (low extracellular K^+ concentration) solutions is caused exclusively by the unequal K^+ concentrations on the two sides of the plasma membrane. If the potassium concentration [K^+] was equal on both sides (symmetrical conditions) on the other hand, then the current to voltage (I-V) relationship would be a line passing through the origin.

If a K^+ current approximately meets the above criteria it can then be considered as a background (leak) K^+ current. Although real K2P channels do not perfectly fullfill these criteria (due to weak voltage dependence, interactions of multiple ions in the channel pore, rectification in symmetrical [K^+]), they provide the best approximation by far, compared with the other K^+ channel families (Leonoudakis, Gray et al. 1998). An example of this small deviation from perfect GHK rectification is the weak inward rectification at depolarised voltages of TWIK-1 due to intracellular Mg^{2+} inhibition (Sepúlveda, Pablo Cid et al. 2015).

2.6.1 The TASK sub-family-What we currently know about K^+ currents elicited from TASK channels expressed on plasma membrane

In 1997, cloning of the first 'true' background mammalian K^+ channel allowed to characterise the TASK family at the molecular, electrophysiological and pharmacological level by identifying blockers specifically targeting each member (Duprat, Lesage et al. 1997). TASK-1 currents for example were studied in cRNA-injected *Xenopus* oocytes and transfected in COS-7 cells revealing physiological characteristics unique to TASK channels such as their sensitivity to variations of extracellular pH in a narrow physiological range. In fact, small pH variations of only 0.5 pH unit around the physiological pH (7.4) could serve as modulators of neuronal activity in forebrain cholinergic neurons, cells of the hippocampus, cerebellum or cortical areas of the brain for examples (Vu, Du et al. 2015) (Chesler and Kaila 1992, Duprat, Lesage et al. 1997).

Other single-channel studies performed on COS-7 cells have shown that the conductance of TASK-1 and TASK-3 channels were equal to 14 and 27 pS respectively under symmetrical 140 mM KCl solution (Kim, Bang et al. 1999). More specifically, in inside-out patches the I-V relationship of TASK-3 showed weak inward rectification with single-channel conductances of 27 pS at -60 mV and 17 pS at +60 mV (Kim, Bang et al. 2000). TASK-2 showed a much higher single channel conductance (60 pS) under similar symmetrical conditions and thus, were considered different from TASK-1 and TASK-3 (Reyes, Duprat et al. 1998). This observation indicates that despite the symmetrical recording conditions, a voltage dependence influencing the curvature of I-V relationships will often occur, with a net outward rectification that does not entirely follow the approximated current rectification predicted by the GHK equation.

2.6.2 Pharmacological characteristics of TASK channels

K2P channels are insensitive or very weakly sensitive to the classical K^+ channel blockers tetraethyl ammonium (TEA), Ba^{2+} , Cs^+ and 4-aminopyridine (4-AP) (Kim 2005). These can nonetheless, be inhibited by the endocannabinoide (meth) anandamide and by local anaesthetics including lidocaine, bupivacaine, halothane, isoflurane, with bupivacaine being a stronger blocker (IC_{50} of 68 µM for TASK-1 and, 81% of inhibition for TASK-2 at 1 mM).

Moreover, TASK-3 was reported to be less sensitive than TASK-1 for methanandamide but was totally inhibited by ruthenium red (RR) (10μM) (Lotshaw 2007). This was attributed to its glutamate residue (E70) in the extracellular M1–P1 linker. Conversely, the low sensitivity of TASK-1 for RR was attributed to a lysine residue at this position (K70). TASK-2 currents were shown to be blocked by quinine (IC_{50} = 22 μM) and quinidine (65% of inhibition at 100 μM) (Reyes, Duprat et al. 1998) and were only slightly sensitive to Ba^{2+} ions with less than 17% of inhibition at 1 mM.

2.7 Sequence similarities between TASK channels

Fabrice Duprat et al., have isolated and characterised TASK-1 from human kidney samples which had only 25 and 28% amino acid homologies with TWIK-1 and TREK-1 accordingly (Fink, Duprat et al. 1996, Lesage, Reyes et al. 1996, Duprat, Lesage et al. 1997). The highest degree of sequence conservation was observed in their two P domains and the M2 segment (~50%) suggesting that these domains are conserved between the different types of K2P channels.

TASK-3 has 62% identical amino acid similarities with TASK-1 whereas TASK-5 has 58% and 56% with TASK-1 and TASK-3 respectively (Karschin, Wischmeyer et al. 2001). Sequences which are mainly conserved within their cytosolic C-terminal sequences. Moreover, the COOH terminus (85 amino acids) of TASK-5 is shorter compared to TASK-1 and TASK-3 and at the very end, a conserved stretch of five amino acids (RRSSV) possibly involved in protein–protein interaction is present (Rajan, Preisig-Müller et al. 2002).

TASK-1 and TASK-3 activity is modulated by pH changes and more specifically by acidic pH_o ranging from pH 6-7. Their pH sensitivity originates from a conserved histidine residue (H98) immediately following the GYG signature sequence in the P1 sequence which was studied by site-directed mutagenesis (Sandoz, Bell et al. 2011); even though, other amino acids were also shown to contribute to their pH sensitivity. Protonation of H98 located outside the trans-membrane domain was linked to conformational changes of the selectivity filter. By rotating and creating an electropositive barrier for K^+ ions traversing the outer mouth of the channel, protonated H98 was suggested to suppress the K^+ pore occupancy and open probability. Although both TASK-1 and TASK-3 possess the same proton-sensing histidine in P1, TASK-1 is more sensitive to extracellular acidification than TASK-3. In fact, 90% of the maximal TASK-1 current is recorded at pH_o 7.7 and 10% at pH_o 6.7 (Duprat, Lesage et al. 1997) with an acid dissociation constant (pKa) value of 7.3. TASK-3 has a similar sensitivity but is shifted towards more acidic values (pH 6.2) (Kim, Bang et al. 2000). TASK-3 is almost fully active at pH 7.4 and is inhibited by acidification with a pKa value of 6.7 (Rajan, Wischmeyer et al. 2000) indicating that both channels are sensible to acidic pH with TASK-1 being more susceptible to small shifts. Equally to TASK-1 and TASK-3, TASK-5 possesses a pH-sensitive histidine

residue (H98) near the K^+ selectivity sequence (GYG) in the pore region. Presence of that residue lead to the hypothesis that TASK-5 could also be sensitive to acidic pH_o.

Swapping M1P1 loops between TASK-1 and TASK-3 was performed to show that the particular domain influences the pH sensor at the selectivity filter, providing an explanation for their different pH_o sensitivities (Clarke, Veale et al. 2008). Furthermore, Czirják and Enyedi created a construct by fusing the C terminus of TASK-3 with the N terminus of TASK-1 to form heterodimers. These were transfected in oocytes where K^+ currents were electrophysiologically characterised. Results showed that large currents, comparable to those of TASK-1 and TASK-3 were elicited. Interestingly, the pH and ruthenium red sensitivity values of the tandem channel from both parent currents had an intermediate pH sensitivity in response to pH modification from 7.5 to 6.5 and a minimal inhibition by 5μM ruthenium red (a feature of TASK-1 channels). Consequently, the heterodimer inherited features asymmetrically from the two parent subunits and was sensitive to a wider pH range than either of the parent homodimers. Insensitivity to ruthenium red was a logical consequence as the binding site for the dye had to be present in both subunits (Czirják and Enyedi 2002).

2.8 Tissue distribution of TASK-1, TASK-3 and TASK-5

TASK channels play an important role in the brain determining the membrane potential, input resistance, excitability of neurons and contribute to the production of cerebrospinal fluid (Kindler, Pietruck et al. 2000). To determine the distribution of TASK channels in the central nervous system, mRNA expression revealed that cholinergic structures such as the cranial nerve motor nuclei, the dorsal motor nucleus of the vagus, spinal cord ventral horn as well as the septal nuclei were found to carry neuronal populations with high expression levels of TASK-1 and TASK-3 (Karschin, Wischmeyer et al. 2001). High expression levels of TASK-1 and TASK-3 were also found in the locus coeruleus the major source of noradrenergic neurons and TASK-3 in all raphé nuclei which contain the majority of all serotonergic neurons. Expression of TASK-1 and TASK-3 was also found in diverse brain neuron clusters (nuclei) or cell populations such as the cerebellar and olfactory bulb granule cells which were not related to a specific neurotransmitter system (Kindler, Pietruck et al. 2000).

The expression pattern of TASK-5 was particularly unique as it appears exclusively expressed in the nuclei of the primary central auditory pathway such as the medulla, the dorsal and ventral cochlear clusters of neurons (Kindler, Pietruck et al. 2000). Outside the auditory system, TASK-5 was only expressed in a few groups of neurons such as the spinal trigeminal sensory and mammillary nucleus, the olfactory bulb and the cerebellum. Interestingly, TASK-5 is the second ion channel associated with the auditory system pathway. Prior to this finding, the voltage-gated K^+ channel subunit $K_v7.4$ or KCNQ4,

implicated in the autosomal dominant deafness 2 (DFNA2) (Holt and Corey 1999, Kubisch, Schroeder et al. 1999) was found in the outer hair cells of the inner ear but also in the cochlear nuclei. The deafness caused by mutations of KCNQ4 could be similarly associated with TASK-5 dysfunctions, provided that TASK-5 channels are functional and expressed at the mRNA levels predicted in the study. The polymorphism observed in the GYG motif of the first pore region of TASK-5 was exactly at the same position as the G285S mutation that disrupted the channel activity in KCNQ4 leading to DFNA2 (Holt, Asako et al. 2006). Thus, future studies focusing on the functional significance of TASK-5 in transgenic animals during development are required to clarify its potential role in processing auditory information. Finally, after cochlear ablation the expression of TASK channels, especially of TASK-1 and TASK-5, diminished in the auditory brain stem neurons (Holt, Asako et al. 2006) and the inferior colliculus (Cui, Holt et al. 2007).

In addition to the high mRNA expression of TASK channels in the brain, TASK-1 and 3 were also shown to be widely distributed in mouse, rat and human tissues where they were suggested to contribute to the maintenance of the resting membrane potentials of multiple cells. Expression of TASK-1 in adult human and mouse tissues was examined by Northern blot analysis. TASK-1 was highly expressed in the brain, heart, lung, pancreas, placenta and to a lower extent in prostate human tissues (Duprat, Lesage et al. 1997). Kim et al.,2000 used RT-PCR to examine the mRNA tissue distribution of TASK-3 in rat tissues and demonstrated that the channel was expressed in the brain, stomach, colon, kidney, lung, liver, spleen, testis and skeletal muscle) (Kim, Bang et al. 2000).

2.9 TASK-5 or $_{h}K_{2P}15.1$ channel

In 2001, two different research groups identified and cloned a novel member of K2P channel family from human brain or testis cDNA (Ashmole, Goodwin et al. 2001, Kim and Gnatenco 2001). The new cDNA encoded a 330-residue polypeptide with a 36kDa molecular mass. The predicted structure of TASK-5 was made up of 4TMS, three cytoplasmic and 2P forming domains in each subunit. It had a large extracellular linker region between M1 and P1 that lacked both a cysteine residue for disulfide bond formation and a glycosylation site. TASK-5 possessed four putative polymorphisms in the TASK-5 coding region at codons 95 (GGG or GAG), 260 (CCC or ACC), 261 (CAC or CCC), and 323 (CTT or CCT) after sequence analysis of three independent EST clones and comparison to the human λ-phage genomic library (Karschin, Wischmeyer et al. 2001, Kim and Gnatenco 2001). The most crucial single nucleotide polymorphism (SNP) observed in this channel was present in the P1 region (position 95) encoding for EYG and leading to a non-functional or non-selective channel. Therefore, it is fundamental to analyse the DNA construct sequence of TASK-5 prior undertaking any experiments.

2.9.1 TASK-5 and its lack of cell surface expression

The sensitivity of TASK-5 to increased [H^+] has yet to be examined as the channel failed to elicit ionic currents either in recombinant or in mammalian cytosolic membranes of COS-7, HeLa or HEK293 cells.

In 2001, Kim and Gnatenco transfected COS-7 cells with GFP-tagged channels or GFP alone (as a control) and compared whole-cell currents recorded from transfected cells either with TASK-1 or TASK-3 (Figure 2.5). TASK-1 and TASK-3 exhibited robust single channel openings with a conductance of 14 and 26 pS (at -80 mV). On the other hand, TASK-5 did not show any single channel openings in all 24 patches from 4 different transfections. Despite intracellular application of ATP (1–4 mM), cAMP (100 μM) stimulating ATP-activated K^+ channels (Dunne 1994, Trapp, Tucker et al. 1997) or GTPγS (100 μM), phorbol myristate acetate (PMA; 10 μM) and arachidonic acid (10 μM) stimulating Ca^{2+} (10 μM) activating calcium-gated K^+ channels,TASK-5 failed to elicit any K^+ currents. Additionally, changes in intracellular or extracellular pH (pH 6.0–8.4) or co-expression of TASK-5 with TASK-1 or TASK-3 did not promote the opening of the channel.

Microinjection of TASK-5 cDNA in *Xenopus* oocytes was also tested where electrophysiological characterisation was undertaken 1-5 days post-injection (Ashmole, Goodwin et al. 2001). The lack of channel activity however lead to two possible suggestions. Either TASK-5 is intracellularly expressed or, needs a functional partner for proper assembly and expression on the plasma membrane.

Finally, replacement of the channel's COOH terminus with TASK-3 resulted in channel expression on the plasma membrane however, this promising approach failed to show any active current that could potentially be elicited from TASK-5 during patch-clamp experiments (Ashmole, Goodwin et al. 2001, Kim and Gnatenco 2001).

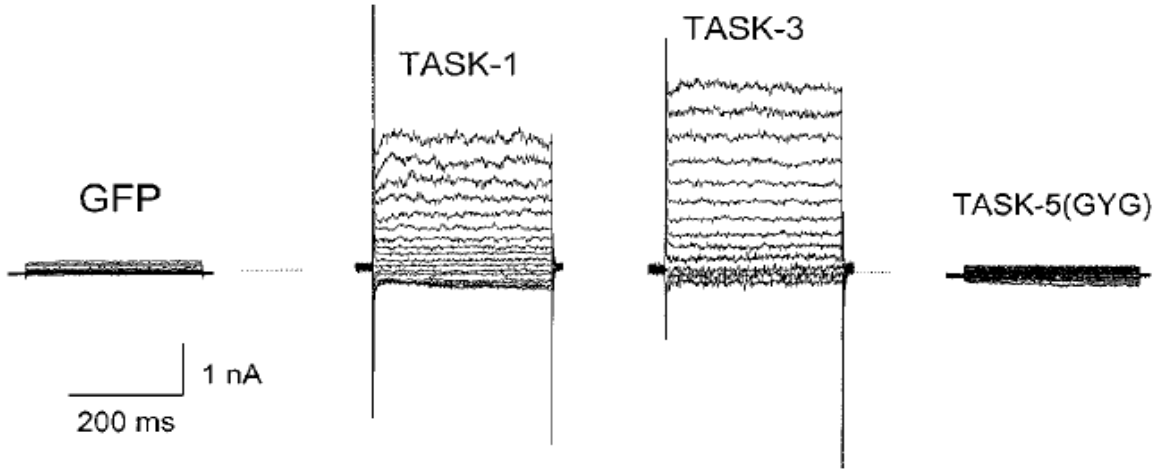

Figure 2. 5 Whole-cell K^+ currents recorded from COS-7 cells transfected with GFP alone, TASK-1-GFP, TASK-3-GFP or TASK-5-GFP. Under identical recording conditions both TASK-1 and TASK-3 elicited large K^+ currents of ~2nA and ~3nA in current amplitude accordingly.TASK-5 did not show any current activity which was comparable to GFP alone. Image adapted from Kim & Gnatenco, 2001.

2.9.2 Evidence that TASK-5 is a mitochondrial channel

In-vitro binding assays

Within the O'Kelly laboratory evidence that TASK-5 was expressed in mitochondria was demonstrated by two different approaches. The first approach consisted of identifying binding partners of TASK-5 through a series of *in-vitro* binding assays either using full-length or smaller fragments of the channel (Roncoroni 2012).

To accomplish this, HEK293 cells were transfected with either eGFP or TASK-5-eGFP, lysed and immobilised on GFP-trap beads. Cells over-expressing GFP-conjugated proteins were lysed and immobilised on GFP-trap beads. Interacting proteins were separated by sodium dodecyl sulfate polyacrylamide gel (SDS-PAGE) electrophoresis and visualised by Coomassie blue staining. Detectable protein bands were analysed by mass spectrometry where two distinct proteins (tubulin beta chain and mitochondrial ATPase subunit beta) were suggested to bind to the full-length of TASK-5 whereas cytochrome bc1 complex subunit 1 was found to bind to the C-terminus of the channel in comparison to eGFP alone. A similar approach was performed for the internal region and N-terminus which however, did not reveal any interacting proteins by mass spectrometry.

Sub-cellular localisation of TASK-5 in transfected HeLa cells using a custom made antibody

The second approach was based on the inability of TASK-5 to show cell surface expression (Kim and Gnatenco 2001) which raised the question whether the channel was intracellularly expressed. To test this hypothesis, members of the group sought to determine TASK-5's cellular expression in transiently transfected HeLa cells with a TASK-5-eGFP DNA construct

using commercially available antibodies against the channel and co-stained with multiple intra-cellular compartments (Roncoroni 2012). However, the antibodies failed to detect the protein by both immunocytochemistry and Western blotting and were hence considered unsuitable for the detection of TASK-5. To overcome the lack of specific targeting tools against the channel, a custom made antibody ($hK_2P15.1$-LR) recognising the last aa (294-308) of the C-terminal was generated for the group by Covalab showing a stronger specificity for TASK-5 both by immunocytochemistry and Western blotting (Roncoroni 2012).

Using the non-commercial antibody and intra-cellular compartments such as the Golgi apparatus (58K Golgi protein), endoplasmic reticulum (PDI), mitochondria (cytochrome bc1) and surface membrane (lectins) the sub-cellular expression of TASK-5-eGFP was revealed following co-localisation analysis of confocal images of immunocytochemistry in transfected HeLa cells (Figure 2.6) (Roncoroni 2012). Markers of intracellular compartments were detected with a Fluorescein isothiocyanate green (FITC) and TASK-5-eGFP with anti-rabbit Texas red secondary antibodies. To study the co-localisation between the two fluorescent signals, a line defining a region of interest (ROI) was traced across a transfected cell. Each fluorescent signal traces (green and red) were quantified and the overlap of their intensity peak positions indicated that there was co-localisation. For non-co-localising signals, the distance between intensity peaks positions was measured (Figure 2.6).

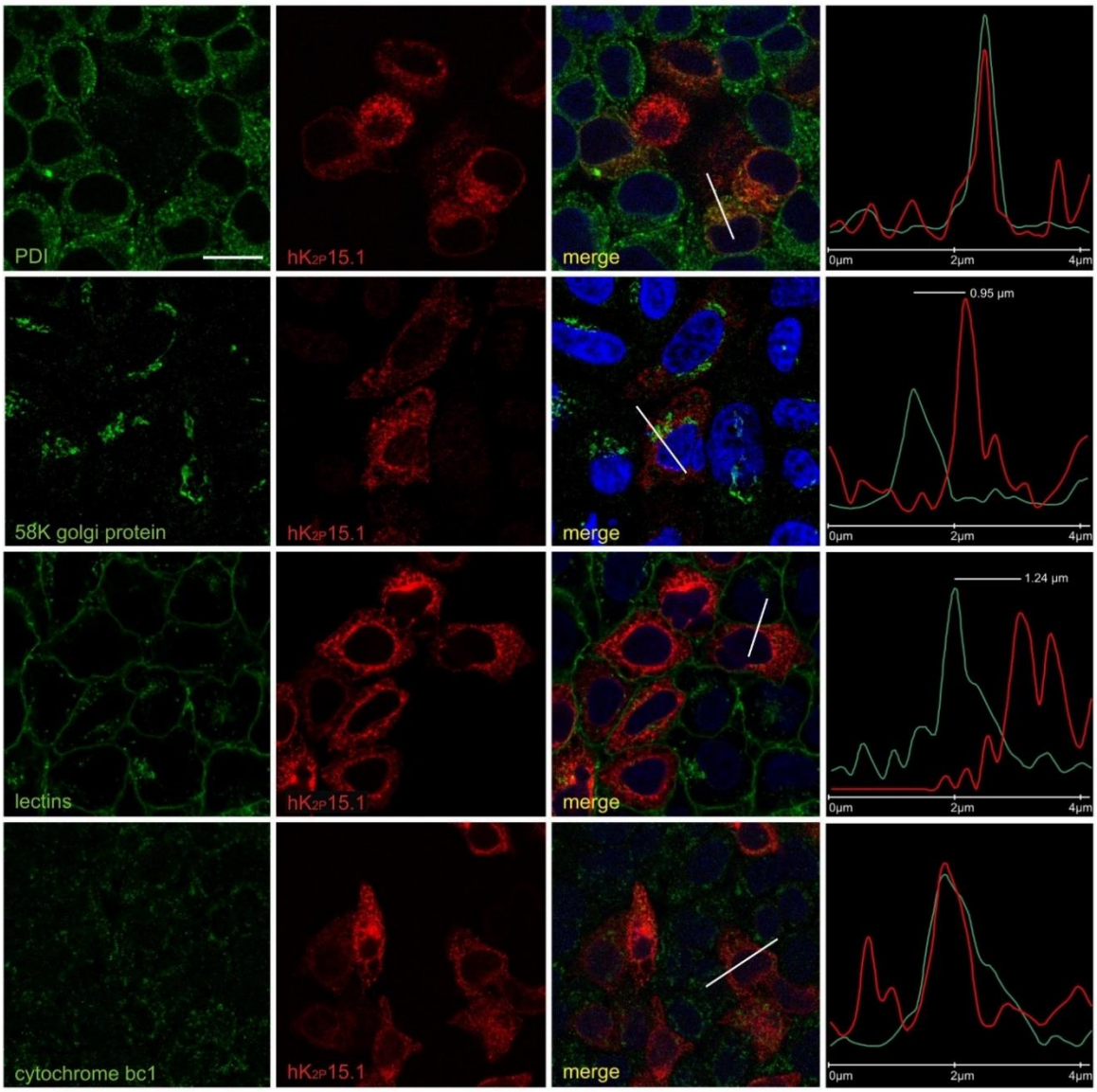

Figure 2. 6 TASK-5 sub-cellular localisation in transfected HeLa cells with TASK-5-eGFP. Confocal images of immunocytochemistry of transfected HeLa cells co-stained with different cellular compartments (lectins, cytochrome bc1, 58k golgi protein and PDI) with a secondary green fluorescence (1:10 00 FITC) antibody. TASK-5-eGFP was targeted with hK2P15.1-LR and a secondary Texas red (1:150) antibody. A ROI was drawn on merged images and co-localisation analysis of the two fluorophores are shown in the last column. True co-localisation was deduced from the overlap of the intensity peak position of the two signals. Scale bars: 25µm. Image adapted from (Roncoroni 2012).

While these data provide evidence of co-localisation, this approach does not provide statistically significant quantification of fluorescent signals (FITC and Texas red). An appropriate analysis should visually, quantitatively and statistically evaluate the co-distribution of two probes in fluorescence microscope images and the negative aspect of such co-localisation quantifications is that they are rarely supported with statistical analysis. Thus, co-localisation of previously acquired confocal images was re-analysed during the current study using ImageJ software where co-localisation test plugin, Costes method and Manders' co-localisation coefficient were adopted (Methods 3.8.3). More precisely, this

consisted of comparing fluorescent signals emitted from blocks of pixels within a selected ROI (R(obs)) to randomly scrambled (R(rand)) pixels within the image background during 200 iterations.

Co-localisation analysis results show that 58K golgi protein is inversely co-expressed with TASK-5-eGFP as negative R(obs) values (-0.288) were extracted from ImageJ (Table 2.1). A negative correlation indicates that the stronger TASK-5-eGFP expression within a selected cell of interest, the less protein will be expressed in the Golgi apparatus. A scatter plot showing individual red pixels that represent TASK-5-eGFP on the x-axis and green pixels for 58K golgi protein on the y-axis was generated to quantitatively illustrate their lack of co-expression (Figure 2.7A). In fact, individual pixels clustered close to the origin instead of the diagonal during which, co-localisation is stronger. Lack of correlation between the cytoplasmic membrane markers (lectins) and TASK-5-eGFP is also shown where R(obs) is close to 0 and, both red and green pixels cluster near the origin of the scatter plot (Figure 2.7B). PDI, a marker for the endoplasmic reticulum has a minimal co-localisation with TASK-5-eGFP (R(obs)=0.126) as few yellow pixels cluster near the origin of the scatter plot (Figure 2.7D). Finally, cytochrome bc1, a marker for the IMM has an average (R(obs)=0.412) but stronger co-localisation level with TASK-5-eGFP compared to the rest cellular compartments as co-localising pixels cluster along the diagonal and reflect the degree of correlation between two fluorescent probes (Figure 2.7C). Importantly, all randomised (R(rand)) background blocks of pixels have lower fluorescent values than pixels selected in a ROI after 200 iterations (0/200) indicating that randomly chosen blocks from the image's background do not show true co-localisation. In fact, R(rand) values should always be close to 0 in order to demonstrate that there is true co-localisation and that results are statistically significant (Dunn, Kamocka et al. 2011).

Cellular compartment	R(obs)	R(rand) Mean ±SD	R(rand)>R(obs)
58K golgi protein	-0.288	0.039±0.021	0/200
Lectins	0.066	0.028±0.003	0/200
Cytochrome bc1	0.412	0.048±0.003	0/200
PDI	0.126	0.095±0.001	0/200

Table 2. 1 R(obs) values extracted from a ROI are compared with background blocks of pixels (R(rand)). Co-localisation analysis between TASK-5-eGFP protein and multiple cellular compartments shows that the channel is preferably expressed in mitochondria R(obs)=0.41. Coste's method provides statistical significance to acquired results as R(obs) values are stronger than R(rand) after 200 iterations. R(rand) values are shown as Mean±standard deviation.

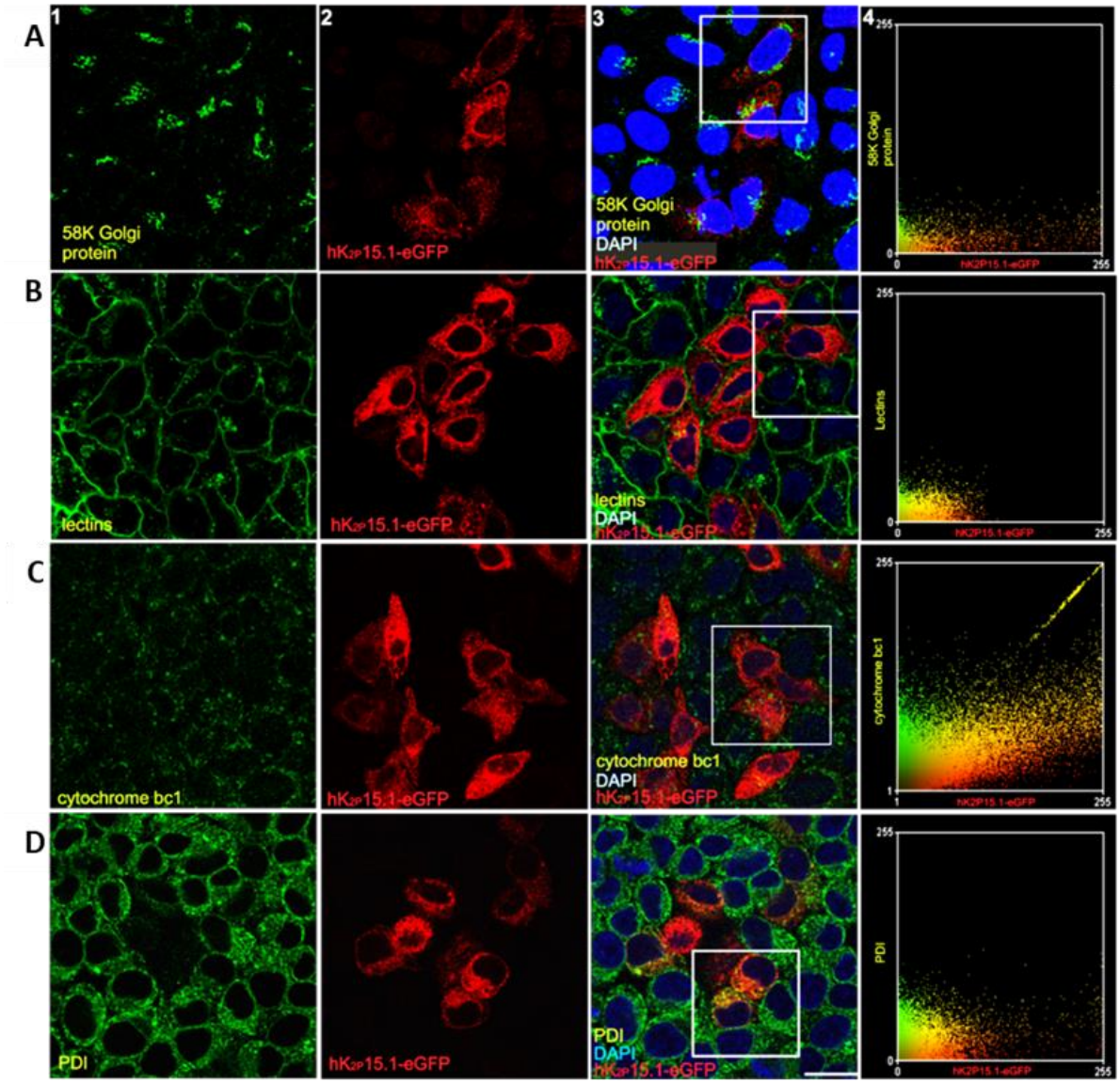

Figure 2. 7 Co-localisation analysis of confocal images of immunocytochemistry where transfected HeLa with TASK5-eGFP were stained with cellular compartments. 58K Golgi, lectins, cytochrome bc1 and PDI were stained with a FITC (520 nm) secondary antibody (1:1000) and TASK5-eGFP with hK2P15.1-LR and a secondary Texas red (1:150) (615 nm) antibody. Co-localisation test was performed on merged images where a ROI was drawn around a double fluorescent cell and scatter plots *(*A4-D4) showing individual fluorescent pixels were obtained from the co-localisation test plugin of ImageJ. Co-localising pixels are shown in yellow and cluster along the diagonal when co-localisation increases as shown in panel C4. The colour components of individual pixels were measured in the colour range between 0 and 255. Scale bars: 25µm. Image (A1:D3) adopted from Roncoroni *et al.,* 2012.

Co-localisation results showed for the first time by immunocytochemistry that TASK-5-eGFP overlapped with cytochrome bc1 (complex III), an intrinsic membrane protein that catalyses the oxidation of ubihydroquinone and the reduction of cytochrome *c* in the inner mitochondrial membrane (Crofts 2004). As the bc1 complex operates through a Q-cycle mechanism that couples electron transfer to generation of the proton gradient that drives ATP synthesis, TASK-5 co-expression may speculate a potential role during mitochondrial energy production.

2.10 Mitochondria

History and background of mitochondria

In 1890, mitochondria were designated as the fundamental living elements of the cytoplasm by being entitled as bioblasts (bio, “life”; blasts, “germs”), the centres of biological function in cells (Altmann 1890). Since then, interest in mitochondria has grown as these organelles have been recognised for their multifunctional roles in metabolism, energy transduction, ion transport, inheritance, signalling and cell death. Several studies have demonstrated that mitochondria could store large amounts of Ca^{2+} and were thus hypothesised to be the main intracellular storage organelles involved in Ca^{2+} cycling. This suggestion was however been set aside lately as this was the main role attributed to the endo-(or sarco) plasmic reticulum (Rizzuto, Duchen et al. 2004). Nevertheless, Ca^{2+} channels still have an important role in mitochondrial dynamics which will be further explained in section 2.12.2.

Mitochondria consist of the matrix which contains the mitochondrial DNA, soluble enzymes or ribosomes, an inner membrane, where important metabolic processes such as the citric acid cycle, oxidative phosphorylation and fatty acid beta-oxidation occur, an intermembrane space; all enclosed by an outer membrane, generally considered to be freely permeable to metabolites and ions (Figure 2.8) (Szabo, Leanza et al. 2012). Under normal physiological conditions, intracellular and extracellular [Ca^{2+}] is in the range of 100nM and 1mM accordingly and mitochondrial Ca^{2+} uptake varies from 100nM to 1mM according to the pathophysiological or excitatory conditions of the cell (Williams, Boyman et al. 2013). Mitochondria also maintain matrix [K^{+}] between 150–180 mM which is higher than the cytoplasmic concentration (~140mM) (Garlid 1996, Kowaltowski, Cosso et al. 2002). Finally, intra-mitochondrial space (IMS) pH is usually close to 6.8 and more basic (pH 7.7) in the mitochondrial matrix indicating that there is a H^{+} movement and accumulation in the IMS (Santo-Domingo and Demaurex 2012).

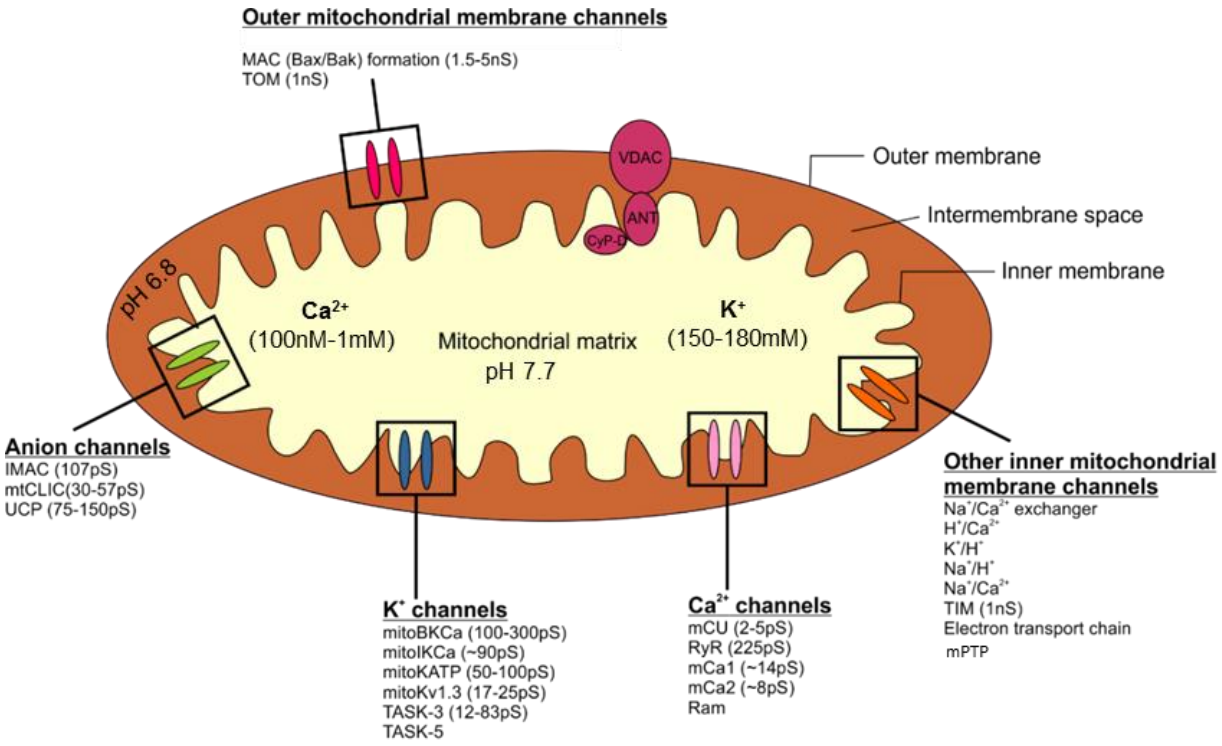

Figure 2. 8 Structure of a mitochondrion. Illustration summarising the various populations of ion channels/exchangers expressed either on the outer or inner mitochondrial membranes together with their respective conductances reported to date. Detailed representation of the mPTP members are shown in purple. Matrix K^+ and Ca^{2+} concentrations maintained under physiological conditions are also shown.

Impact of ion transport in mitochondria

Mitochondrial channels are important for the control of the integrity of the organelles as they transport ions and play a key role in energy metabolism, regulate the mitochondrial matrix volume, respiration and membrane potential. Mitochondrial bioenergetics have been revealed through a series of findings and theoretical considerations including the description of the Krebs cycle, the oxidative phosphorylation process and the chemiosmotic hypothesis; resulting in the production of ATP in aerobic organisms (Mitchell 1961). The chemiosmotic hypothesis is sub-divided into three main processes with (*a*) the flow of electrons down the electron transport chain which is coupled to H^+ pumping from the matrix to the intermembrane space to establish the proton motive force (Δ_{H^+}), (*b*) the H^+ translocation down the electrochemical proton gradient across the mitochondrial inner membrane which is reversibly coupled to ATP phosphorylation through the ATP synthase (F_1F_O ATPase), (*c*) exchange-diffusion carrier proteins and ion channels being present on the inner and outer membranes to transport metabolites and selected ions into and out of the matrix in order to control the organelle integrity (O'Rourke 2007). Emphasis to the last chemiosmotic process will be given through the presentation of various ionic carriers and channels expressed either on the outer or inner mitochondrial membrane in the following section.

2.11 Outer mitochondrial membrane channels

MAC

Although debate is ongoing about whether VDAC constitutes a route for cytochrome *c* release, another candidate has emerged as a possible outer membrane permeation pathway (MOMP) (Antonsson, Montessuit et al. 2000, Dejean, Martinez-Caballero et al. 2005, Dejean, Martinez-Caballero et al. 2006, Adams and Cory 2007)(Dejean et al., 2005; Dejean et al., 2006; Antonsson et al., 2000; Adams & Cory, 2007). In 2001, a novel high-conductance channel was observed in proteoliposomes prepared from mitochondrial outer membranes that were isolated from cells undergoing apoptosis (Pavlov, Priault et al. 2001). This mitochondrial apoptosis–induced channel (MAC) was formed by the pro-apoptotic Bcl-2 family proteins Bax and/or Bak, had a fully open conductance of 1.5-5 nS which was voltage independent and, unlike VDAC, was partially cation selective ($P_{K^+} > P_{Cl^-}$). Moreover, MAC was able to make the mitochondrial outer membrane permeable to apoptosis-associated proteins normally constrained within the intermembrane space, such as cytochrome *c* and Smac/DIABLO (Green and Kroemer 2004, Martinez-Caballero, Dejean et al. 2005). Once in the cytoplasm, these proteins triggered a chain of downstream cytosolic enzyme pathways including effector caspases that execute cell death (Youle & Strasser, 2008) (Peixoto, Lue et al. 2011).

TOM/TIM

Other channels such as the protein import machinery translocases (TIM and TOM), as well as the respiratory complex I were successively added to the OMM channels family (Uribe-Carvajal, Luévano-Martínez et al. 2011). The insertion and translocation of mitochondrial pre-proteins encoded by the nucleus require specialised molecular machinery consisting of complexes of proteins on the outer and inner membranes. The principal proteins of the translocase of the outer mitochondrial membrane (TOM) and its partner on the inner membrane, TIM, can form large conductance (1nS both) channels which have partial cation selectivity ($P_{K^+} > P_{Cl^-}$) between +20 and +30mV (Grigoriev, Muro et al. 2004).

2.12 The inner mitochondrial membrane

Mitochondria have long been considered to be poorly permeable to cations and anions due to the strict control of IMM permeability for efficient ATP synthesis. However, there is evidence that various ion channels along with antiporters and uniporters are present in the mitochondrial inner membrane (Szabo, Leanza et al. 2012). These channels are important for energy supply and some are even decisive factors in determining whether a cell lives or dies. The electrochemical driving forces for ion movement across the IMM are critical due to the very high negative membrane potential ($\Delta_{\psi m}$ ~120-180mV, negative in the matrix) created by the efflux of protons from the matrix during oxidative phosphorylation (Logan, Pell et al. 2016). The electrochemical gradient is regulated by two components: (a) the electrical gradient i.e the voltage difference across the membrane generating a membrane potential or (b) the chemical gradient or difference in ion concentration across the two sides of the membranes (Δp_{Ion}). The combination of these two factors determines the thermodynamically favourable direction for ion movement across the mitochondrial membranes (Szabo, Leanza et al. 2012).

mPTP

The mitochondrial permeability transition pore (mPTP) requires the association of different proteins such as the voltage-dependent anion channel (VDAC), localised in the OMM, the adenine nucleotide translocator (ANT) in the IMM together with the peripheral benzodiazepine receptor, the Bcl-2 family proteins, the hexokinase bound to porin, cyclophilin-D (CyP-D) and the intermembrane space creatine kinase (mtCK) within the matrix (Beutner, Ruck et al. 1996, Beutner, Ruck et al. 1998, Bernardi 1999).
The major candidates believed to represent the minimum mPTP configuration with a total conductance of ~3.4nS are VDAC and ANT coupled to CyP-D. VDAC forms an outer membrane pore with a diameter of 2.5–3 nm in the full conductance state where it is partially anion selective in the open state, allowing the passage of molecules of up to ~5kDa such as

ATP, ADP, and P_i, but also permits the free diffusion of cations including Ca^{2+}, K^+, and Na^+ (Rostovtseva, Tan et al. 2005). VDAC gating is highly voltage dependent with peak currents near 0 mV which dramatically reduce at positive or negative voltages in the range of 20-40 mV (Gincel, Zaid et al. 2001, Levadny, Colombini et al. 2002). Peak currents are also reduced by the application of ruthenium red at micromolar concentration (5μM) (Gincel, Zaid et al. 2001, Levadny, Colombini et al. 2002). ANT forms the inner part of mPTP by binding to the inner face of VDAC at contact sites between the inner and outer mitochondrial membranes. CyP-D is an ubiquitous protein endowed with matrix peptidyl–prolyl cis–trans isomerase activity that binds to ANT's matrix surface enabling a Ca^{2+}-triggered conformational change converting mPTP from a specific transporter to a non-specific pore (Halestrap and Brenner 2003). Pathologically, mPTP opening is induced by elevated mitochondrial matrix Ca^{2+}, ROS, inorganic phosphate and intracellular acidification (Szabo et al., 1992; Giorgio et al., 2013). In contrast, mPTP is inhibited by ATP/ADP and Mg^{2+} (Kowaltowski, Naia-da-Silva et al. 1998, Crompton 1999)

2.12.1 Inner mitochondrial membrane potassium channels

The K^+ cycle

The so-called K^+ cycle can potentially control the tightness between respiration (Kreb's cycle) and ATP synthesis by maintaining a balance between energy supply and demand in the cell via the magnitude of $\Delta\Psi_m$ (Szabo, Leanza et al. 2012).

In isolated mitochondria, the high negative membrane potential induces K^+ influx from the cytoplasm to the mitochondrial matrix preventing excessive matrix swelling (Garlid and Paucek 2003). Thus, this process maintains the structural integrity of the organelle or prevents matrix shrinkage which can then inhibit respiration (Heinen, Camara et al. 2007). In energised mitochondria when $\Delta\Psi_m$ is highly negative (–180/-200 mV), K^+ influx results in water uptake through mitochondrial aquaporins (Amiry-Moghaddam, Lindland et al. 2005) resulting in mitochondrial swelling (Szabo, Leanza et al. 2012). Excess matrix $[K^+]$ is then exported from the matrix by the electroneutral K^+/H^+ antiporter, which is regulated to sense volume changes via changes in pH and $[Mg^{2+}]$ (Szabo, Leanza et al. 2012). Volume changes of mitochondria may also have an impact on Ca^{2+} signalling within cells by altering the architecture of contact points between the endoplasmic reticulum and mitochondria; however, this hypothesis remains to be confirmed (Rizzuto, Marchi et al. 2009, Garcia-Perez, Schneider et al. 2011). Furthermore, K^+ influx may lead to formation of the so-called donut-shaped mitochondria during hypoxia or stress however, the significance of such shape change is still undefined (Liu and Hajnoczky 2011). Increases in extracellular $[K^+]$ can occur during neuronal activity and under pathological conditions such as ischaemia, leading to a compromised neuronal function. Astrocytes for example contribute to the clearance of

excess [K^+] by taking up K^+ from the cytoplasm into mitochondria (Kozoriz, Church et al. 2010). Thus, mitochondria seem to act not only as a safety sink for cytoplasmic Ca^{2+} but also for excess extracellular K^+.

The mitochondrial ATP-sensitive potassium channel

In 1991, Inoue et al. reported the presence of an ATP-sensitive K^+ channels in rats' liver mitochondrial inner membrane using the direct mitoplast patch-clamp method (Inoue, Nagase et al. 1991). They described a channel with a single channel conductance of 9–10 pS in asymmetrical KCl solutions100 mM (pipette) /33 mM (bath) with a nearly linear current to voltage (I-V) curve and a slight outward rectification. Remarkably, since its initial discovery a variety of mitoKATP channel conductances have been reported. In 1992, mitochondria from rat liver and bovine hearts reconstituted in lipid bilayers recorded a conductance of 30 pS in symmetrical 1M KCl solution (Paucek, Mironova et al. 1992). A conductance of 56 pS in symmetrical 150 mM KCl solution from lipid bilayers was observed nearly a decade later (Zhang, Chen et al. 2001) while Bednarczyk et al. observed a conductance of ~ 103 pS under the same conditions (Bednarczyk, Kicinska et al. 2004, Bednarczyk, Dolowy et al. 2005). The differences in conductance can be attributed to variances in the preparations, concentrations of charge carriers as well as the presence of modulators such as Mg^{2+} and ATP. They also reflect the complexity of studying mitoKATP channels and raise the possibility that there may be more than one type of channel that respond to known activators and inhibitors of mitoKATP channels. Most of researchers do agree on a pharmacological sensitivity to ATP in the presence of Mg^{2+} ions.

In fact, in single channel recordings, addition of 0.5 mM ATP inhibited most of the channels' activity in the presence of 0.1 mM Mg^{2+} and increasing ATP concentration to 1 mM gradually inhibited the channel until complete closure (Jiang, Ljubkovic et al. 2006). The Mg^{2+}/ATP-inhibited channel could be activated by the plasma membrane ATP-sensitive K^+ channel (KATP channel) openers cromakalim and diazoxide which were hypothesised to be beneficial during cardioprotection. In the absence of Mg^{2+} and ATP, mitoKATP was completely insensitive to the cardioprotection blockers glyburide (IC_{50} 1-6 μM) and 5-hydroxydecanoate (5-HD) (IC_{50} 45-75 μM) (Jaburek, Yarov-Yarovoy et al. 1998). On the other hand, in the presence of Mg^{2+}, ATP or a pharmacological opener such as diazoxide, mitoKATP could become highly sensitive to glyburide and 5-HD (Jaburek, Yarov-Yarovoy et al. 1998). Diazoxide was much more effective on the mitochondrial than on the plasma membrane channel and was widely used to study the pathophysiological roles of mitoKATP (Garlid, Paucek et al. 1997, Szewczyk, Kajma et al. 2010).

Mitochondrial voltage-gated potassium channel (mitoKv1.3)

In 1996, the voltage-gated (Kv) channel potassium channel (Kv1.3) was identified by electron microscopy, immunological studies and patch clamp of mitoplasts in the inner mitochondrial membrane of T lymphocytes, macrophages, hippocampal neurons and presynaptic neurons (Szabo, Bock et al. 2005, Vicente, Escalada et al. 2006, Bednarczyk, Kowalczyk et al. 2010, Gazula, Strumbos et al. 2010); the cell membrane of kidney cells (Yao, Chang et al. 1996), central nervous system (Mourre, Chernova et al. 1999) and epithelia cells (Grunnet, Rasmussen et al. 2003). Patch-clamp experiments on mitoplasts from Jurkat T-cells known to endogenously express mitoKv1.3 (Cahalan, Chandy et al. 1985) or transfected Kv1.3-deficient CTLL-2 cells have shown that a channel with biophysical characteristics analogous to those of Kv1.3 expressed on the cell membrane was present in the IMM. The conductance of the channel was 17-25 pS and a weak rectification was observed at potentials more positive than +30 mV in symmetrical 114 mM K^+ gluconate solution equally to Kv1.3 (Schilling, Quandt et al. 2000). The channel was shown to be sensitive to specific inhibitors such as 2nM Margatoxin (MgTx), K^+ channel blocker TEA (100mM) or 20nM Charybdotoxin (ChTx) a neurotoxin usually used to block calcium-activated potassium (K_{Ca}) channels (Szabo, Bock et al. 2005).

Two-pore potassium channel TASK-3

2.12.1.1 Controversial role of TASK-3 in cell survival and death

During the early 2000s, the functional role of TASK-3 elicited the curiosity of numerous researchers as there was clear indication that this channel had the paradoxical ability to either induce (Lauritzen, Zanzouri et al. 2003) or prevent apoptotic cell death (Liu, Cotton et al. 2005) and promote cell proliferation (Mu, Chen et al. 2003, Pei, Wiser et al. 2003).

In cultured rat granule neurons, the activity of TASK-3 channel was shown to be linked to apoptosis induction while migrating to their final destination in the cerebellar cortex (Lauritzen, Zanzouri et al. 2003). Moreover, during *in vitro* studies performed on rat hippocampal neurons, over-expression of the channel lead to cell death (Nadeau, McKinney et al. 2000). Survival of rat granule neurons on the other hand was demonstrated by expression of TASK-3^{G95E} dominant-negative mutant, confirming that the TASK background K^+ channel significantly contributed to the K^+-dependent death of these cells. The mechanism by which TASK-3 channels contribute to the initiation of granule cell death is however, not completely understood but their ability to allow K^+ ions exit the cytoplasm along with Cl^- and water movements may be linked to the activation of the apoptotic machinery such as the intracellular enzymes caspases or nucleases (Maeno, Ishizaki et al. 2000). Innamaa and co-workers reported that increased TASK-3-specific immunostaining was

associated with a distinct prognostic advantage and patients having ovarian cancer with strong TASK- 3 immunopositivity were characterised with increased survival (Innamaa, Jackson et al. 2013). Increased TASK-3 expression was also found to be associated with reduced migration and invasion of breast cancer cells (MCF-7) (Lee, Park et al. 2012). In addition, Meuth and his co-workers demonstrated the existence of a TASK-3-dependent cell death pathway in glioma cell lines (LN319 and U373) (Meuth, Herrmann et al. 2008).

In contrast, the potential pathological significance of TASK- 3 channels emerged when amplification of the TASK-3 coding gene (*KCNK9*) was reported in 10% of malignant breast tumours investigated in a study in 2003, along with a 5–100-fold over-expression of the channel protein in 44% of breast cancer or 35% of lung cancer specimens by promoting cancer cell survival in the poorly oxygenated areas (Mu, Chen et al. 2003). Although *KCNK9* is situated at the chromosomal region 8q24.3 which is in proximity of a well-known oncogene (c-myc), amplification of *KCNK9* alone was found to be present in a number of pathological cases, suggesting its potential causative role in tumour development (Mu, Chen et al. 2003). Over-expression of the wild-type TASK-3 protein enhanced tumorigenicity of mouse embryonic fibroblasts (C8) and shortened the time for tumour formation in athymic nude mice. Moreover, cultured C8 cells became more resistant for hypoxia and serum deprivation (Pei, Wiser et al. 2003). It is also hypothesised that *KCNK9* over-expression in breast tissue may occur due to acquired relative hypomethylation and subsequent functionally biallelic-expression which may be equivalent to duplication of an active allele (Skaar, Gould et al. 2014). The functional relationship of *KCNK9* methylation/expression of Skaar, Gould et al., was also consistent with Dookeran, Zhang et al, as they observed increased *KCNK9* expression together with relative hypomethylation at functional loci in triple negative breast cancer sub-type (Dookeran, Zhang et al. 2017). Interestingly, the reduction of TASK-3 expression in melanoma cells (WM35 and A2058) compromised mitochondrial function and cell survival (Kosztka, Rusznák et al. 2011) decreased the total DNA content, altered the cell morphology and induced apoptosis (Cheng, Gulbins et al. 2011).

The Ben cell line (lung carcinoma) is known to have naturally over-expressed TASK-3 channels. Transfection of these cells with TASK-3^{G95E} a dominant negative mutation resulted in a significant reduction of cell proliferation (Pei, Wiser et al. 2003). Moreover, over-expression of TASK-3 channels was shown to effectively reduce the TNF-induced cell apoptosis whereas the non-K^+-permeable point mutant (TASK-3^{G95E}) did not have the ability to do so (Pei, Wiser et al. 2003).

Based on these experiments, TASK-3 activity may either induce or prevent cell apoptosis indicating that its activity is specific for each tissue. The modus operandi however, of TASK-

3 channels in contributing to the genesis and/or increased survival of malignantly transformed cells still awaits clarification. A potential mechanism could be the amplification of *KCNK9* gene (along with the over-expression of its encoded protein) that could favour tumour formation, most likely via increasing the resistance of cancer cells to hypoxia and serum deprivation. This mechanism would increase the survival of cancer cells especially in the poorly oxygenated areas of solid tumours leading to the assumption that *KCNK9* can be considered as an established oncogene.

2.12.1.2 Localisation of TASK-3

Shortly after the contradictory hypotheses that TASK-3 may or not enhance tumourigenicity in different cancer types, the distribution of the channel's immunopositivity was reported (Pocsai, Kosztka et al. 2006). In this study, three different TASK-3-specific antibodies, developed by Pocsai et al, were employed to assess TASK-3 expression of metastatic human (HT199 and HT168-M1) and benign melanoma (WM35) cells both in tissue sections and in cell cultures using immunocytochemistry. In tissue preparations the presence and distribution of the channel was distinct and strong in most melanocytes. In cultured melanocytes, all preparations showed distinctly strong TASK-3-immunopositivity in the peri-nuclear region along with a sub-cellular distribution and a low intensity plasma membrane labelling.

Two years later, Rusznak et al, used the former indication pointing out that TASK-3 expression was mostly present intracellularly to perform a more in depth investigation of the channel's expression in organelles of malignantly transformed melanoma (WM35) cells, human keratinocytes (HaCaT) and TASK-3 negative murine skeletal myoblast (C2C12) cells (Rusznak, Bakondi et al. 2008). Data demonstrated that endogenous TASK-3 co-localised with a mitochondrion specific fluorescent dye in melanoma cells as well as healthy keratinocytes. Finally, to exclude a potential cross-reaction arising from non-specific binding of the antibody used with mitochondrial proteins, C2C12 cells were transiently transfected with a TASK-3 protein encoding plasmid and immunocytochemistry results confirmed the aforementioned co-localisation (Rusznak, Bakondi et al. 2008).

2.12.1.3 TASK-3 mitochondrial expression and electrophysiological properties

Two different types of potassium channels were identified in the inner mitochondrial membrane of rat embryonic hippocampus in symmetrical 150/150 mM KCl solution (Kajma and Szewczyk 2012). The first channel was similar to the large-conductance calcium-activated potassium channel (BK_{Ca}) expressed on the cell membrane and the second channel displayed voltage-dependent characteristics. At positive holding potentials (between +20 mV and +80 mV) an outwardly rectifying channel with a single-channel conductance of 67.84 pS was observed whereas at negative potentials (between − 80 mV and − 20 mV) its

conductivity reached 11 pS. Moreover, changing the pH of the bath solution from 7.2 to 6.2 resulted in complete blockade of the channel which was not reversible.

Another recent electrophysiological study of the properties of TASK-3 was described in mitoplasts of human keratinocyte cells in symmetrical solution (150/150 mM KCl) (Toczylowska-Maminska, Olszewska et al. 2014). Single-channel current traces were recorded at positive voltages (+90mV) with a conductance of 83.3±1 pS and 11.9±0.2 pS at negative (-90mV) voltages. As TASK channels were known to be blocked by local anaesthetics such as lidocaine and acidic pH, Toczylowska-Maminska et al, studied the channel activity in 1mM lidocaine and a recording solution of pH 6.2 similarly to Kajma and Szewczyk et al. Results showed that there was no channel activity supporting the identity of TASK-3.

2.12.2 Inner mitochondrial membrane Ca^{2+} channels

Mitochondrial Ca^{2+} conductance plays a central role in cellular physiology and pathophysiology and Ca^{2+} influx from the cytosol is depend on $\Delta\Psi_m$ and ATP synthesis (Jouaville, Pinton et al. 1999, Territo, Mootha et al. 2000). Calcium uptake can also regulate the mitochondrial motility and morphology (Yi, Weaver et al. 2004), and may trigger cell death during stress conditions (Hajnoczky, Csordas et al. 2006). Under normal circumstances, intra-mitochondrial Ca^{2+} uptake provides a supply for the reduction of the Krebs cycle reducing equivalents (dehydrogenases) (Hansford, Hogue et al. 1990) to drive respiratory chain activity and ATP synthesis (activation of the ATP synthase). Thus, the ATP demand to fuel energy-requiring processes in the cytosol such as ion pumping, contraction or exocytosis is fulfilled (Balaban 2009, Tarasov, Griffiths et al. 2012). Mitochondrial Ca^{2+} is also a key regulator for the generation of reactive oxygen species (ROS) which intimately link to physiological redox signalling pathways (Feissner, Skalska et al. 2009). Moreover, $[Ca^{2+}]$ within the mitochondrial matrix is regulated by a variety of Ca^{2+} efflux mechanisms including the mitochondrial Na^+/Ca^{2+} and H^+/Ca^{2+} exchangers, but neither of which have yet been characterised by conventional patch-clamping (Bernardi 1999). Depending on the concentration of Na^+, H^+ and Ca^{2+} across the mitochondrial inner membrane these exchangers contribute to either Ca^{2+} uptake or release. In this section, mitochondrial Ca^{2+} channels expressed on the IMM regulating Ca^{2+} uptake will briefly be presented. This will provide an understanding of the Ca^{2+} overload mechanism usually occurring during increased heart workload or β-adrenergic receptors stimulation (in myocardium) and how Ca^{2+} -activated K^+ channels (mitoKCa) liaise during such pathological condition.

During Ca^{2+} overload i.e when cytoplasmic concentrations are greater than ~200 nM and up to ≥ 1 μM, a progressive increase in mitochondrial Ca^{2+} uptake (from 0.1 to 10 μM or more)

is induced by the mitochondrial Ca^{2+} uniporter (MCU), voltage-dependent Ca^{2+} channels, the rapid mode of mitochondrial Ca^{2+} uptake (RAM) and the mitochondrial ryanodine receptor (mRyR) (Sparagna, Gunter et al. 1995, Kirichok, Krapivinsky et al. 2004, Altschafl, Beutner et al. 2007, Michels, Khan et al. 2009). Significant matrix Ca^{2+} influx also occurs during opening of the mitochondrial permeability transition pore (mPTP) which occurs after the interaction of cyP-D with large quantities of Ca^{2+} ions (Basso, Fante et al. 2005). Under such pathological conditions, mitochondrial Ca^{2+} overload is linked to several cascade pathways that contribute to excessive generation of ROS and initiation of cell death (Brookes, Yoon et al. 2004, Hajnoczky, Csordas et al. 2006, Feissner, Skalska et al. 2009).

Mitochondrial Ca^{2+} uniporter (MCU)

The channel activity of MCU was investigated by patching mitoplasts isolated from COS-7 cells at the single-channel configuration demonstrating that the channel had a highly selective mitochondrial Ca^{2+} conductance ranging from 2.6 to 5.2 pS at -160 mV driven by the negative mitochondrial matrix potential (Kirichok, Krapivinsky et al. 2004). Kirichok et al., also showed that MCU conductance saturated at high [Ca^{2+}] (millimolar range) and was largely open when $\Delta\Psi_m$ reached −200 mV but was generally closed when $\Delta\Psi_m$ was less negative (−80mV). MCU is inhibited by 200nM ruthenium red (IC_{50}, 100nM) or ruthenium 360 (IC_{50}, 5 nM) (Kirichok, Krapivinsky et al. 2004) as well as external EGTA, Mg^{2+} (IC_{50}, 50μM) or by external ATP ($IC_{50,}$ 0.6 mM) (Litsky and Pfeiffer 1997).

Rapid mode of mitochondrial Ca^{2+} uptake (RAM)

A rapid mode of Ca^{2+} uptake with kinetics hundreds of times faster (millisecond time scale) than the classical MCU activity has been reported in isolated liver, heart, and brain mitochondria (Hoppe 2010). Interestingly, unlike MCU, Ca^{2+} uptake is inhibited by increasing the extra-mitochondrial [Ca^{2+}] (Sparagna, Gunter et al. 1995, Buntinas, Gunter et al. 2001, Hoppe 2010). Hence, to observe RaM activity the basal extra-mitochondrial Ca^{2+} levels had to drop below ~100 nM for a period of time in order to permit removal of Ca^{2+} from a high-affinity external binding site on the channel (Sparagna, Gunter et al. 1995). Moreover, RAM was shown to be inhibited by ruthenium red but variations on its blocking effect were observed between samples and concentrations tested. In fact, ruthenium red was suggested to activate Ca^{2+} uptake at lower nM concentrations and inhibit it at higher concentrations indicating that there may be two ruthenium red binding sites involved. One with a highest affinity site that would lead to activation of Ca^{2+} uptake while binding of ruthenium red to the lowest site would inhibit the channel (Sparagna, Gunter et al. 1995).

Mitochondrial ryanodine receptor

Presence of a mitochondrial RyR was controversial within the literature as immunoreactivity for RyRs around perinuclear mitochondria could be detected but there was no evidence supporting the localisation of the channel in the IMM (Beutner, Sharma et al. 2001). A couple of years later, research demonstrated that in isolated rat heart mitochondria gold-labelled antibodies against RyRs predominantly detected the channel in the cristae of the IMM by electron microscopy (Salnikov, Lukyanenko et al. 2009). Peak single channel conductance of mRyR channel activity was ~225 pS using symmetrical 150 mM caesium (Cs^+) solution and up to 660pS in 300mM symmetrical Cs^+ between -30 and +20mV (Altschafl, Beutner et al. 2007). Moreover, RyR was inhibited by low concentrations of ruthenium red (IC_{100} 1–5µM) and Mg^{2+} (IC_{50} ~0.33mM) alike MCU (Beutner, Sharma et al. 2001). The channel appeared to allow rapid sequestration of Ca^{2+} at relatively low concentrations and thus, could account for a physiological Ca^{2+} uptake in heart cells. It has also been suggested that as the ryanodine-sensitive pathway becomes inhibited, MCU might take over and stimulate Ca^{2+} uptake during pathological and higher external [Ca^{2+}] (Beutner, Sharma et al. 2005).

Voltage-dependent mitochondrial Ca^{2+} channels mCa1 and mCa2

mCa1 and mCa2 were detected in mitoplasts from failing human myocytes associated with deep changes of intracellular Ca^{2+} homeostasis (Bers 2008). Voltage steps to -100 mV elicited Ca^{2+} currents with a conductance of 13.7 pS which was referred to the mitochondrial Ca^{2+} channel type 1 (mCa1) and a lower conductance of 7.7pS for mCa2 (Michels, Khan et al. 2009). Equally to MCU, mCa1 was partially inhibited by 200 nM ruthenium 360 whereas mCa2 was sensitive to higher ruthenium 360 concentrations (10 µM) (Yi, Weaver et al. 2004).

2.12.2.1 Calcium-activated mitochondrial potassium channels (mitoKCas)

mitoBKCa

The big conductance potassium channel (mitoBKCa) and the intermediate conductance channel (mitoIKCa) are two types of calcium-activated K^+ channels that have been described in various cell types. MitoBKCa was identified in mitochondria of a glioma cell line, in ventricular cells, rat skeletal muscle and brain adopting Western blot, electron microscopy and immunofluorescence microscopy approaches (Skalska, Bednarczyk et al. 2009). The channel displayed a conductance of 100-300 pS in the range of +/-60 mV in symmetrical 150mM KCl solutions which was observed by direct patch clamping of mitoplasts isolated from mammalian cells (Siemen, Loupatatzis et al. 1999, Xu, Liu et al. 2002) or during planar lipid bilayer experiments (Skalska, Piwonska et al. 2008). The channel was shown to be activated by micromolar concentrations of Ca^{2+}, the drugs NS1619, NS11021 (Bentzen, Osadchii et al. 2009, Aon, Cortassa et al. 2010) or, 12,14-dichlorodehydroabietic acid (diCl-

DHAA) (Samavati, Monick et al. 2002) and was blocked by specific inhibitors such as Charybdotoxin (ChTx) (EC_{100}, 200nM) (Skalska, Bednarczyk et al. 2009), iberiotoxin ($EC_{100,}$ 50nM) (Cheng, Gu et al. 2008, Cheng, Gulbins et al. 2011) and paxilline (EC100 5μM) (Heinen, Aldakkak et al. 2007).

mitoIKCa

MitoIKCa was characterised by patch clamping mitoplasts isolated from human colon carcinoma cells (De Marchi, Sassi et al. 2009) of human cervix adenocarcinoma cells (HeLa) and mouse embryonic fibroblasts displaying a conductance of 10-90 pS, being voltage-insensitive and responding to [Ca^{2+}] in the sub-μM range (Sassi, De Marchi et al. 2010). Interestingly, molecular weights, biophysical and pharmacological properties of mitoIKCa and IKCa (expressed on the plasma membrane) were found to be indistinguishable (Sassi, De Marchi et al. 2010). The channel was selectively inhibited by clotrimazole, iberiotoxin, apamin and TRAM-34 (Szabo, Leanza et al. 2012). In a recent study, IKCa as well as the voltage dependent Kv1.3 channel expressed on the plasma membrane, were shown to be both inhibited by 100 nM ChTx, similarly to mitoBKCa indicating that their corresponding mitochondrial channels could also be sensitive to this blocker (Guéguinou, Chantôme et al. 2014).

2.12.3 Mitochondrial anion channels

IMAC

The mitochondrial inner membrane is also home to anion-selective ion channels with anionic conductances ranging from 5 pS to 1 nS including the ~107 pS. The first anion channel identified in brown adipose tissues of mice mitoplasts by patch-clamp studies performed in symmetrical 150 mM KCl solutions was a ~107 pS channel that was also referred to as the centum picosiemen channel (Sorgato, Keller et al. 1987). This channel had a minor anion selectivity (P_{Cl^-}/P_{K^+} = 4.5), a strong voltage sensitivity (being open between -30mV and +80mV), sensitive to ATP (2mM) with 62% inhibition at 0mV and 38% at +30mV, nifedipine, the amphiphilic amine propranolol at micromolar ranges or reduced matrix pH (pH< 7.2) (Borecky, Jezek et al. 1997, Kominkova, Malekova et al. 2010). Although the ~107pS channel has been tentatively identified as the inner membrane anion channel (IMAC) in brown-fat mitoplasts in symmetrical 150mM KCl solution (Borecky, Jezek et al. 1997); this possibility was not definitive as other candidates (e.g., the 15-pS channel) have also been proposed. IMAC was shown to be permeable to a variety of inorganic (e.g., $SCN^- > NO_3^- > Cl^- > P_i$) and organic (e.g., oxaloacetate > citrate > malate> ATP) anions (Beavis 1992, Powers, Smith et al. 1994). It was also shown to be inhibited by protons and Mg^{2+} and by cationic amphiphiles including amiodarone (IC_{50} ~ 1 μM), amitriptyline (IC_{50} ~ 10 μM),

dibucaine (IC_{50} ~ 20 µM), propranolol (IC_{50} ~ 25 µM) (Beavis 1992). The identity of IMAC has nevertheless some discrepancies as some studies demonstrate that IMAC is permeable to ATP (Powers, Smith et al. 1994) in contrast to others, supporting that the channel is inhibited by ATP (Ballarin and Sorgato 1995, Kominkova, Malekova et al. 2010, Tomaskova and Ondrias 2010).

UCP

The uncoupling protein (UCP) is another mitochondrial anion channel isolated from rat heart mitochondria that exhibits 150 or 75 pS conductance in symmetrical 100 mM KCl solution indicating that it is either a dimer of two monomeric channels or a monomeric channel with a 50% sub-conductance state (Tomaskova, Gaburjakova et al. 2007). UCP was shown to be voltage sensitive (open between -80mV and +40mV) and strongly discriminating against cations (PCl^- /PK^+ ~17). UCP is inhibited by transport inhibitors GTP or GDP (IC_{50} 50µM), ATP and ADP (EC_{100} 800µM) in a reversible way whereas pH changes and divalent cations (Mg^{2+} and Ca^{2+}) from the matrix side did not influence its channel activity (Huang and Klingenberg 1996).

mtCLIC

Another intracellular chloride channel was later identified known as either mtCLIC or CLIC4 which was localised in the IMM of differentiating mouse keratinocytes but little is known to date about its biological function and pharmacological character (Fernandez-Salas, Sagar et al. 1999). Isolated mtCLIC was shown to have two distinct conductances of 31 pS and 57 pS in symmetrical solution (140 mM KCl) when lipid bilayers were patched between -80 and +80mV (Littler, Assaad et al. 2005). It was suggested that increases in *CLIC4* gene expression could be linked to differentiation of keratinocytes (Fernandez-Salas, Sagar et al. 1999), adipocytes (Kitamura, Nishizuka et al. 2001) as well as fibroblasts into myofibroblasts (Ronnov-Jessen, Villadsen et al. 2002). One of the most interesting functions of mtCLIC is its involvement in apoptosis (Fernandez-Salas, Sagar et al. 1999, Fernandez-Salas, Suh et al. 2002). Upregulation of p53 was demonstrated to involve increases in both mtCLIC mRNA and mtCLIC protein expression (Fernandez-Salas, Sagar et al. 1999, Fernandez-Salas, Suh et al. 2002). During this scenario, mtCLIC appeared to be a direct transcriptional target for p53, as Fernández-Salas, Suh et al., have identified several functional p53-binding consensus elements in the mtCLIC promoter sequences. Over-expression of mtCLIC during transient transfection was shown to reduce mitochondrial membrane potential, release cytochrome *c* into the cytoplasm, activate caspases and induce apoptosis in mouse keratinocytes (Fernández-Salas, Suh et al. 2002). In addition, a role for mtCLIC in

mitochondrial electron transport, i.e., interaction with proton complexes to regulate pH and mitochondrial function was suggested (Fernández-Salas, Suh et al. 2002).

2.13 Biosynthetic and post-golgi targeting of mitochondrial proteins

During co-localisation analyses performed by Roncoroni et al., TASK-5 was found to co-localise with lamin AC, a nuclear membrane protein involved in nuclear stability and gene expression (Roncoroni 2012). Based on this evidence, the TASK-5 gene is suggested to be translated within the cell nucleus, transcribed into a protein in the ER which however never reaches the plasma membrane due the inability of the channel to proceed beyond the ER in the secretory pathway of the Golgi apparatus.

Trafficking to the cell membrane was shown to involve both post transcriptional modifications (PTM) such as glycosylation or phosphorylation and binding with auxiliary proteins within the TASK channel family. Once correctly folded and assembled, membrane proteins bind the coatomer protein complex 2 (COP-II), which is involved in their transport from the ER to the Golgi complex (Orci, Schekman et al. 1996). Both TASK-1 and TASK-3 possess forward trafficking motifs which enable the interaction with COP-II and the anterograde transport of the channels to the Golgi complex (Nishimura, Bannykh et al. 1999, Nufer, Guldbrandsen et al. 2002, Zuzarte, Rinne et al. 2007, Ma, Zhang et al. 2011, Ma, Zhang et al. 2011). As for all K_2P channels, TASK-1 and TASK-3 possess either N- or C-terminal interaction sequences for the coatomer protein complex 1 (COP-I) subunit β (β-COP). Interaction with β-COP is responsible for the retrograde transport of the channels from the Golgi complex to the ER and for the channels retention within the ER (O'Kelly, Butler et al. 2002, Zuzarte, Heusser et al. 2009). To date, this mechanism has been demonstrated for both TASK-1 and TASK-3 and for the TREK channel $K_{2P}2.1$ (Kim, Bang et al. 2000, O'Kelly, Butler et al. 2002). This retrograde transport to the ER mediated by β-COP interaction is however, impaired by the competitive binding of the channel with the cytosolic adaptor protein 14-3-3 (O'Kelly, Butler et al. 2002, O'Kelly and Goldstein 2008, Arakel and Schwappach 2018).14-3-3 has been shown to bind to the last three amino acids (aa) of both TASK-1 and TASK-3 C-termini in a phosphorylation dependent manner and enable the channels to escape β-COP-dependent retrograde transport from the Golgi complex to ER (O'Kelly, Butler et al. 2002). Following phosphorylation of S393 in TASK-1 and S372 in TASK-3 the adaptor protein 14-3-3 is recruited to the C-terminal motifs RRSSPV and RRKSPV in TASK-1 and TASK-3 respectively (O'Kelly, Butler et al. 2002). A similar motif was shown to be present in TASK-5 sequence where the possibility of binding with 14-3-3 has been shown for TASK-5 C-terminus through two-hybrid techniques (Rajan, Preisig-Muller et al. 2002). Therefore, exclusion of TASK-5 from the cell surface and impairment in exchanging K^+ ions across the cell membrane in transiently expressed recombinant systems could be related to a potential

binding to β-COP (Ashmole, Goodwin et al. 2001, Karschin, Wischmeyer et al. 2001, Kim and Gnatenco 2001).

Co-localisation analyses also indicated that TASK-5 has a putative mitochondrial expression with cytochrome bc1. How proteins are trafficked through the confines of the cell and integrated into the appropriate intracellular compartment revealed elaborate cellular protein translocation and sorting systems to fulfill their specific functions. More specifically, sophisticated molecular machines serve to recognise incoming precursor proteins and integrate them into the functional framework of mitochondria (Stojanovski, Bohnert et al. 2012). Mitochondria contain their own genetic material and machineries to manufacture their own RNAs and proteins. However, the small circular mitochondrial genome encodes only a few proteins. All remaining mitochondrial proteins (approximately 99%) are encoded by the nuclear genome and synthesised on cytosolic ribosomes in their precursor forms (Stojanovski, Bohnert et al. 2012). To acquire their mature, functional state these precursor proteins need to be efficiently targeted and imported into mitochondria and sorted to the correct sub-mitochondrial compartment. During the last few years, the presence of at least six distinct translocation and assembly machineries within mitochondria were identified (Sickmann, Reinders et al. 2003, Reinders, Zahedi et al. 2006, Pagliarini, Calvo et al. 2008)**.** TOM, mitochondrial import 1 (Mim1) and the sorting and assembly machinery (SAM) on the OMM or TIM in cooperation with the pre-sequence translocase-associated import motor (PAM) in the IMM are complexes which sort precursor proteins to the organelle in a translocation-competent state (Wiedemann, Frazier et al. 2004, Waizenegger, Schmitt et al. 2005, Stojanovski, Bohnert et al. 2012, Dudek, Rehling et al. 2013). Precursor proteins must be kept in an unfolded or loosely folded conformation to allow their passage through the tightly gated membrane pores. This is achieved by the binding of cytosolic factors to nascent precursors that stabilise them in a translocation-competent form and guide them to dedicated receptors on the mitochondrial surface. The best characterised machineries that escort mitochondrial precursor proteins through the cytosol are the Hsp90/p23 and Hsc70/Hsp40 chaperone systems (Young, Hoogenraad et al. 2003, Zara, Ferramosca et al. 2009) and cytosolic proteins such as the arylhydrocarbon receptor-interacting protein (AIP) (Yano, Terada et al. 2003).

Additionally, approximately one-half of mRNAs coding for mitochondrial proteins were reported to be localised to the mitochondrial surface (Marc, Margeot et al. 2002, Garcia, Darzacq et al. 2007). The Pumilio-Fem-3 binding factor (PUF) proteins are defined by the presence of a Pumilio (PUM-HD) domain. This domain is crucial for PUF protein function and has the capacity to bind to the 3′ untranslated region (UTR) of mRNAs, regulate transcript localisation, translation and be involved in the targeting of mRNAs to mitochondria

(Zamore, Williamson et al. 1997, Wickens, Bernstein et al. 2002) (Garcia-Rodriguez, Gay et al. 2007, Saint-Georges, Garcia et al. 2008). PUF also localises to mitochondria where it regulates not only mitochondrial biogenesis but also mitochondrial motility during inheritance (Garcia-Rodriguez, Gay et al. 2007).

Based on this information, it is hypothesised that TASK-5 mRNA/proteins undergo a series of post transcriptional modifications in order to ensure selective targeting in the IMM. To date, it remains elusive why TASK-5 proteins previously synthesised in the ER were not detected in the Golgi apparatus by immunocytochemistry as there is evidence of protein trafficking within mitochondria from the Golgi complex but also, the presence of an N-glycosylation site on TASK-5 channel. A possible explanation would be a rapid import machinery from Golgi to the organelles in response to metabolic changes and/or cellular stimuli occurring during TASK-5 over-expression and thus, inability to estimate their co-localisation during a limited window of time.

2.14 Cyto-protective or pro-apoptotic role of mitochondrial channels

As previously mentioned, mitochondrial channels expressed on the OMM and IMM are key regulators of cell survival and death by protecting cells from death in neurodegenerative diseases, ischemia/reperfusion injury in heart; or enhancing cell death (Ryu, Peixoto et al. 2010).

There are at least two mitochondrial channels involved in controlling cell death on the OMM such as MAC and mPTP (Crompton 1999, Kinnally and Antonsson 2007). MAC is the cytochrome *c* release channel formed by the pro-apoptotic Bcl-2 family proteins Bax and/or Bak post apoptotic stimulations or DNA damage. Release of cytochrome *c* into the cytosol initiates an apoptotic signalling cascade by forming apoptosomes which finally activate the executioners such as caspases and proteases (Ryu, Peixoto et al. 2010). Mitochondrial matrix Ca^{2+} overload and oxidative stress (ROS generation) induce a complete loss of $\Delta\psi_m$ due to the opening of mPTP which results in metabolic imbalance, cell swelling and plasma membrane damage (Halestrap 2009, Lemasters, Theruvath et al. 2009).

On the other hand, two types of K^+ channels expressed in the mitochondrial inner membrane revealed to be protective against ischemia- or reperfusion-induced injury in cardiac cells as well as apoptosis and mPTP activation (Akao, Ohler et al. 2001, Hausenloy, Yellon et al. 2004, Juhaszova, Zorov et al. 2004). These were mitoK_{ATP} and mitoK_{Ca} present in the IMM (Inoue, Nagase et al. 1991, Xu, Liu et al. 2002).

Although the exact regulatory pathway by which mitoK_{ATP} is activated and its molecular structure are still vague, its role in myocardial protection after ischemic or pharmacological preconditioning was demonstrated in several studies (Garlid, Paucek et al. 1997, Fryer, Hsu

et al. 1999). It has been proposed that during ischemic preconditioning (IPC) the translocation of protein kinase C (PKC) isoforms from the cytosol to the IMM in mitochondria is triggered (Wang, Hirai et al. 1999, Wang, Takashi et al. 2001). The translocated PKC has been proposed to regulate mitoK_{ATP} channel through the C-terminus where blockade of PKC transfer prevented IPC in both animals and humans (Speechly-Dick, Grover et al. 1995). Activation of the mitoK_{ATP} channel by phorbol 12-myristate 13-acetate (PMA), a PKC activator, was found to protect the integrity of isolated mitochondria by preventing the opening of mPTP and cytochrome *c* release and thus, prevent ischemia (Korge, Honda et al. 2002). However, this hypothesis needs to be further extended as it has also been reported that mitoK_{ATP} was involved in cancer cell apoptosis. An example is the treatment of leukaemic cells with the channel activator diazoxide which antagonised the division of these cells by causing mitochondrial membrane depolarisation promoting cell death (Holmuhamedov, Lewis et al. 2002). In this case, mitoK_{ATP} could be used as a new possible target for anticancer therapy (Pathania, Millard et al. 2009).

MitoBK_{Ca} and MitoIK_{Ca} have been proposed to be activated under pathophysiological conditions which increase mitochondrial Ca^{2+} uptake preventing excessive mitochondrial Ca^{2+} accumulation. Opening of mitoBK_{Ca} as for mitoK_{ATP} was reported to protect against damage of the heart and other organs caused by ischaemia and reperfusion. Mitochondrial BK_{Ca} channels are also activated by hypoxia (Cheng, Gu et al. 2008) and seem to protect cardiomyocytes isolated from chronically oxygen deprived rats (Borchert, Yang et al. 2011). The protective effect of BK_{Ca} openers has been attributed to increased matrix K^+ uptake and volume regulation improved respiratory control (Aon, Cortassa et al. 2010), inhibition of mitochondrial Ca^{2+} overload (Wang, Yin et al. 2004, Kang, Park et al. 2007) and prevention of mPTP opening (Cheng, Gu et al. 2008). The effect of BK_{Ca} modulators on death or survival is still not well-defined but BK_{Ca} channel inhibition by pro-apoptotic Bax molecules might contribute to the opening of mPTP occurring during cell death (Cheng, Gulbins et al. 2011).

In addition to these two K^+ channels, Kv1.3 was found to be a crucial factor for T-cell proliferation and volume regulation in mitochondria (Chandy, Wulff et al. 2004) indicating that inhibition of the channel in these particular cells could potentially suppress the effector memory T-cell proliferation making these blockers a promising tool for the therapy of autoimmune diseases (Beeton, Wulff et al. 2001). The channel had a fundamental role in apoptosis regulation as mitoKv1.3 inhibition by either Bax protein or toxins such as MgTx was required for induction of apoptosis, at least in lymphocytes (Szabo, Bock et al. 2008).

This resulted in $\Delta\Psi_m$ depolarisation and ROS release, which are upstream of both cytochrome *c* release and mPTP activation.

Lastly, although the physiological roles of TASK-3 are still under investigation, evidence indicates that ischemic preconditioning (short episodes of ischemia that increase tissue tolerance to a lethal insult) can be mimicked by the administration of openers of these mitochondrial K^+ channels (Busija, Gaspar et al. 2008, Gaspar, Snipes et al. 2008, Watanabe, Katsura et al. 2008). It has been suggested that the transport of K^+ ions into mitochondria causes changes in the volume of the mitochondrial matrix, the mitochondrial membrane potential, the rate of generation of reactive oxygen species and Ca^{2+} influx (Dębska, May et al. 2001, Dos Santos, Kowaltowski et al. 2002, Sato, Saito et al. 2005, Bednarczyk, Barker et al. 2008) to protect the cells from death (Szewczyk, Jarmuszkiewicz et al. 2009, Szewczyk, Kajma et al. 2010).

Chapter 3

Materials and Methods

3.1 Molecular biology

3.1.1 TASK-5 DNA construct

TASK-5-eGFP construct possessing a C-terminal eGFP tag was expressed in pEGFP-N1 vector and kindly donated by Dr. Ian Ashmole (University of Leicester, United Kingdom) (Appendix 1).

3.1.2 Bacteria cultures

Bacteria cultures were used for DNA preparation (Method 3.1.3).

Cultures were initiated from bacteria frozen at -80°C in Luria Bertani (LB) broth (10 g/l bactotriptone, 10 g/l NaCl, 5 g/l yeast extract) containing 20% glycerol (glycerol stock) and the appropriate selective antibiotic (50 µg/ml kanamycin). To perform midi or maxiprep purifications (Methods 3.1.3), frozen bacteria cultures (10µl) were initially diluted in 5ml LB containing 5µl of the appropriate selective antibiotic and grown for at least 3 hours. Once the media was cloudy haze, this was further diluted either in 100ml or 500ml of LB with the appropriate antibiotic overnight (o/n). Unless otherwise stated, bacteria growth was performed at 37°C. Samples of bacteria cultures were stored at -80°C in LB broth containing 20% glycerol and all cultures were handled in sterile conditions.

3.1.3 DNA preparation

DNA required to transiently transfect (Method 3.2.2) cells was prepared through midi or maxiprep purifications.

To perform midi or maxiprep purifications a QIAGEN purification kit was employed. Bacteria culture was centrifuged at 4 000 g, at 4°C for 30 minutes and the resultant pellet was re-suspended in 10 ml of cell re-suspension buffer (50 mM TrisHCl pH 8.0, 10 mM EDTA, 100 µg/ml RNaseA). Bacteria were then lysed by adding 10 ml of cell lysis buffer (200 mM NaOH, 1% SDS) and the lysate was incubated 5 minutes at room temperature (RT). To neutralise the lysis buffer and to precipitate bacterial proteins and genomic DNA, 4 ml of ice cold 3.0 M potassium acetate was added. The solution was incubated on ice for 20 minutes, after which it was centrifuged at 20 000 g, 4°C for 30 minutes. The supernatant was centrifuged again at 12 000 g, 4°C for 15 minutes. The resulting supernatant was added to a filter column already equilibrated with 10 ml of column equilibration buffer (750 mM NaCl, 50 mM MOPS pH 7.0, 15% isopropanol and 0.15% Triton X-100). The solution was let flow to allow binding between the DNA and the column. To wash the DNA, 10 ml of wash buffer (1 M NaCl, 50 mM MOPS pH 7.0, 15% isopropanol) was added to the column and the buffer was let flow through it twice. The DNA was eluted in 5 ml pre-warmed (at 65°C) elution buffer (1.25 M NaCl, 50 mM TrisHCl pH 8.5, 15% isopropanol), precipitated by adding 0.7

volumes isopropanol and immediately centrifuged at 20 000 g, 4°C for 30 minutes. The resultant pellet was washed in 2 ml of 70% ethanol and centrifuged at 20 000 g, 4°C for 10 minutes. The DNA pellet was finally re-suspended in 20-30 µl of de-ionised water.

3.1.4 DNA quantification

DNA obtained from minipreps and maxipreps (Methods 3.1.3) was quantified through spectrophotometry on a Nanodrop 2000. Blank and sample concentrations were estimated by their light absorption at 260 nm λ (OD_{260}). DNA quality and purity was assessed by comparing the light absorption values of the sample at 230 nm (OD_{230}) compared to OD_{260} and at 280 nm (OD_{280}) compared to OD_{260}. Ratio OD_{260}/OD_{230} greater than 1.5 indicated negligible DNA contamination by organic compounds or guanidium salt (present in DNA purification columns); ratio OD_{260}/OD_{280} greater than 1.8 was index of protein-free samples.

3.1.5 DNA sequencing

Plasmid DNA was supplied to Geneservice - Source BioScience plc at the concentration of 100 ng/µl diluted in water; sequencing primers were supplied at the concentration of 3.2 pmol/µl.

3.2 Tissue culture

3.2.1 Cell cultures

Cell cultures were used for cell transient transfection, binding assays from cells' lysates, Western blot analysis, Mitotracker red staining, mitochondrial isolations, immunocytochemistry and planar patch-clamping.

Cultures were initiated from cells frozen in liquid nitrogen in freezing media (90% fetal bovine serum (FBS), 10% DMSO). COS-7 cells were maintained in standard growing conditions of 20% O_2 and 5% CO_2 at 37°C and cultured on 25 cm^2, 75cm^2 flasks or 6 wells plates in standard culture medium composed by Dulbecco's Modified Eagle Medium (DMEM) (Invitrogen) with 10% Fetal Bovine Serum (FBS), 50u/ml Penicillin (Invitrogen) and 100 µg/ml Streptomycin (Invitrogen). HeLa cells were cultured in RPMI with identical serum and antibiotics conditions as previously described. Every 2/3 days cultures were split by Trypsin (Invitrogen) treatment in order to not exceed 70-80% confluence. Antibiotics were omitted during transfection. All cell cultures were handled in sterile conditions.

3.2.2 Transient transfection

COS-7 and HeLa cells were transiently transfected prior to binding assays, Western blot analysis, immunocytochemistry, mitochondrial staining and isolation, flow cytometry and planar patch-clamping. Transfections were performed on cells plated in 6 well plates or T25-75cm^2 flasks.

During immunocytochemistry experiments, 2 x 10^5 cells were seeded on glass coverslips in 6 well plates 12h pre-transfection. For both COS-7 and HeLa transfection, 5µg DNA was diluted in 50µl of 150mM NaCl; in another tube, 10µl jetPEI (Polyplus transfection) was diluted in 250µl of 150mM NaCl and both tubes were vortexed during 10 seconds.

Diluted JetPEI reagent was added to the DNA-NaCl solution, vortexed for 15 seconds and incubated for 15-30 minutes at RT. JetPEI-DNA solution was then added dropwise on the adherent cells which were let to incubate at 37°C, 20% O_2 and 5% CO_2 during 4h in media containing only FBS. Four hours post-transfection, media was replaced with media containing FBS and antibiotics. COS-7 cells were used for experiments 24h post-transfection while HeLa were over-expressing the GFP-tagged channel only 48h post-transfection.

3.3 Protein detection

3.3.1 Protein immunoprecipitation

Transfected COS-7 cells suspended in lysis buffer (Table 3.1) and homogenised for 10-15 minutes with a pestle and mortar. The cell lysate was centrifuged at 1 000g for 5 minutes at 4°C and supernatant was re-suspended in 200-400µl lysis buffer. Supernantant was then incubated with 40µl GFP-trap beads (GFP-Trap_A, Chromotek) and uniformly rotated for either 1 h at RT or overnight at 4°C. Once the rotation was over, the sample was centrifuged, the supernatant containing unspecific proteins was discarded and beads were washed three times with wash buffer (Table 3.1) so that the rest of unspecific proteins that did not bind to beads were also discarded. As the eGFP tag of the channel was bound to agarose beads, the release of the former was completed with 40µl 4X SDS sample buffer for Western blot experiments.

3.3.2 Protein electrophoresis

Protein electrophoresis was performed to study the GFP-trap beads based purification efficiency, verify TASK-5 protein transient expression levels and targeting capacitance of the custom antibody against TASK-5 proteins.

Protein samples were suspended in 4x loading buffer (8% SDS, 250 mM TrisHCl pH 6.8, 35% glycerol, bromophenol blue, 50 mM DTT) incubated at 95°C for 5 minutes and centrifuged at 12 000 g for 1 minute.

Polyacrylamide gels were prepared by polymerising a short 4 % polyacrylamide layer on top of a main 12% polyacrylamide layer. Preparation of 4 % polyacrylamide (3.84% acrylamide (Biorad), 0.16% bis-acrylamide (Biorad), 125 mM TrisHCl pH 6.8, 0.1 SDS, 0.1% tetramethylethylenediamine (TEMED), 0.05% ammonium persulfate (APS)) and 12 %

polyacrylamide (11.68% acrylamide, 0.32% bis-acrylamide, 375 mM TrisHCl pH 8.8, 0.1% SDS, 0.05% TEMED, 0.05% APS) .

Samples were separated by SDS gel electrophoresis on 12 % polyacrylamide gels in running buffer (25 mM Tris, 192 mM glycine, 0.1% SDS) for 1 hour at 120mV and transferred to a hybond ECL nitrocellulose membrane (GE Health care Life Sciences) for 1h at 100mV. Proteins were then detected with a PIERCE enhanced chemiluminescent substrate (Life technologies) in dark conditions.

3.3.3 Antibodies

Antibodies were obtained from the following suppliers and used at the concentrations indicated: Abcam (Cambridge, UK); mouse anti-eGFP (ab1218, 0.5µg/ml), goat anti-rabbit FITC (ab97050, 1:1000), mouse anti-MTCO2 or COX II (ab110258, 1mg/ml), Vectashield with DAPI (H-1200),DAKO or Prolong Diamond anti-fade mountant with DAPI, secondary goat α-mouse-HRP (P0447,1:10000), goat α-rabbit-HRP (P0448, 1:2000), Life Technologies; goat anti-human K_{2P}9.1 (sc-11320, 200µg/ml),Santa Cruz ;Mitotracker Red CMXRos (M7512, 250nM); Vector Labs, secondary antibodies rabbit α-goat-Texas red (TI-5000, 1:150), goat α-rabbit-Texas red (TI-1000, 1:150), horse α-mouse-Texas red (TI-2000, 1:150); Covalab S.A.R.L. $_{h}K_{2P}$15.1-LR (1:50).

3.3.4 Immunocytochemistry

Immunocytochemistry was performed on cells seeded in 6 well plates to investigate either the endogenous expression of TASK-3 and TASK-5 channels in HeLa and COS-7 cells, detect non-cytotoxic Mitotracker red staining concentrations or study the co-localisation of TASK-5-eGFP with Mitotracker red and COX II.

Trypsinised cells with a 50-80% confluence were seeded and left to settle and grow for 2 hours on sterile coverslips. Media was aspirated and cells were washed 3 times with 1ml PBS. Cells were fixed in 1ml filtered 4% paraformaldehyde (PFA) in PBS for 7 min at RT. PFA was rinsed with 1 ml PBS and its auto-fluorescence was quenched by adding 1 ml 100mM Glycine (Fischer) diluted in PBS for 10 minutes at RT. Cells were then permeabilised by adding 1 ml 0.1% Triton X-100 (Sigma) in PBS for 7 minutes at RT. Triton X-100 was washed 3 times with 1 ml PBS. Incubation with 3% BSA in PBS for 1h at RT or a moisturised environment at 4ºC overnight was performed to minimise non-specific antibody binding. Primary antibody was then added to cells at a concentration shown in section 3.3.3. During the antibody incubation, Parafilm was placed on top of the antibody solution to avoid evaporation. For each well, antibody diluted in 100µl of 1% BSA, 0.1% Triton in PBS was used for a 1h incubation at RT. After antibody hybridisation, cells were washed in PBS 3 times. Cells were then incubated with a secondary antibody diluted in 0.1% Triton in PBS for

1h at RT protected from light. Cells were finally washed 3 times in PBS, mounted with Vectashield with DAPI and stored at 4ºC.

3.5 Flow cytometry

Flow cytometry experiments were performed on isolated mitochondria from either non- or transfected HeLa or COS-7 cells with the aim to sort organelles over-expressing TASK-5-eGFP.

Fluorescence-activated flow cytometry (FACS) was performed using a three-laser BD Biosciences FACS Aria I cell sorter. Using sterile PBS as sheath fluid (100µm diameter) at low pressure (20psi), mitochondrial analyses were performed after appropriate voltage settings of the forward angle light scatter (FSC) and side angle light scatter (SSC) detectors. Excitation of GFP-tagged and Mitotracker red-stained mitochondria was achieved using a 488nm (Blue, Coherrent Sapphire Solid state) laser. Bandpass filters within the range 530/30 (515 – 545nm) and 610/20 (600 – 620nm) were used to collect the respective fluorescence emissions. Discrimination of mitochondria from cellular debris and background/electronic noise was performed by appropriate gating on the FSC-A vs SSC-A scatter plots. Systematic confirmation of the validity of this gating was obtained by labelling transfected mitochondria with the mitochondrial dye MitoTracker red CMXRos. Briefly, transfected mitochondria were suspended in 500µl external mitochondrial recording solution (Table 3.4) and were analysed on the flow cytometer by the BD FACSDiva operating software v5.0.3 (BD Biosciences). In order to sort double fluorescent (GFP and Mitotracker red) mitochondria the purity mode setting was selected allowing to specifically collect mitochondria expressing the channel. An average of 1500-3000 events (i.e mitochondria) per second were collected into a 1.5ml sterile eppendorf tube containing external mitochondrial recording solution. Non-fluorescent mitochondria were collected into a different waste tube for disposal.

3.6 Manipulation of organelles

3.6.1 Mitochondrial isolation

Isolated mitochondria were used during flow cytometry or planar patch-clamp studies.

The standard mitochondrial isolation protocol was followed, as outlined in (Wieckowski, Giorgi et al. 2009) with several optimisations (Chapter 4, section 4.5). All experimental steps were performed at 4°C unless otherwise stated.

3.6.2 Mitoplasts

In order to study the electrophysiological characteristics of TASK-5 in the IMM, mitochondria were stripped of their OMM by osmotic shock resulting in the formation of mitoplasts.

This was achieved by incubating the mitochondrial pellet into a hypotonic solution (Table 3.2) for 20 minutes during which, a solute imbalance generated an osmotic pressure within mitochondrial matrix inducing the OMM to burst. In order to decant the broken outer membrane debris, the organelles were centrifuged for 10minutes at 10,000g at 4°C and re-suspended in a hypertonic solution (Table 3.2) to restore the isotonicity. A last centrifugation step was performed for 10minutes at 10,000g at 4°C where the pellet was suspended in external mitochondrial patching solution or fixed in fixative (Methods 3.8.4) to study the efficacy of the swelling procedure by transmitted electron microscopy (TEM).

3.7 Electrophysiology – Planar patch-clamping

3.7.1 Whole-cell recordings

Potassium currents elicited either from whole non- or transfected cells, mitochondria or mitoplasts were studied on a planar planar patch-clamp system (port-a-patch, Nanion Technologies GmbH, Germany) where samples were mounted on NPC-1 chips.

NPC-1 chips (Nanion Technologies GmbH, Germany) have a core structure made of planar borosilicate glass slide with a micron-sised patch aperture. During the experiments, two types of NPC-1 chips were used; 2-3.5 MOhm resistance for whole-cell recordings and 10-15 MOhm (highest chip resistance commercially available) for whole-mitochondrial or mitoplast recordings. Electrodes were made of silver (Ag) wires which were regularly coated with house hold thin bleach for minimum 30 minutes in order to form a thin chloride (AgCl) coat enabling current to pass.

Internal and external solutions (5µl) were placed in the inner and outer part of each NPC-1 chip in order to cover each side of the aperture. Air bubbles were removed by gently flicking the chip which was subsequently screwed on the chip holder. Once the Faraday cage (Appendix 2) was positioned over the chip holder, 100-200µl of external solution were applied on the top external side of the aperture. Whole-cell or organelle recordings were conducted according to Nanion's procedure and optimised where necessary. Detailed parameter settings allowing to reach the whole-cell/organelle configurations are summarised in Chapter 6 (sections 6.3-4). Seal enhancer solution was washed with a perfusion system connected via a tubing system to the Faraday cage. This system also enabled to exchange external recording solution with solutions containing mitochondrial channel blockers at a flow rate of 13µl/sec. To measure the inhibitory effect of selected blockers or altered pH on isolated organelles, current recordings were measured 10minutes post-application to ensure complete channel inhibition.

All experiments were performed at RT. Solutions used to record K^+ currents from cells were provided by Nanion where their composition is summarised in Table 3.3. Solutions for whole-mitochondria/mitoplasts recordings were prepared according to published studies and adjusted for an appropriate use on the port-a-patch (Table 3.4).

Unless otherwise stated, voltage steps of 1s duration each with a holding potential of -50 mV were applied between −100 to +80 mV (with 20mV increments). As the electrophysiological characterisation of TASK-3 channel in mitochondria was performed between -90 and +90mV (Toczyłowska-Mamińska, Olszewska et al. 2014), decision to perform experiments in similar voltage clamp steps was undertaken to compare acquired results with published data. Liquid junction potential was empirically measured and was close to 3mV. Leak currents were not subtracted during data analysis. Ion currents were low-pass filtered at 1 kHz and sampled at a frequency of 10 kHz. Series resistance (Rs) were not compensated as studying rapid ionic currents were not of interest and would be more difficult to distinguish small currents due to larger noise contamination.

Membrane potential (V_m) was calculated according to the GHK equation:

$$V_{\mathrm{m}} = \frac{RT}{F} \ln\left(\frac{p_{\mathrm{K}}[\mathrm{K}^+]_{\mathrm{o}} + p_{\mathrm{Na}}[\mathrm{Na}^+]_{\mathrm{o}} + p_{\mathrm{Cl}}[\mathrm{Cl}^-]_{\mathrm{i}}}{p_{\mathrm{K}}[\mathrm{K}^+]_{\mathrm{i}} + p_{\mathrm{Na}}[\mathrm{Na}^+]_{\mathrm{i}} + p_{\mathrm{Cl}}[\mathrm{Cl}^-]_{\mathrm{o}}} \right)$$

This equation was used to determine the resting membrane potential in cells, in which K^+ and Cl^- were the major contributors to the membrane potential. During the study, Na^+ ions were omitted from the recording solutions, therefore the corresponding relative permeability value was set to zero. *R* corresponds to the universal gas constant (8.314 $J.K^{-1}.mol^{-1}$). *T* to temperature in Kelvin (K = °C + 273.15). *F* is the Faraday's constant (96485 $C.mol^{-1}$). $p_{K, Na,Cl}$ is the membrane permeability for K^+,Na^+, Cl^-. Normally, permeability values are reported as relative permeabilities with p_K having the reference value of one (because in most cells at rest p_K is larger than p_{Na} and p_{Cl}). For a typical neuron at rest, $p_K : p_{Na} : p_{Cl} = 1 : 0.05 : 0.45$. $[K^+,Na^+, Cl^-]_o$ is the concentration of K^+ in the extracellular fluid. $[K^+,Na^+, Cl^-]_i$ is the concentration of K^+ in the intracellular fluid.

Ohm's law equation: V= I*R was another fundamental equation used to determine suitable chip resistances for mitochondrial patch-clamp experiments where V represents voltage in Volts, I the current in Amperes (A) and R the resistance in Ohm (Ω).

PatchControl (Nanion) and Clampex 10.2 softwares were simultaneously operated during experiments. PatchControl applied pre-programmed parameters including suction strength, duration and reading membrane or series resistances and whole-cell capacitances. Once

the whole-cell configuration was reached, voltage clamp protocol was applied and current amplitudes were recorded using Clampex with a patch-clamp amplifier (Axopatch 200B, Molecular Devices) and an axon Digidata 1322A (Axon instruments). Acquired current data were then analysed using Clampfit 10.2. Inclusion criteria for analysis were; (i) the current evoked at -100mV must not be more than half of the maximal leak current recorded, (ii) current-voltage (IV) relationship must have a negative reversal potential for whole-cell experiments.

3.7.2 Whole-organelle recordings

Identically to whole-cell recordings, the planar patch-clamp protocol was optimised for organelles usage.

The ionic composition of external and internal solutions was synthesised in order to reduce potential ionic contamination from active Ca^{2+} and Cl^- channels, especially in the outward direction. Based on published studies where mitochondrial K^+ channels were identified and characterised in symmetrical K^+ conditions (150mM KCl) (Rusznak, Bakondi et al. 2008, Kajma and Szewczyk 2012, Toczylowska-Maminska, Olszewska et al. 2014) we sought to use identical [K^+] in order to compare acquired with published data. The composition of these solutions is summarised in Table 3.4 where 150mM KCl was used in the external and 80mM K-Fluoride (Sigma, 449148) was combined with 70mM KCl in the internal recording solution.

3.7.3 Pharmacological study of mitochondrial channels

The mitochondrial K^+ channel activity was inhibited by Charybdotoxin (Sigma, C7802), ATP (Sigma, A6419) and two commonly used K_v channel blockers Tetraethylammonium chloride (Sigma, T2265) and 4-Aminopyridine (Sigma, A78403). Ca^{2+} channels were blocked by ruthenium red (RR) (Sigma, R2751). The blocker concentrations used during the study are summarised in Table 3.5. The percentage of residual current upon application of each blocker was calculated according to the following equation:

$$\% \text{ Residual current} = \frac{\text{Current with blocker}}{\text{Current without blocker}} \text{ x100}$$

3.8 Microscopy

3.8.1 Epifluorescence microscopy

Immunocytochemistry images (Methods 3.4.3) were acquired with the inverted Zeiss Axiovert 200 or the upright Zeiss Axioplan2 (Zeiss) microscopes. Different lasers emitting at specific wavelengths (λ) were employed such as FITC (525nm), Texas red (615nm) and

GFP (510nm). Each image was generated at 512 pixels x 512 pixels with 8 bit colour resolution. Images were acquired with a 63x magnification objective or a 100x oil immersion objective lenses. Detector sensitivity for each channel was set to the maximum exposition time which gave no signal in control samples (no primary antibody).

3.8.2 Confocal microscopy

Fixed cells mounted on glass slides by immunocytochemistry were analysed by confocal microscopy. Confocal images were later analysed with LAS X software and ImageJ to quantify the co-localisation of $hK_{2P}15.1$-eGFP with Mitotracker red or COX II and study the endogenous expression of TASK-5 or TASK-3 in COS-7 or HeLa cells.

Images were acquired by the inverted Leica SP8 AOBS confocal microscope using a plan Apochromat 63x N.A.1.30 glycerol immersion objective. To specifically excite each fluorophore used during the immunofluorescent staining (method 3.4.3), different lasers emitting at specific wavelengths (λ) were employed. DAPI (nuclear stain) was excited at 405 nm λ; green fluorescent stain (eGFP) at 488 nm λ and red dyes (Mitotracker or Texas red) at 561 nm λ. Emission was collected with a bandwidth of 412-522nm (DAPI), 494-561nm (eGFP) and 575-702nm (red dyes).

3.8.3 Co-localisation analysis

Costes method provides a quick and effective way of distinguishing labelled structures from background based on an analysis that determines the range of pixel values in which a significantly ($p<0.05$) positive Pearson's correlation coefficient (PCC) is obtained (Costes, Daelemans et al. 2004).This test was performed by randomly scrambling the blocks of pixels (instead of individual pixels, because each pixel's intensity was correlated with its neighbouring pixels) in one image, and then measuring the correlation of this image with the other (unscrambled) image. This process was repeated for 200 iterations until R(rand) values dropped to zero meaning that threshold for subsequent calculations has been found. Only those pixels whose red and green intensity values (R(obs)) were both above their respective thresholds (R(rand)) were considered to be pixels with co-localised probes.

Single z-stacks of confocal images were quantified with LAS AS Lite software to verify signal co-localisation between the two stains of interest. Alternatively, co-localisation analysis was performed on ImageJ software through the co-localisation test plugin where Costes' method estimates background thresholds. PCC values ranged from 1 where fluorescence intensities were perfectly and linearly related, to −1 where fluorescence intensities were perfectly, but inversely related to one another. Values near zero reflected distributions of fluorescent probes that did not correlate with each other.

Manders' Co-localisation Coefficient (MCC) test produced scatter plots representing co-localising pixels. The intensity of one fluorophore was plotted against the intensity of the

second one for each pixel. During strong co-distribution pixels clustered along the diagonal. In contrast, lack of co-localisation was reflected by the distribution of pixels into two separate groups through the x and y axes.

When co-localisation was not noticeable but statistically significant due to the higher R(obs) value than its threshold R(rand), co-localisation finder plugin was used on ImageJ. The plugin merged the red and green channels to an RGB image and highlighted the co-localised pixels in white. Pixels were considered 'co-localised' when their intensities were higher than the threshold of their channels and if the ratio of their intensity was higher than the ratio setting value (set at 50% by default).

3.8.4 Transmission electron microscopy

Aliquots of isolated mitochondria or mitoplasts were fixed for a minimum of 1h in 3% glutaraldehyde, 4% formaldehyde in 0.1M PIPES buffer at pH 7.2. Specimens were then embedded in alginate according to method one of (Page, Lagnado et al. 1994). Briefly, the samples were centrifuged, decanted and the pellet mixed with a small volume of 5% (aqueous) sodium alginate. Small drops of the mixture were then pipetted into 2 ml of 50/50 0.1M CaCl2 and 0.1M PIPES and left to set overnight. Calcium alginate beads containing mitochondria or mitoplasts could then be treated similarly to pieces of tissue without the need for further centrifugation. Beads were rinsed in 0.1M PIPES buffer (pH 7.2), post-fixed in 1% osmium tetroxide in 0.1M PIPES at pH 7.2 for 1h, rinsed in buffer, then distilled water and then block stained in 2% uranyl acetate for 20minutes. Samples were then dehydrated in an ethanol series and embedded in TAAB resin (TABB laboratories, Aldermaston, UK). Gold/silver (80 nm) sections were cut using glass knives using an OMU III ultramicrotome (Leica Microsystems, Milton Keynes, UK) post stained with Reynolds lead stain and viewed on a Hitachi H7000 microscope fitted with an EMSIS Megaview III digital camera (MÜnster, Germany).

3.9 Statistical analysis

All data are presented as the mean ± standard error of the mean (SEM) which was calculated as the standard deviation divided by the square root of the number of samples (n). The significance between sets of data was calculated in IBM SPSS statistical software using a Student's t-test or one-way analysis of variance (ANOVA) with Tukey's post-hoc test. The levels of significance were *p<0.05,**p<0.01, ***p<0.001, ****p<0.0001.

3.10 Composition of solutions

The composition of buffers used during total cell lysate or mitochondrial isolation and swelling experiments is summarised below. Concentration of all solutions is shown in mM except for Table 3.5.

Table 3. 1 Composition of total cell lysate or washing solutions.

Solutions	Tris-HCl	NaCl	Nonidet P40	Protease inhibitors
Lysis buffer	10	150	1% v/v	1 tablet in 10ml PBS
Wash buffer	10	150	1% v/v	-

Table 3. 2 Composition of solutions during isolation or swelling of mitochondria.

Solutions	Sucrose	Mannitol	EGTA	Tris-HCl	KCl	HEPES	$CaCl_2$	Protease inhibitors
Isotonic	-	-	-	-	150	10	0.1-0.2	
Hypotonic	-	-	-	-	-	5	0.1-0.2	
Hypertonic	-	-	-	-	750	30	0.1-0.2	
$IB_{cells}1$ buffer	75	225	0.1	30	-	-		1 tablet in 10ml PBS
$IB_{cells}2$ buffer	75	225	-	30	-	-		1 tablet in 10ml PBS

Table 3. 3 Electrophysiological solutions used for K^+ channel recordings in whole-cell configuration. Osmolarity of solutions was equal to 298-300 mmol/kg.

Solutions	KCl	NaCl	$MgCl_2$	$CaCl_2$	EGTA	HEPES	D-Glucose	K-Fluoride
External	4	140	1	2	-	10	5	-
Internal	50	10	-	-	20	10	-	60
Seal Enhancer	80	-	10	35	-	10	-	-

Table 3. 4 Electrophysiological solutions used for K^+ channel recordings in whole-organelle configuration. Osmolarity of solutions was equal to 298-300 mmol/kg.

Solutions	KCl	$MgCl_2$	$CaCl_2$	EGTA	HEPES	D-Glucose	K-Fluoride
External	150	0.1	0.1	-	10	5	-
Internal	70	-	-	2	10	-	80

Table 3. 5 Concentration of K^+ and Ca^{2+} blockers added to the external mitochondrial recording solution. Osmolarity of solution was equal to 360 mmol/kg when IC_{100} concentrations of TEA, 4-AP, ATP, Charybdotoxin and Ruthenium red were simultaneously applied to organelles.

Blockers	Ic_{50}	Ic_{100}
Charybdotoxin	2nM	200nM
ATP	0.5mM	1mM
TEA	10mM	20mM
4-AP	200μM	10mM
Ruthenium red	5μM	10μM

List of Accompanying Materials: All data supporting this study are openly available from the University of Southampton repository at: **doi:10.5258/SOTON/D0741**

Chapter 4

Optimisation of key methodologies

4.1 Introduction

The ultimate aim of this thesis is to determine if TASK-5 is a functional mitochondrial channel therefore, a key requirement to achieve this is to isolate and examine the electrophysiological characteristics of TASK-5 in transfected mitoplasts. As the adopted planar patch-clamp system does not enable visualisation of samples, a model cell over-expressing fluorescently tagged TASK-5 channels in mitochondria was established followed by a qualitative selection of fluorescent organelles by flow cytometry. This decision was taken based on the lack of reliable and specific fluorescent staining against TASK-5 that would allow direct mitochondrial channel visualisation. The experimental set up presented here, required considerable amount of optimisation and coordination of precise experimental procedures to ensure that the mitoplasts studied by planar patch-clamping were both viable and over-expressing the channel in question.

1. Isolation of mitochondria over-expressing TASK-5 from cells stained with Mitotracker red.

To determine if TASK-5 elicits K^+ currents in the IMM, a first and fundamental experimental step to perform was to transiently transfect (Methods 3.2.2) COS-7 or HeLa cells with the eGFP-tagged TASK-5 construct. This would allow to discriminate current differences between endogenous and enhanced TASK-5 mitochondrial expression. Acceptable transient transfection was attained once a DNA: transfection reagent ratio resulted in the expression of the fluorescently labelled proteins in a significant number of cells without inducing cytotoxicity. To ascertain that TASK-5 is present in mitochondria, cells were stained with Mitotracker red a fluorescent probe that passively diffuses across the plasma membrane and accumulates in active mitochondria according to their highly negative membrane potential. Both transient transfection and Mitotacker red staining are considered important steps of the strategy as it allowed to determine the viability of mitochondria prior performing any subsequent experiments. The incubation period of transfected cells with the fluorescent dye was also optimised so that cellular and organelle toxicity was maintained at low levels. Mitochondria were subsequently isolated and analysed by flow cytometry in order to collect healthy mitochondria over-expressing TASK-5.

Protein detection by SDS-electrophoresis

Immunoprecipitation followed by Western blot analysis (Methods 3.3.1-3.3.2) was also optimised as it provided the first evidence that an antibody and more specifically the custom $_hK_{2P}$15.1-LR could detect TASK-5 proteins in comparison to other commercially available antibodies which failed to target the channel (Chapter 2, section 2.9.3) (Roncoroni 2012). Immunoprecipitation of the GFP-tagged channel consisted of incubating GFP-trap beads with transfected cell lysates during which GFP-tagged proteins would bind to beads and

separate from the remainder unspecific proteins present in the lysate. To elute sufficient amounts of TASK-5 proteins from beads and reduce contamination from unspecific proteins, several optimisations were carried out.

2. Isolation of mitochondria and usage of transmission electron microscopy to confirm OMM removal and generation of mitoplasts.

To study K^+ currents elicited within organelles, isolation of mitochondria had to be accomplished prior sorting these by flow cytometry. After a series of optimisations including the determination of optimal centrifugation speeds and solution volumes; a pellet consisting of crude isolated mitochondria was obtained. The mitochondrial pellet was subjected to transmission electron microscopy (TEM) and used to determine conditions necessary for successful removal of the OMM; a step which was imperative to access the IMM for electrophysiological recordings. By incubating mitochondria in hypotonic conditions for a range of incubation periods, optimal swelling conditions (time and solution tonicity) were determined. This approach allowed to directly observe the extent of OMM rupture and mitochondrial matrix structure fluctuations.

3. Electrophysiological characterisation of TASK-5 currents in isolated mitoplasts using optimal recording solutions for planar patch-clamping.

To record K^+ currents elicited within organelles and ultimately identify currents generated by TASK-5 in the IMM, recording solutions suitable to planar patch-clamp electrophysiology were designed. Identification of mitochondrial recording solutions was essential to the proper characterisation of a background K^+ channel expressed in an intracellular compartment. During the optimisation phase, the presence of potassium fluoride (KF) ions within the internal mitochondrial solution was found to be vital to enable complete formation of giga-seals.

4.2 Isolation of mitochondria over-expressing TASK-5

4.2.1 Transient transfection of cultured cells

Laboratory techniques such as protein electrophoresis or isolation of mitochondria followed by planar patch-clamp electrophysiology required considerably large amounts of cells (compared to immunocytochemistry) in order to detect TASK-5 protein or sort sufficient mitochondria by flow cytometry. Thus, several DNA concentrations (5 µg, 10 µg, 15 µg, 20 µg) and transfection reagent (150mM NaCl) volumes (5-40µl) were assessed (Table 4.1) to comply with an increase in surface area where cells were cultured. Fluorescence intensity and localisation within cells was compared to control conditions where COS-7 were transfected with an eGFP DNA construct (Figure 4.1, Panel A). A bright and distinct green fluorescence that was mainly retained intracellularly rather than on the outer cellular membrane (Figure 4.1 Panel B and C) in comparison to eGFP alone (Figure 4.1 Panel A) was observed both in COS-7 and HeLa cells.

Cell line	DNA	150mM NaCl-DNA	JetPEI	150mM NaCl-JetPEI	Transf. efficiency (%)
COS-7	5	150	5	350	0
	10	150	10	350	50-60
	15	150	15	350	50-60
HeLa	10	150	10	350	10-20
	15	150	15	350	10-20
	15	50	30	250	40-50
	20	50	40	250	40-50

Table 4. 1 Optimisation of transfection reactions using a range of DNA concentrations and transfection reagents. Several DNA concentrations (µg) or JetPEI (µl) and 150mM NaCl (µl) were tested on either COS-7 or HeLa cells, prior to identifying the most efficient transfection efficiency (%).

Preliminary experiments performed on COS-7 cells revealed by epifluorescence microscopy that application of 10 µg (Figure 4.1, left Panel B) or 15 µg (Figure 4.1, right Panel B) DNA could most efficiently transfect cells with a 50-60% transfection rate compared to the first condition (5µg) where no fluorescent cells were observed (data not shown). As the transfection efficacy did not improve while increasing DNA concentration or incubation time (48h), decision to use 10µg instead of 15µg DNA was taken to limit potential cytotoxicity but also consume less DNA during each procedure.

Application of aforementioned conditions to HeLa cells on the other hand had a poor (10-20%) transfection efficiency (Figure 4.1, left Panel C) even 48-72h post-transfection, indicating that several parameters such as DNA concentration, JetPEI volume or incubation period should be modified. Optimisation of the NaCl volumes in which DNA and JetPEI were diluted was subsequently carried out in order to increase the percentage of transfected cells to at least 50%. By decreasing DNA-NaCl volume to 50µl and JetPEI-NaCl to 250µl (Table 4.1) and by increasing JetPEI volume to 30µl, the number of transfected HeLa cells

increased to 40-50% (Figure 4.1, right Panel C). Trials to increase the efficiency up to 60-70% by increasing the DNA concentration (20μg) or changing NaCl volumes did not however, increase transfection efficiency, leading to the conclusion that 15μg DNA and 30μl JetPEI together with a 48h incubation post-transfection were optimal conditions for the particular cell line.

It is also important to note that a time interval of 12-18 h was essential prior proceeding to the following experimental approaches (Mitotracker red staining or immunocytochemistry) for both cellular and mitochondrial recovery purposes as, deterioration of cells and organelles structure (i.e rounder, less adherent cells or donut-shaped mitochondria) was observed if this step was not taken into consideration.

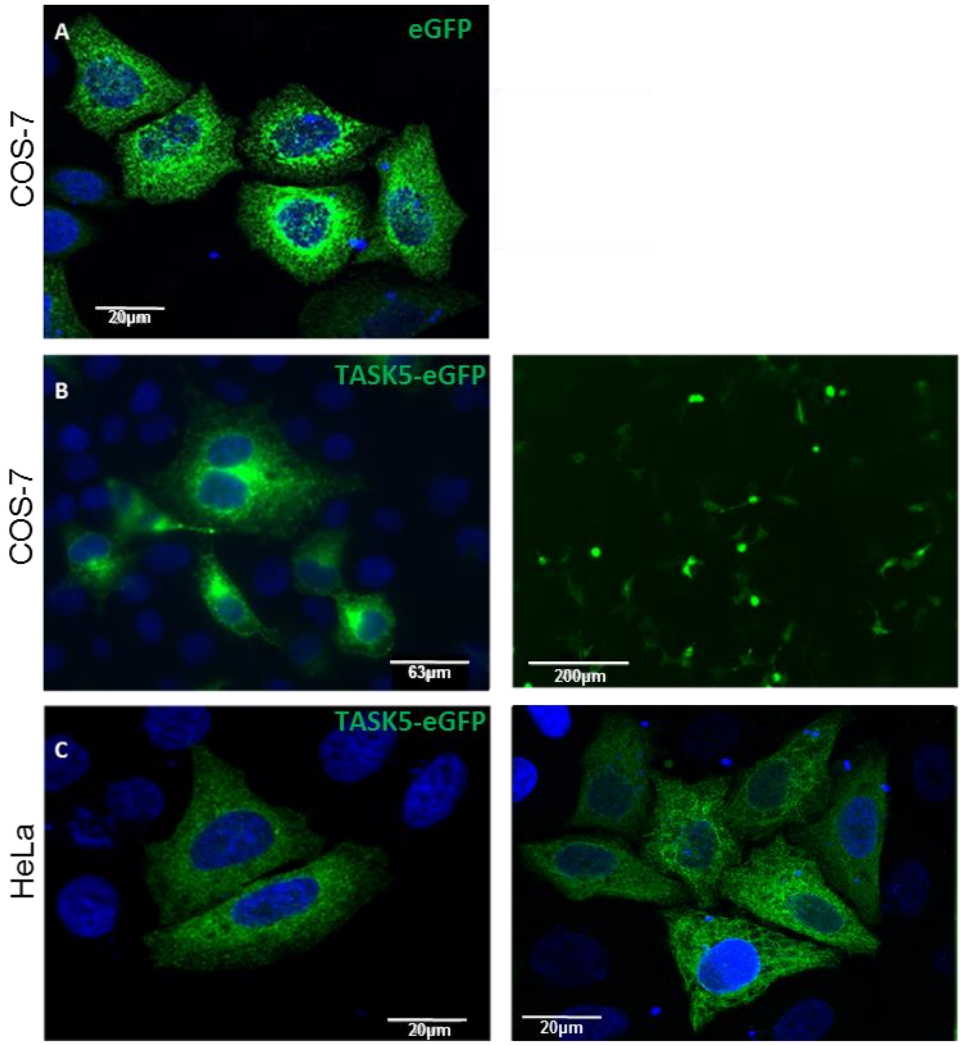

Figure 4. 1 Transient transfection of COS-7 or HeLa cells with a TASK-5-eGFP DNA construct. A. Confocal image of COS-7 cells transfected with 5μg eGFP DNA construct was used as a control sample. **B.** Epifluorescence images of transfected COS-7 cells with 10 μg DNA had a transfection efficiency of up to 50%. **C.** Confocal images of transfected HeLa cells with 15 μg DNA reached a 30-40% transfection efficiency. DAPI staining was also used to visualise the nuclei. Scale bars are reported in μm.

4.2.2 Identification of TASK-5-eGFP protein by SDS-PAGE electrophoresis

The targeting capacitance of $hK_{2P}15.1$-LR antibody was investigated on COS-7 cell lysates transfected with eGFP or TASK-5-eGFP by agarose bead immunoprecipitation (Methods 3.3.1) followed by SDS-PAGE electrophoresis (Methods 3.3.2).

Immunoprecipitated lysates of transiently transfected cells with eGFP or TASK5-eGFP were first probed with an anti-eGFP antibody in order to examine the protein product band sizes (Figure 4.2A). Both eGFP (33kDa) and TASK5 (36kDa) coupled to eGFP (~70kDa) were detected at the predicted protein sizes. Subsequently, eluted TASK5-eGFP proteins from beads together with supernatants that should only contain non-specific proteins were probed with $hK_{2P}15.1$-LR antibody (Figure 4.2B). A single band corresponding to the expected protein size of TASK-5- eGFP is visualised within the lane containing eluted proteins from beads in comparison to its supernatant where the 70 kDa band was absent. This indicates a high binding specificity of GFP-trap beads for GFP-tagged proteins which is also confirmed by an absence of eGFP protein within the eGFP supernatant collected post-incubation. Bands of ~110kDa size at the top of each nitrocellulose membrane were also observed. The polyclonal origin of $hK_{2P}15.1$-LR could be a possible explanation for the appearance of the non-specific bands as it is well known that such antibodies produce large amounts of non-specific interactions with multiple epitopes which can create background signal during some applications.

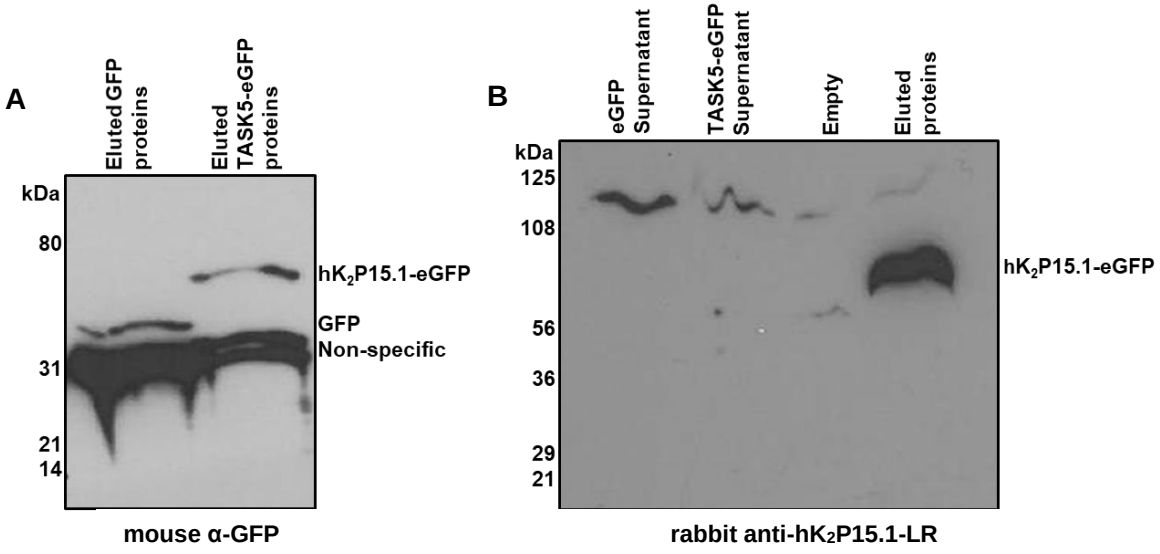

Figure 4. 2 SDS-PAGE electrophoresis of transiently transfected COS-7 cell lysates post-immunoprecipitation with GFP-trap agarose beads. Supernatants collected post-immunoprecipitation along with cell lysates of transfected COS-7 cells with either eGFP or TASK5-eGFP are shown. **A**. Distinct bands of ~33kDa or ~70kDa that correlated with the expected eGFP or TASK5-tagged GFP protein sizes are observed. Bands were detected using a mouse anti-eGFP antibody (1:1 000). Non-specific bands are also observed. **B** TASK5-eGFP was detected at the expected protein size (70kDa) using the hK2P15.1-LR antibody. Within both eGFP and TASK5-eGFP supernatants, larger unspecific bands were observed at ~110kDa due to the polyclonal origin of the antibody.

4.2.3 Determination of non-toxic conditions for mitochondrial staining with Mitotracker red

Mitotracker staining allowed to perform co-localisation analyses with TASK-5-eGFP, sort double fluorescent mitochondria and ensure that the channel is expressed in the organelles. Several concentrations of Mitotracker red were tested on COS-7 or HeLa cells in order to identify the optimal concentration that would result in viable mitochondria post transient transfection.

Epifluorescence and confocal images (Figure 4.3 A-C) show the reduction of red fluorescence intensity and background staining while Mitotracker red concentration decreases from 100 to 25nM. Even though, the exposure time during which epifluorescence images with 100 nM Mitotracker red was longer (2 ms) than usual (0.9-1.2 ms) resulting in a background dominated by red fluorescence, the structure of organelles could not be distinguished from other cytoplasmic compartments due to a high internalisation level of the dye (Figure 4.3A). Therefore, Mitotracker concentrations were tested at 50 nM and 25 nM (Figure 4.3B and C). Despite a clear reduction of red background with 50 nM Mitotracker, "donut"-shaped mitochondria (Figure 4.3D and E) were observed indicating that organelles underwent stress as stated in section 2.12.1 (Ahmad, Aggarwal et al. 2013). Cells were then incubated with 25 nM Mitotracker red during which, elongated, highly branched mitochondria were observed (Figure 4.3D and E). Optimising Mitotracker red concentration minimised mitochondrial toxicity but not totally eliminated it as a minor sub-population of organelles lost their ultrastructure and adopted a rounder shape post-transfection (Chapter 5, Figure 5.1).

The period of incubation of Mitotracker was also crucial as the longer the incubation the more mitochondria started losing their ultrastructure. According to the manufacturer's protocol, cells should be incubated between 15-45 minutes. Initially, cells were incubated for 30 minutes with the dye but mitochondria were faintly labelled (data not shown). Incubating cells for 1 h with Mitotracker red was toxic to mitochondria resulting in rounder shapes as shown in Figure 4.3D and E. Thus, the optimal incubation period for staining mitochondria was estimated as 45 minutes at 37°C.

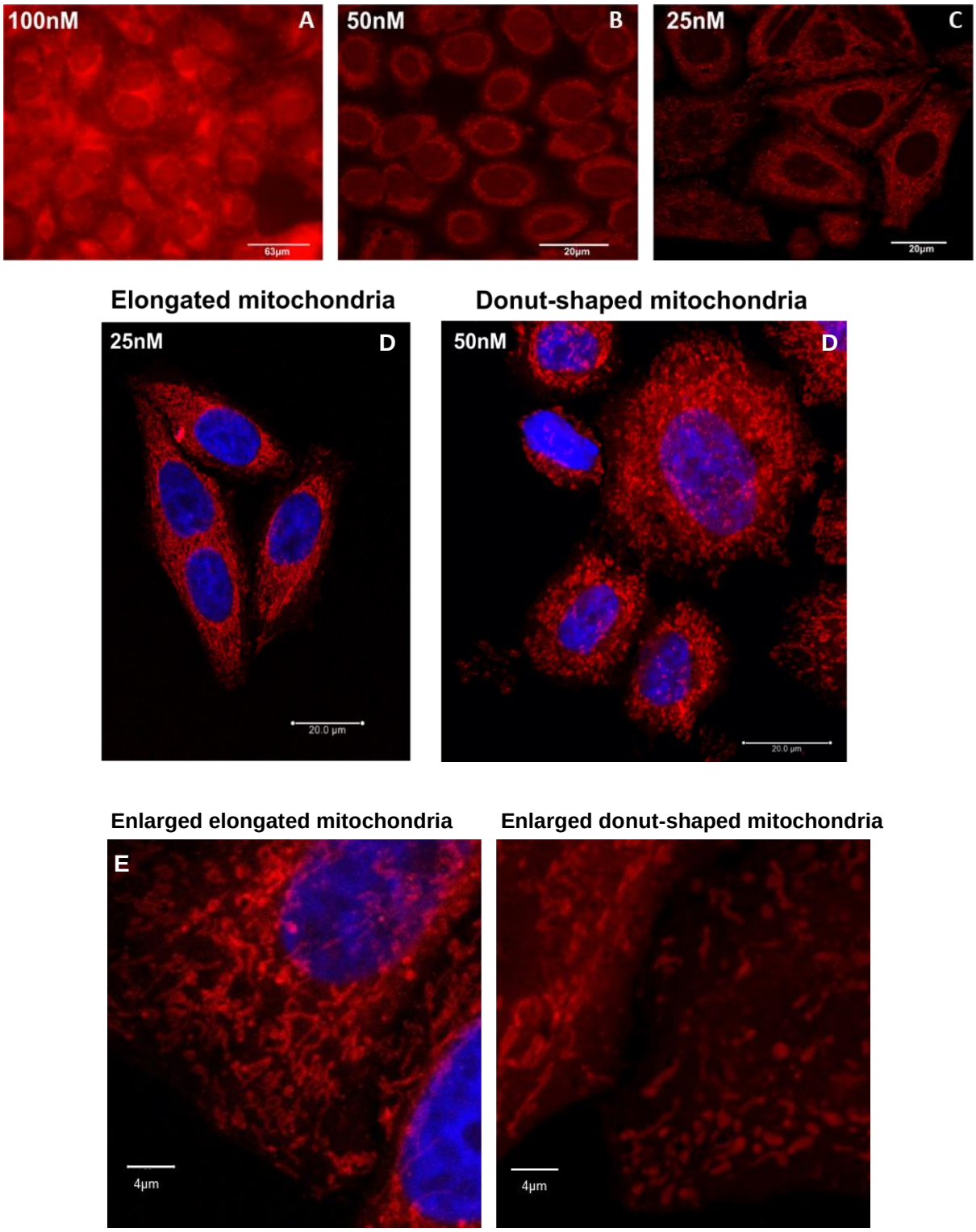

Figure 4. 3 Epifluorescence and confocal images of mitochondria stained with Mitotracker red. COS-7 cells were stained with **A.** 100 nM or **B.** 50 nM Mitotracker red and HeLa cells with **C.** 25 nM or **D.** 50nM. Immunocytochemistry images of donut-shaped mitochondria incubated in 50 nM Mitotracker red (D) show the cytotoxic impact of the dye on mitochondrial ultra-tructure in contrast to the elongated (normal) organelles incubated with 25 nM Mitotracker red. **E.** Enlarged sections of mitochondria showing the ultrastructure of elongated and donut-shaped organelles can be observed. DAPI staining was used to visualise the nuclei. Scale bars are reported in µm.

4.2.4 Isolation of mitochondria by differential centrifugation

The procedure of isolating mitochondria from HeLa or COS-7 cells was modified from a protocol published by Wieckowski, Giorgi et al., in 2009. Modifications were performed to isolate large concentrations of mitochondrial samples from cells in suspension and sort a sufficient amount of organelles prior patching.

Wieckowski et al. (2009) washed cells in 10 ml of mitochondrial buffer 1 (IB_1) during the first homogenisation step, a volume that did not allow efficient cell lysis as cells and/or organelles were highly diluted within the mortar which made it challenging to lyse cells by the pestle. Therefore, IB_1 volume was reduced to 3ml (in a stepwise manner) which resulted to an increased cell lysis rate. To verify the extent of cellular homogenisation, 10 µl of the cell lysate containing cells previously incubated with Mitotracker red were collected every 3-5 minutes and cell integrity was examined by epifluorescence microscopy. Cell lysate samples were collected after 15 series of 25 strokes and epifluorescence images revealed that cells maintained a whole-cell morphology (Figure 4.4 A). After 40 repetitions of 25 strokes lasting approximately 15-20 minutes, the majority of cells lost their cell integrity releasing their contents (organelles) in IB_1 solution. Crude mitochondria stained with Mitotracker red are visualised by epifluorescence microscopy as shown within the selected region of interest (ROI, Figure 4.4B).

Subsequently, homogenised cells were centrifuged at 600 g for 5 minutes and the pellet containing unbroken cells was discarded. However, cell membrane fragments were still present in the supernatant as shown in Figure 4.4B (outside the ROI), indicating that the centrifugation speed was not rapid enough to pellet cell debris. As a result, the centrifugation speed increased to 1000 g resulting in cleaner samples (data not shown). Wieckowski et al. washed the supernatant containing mitochondria, lysosomes and microsomes in 20 ml IB_2, followed by two centrifugation steps at 7 000 g for 10 minutes. Re-suspending the pellet in such large volume and centrifuging at this speed did not allow to visibly detect the mitochondrial pellet. Therefore, the protocol was modified by re-suspending the pellet in 1 ml of IB_2 followed by a centrifugation at 10 000g for 10 minutes. This allowed to mainly pellet mitochondria along with ER debris, lysosomes and membrane fragments (Figure 4.5). The pellet was lastly re-suspended in 40-1000µl of IB_2 or external mitochondrial solution, according to the requirements of the following experiment.

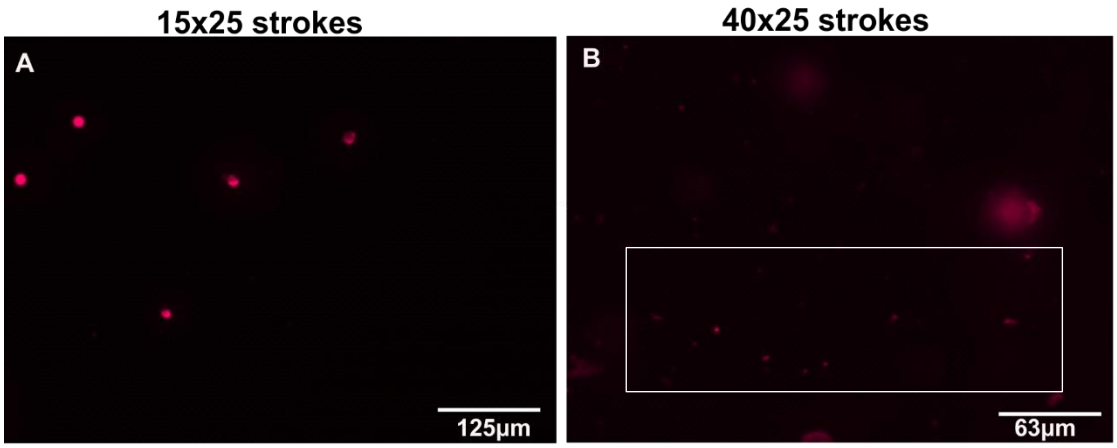

Figure 4. 4 Isolation of mitochondria through a homogenisation procedure of COS-7 cells, previously incubated with Mitotracker red. Epifluorescence microscopy images of homogenised cells after **A.** 15 repetitions of 25 strokes, where cells kept their cell integrity (round structures). **B.** Optimal mitochondrial isolation was reached after 40 repetitions of 25 strokes where most of cells were lysed, releasing mitochondria (ROI) within IB_1 buffer. Scale bars are shown in µm.

4.3 Swell induction and rupture of the outer mitochondrial membrane

Mitoplasts isolated from HeLa were obtained by inducing an osmotic shock to the organelles. Isolation of mitochondria was performed in physiological and isotonic mitochondrial conditions, where 75 mM sucrose and 225 mM mannitol maintained their physiological ultrastructure (Methods 3.6.1) (Morikawa, Kanematsu et al. 2014). By reducing the concentration of sucrose to 15 mM and incubating mitochondria in such hypotonic conditions for more than 5 minutes, osmotic stress was induced, allowing water from the solution to enter the mitochondrial matrix (Morikawa, Kanematsu et al. 2014). Pressure caused by water across the intra-mitochondrial space was applied (swelling) which ultimately, induced the OMM to burst. In order to restore mitoplast isotonicity and maintain their functionality, mitoplasts were incubated in a hypertonic solution (Table 3.2) for 10 minutes.

Rupture or partial rupture of the outer membrane was assessed by TEM during which mitochondria were incubated in hypotonic conditions for 10 or 30 minutes (Figure 4.5). During the first 10 minutes of incubation, the majority of organelles retained their double membrane structure with fissures in the OMM indicating that rupture of the membrane was incipient but incomplete. Mitochondria were then incubated in hypotonic solution during an extended period of time (30 minutes) during which, organelles totally lost their cristae and matrix structure (indicated with an *, Figure 4.5) adopting a vesicle-looking shape. Hence, to maintain the ultra-structure of organelles while being able to strip off the OMM, mitochondria were incubated for 20 minutes in hypotonic followed by 10 minutes in hypertonic solution.

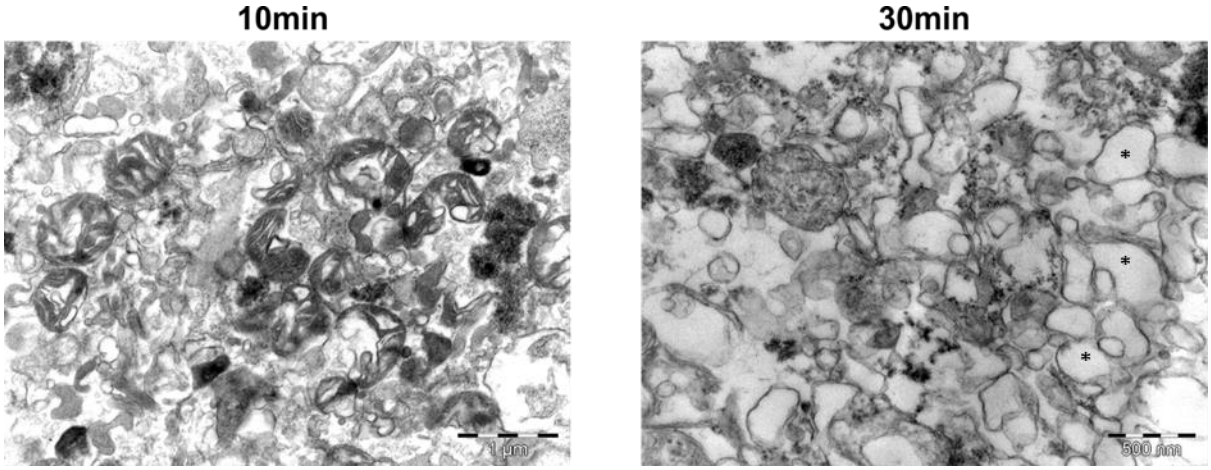

Figure 4. 5 Transmission electron micrographs of isolated mitochondria from HeLa cells. Mitochondria were incubated in hypotonic solution for 10 or 30 minutes. Intact mitochondria with a conserved matrix structure (non-swollen) and an OMM were observed post 10minute incubation. Organelles incubated for 30 minutes in hypotonic solution lost their ultra-structure adopting a vesicle structure with swollen matrices indicated with an *. Cell membrane or intracellular debris were observed in light grey within the background. Scale bars of 500nm and 1µm are indicated at the right bottom of each image.

4.4 Design of optimal mitochondrial recording solutions for planar patch-clamping

During the last decade, numerous publications of automated patch-clamping performed on cells and very recently in intracellular organelles have emerged. As the electrophysiological characterisation of mitochondrial K^+ channels at the whole-cell configuration has not been widely explored to date, identification of suitable recording conditions was imperative prior performing any patch-clamp experiments.

Composition of the external and internal recording solutions was chosen based on several published works performed on isolated mitochondria with conventional patch-clamp rigs (Method 3.6.2 and Table 3.4) (Sorgato, Keller et al. 1987, Dahlem, Horn et al. 2004, Orij, Postmus et al. 2009, Kajma and Szewczyk 2012, Bednarczyk, Wieckowski et al. 2013). The first criterion to comply with was to use symmetrical K^+ solutions to limit the exchange/contamination of other ions and principally record K^+ currents across mitochondrial membranes. Under such conditions, current amplitudes would increase in a sigmoidal manner as a function of the permeant ion concentration (activity). This would also reveal mitochondrial K^+ current patterns including reversal potential or current rectification. The second principle was to determine the concentration of solutes required to maintain the physiological structure and functionality of isolated mitochondria *in vitro*. Published mitochondrial studies performed on standard electrophysiological rigs, used symmetrical solutions of 150 mM KCl with a marginally more alkaline pH (7.4) (compared to cells (pH7.2)) as mitochondrial matrix pH is known to be more alkaline (pH 7.4) than the cytoplasm (7.2) (Sorgato, Keller et al. 1987, Dahlem, Horn et al. 2004, Orij, Postmus et al. 2009, Kajma and Szewczyk 2012, Bednarczyk, Wieckowski et al. 2013).

During the mitochondrial solution design it was observed that potassium fluoride (KF) ions were absent from internal recording solutions used in published conventional patch-clamp studies. Therefore, initial trials (presented in Chapter 6) were performed using internal solutions devoid from KF (Trial A, Table 4.2). Establishing contact and subsequently gigaohm seals between the mitochondrial membranes and the chip apertures was however unsuccessful, supporting the conclusion that F^- ions were essential to mitochondrial seal formation on a planar patch-clamp system. Internal solution containing 150mM KF, devoid from Cl^- ions was thereafter tested (Trial B) in order to confirm previous observations regarding the importance of F^- ions. Seals formed successfully under these conditions and gigaohm seals were achieved several minutes post-application of a seal enhancer solution. Current amplitudes at +80mV are summarised in Table 4.3 with their corresponding I-V curves presented in Chapter 6, section 6.4.

Despite meeting the symmetrical [K^+] requirements between internal and external recording solutions an ionic imbalance between fluoride and chloride ions was generated. However, the effect of fluoride ions on mitochondrial ion channel conductances has not been examined to date. Internal solution with higher concentration of KCl than KF was subsequently tested on mitochondria (Trial C). Equally to Trial A however, mitochondrial seals could not reach the gigaohm resistance suggesting that higher [F^-] than [Cl^-] was central to achieve gigaseals and thereafter the whole-cell configuration. Taking into consideration the internal recording solution suitable for whole-cell recordings provided by the manufacturer (Table 3.3) where 60mM KF and 50mM KCl were used; 80mM KF and 70mM KCl were accordingly tested (Trial D). This significantly improved seal stability (as observed in Trial B) and enabled the maintenance of the whole-mitochondrial configuration for several minutes. Equally to Trial B, K^+ currents elicited from perforated mitochondrial membranes were recorded at +80 mV (Table 4.3). Corresponding current to voltage curves are presented in Chapter 6 where detailed curve kinetics are provided.

Table 4. 2 Solute composition of external and internal recording solutions suitable for planar patch-clamping. All concentrations are shown in mM. Absence of several solutes within either external or internal solution are indicated by -.

Trial A							
	KCl	**MgCl2**	**CaCl2**	**HEPES**	**EGTA**	**K-Fluoride**	**D-Glucose**
External	150	0.1	0.1	10	-	-	5
Internal	150	-	-	10	20	-	-

Trial B							
	KCl	**$MgCl_2$**	**$CaCl_2$**	**HEPES**	**EGTA**	**K-Fluoride**	**D-Glucose**
External	150	0.1	0.1	10	-	-	5
Internal	-	-	-	10	20	150	-

Trial C							
	KCl	**$MgCl_2$**	**$CaCl_2$**	**HEPES**	**EGTA**	**K-Fluoride**	**D-Glucose**
External	150	0.1	0.1	10	-	-	5
Internal	90	-	-	10	20	60	-

Trial D							
	KCl	**$MgCl_2$**	**$CaCl_2$**	**HEPES**	**EGTA**	**K-Fluoride**	**D-Glucose**
External	150	0.1	0.1	10	-	-	5
Internal	70	-	-	10	20	80	-

Trial E							
	KCl	**$MgCl_2$**	**$CaCl_2$**	**HEPES**	**EGTA**	**K-Fluoride**	**D-Glucose**
External	120	0.1	0.1	10	-	-	5
Internal	40	-	-	10	20	80	-

Table 4. 3 Maximal mitochondrial K^+ currents recorded at +80mV in gradient or symmetrical K^+ solutions with several KF concentrations. All currents measured (in pA) after a voltage stimulation at +80mV were recorded in multiple KF (in mM) combinations. Results are Mean±SEM.

Internal solution [KF]	**Gradient K^+**	**Symmetrical K^+ (150)**		**Symmetrical K^+ (120)**
	60	150	80	40
Current at +80mV	1064.48	699.32	636.17	228.47
±SEM	166.79	159.31	107.41	30.26

Finally, symmetrical (120 mM) K^+ solutions were tested to determine the effect of marginally lower symmetrical [K^+] along with a greater [F^-] than [Cl^-] ratio on mitochondrial current amplitudes and kinetics (Trial E). Comparison of currents recorded within 4 different [KF] in gradient or symmetrical conditions at +80 mV (Table 4.3) revealed a concentration dependent outward amplitude. In fact, bathing mitochondria in gradient solutions (provided by Nanion) that were more suitable for cell membranes (Table 3.3), induced a significantly higher outward rectification, reaching a maximal current amplitude of ~1 nA compared to mitochondria bathed in symmetrical conditions (228-699 pA). Nevertheless, bathing mitochondria in an external solution with significantly lower [K^+] (4mM) than the mitochondrial matrix (150mM) would certainly induce an osmotic shock to organelles as a result of [K^+] imbalance across organelle membranes. Under symmetrical 150 mM [K^+] with a gradual decrease of [KF] (80 mM) in the internal solution did not considerably alter current amplitudes indicating that F^- ions might not have affected K^+ ion transport. Decreasing symmetrical [K^+] to 120 mM strongly reduced current amplitudes on the other hand, demonstrating that K^+ channels were the main active ion conductors under such conditions. As current amplitudes recorded under 120mM [K^+] solutions were considerably low, the use of symmetrical 150 mM [K^+] with 80 mM KF in the internal solution was taken in order to better study residual currents post-blocker application.

4.5 Conclusions

A key challenge of this thesis was to achieve optimal conditions of each independent protocols and subsequently perform the experimental techniques in series while preserving toxicity of mitochondria as low as possible. Characterisation of K^+ currents *ex vivo* was particularly demanding as mitochondrial physiology was affected after undergoing several stress inductions such as transient transfection, differential centrifugations and sorting by flow cytometry. It was also important to ensure that ionic currents were recorded from mitochondrial membranes and not any other intracellular compartment. Therefore, a series of experimental techniques (Figure 4.6) were optimised in such a way to allow efficient characterisation of the IMM channel in recording solutions that maintained the organelle ultra-structure and function close to physiological ranges.

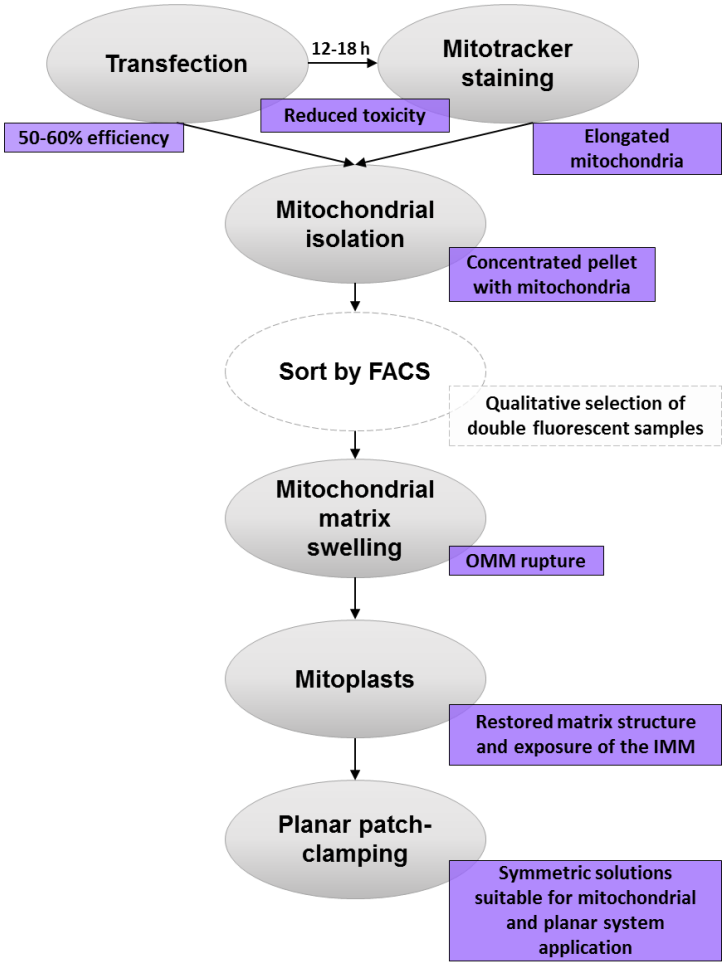

Figure 4. 6 Diagram outlining various experimental steps and outputs of the study. Techniques that required optimisation are shown in grey circles together with their optimal outputs (purple squares) achieved within the study. Detailed explanation of mitochondrial sorting by FACS (light grey circle) will be covered in Chapter 5. Experimental approaches were performed in series starting from a transient transfection, followed by Mitotracker red staining, ending to the electrophysiological characterisation of mitoplast K^+ currents on a planar patch-clamp system.

4.5.1 Transient transfection and Mitotracker red staining

Choosing a transfection reagent that balances efficient nucleic acid delivery and low cellular toxicity to cells was imperative to achieve reliable experimental results. Identification of optimal transient transfection conditions that allowed the over-expression of sufficient amounts of TASK-5-eGFP channel while maintaining low cellular toxicity was attained. Transient transfection was a key experimental procedure of the research's strategy as over-expression of the channel allowed to demonstrate the mitochondrial expression of TASK-5 during co-localisation analyses and recognise K^+ currents by planar electrophysiology. Subsequently, immunoprecipitation and Western blot analyses demonstrated that the protein of interest is translated into a protein in COS-7 cells which was effectively targeted by the custom antibody. The power of the antibody in targeting TASK-5 was also demonstrated for the first time in cell lysate samples but also by immunocytochemistry as TASK-5-eGFP adequately co-localised with $hK_{2P}15.1$-LR in transfected COS-7 cells (Appendix 5).

Optimal Mitotracker red concentration that could stain mitochondria without inducing mito-toxicity and producing high levels of red background was identified. Elongated, tubular and highly branched mitochondria were observed in non-transfected cells stained with 25 nM Mitotracker red, indicating a healthy condition (Friedman and Nunnari 2014). Over-expression of the channel together with mitochondrial staining however resulted in few donut-shaped mitochondria (Chapter 5, Figure 5.1) which could possibly be to the over-expression of TASK-5 affecting the K^+ cycle, $\Delta\psi_m$ and entrance of water (section 2.12.1). The use of stably transfected cells could induce less cytotoxicity to mitochondria as permeabilisation of mitochondrial membranes would only be triggered by Mitotracker red internalisation.

4.5.2 Mitochondrial isolation

Optimal centrifugation speeds and buffer volumes were determined resulting in a pellet containing abundant isolated mitochondria as shown in Figure 4.5. Subsequent repetitions of the mitochondrial isolation protocol led to the conclusion that the volume in which cells were lysed together with the centrifugation speed and the duration of this procedure were crucial. In fact, the speed and time of centrifugations had to be highly precise as a small change could modify the whole experiment and result to a negligible amount of isolated mitochondria. Following isolation of organelles, flow cytometry was performed to specifically sort GFP-tagged mitochondria. Detailed information on the flow cytometry and sorting processes is covered in Chapter 5 nevertheless, it is worth mentioning that sorted mitochondria were ultra-centrifuged post-FAC sorting as it was not possible to collect sorted mitochondria with a normal benchtop microcentrifuge even at its highest speed competence (~20,000g).

Centrifugations at 10, 15 and 20,000g were initially tested prior to perform ultra-centrifugation at 40,000g for 20 min which enabled to pellet sorted mitochondria and re-suspend the later in hypotonic solution to form mitoplasts.

4.5.3 Mitoplasts formation

Mitochondria respond to changes in osmotic pressure generated by the solute composition of the solution in which these are incubated and can undergo rapid, reversible volume/shape alterations due to the permeability of their outer membrane. During this study, rupture of the outer membrane was caused by incubating organelles in a hypotonic solution (i.e lower sucrose and K^+ ions concentrations than mitochondrial solution buffers used during their isolation) which allowed water to enter into the mitochondrial matrix, induce an osmotic pressure to the inter-membrane space and rupture the OMM.

Transmission electron microscopy was used to demonstrate that isolation of mitochondria through differential centrifugations was successful despite the partial cellular debris contamination but also, to observe structural alterations of mitochondria in hypotonic solution following 10 or 30 minute incubation in hypotonic solution. Increase in matrix volume was observed after a 30 minute incubation which may be related to an increase in respiration rate increasing ATP production (Halestrap 1987, Halestrap 1989, Lim, Javadov et al. 2002). A possible explanation would be that during energetic stress, i.e when the need for ATP is high and $\Delta\Psi_m$ decreases, an increase in matrix volume could further activate the respiratory chain as observed in ischeamic mitochondria following reperfusion and leading to the deterioration of mitochondrial functions (Lim, Javadov et al. 2002). What is more, increased K^+ influx and/or matrix swelling were associated with other cellular processes which have an impact on the reactive oxygen species (ROS) generation, like matrix alkalinisation (Garlid and Paucek 2003), mild uncoupling of the proton gradient (Holmuhamedov, Jahangir et al. 2004), or enhancement of fatty acid oxidation (Halestrap 1987). Mitochondrial swelling was also associated with cytochrome *c* release during apoptotic cell death. Cytochrome *c* can be released from mitochondria through mPTP-dependent or -independent mechanisms (Newmeyer and Ferguson-Miller 2003). Recently, Gogvadze et al. suggested that release of cytochrome *c* might occur via moderate modulation of mitochondrial volume irrespective of the mechanism leading to mitochondrial swelling (Gogvadze, Robertson et al. 2004). Therefore, it remains uncertain whether mitoplasts that undergo an osmotic shock, a transient transfection and differential centrifugations will entirely preserve their functional characteristics. Nevertheless, as the aim of the study was not to investigate the activity of TASK-5 during physiological conditions but instead, determine whether the channel could generate K^+ currents in mitochondria; assessment of the electrophysiological character of the channel was considered suitable.

Electrophysiological study and pharmacological application of channel blockers will then enable to compare membrane resistances or current amplitude differences between mitochondria and mitoplasts to conclude that OMM rupture was successful (Chapter 6 and 7).

4.5.4 Mitochondrial recording solutions suitable to the planar patch-clamp system

Optimal solutions for planar patch-clamp of mitochondrial membranes needed to be defined empirically. In order to characterise the electrophysiological properties and kinetics of an ion channel, the use of symmetrical solutions for the main permeant ion of interest, in this case K^+, was required. Symmetrical K^+ conditions allowed to determine the direction of K^+ ions flowing across mitochondrial membranes which was deduced to be mainly outwardly (to the matrix) rectifying at positive voltage steps as we would expect from active K^+ channels (Chapter 5). Moreover, internal and external recording solution concentrations were established according to published records performed on conventional patch-clamp rigs, commonly using 150mM KCl. The reason explaining this was mainly due to the higher mitochondrial matrix [K^+] that was close to 150 mM at rest compared to cytoplasmic [K^+] at 120-140 mM (Lodish 2000, Kaasik, Safiulina et al. 2007).

Patching mitochondria in conditions that are to date proposed to be most appropriate for K^+ channels characterisation and not inducing any electrochemical gradient imbalance to the organelles were hence tested on the planar patch-clamp system. Results were compared with published data from conventional patch-clamp studies and showed that under symmetrical KCl conditions seal establishment failed, linking this to the absence of fluoride ions in the internal solution. Although the molecular mechanism of improving seal stability and leakage upon addition of KF or phosphate salts is currently not well understood, Kostyuk et al., were the first to report this observation (Kostyuk, Krishtal et al. 1975). Decades later, Yatani and Brown have demonstrated that application of intracellular KF improved seal formation but also activated muscarinic atrial K^+ (K^+[ACh]) channels in guinea myocytes upon application of Mg^{2+} ions at mM concentrations (Yatani and Brown 1991). In 2008, during the process of screening hERG K^+ channel adopting the planar patch-clamp system PatchXpress 7000A, Zeng et al., showed that partial substitution of KCl with KF in the internal recording solution improved patch-clamp sealing and stabilised the whole-cell configuration (Zeng, Penniman et al. 2008). This resulted in longer, more stable gigaohm seals but also indicated that F^- ions did not significantly change the biophysical properties or the pharmacology of hERG channel (Zeng, Penniman et al. 2008). Recent published works on automated patch-clamp experiments also reported that fluoride improved seal quality and did not affect reversal potential or pharmacology of voltage-gated sodium (Nav1.7) or potassium channels (Kv1.3) in Chinese hamster lung (CHL) or T-cells accordingly (Li, Lu et

al. 2017), or the human *ether-a-go-go-* (hERG) potassium channel in Chinese hamster ovary cells (Zeng, Penniman et al. 2008).

Five years later, Zeng et al., published another paper related to the critical role of F^- or halide ions on hERG channel properties using PatchXpress 7000A (Zeng, Balasubramanian et al. 2013). In this study, they examined the effects of complete replacement of Cl^- in internal solution with halide ions such as F^- or Br^- and found that: (a) F^- slightly shifted the voltage dependence of hERG channel activation to more positive voltages, while Br^- to more negative voltages; (b) F^- decreased hERG activation, while both F^- and Br^- induced faster channel closure; (c) neither F^- nor Br^- had an effect on hERG inactivation kinetics. Therefore, complete replacement of Cl^- with F^- had subtle effect on hERG activation and generated similar current kinetics with conventional patch-clamp studies.

Taking into consideration the aforementioned information, F^- ions are essential for gigaseal establishment during planar patch-clamp electrophysiology. Nevertheless, it is important to keep in mind that presence of halide ions in the internal solution may also affect the activation/deactivation or physiological properties of some mitochondrial channels. In fact, fluoride ions could potentially lead to the activation of anion channels as fluorine has similar ionic radius with chlorine (James N. Spencer 2010). Even though the ion selectivity of mitochondrial chloride channels remains to date vague, it is imperative to control the solute composition of the internal solution to correctly interpret currents of interest.

Chapter 5

Experimental strategy undertaken to characterise TASK-5 channel in mitoplasts

5.1 Introduction

Based on co-localisation re-analysis results performed in Chapter 2 demonstrating that TASK-5 could be co-expressed with the IMM protein complex cytochrome bc1 but not with extracellular membrane lectin markers, additional co-localisation analyses were undertaken to further validate the mitochondrial expression of the channel. More precisely, co-localisation analyses between eGFP-tagged channel and Mitotracker red or cytochrome *c* oxidase subunit (COX) II was investigated by immunocytochemistry and confocal microscopy in transfected HeLa cells with TASK-5-eGFP. An approach demonstrating that TASK-5 has a putative and partial mitochondrial localisation within the IMM.

Sorting microscopic organelles such as mitochondria according to their fluorescence identity by flow cytometry or incubating organelles in optimal swelling conditions to partially expose IMM will be presented in this chapter. These approaches provide the last piece of evidence to validate the effectiveness of optimised techniques (presented in Chapter 4) that consist of the research strategy designed to characterise TASK-5 prior planar patch-clamping.

5.2 Mitochondrial expression of TASK-5-GFP in transiently transfected cells

5.2.1 Co-localisation between the GFP-tagged channel and Mitotracker red

To analyse the co-localisation level between the two fluorophores, a ROI around cells over-expressing the GFP-tagged channel and co-stained with the red fluorescent probe was defined (Figure 5.1). Pearson's correlation coefficient value between red and green fluorescent pixels was significant (R(obs)=0.421) as the mean R(rand) value was lower than R(obs) after 200 iterations (Coste's method) (Table 5.1), confirming the mitochondrial expression of the channel. A scatter plot showing how green and red fluorescent pixels cluster along with the diagonal emphasises the co-localisation level between the two fluorophores. Co-localisation level of endogenous TASK-5 proteins with Mitotracker red is also demonstrated by epifluorescence microscopy in HeLa cells where a clear fluorescence staining overlap can be visualised (Appendix 3).

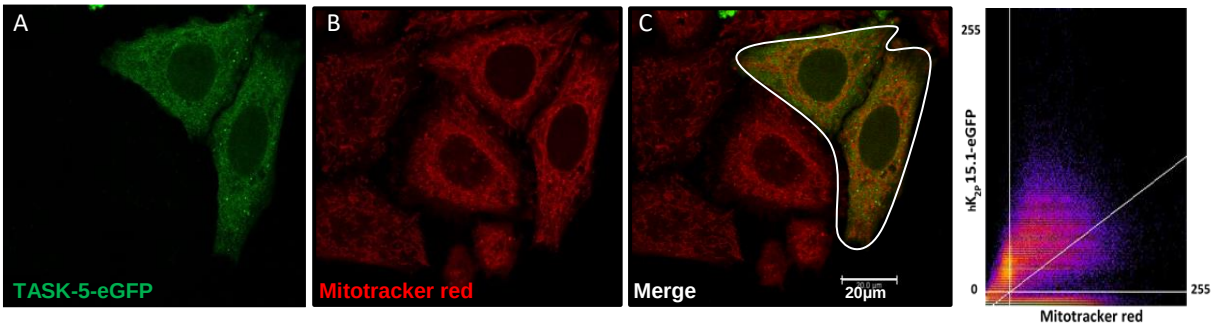

R(obs)	R(rand) Mean±SD	R(rand)>R(obs)
0.421	0.002±0.011	0/200

Table 5. 1 Co-localisation PCC values between TASK5-eGFP and Mitotracker red. PCC values obtained upon application of Costes' randomisation statistical analysis allowed to determine the co-localisation level between Mitotracker red and TASK-5-eGFP on ImageJ. As R(rand) values were lower than R(obs) during all 200 iterations, co-localisation between the two fluorophores was considered significant ($p<0.05$).

Figure 5. 1 Confocal image of immunocytochemistry of transiently transfected HeLa cells with TASK-5-eGFP, stained with 25nM Mitotracker red. Co-localisation analysis was performed by drawing a ROI line around cells (panel C) which were both expressing the GFP-tagged channel (panel A) and stained with Mitotracker red (panel B). Co-localisation test performed on ImageJ resulted in a scatter plot showing the co-localising pixels in pink grouped along the diagonal. Purple pixels designate the non-colocalising eGFP and Mitotracker red pixels. The colour components of individual pixels were measured in the colour range between 0 and 255. Scale bar: 20µm.

5.2.2 Co-localisation between the GFP-tagged channel and COX II

COX II is a protein complex that catalyses the reduction of oxygen to water in the respiratory chain in the IMM (Capaldi, Malatesta et al. 1983). Co-localisation analysis of immunocytochemistry of transfected HeLa cells stained with a primary COX II and a secondary Texas red antibody was performed (Figure 5.2). Despite an absent yellow fluorescence emission that would usually indicate visual co-localisation between proteins, Pearson's

method showed that TASK-5 co-expressed with COX II in the IMM. In fact, reasonable R(obs) and higher values than R(rand) were obtained after 200 iterations (Table 5.2). Additionally, scatter plots obtained on ImageJ poorly demonstrated co-localising pixels as the fluorescence emission of COX II antibody was relatively weak. To visibly demonstrate the co-expression degree between fluorophores, a co-localisation finder plugin on ImageJ allowed the detection of co-localising fluorescent points on a single z-stack where co-localising pixels were highlighted with an artificial white shade. Therefore, the experiment further supports that TASK-5 is present in the IMM and emphasises that there are a number of different methods that can be used to measure co-localisation of immunocytochemistry images.

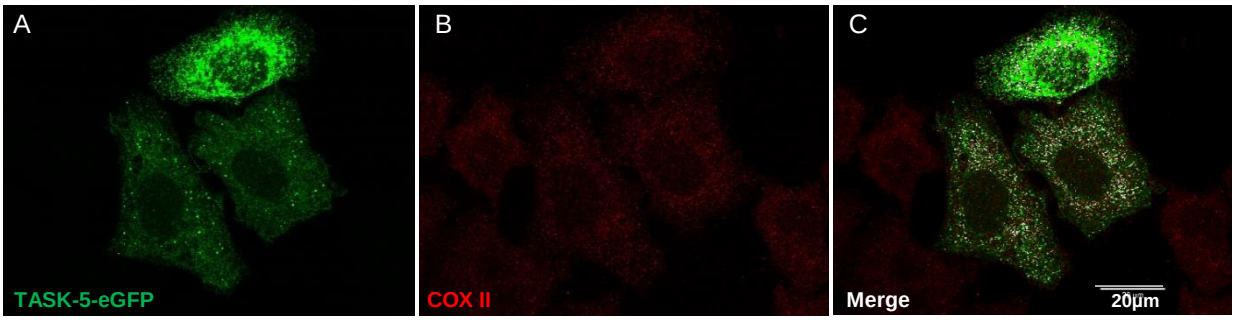

R(obs)	R(rand) Mean±SD	R(rand)>R(obs)
0.401	0.000±0.002	0/200

Table 5. 2 Co-localisation PCC values between TASK5-eGFP and COX II. PCC values obtained upon application of Costes' randomisation statistical analysis allowed to determine the co-localisation level between COX II and TASK-5-eGFP on ImageJ. As R(rand) values were lower than R(obs) during all 200 iterations, co-localisation between the two fluorophores was considered significant ($p<0.05$).

Figure 5. 2 Confocal image of immunocytochemistry of transiently transfected HeLa cells with TASK-5-eGFP stained with COX II. Transfected cells (panel A) were stained with a primary COX II antibody (5µg/µl) (panel B) and an anti-mouse Texas red (1:150) secondary. Merged image of green and red fluorophores along with artificial white points (panel C) indicating co-localising pixels between TASK-5-eGFP and COX II. At the top of the image a brighter HeLa cell with higher eGFP uptake was excluded from the co-localisation analysis in order to properly set the background R(rand) threshold. Scale bar: 20µm.

5.3 Flow cytometry on isolated mitochondria

The main weakness of certain planar patch-clamp systems is that visualisation of samples is not applicable. Thus, it was critical for the success of this strategy to ensure that the samples used for planar patch characterisation derived from TASK-5-eGFP positive mitochondria. To ascertain that patched organelles would over-express the GFP-tagged channel, a selection procedure was conducted on a flow cytometer embedded with an airflow sorter. More specifically, a blue laser exciting both eGFP-tagged and Mitotracker red stained mitochondria detected their respective fluorescence emission wavelengths within the FITC and Texas red band pass filter range (Methods 3.5).

The quartile gating (Q) parameters of the forward (FSC-A) versus side (SSC-A) light angle scatters were established based on four populations of mitochondria. These settings allowed to differentiate between TASK-5 positive organelles used for patch-clamping and TASK-5 negative organelles that were discarded together with cell debris. Control gating was set up with mitochondria isolated from non-transfected cells which were not stained with Mitotracker red. The population of non-stained mitochondria (events) together with cell fractions clustered in the third quartile (Q3) indicating that the flow cytometer did not detect any fluorescent events or the size of these last was particularly small (Figure 5.3 A). Subsequently, isolated mitochondria from transfected but not stained with Mitotracker red cells were detected in Q4 whereas non-transfected mitochondria, stained with Mitotracker red in Q1 accordingly (Figure 5.3 B,C). During data acquisition, a linear line in Q2 (Figure 5.3B) appeared as an emission spectra overlap indicating that fluorescence from more than one fluorophore (dual fluorescence) was detected. To address this spectral overlap fluorescence compensation was applied to minimise the detection of ‘false’ double fluorescent organelles. Mitochondria over-expressing TASK-5 and stained with Mitotracker red were lastly detected in Q2 (Figure 5.3D). As the sample also contained single positive Texas red fluorescent events, a ROI gate that would specifically select double positive events was shifted to the right in order to reduce contamination from single red events.

It is also essential to note that during each experimental acquisition FSC-A and SSC-A scatter plots were modified according to the size and fluorescence intensities of the samples. Once the gating parameters were set, sorting was performed where more than 60,000 events could be selected and re-suspended in suitable isotonic mitochondrial solution.

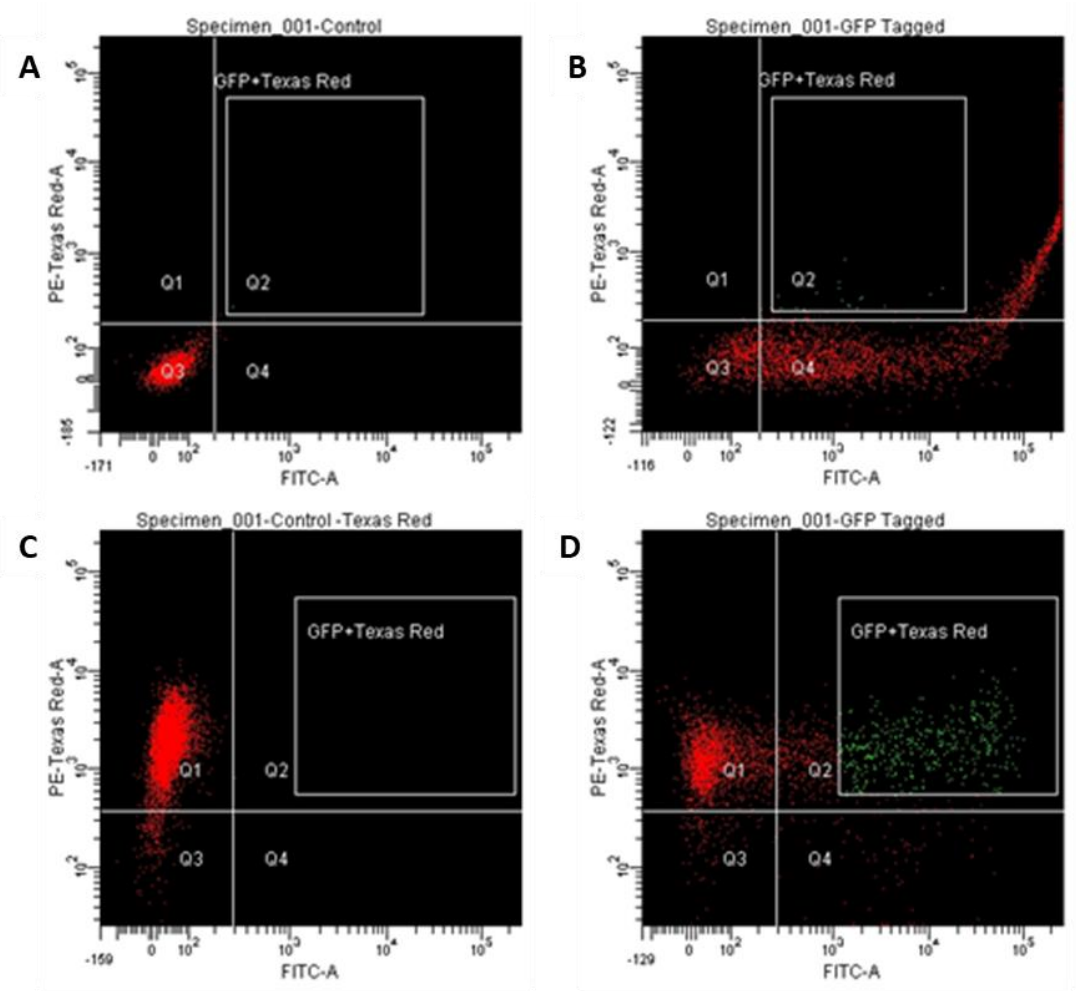

Figure 5. 3 FSC-A versus SSC-A scatters (Texas Red vs FITC) showing different populations of isolated mitochondria. Four different populations of isolated mitochondria are shown in each quartile. Control mitochondria collected from unstained cells were detected in Q3. Mitochondria expressing the GFP-tagged channel were observed in Q4 and those with Mitotracker red where observed in Q1. Transfected mitochondria which were also stained with Mitotracker red were observed in Q2 where a gate was drawn to select and sort double fluorescent organelles. Number of fluorescent events detected ranged between -185 and $1x10^5$. Negative FSC values were set to visualise non-transfected samples.

5.3.1 Epifluorescence microscopy on sorted mitochondria

To examine the efficiency of the sorting process, epifluorescence microscopy on sorted events in suspension was performed. Double stained mitochondria were suspended in ~500µl external recording solution and centrifuged at 20,000g for more than 30 minutes, a speed that was insufficient to pellet isolated organelles. Therefore, ultra-centrifugation at 40,000g and 4°C was adopted to pellet and re-suspend sorted organelles in smaller volumes during mitoplast formation. Results showed that the Mitotracker red mitochondrial population also expressed the GFP-tagged channel providing strong evidence that the sorting procedure was efficient (Figure 5.4). Merged image of the two fluorophores (FITC and Texas red) resulted in a clear yellow fluorescence emission confirming the degree of co-localisation (Figure 5.4C). Confirmation that fluorescent events were exclusively isolated mitochondria and not cell

membrane debris was also demonstrated as Mitotracker red is a dye that is specifically taken up by healthy mitochondria and does not internalise in other intracellular compartments.

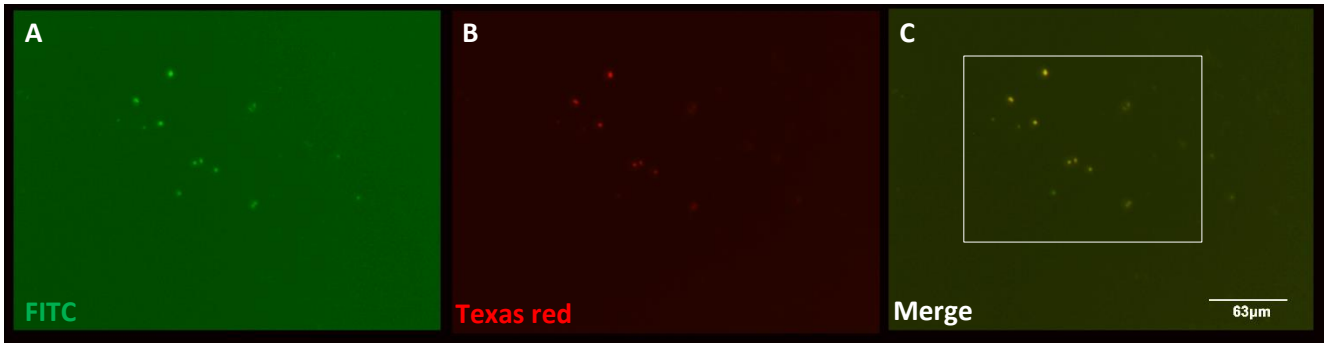

Figure 5. 4 Epifluorescence microscopy images confirming the co-localisation of the GFP-tagged channel with Mitotracker red in sorted mitochondria. A Sorted GFP-tagged mitochondria expressing TASK-5 channel. **B.** Sorted mitochondria stained with Mitotracker red. **C.** Merged image of sorted double fluorescent mitochondria emitting a yellow fluorescence. Scale bar: 63µm.

5.4 Mitoplast formation

The final step prior to patch organelles was to form mitoplasts and expose their IMM where TASK-5 is expressed. Optimal swelling conditions were identified in Chapter 4 concluding that incubation of isolated mitochondria in hypotonic solution for 20 minutes followed by 10 minutes in hypertonic conditions would generate mitoplasts stripped off their outer membrane. Magnification of TE micrographs of isolated mitochondria that have partially lost their OMM but not their ultra-structure are presented after being incubated in hypotonic solution (Figure 5.5). In fact, the isotonicity of organelles was significantly restored once incubated in hypertonic solution in comparison to mitochondria that underwent non-reversible structure deterioration during a 30 minute incubation (Figure 4.6). Isolated mitoplasts from HeLa cells had nevertheless preserved OMM fragments or double membrane ‘caps’, pointing out that OMM burst was not entirely attained.

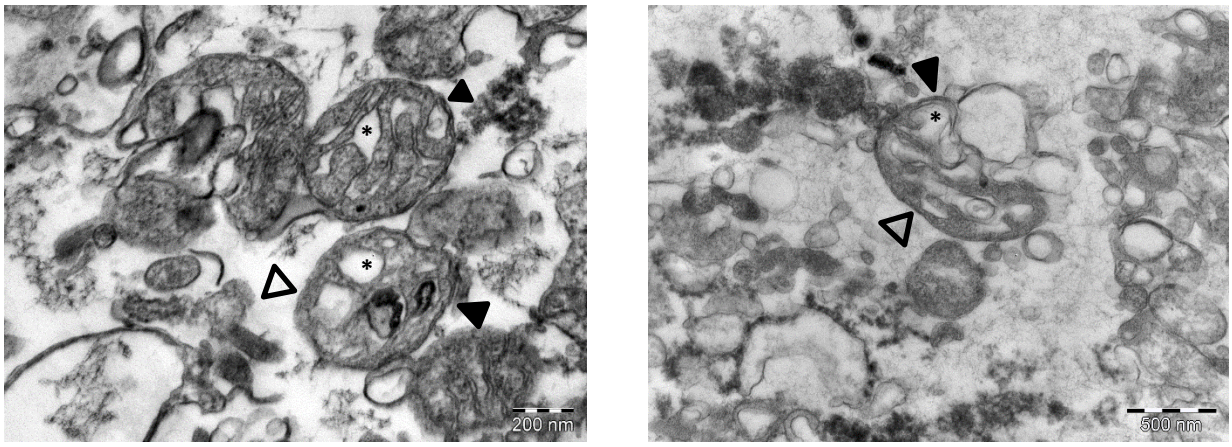

Figure 5. 5 Transmission electron micrographs of non-transfected and non-sorted mitoplasts. Isolated mitoplasts with a conserved matrix structure (shown with an *) and an exposed IMM (open arrow). Closed arrows indicate double membrane fragments where the OMM is conserved. Cell debris such as rough endoplasmic reticulum fragments with ribosomes can be observed in the background. Scale bars: 200 and 500nm are indicated at the right bottom of each image.

5.5 Conclusions

5.5.1 Localisation of TASK-5 in mitochondria

Qualitative and quantitative analysis of confocal images was undertaken as the degree of overlap between that GFP-tagged channel and intracellular markers, Mitotracker red or COX II was not always detectable visually. To do so, two widely accepted measures of co-localisation (PCC and MCC) were applied during the study providing additional evidence to the mitochondrial expression of TASK-5.

Co-expression of TASK-5 with a mitochondrial probe that specifically internalises within the organelles according to their membrane potential was demonstrated at the endogenous and transient transfection level. Results suggest that over-expression of the channel moderately altered $\Delta\psi_m$ or induced modest mitochondrial stress as the fluorescent probe can only internalise in active mitochondria with a highly negative membrane potential which can easily be washed out of organelles during $\Delta\psi_m$ hyper- or depolarisation. In fact, TASK-5 over-expression is hypothesised to generate inward currents that would depolarise $\Delta\psi_m$ due to the entrance of positively charged K^+ ions within the matrix. Mitotracker red staining of the matrix demonstrates that the $[K^+]$ is maintained within physiological concentrations due to mainly the expulsion of K^+ ions by the K^+/H^+ antiporter. This may also suggest that matrix acidification can occur due to the higher H^+ influx in response to TASK-5 over-expression which can function as a feedback loop inhibiting the activity of the channel.

Evidence reinforcing the putative mitochondrial expression of TASK-5 was also demonstrated by its co-expression with COX II (or complex IV). COX II is another component of the respiratory chain in the IMM involved in the transfer of electrons from cytochrome *c* to oxygen (Capaldi, Malatesta et al. 1983). Despite no apparent co-localisation between the two fluorophores, PCC values were shown to be significant and co-localising pixels were visualised using ImageJ software.

Acquired data lead to the conclusion that TASK-5 may be a mitochondrial channel that is co-expressed with complexes III and IV of the electron transport chain in the IMM suggesting that K^+, H^+ transport and ATP synthesis across the IMM may be inter-linked. As previously described in Chapter 2 (section 2.12.1), H^+ ejection by the electron transport chain during ATP synthesis generates an electrical membrane potential depolarisation which drives K^+ influx to the mitochondrial matrix by diffusion ("K^+ leak") and via the mitochondrial K^+ channel (mitoK) (Garlid and Paucek 2003). Net uptake of K^+ salts is then accompanied by osmotically obligated water resulting in matrix swelling (Garlid 1988) which is restored by the K^+/H^+ antiporter (Figure 5.6). Based on this evidence, a proposed role of endogenous TASK-5 channel under physiological conditions would be that K^+ leak would regulate matrix volume

through the electron transport chain and K^+ cycle. Detailed physiological role of TASK-5 in mitochondria is further discussed in Chapter 8.

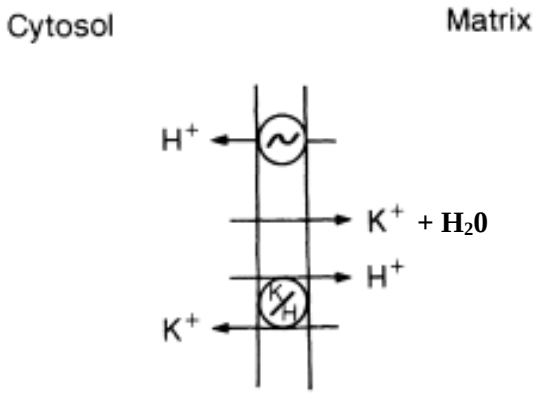

Figure 5. 6 The K^+ cycle in mitochondria. Three independent and physiologically essential transport processes of mitochondria are outlined. During ATP synthesis, an equal rate of electrogenic H^+ pumping coupled to electron transport towards the cytosol is generated, altering $\Delta\psi_m$. Electroneutral K^+/H^+ antiport is regulated to balance the activation of K^+ uniport towards the matrix upon membrane depolarisation. The energy used by the cycle is the cost of providing volume homeostasis to mitochondria. Image adopted from Garlid, 1988.

Moreover, this finding also suggests that only a fraction of the putative mitochondrial population expresses the protein after being transiently transfected. More precisely, based on the R(obs) values extracted from the co-localisation analyses between TASK-5-eGFP and cytochrome bc1, Mitotracker red or COX II, correlation coefficient values propose that ~40% (R(obs)= 0.4) of the total mitochondrial population over-express TASK-5-eGFP. Possible rationale would be that either transient transfection efficacy of JetPEI was insufficient, or the translated protein was distributed within other intracellular compartments such as endocytic vesicles or nuclear membrane. Another hypothesis could be that TASK-5 DNA may be excluded by cells to reduce cytotoxicity for a yet unknown reason or that it was degraded by nucleases post-transfection. This finding was nevertheless taken into consideration and explains why sorting by flow cytometry was an additional and fundamental step to the experimental strategy. In fact this approach allowed to sort organelles (red fluorescence) according to their green fluorescence with a high purity rate and ensure that K^+ currents studied by planar electrophysiology would be elicited from TASK-5.

5.5.2 Sorting mitochondria by flow cytometry

Despite the microscopic size of a mitochondrion (1-10μm in diameter), flow cytometry was an effective and reliable technique for sorting organelles. Control samples enabled scatter plot gating and setting up the boundary of each quartile in order to accurately select mitochondria emitting a green and red fluorescence. During the procedure, more than 60,000 events were sorted and re-suspended in isotonic mitochondrial recording solution

according to their purity. Collecting mitochondria in external recording solution enabled to maintain their ultra-structure and to some extent, mimic their physiological (cytosolic) environment prior being stripped off their OMM or patched for whole-mitochondrial studies. Ultra-centrifugation of organelles was also a crucial step as it allowed to pellet organelles over-expressing TASK-5 prior being stripped off their OMM. Epifluorescence microscopy was finally adopted to confirm that sorted organelles did over-express TASK-5 and samples were free from cell membrane debris.

5.5.3 Investigation of mitoplast formation by TEM

Transmission electron microscopy was a valuable approach to visualise isolated mitochondria and allowed to identify the optimal swelling conditions to rupture the OMM without altering the mitochondrial matrix and cristae shapes of organelles. Results showed that organelles were not totally stripped off their OMM and conserved several outer membrane caps. A hypothesis explaining this observation would be the ultra-thin sectioning of the mitochondrial samples embedded into the resin. More precisely, the orientation and distribution of fixed organelles is usually not identical within the resin, resulting in cross-sectioning of different levels of the sample. Hence, the presence of OMM caps may suggest that the OMM was totally conserved but not visible within the particular cross-section. Even though, electrophysiological access to the IMM of partially swollen mitoplasts can be debated based on these data, evident inhibition of IMM channels during pharmacological assays is demonstrated in Chapter 7.

Chapter 6

Measurement of the electrical activity of plasma or organellar membrane channels at the whole-cell configuration on a port-a-patch

6.1 Introduction

The port-a-patch is a miniaturised planar patch-clamp system that enables whole-cell current recordings in individual cells. For this experimentation, pipettes usually used in conventional patch-clamping were replaced with NCP-1 chips to enable access to cell membranes (due to their conical shaped aperture). In contrast to the classic patch-clamp technique, cells move towards the chip aperture instead of glass pipettes to the cells by suction (or negative pressure) application. This is achieved by PatchControl software which applies suction pulses (using a computer controlled pump) until the whole-cell configuration is reached. PatchControl has the advantage of automatically controlling pre-set parameters and offering information on membrane resistances, organelles surface areas along with pressure amplitudes (Rusznak, Bakondi et al. 2008, Kajma and Szewczyk 2012, Toczylowska-Maminska, Olszewska et al. 2014).

Recordings of whole-cell seals were primarily undertaken with the aim of understanding how the planar patch-clamp software was operating, how to identify suitable suction intensities that would rupture cell membranes without impairing their structure/functions and most importantly, how to examine K^+ currents. Measurement of K^+ currents elicited at the whole-cell configuration in COS-7 was attained by incubating cells in gradient K^+ solutions provided by the manufacturer (Methods Table 3.1). Once the configuration was finalised and preliminary current recordings from COS-7 were made, mitochondrial currents were characterised in gradient solutions. Modifications to pre-set parameters in PatchControl software were performed in order to optimise seal formation and gently rupture their membranes to reach the whole-organelle configuration. Earlier experimental studies (Rusznak, Bakondi et al. 2008, Kajma and Szewczyk 2012, Toczylowska-Maminska, Olszewska et al. 2014), adopted K^+ solution concentrations symmetrical to the matrix [K^+] in order to not affect mitochondrial physiological millieu and determine K^+ transport direction to characterise K^+ channels. The symmetrical solutions adopted in these studies were however not suitable to the planar patch technique due to an absence of F^- ions in the internal recording solution. Symmetrical solutions were adjusted and optimised to study mitochondrial K^+ currents on a planar patch-clamp system. Identical conditions were subsequently applied to mitoplasts.

Datasets acquired using the methodology presented in this thesis where compared with mitochondrial published studies to reinforce the suggestion that the proposed methodology can be used to patch mitochondria despite its inability to offer visual / physical evidence.

6.2 Establishing the planar-patch whole-cell configuration

Preliminary current recordings were performed on non-transfected cells and subsequently on isolated mitochondria or mitoplasts to optimise recording conditions. Currents recorded at the whole-cell configuration were processed and subsequently used as reference data where series resistances, membrane capacitances and current amplitudes were compared with recordings performed on whole-organelles and available published studies.

A fundamental prerequisite to the experimental methodology is the selection of an appropriate NPC-1 chip (a function of the samples studied). Ohm's law (Methods 3.7.1) defines that during a constant voltage (V) stimulation, the smaller the current (I) elicited within a cell/organelle, the higher resistance (R) the pipette or chip should have to form a seal. Thus, NPC-1 chips with a 2-3.5 MOhm resistance and 1 μm aperture were selected for cells that elicited currents at the whole-cell configuration within the nano Ampere (nA) range. For mitochondrial experiments, NPC-1 chips of 10-15 MOhm resistance (highest resistance available at Nanion) were used due to the smaller current amplitudes recorded from mitochondria compared to cells (Kane and Pavlov 2013, Rinné, Kiper et al. 2017).

To study whole-cell currents on the planar patch-clamp system, PatchControl software was adopted, allowing to pre-define and adjust protocols according to the samples tested. Experimental length, suction strength and duration of the holding membrane potential were variable parameters that were controlled within the PatchControl software. Briefly, automated parameters consisting of cell catching, gigaseal formation, whole-cell formation, blocker application (during pharmacological assays) were performed sequentially before recording K^+ currents. To facilitate gigaohm seal formation, seal enhancer solution (Table 3.3) was administrated during the sealing procedure and replaced with external solution before reaching the whole-cell/organelle configuration (Figure 6.1), via an external perfusion system. The external perfusion system consists of a software controlled magnetic pinch valve panel with three different suspended syringes that contain solutions that could also be administrated manually (Appendix 2). For this set of experiments, the exchange of solution was performed in such a way as to not disturb the seal. Establishing the whole-cell configuration also relies on the cell quality (low passage, 50% confluence) but also on an appropriate manipulation of pre-set parameters presented in the following section.

Once the whole cell configuration is established, PatchControl software and suction pulses are automatically paused allowing Clampex to apply a voltage clamp protocol or command voltage (Vc) to control the voltage across the membrane (Vm). The difference between Vm and Vc are thereafter detected by the amplifier and converted into a current (I) which was injected into the cell in order to make Vm equal to Vc. The amount of current required to keep

Vm=Vc was dependent on the solute composition of the external and internal recording solutions where ion channels were in- or activated and recorded.

6.2.1 Potassium currents recorded in whole-cell configuration on the planar patch-clamp system

Preliminary trials aiming to examine K^+ currents elicited from cell membranes were first performed to examine current characteristics following voltage stimulations. Cells in suspension with a cytoplasmic milieu of ~140 mM K^+ were bathed in external recording solution (4 mM K^+) (Figure 6.1). A series of suction pulses along with predefined set of parameters were used to attract a single cell towards the aperture of a 2-3.5 MOhm resistance chip. Once the whole-cell configuration is reached through the application of short and brief suction pulses that rupture the cell membrane, internal (110 mM K^+) solutes come into contact with cytoplasmic solutes. The higher [K^+] of both cytoplasmic milieu and internal solution compared to external solution was suggested to mainly induce an outward movement of ions due to the electrochemical gradient concentration difference generated across the cell membrane. In other words, the greatest cytoplasmic and internal [K^+] compared to external recording solution, results in the generation of outward K^+ movements (or exit) towards the internal solution in order to reach the so-called equilibrium K^+ potential (or reversal potential) across the membrane.

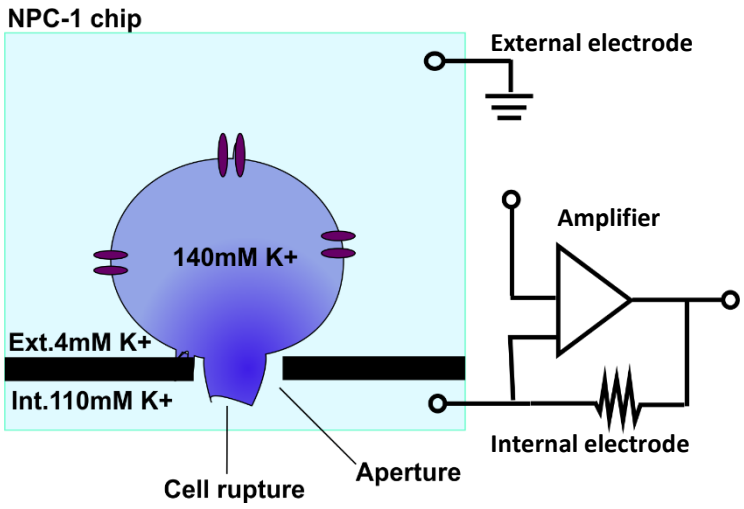

Figure 6. 1 Illustration of the whole-cell configuration on a planar patch-clamp system. A cell bathed in external K^+ solution (4mM) forms a seal on the aperture of an NPC-1 chip (indicated with a line), placed on top of the internal K^+ solution (110mM). Application of suction pulses allow to rupture the extracellular membrane and reach the whole-cell configuration. Difference in [K^+] (Vm) between internal and intracellular cytoplasmic (140mM) solutions is recognised by the amplifier's (right) electrodes bathed in solution once a voltage clamp protocol (Vc) is applied. Difference between Vm and Vc is converted to current which is then recorded. Ion channels expressed on the extracellular membrane are represented in purple.

Pre-set parameters

A complete electrophysiological experiment is sub-divided into four main automated steps; cell contact, gigaseal formation, whole-cell configuration and current recordings are performed in the order illustrated in Figure 6.2. Starting from the 'wait for contact' parameter step where positive pressure measured in milliBar (mB) (light red: R<10 MOhm; 20 mB) is applied within the chip holder. This prevents debris or dust clogging in the chip aperture but can also allow the evaluation of the condition of the chips (humidity or cracked glass apertures increase a chip's resistance). Therefore, if the resistance was higher than 10 MOhm during the 'wait for contact' process, the experiment was automatically interrupted. Conversely, if the measured resistance is lower than 10 and closer to 2-3.5 MOhm, the software moves to adjust the pipette offset (VpOffset) step during which the current passing through the pipette is 'zeroed' when the electrode is in contact with the external solution. Offset correction enables re-setting the internal circuitry and avoiding contamination from leak currents generated by the planar instrument. Negative pressure is then applied (dark red: -30mB; Figure 6.2) to 'pull' a cell towards to aperture, followed by higher suction pulses during the wait for cell step (orange: R>10 MOhm; -50 to -100mB with 10mB increments; Figure 6.2). Chip resistance progressively increases to form a cell membrane contact and subsequently, a gigaOhm (1 000 MOhm) resistance seal following the wait for seal (yellow: R>100 MOhm; -60 to -150mB with 10mB increments), improve seal 1 (dark green: R>500 MOhm; -80 to -200mB with 10mB increments) and improve seal 2 (light green: R>1 GOhm; -200mB)] parameters. Once a gigaseal is established, continuous and brief suction pulses are applied to maintain whole-cell configuration step (blue: Cslow>4 pF and Rs<40 MOhm; -100 to – 250mB with 50mB increments).

During the "whole-cell patch" process, several resistances arise and should be taken into consideration to properly interpret acquired results. These are the access resistance (Ra) which is synonymous to the chip resistance and the series resistance (Rs) generated between the chip aperture and port-a-patch ground. If Rs is sufficiently large to introduce significant current errors due to unwanted generation of electrical noise from the rig, series resistance compensation should be undertaken. Usually, an electronic trick that can effectively reduce resistance and accounts for 10% of total Rm is called Rs compensation or correction (Barbour 2014). Thus, the lower the series resistance, the less current contamination will occur. A threshold of Rs<40 MOhm was set during whole-cell experiments. Another parameter that was taken into consideration was the membrane capacitance (measured in farads) which a measure of how many ions need to be transferred to set up a given potential difference across membranes, i.e how quickly Vm can respond to a change in current (Hille 2001). The total membrane capacitance (Cm) of a cell is also a quantity directly proportional to the membrane

surface area with 1μF/cm^2 (or 0.01 pF/μm^2) being used to determine the surface area of the cells studied (Neher and Marty 1982, Streit and Lux 1987). The higher the capacitance, the slower the ions will cross membranes. Slow capacitance (Cslow) is the storage of charge in a cellular membrane based on the size of a cell (Hille 2001). Therefore, if Cslow is higher than the pre-set threshold value of 4 pF that indicates that the whole-cell configuration was established the software automatically pauses (no pressure is applied). Clampex then takes over by applying voltage-clamp protocols and records ionic currents.

Addition and removal of the seal enhancer was also found to be fundamental to achieving the gigaseal configuration. Its high [Ca^{2+}] content is anticipated to improve seal formation between the cell membrane and chip aperture. In this set of trials the enhancer was applied once resistance was higher than 50 MOhm (yellow step), a fact that indicates that a cell is captured within the aperture. Removal of the seal enhancer was strictly done before the whole-cell configuration (light blue; Figure 6.2) in order to avoid significant Ca^{2+} entrance within the cytoplasm and activation of Ca^{2+} channels. Combining aforementioned criteria, the overall gigaseal formation success rate was ~70%, based on the number of chips discarded when seal establishment failed.

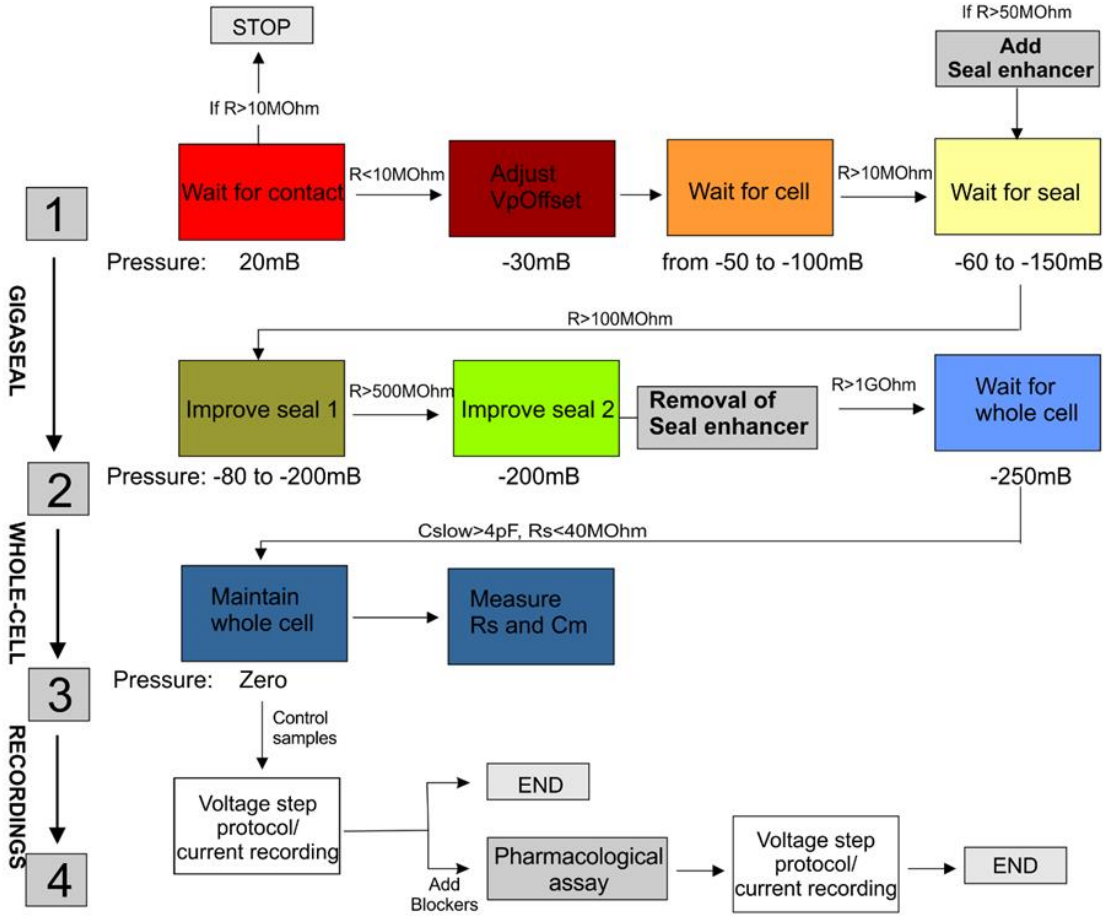

Figure 6. 2 Pre-set parameters and settings in PatchControl leading to the whole-cell configuration in COS-7 cells. Diagram illustrating automated steps enabling to form a gigaseal (sections 1 to 2) and later, reach the whole-cell configuration (sections 2 to 3) in a colour coded manner. Voltage stimulations and pharmacological blockers were only applied once the whole-cell configuration was attained (sections 3 to 4). In order to proceed to the following step, conditions such as membrane resistance, capacitance and positive or negative pressures were set. If the requirements were not met, the software automatically stops. The addition and removal of the seal enhancer was fundamental to the whole procedure and should be performed at specific steps.

Ionic currents elicited at the whole-cell configuration in a single COS-7 cell were recorded in gradient (or asymmetric) recording solutions (Table 3.3) and application of a voltage clamp protocol between -100 mV and +80 mV led to large outward rectifying currents in the nA range (Figure 6.3A). An outward rectification (starting at -50 mV) with a maximal current amplitude of ~3.5 nA at +80 mV and a relatively minimal inward rectification at negative voltage steps were observed. Recorded current amplitudes were analysed and plotted as current to voltage (I-V) curves in order to study the current to voltage relationship, observe how channels respond to voltage stimulation but also investigate the voltage-dependence and reversal potential (V_{rev}).

Strong outward rectification at positive voltages (between +20 and +80 mV) and weak inward rectification at negative voltages (between -65 and -100 mV) were observed (Figure 6.3B). What is more, direct measurement of V_{rev} close to -65 mV was seen on the I-V curve and

indicated that no net ionic flow passed through the cell membrane (i.e at 0 pA). The solute composition of internal and external recording solutions generated a V_{rev} similar to the predicted GHK equation (-65 mV) (Methods 3.7.1) which was close to the equilibrium K^+ potential (E_{K+}=-80 mV). This result indicated that the dominant ion flowing through cell membranes was K^+. In fact, electrochemical gradient imbalance generated between the low [K^+] in the external recording solution and the cell cytoplasm along with voltage stimulations, increased the activation of voltage-dependent or –independent K^+ channels and permeability of these ions (p_K). Therefore, reversal potential (V_{rev}) approached a value of the most permeant ion at equilibrium, i.e the theoretical potassium equilibrium potential (E_K =-80 mV). Probability that K^+ ions would preferably pass through the membrane compared to other ions (Na^+, Cl^-, Ca^{2+}) was hence higher (p_K>>p_{Na}>p_{Cl-}) but not exclusive as these will still pass in lower amplitudes inducing minimal current contamination.

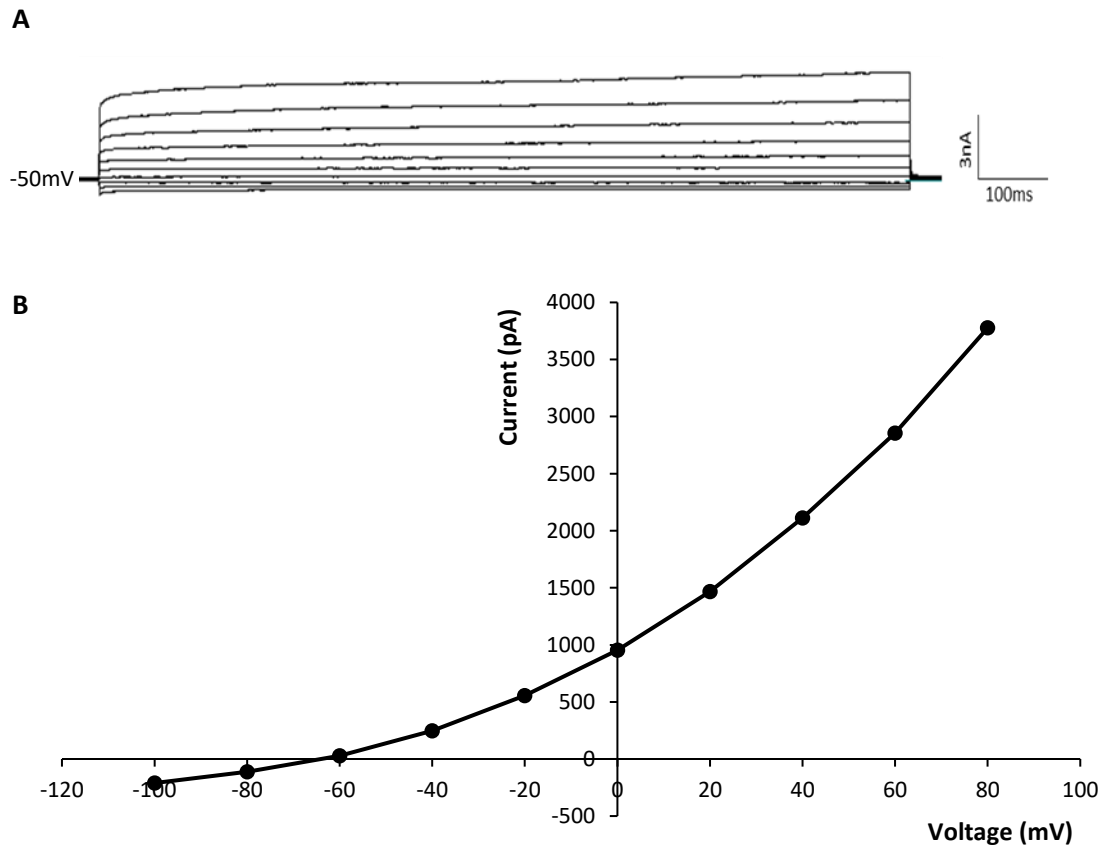

Figure 6. 3 COS-7 currents recorded at the whole-cell configuration during a voltage-clamp protocol and its corresponding I-V curve. A. Each current trace was generated upon a voltage–clamp protocol applied from -100 to +80 mV with 20 mV increments and recorded 5-10mins post-SE removal. Membrane potential was set to -50 mV and a strong outward rectification was mainly observed at positive voltage steps reaching a maximal value of ~4 nA at +80 mV. **B.** Current to voltage relationship was plotted as an I-V curve and equally, demonstrated a relatively strong outward rectification at +80 mV with a nearly absent inward rectification. Reversal potential was observed at -65 mV indicating that no current could flow through the membrane during this voltage stimulation.

To investigate the homogeneity of acquired current data in Figure 6.4A, a mean I-V curve representing the average whole-cell current values in response to each voltage step was plotted in Figure 6.4B. Similarly to Figure 6.3, recorded currents had a strong outward rectification at positive voltages, weak inward rectification at negative voltages and a reversal potential close to -65 mV. Steepness of the curve revealed a weak voltage dependence at positive voltages that may indicate an activation of voltage-dependent K^+ channels. Cell membranes express diverse populations of K^+ channels which are activated by multiple factors as stated in section 2.4 and amongst these, voltage stimulations. Therefore, mean rectification observed may represent multiple active ion channels and principally K^+ channels due to the solute composition of recording solutions and the application of a voltage protocol.

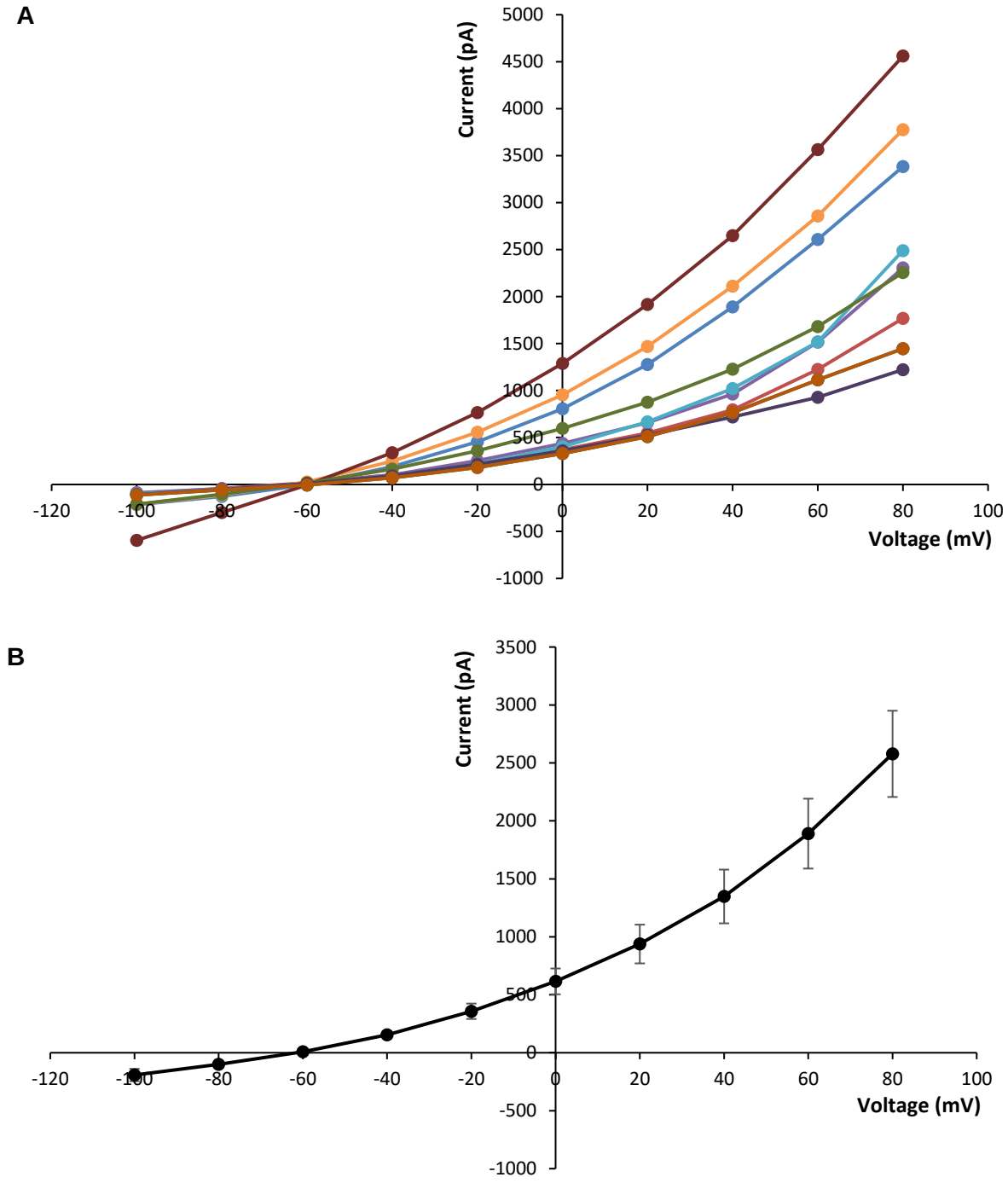

Figure 6. 4 Current to voltage relationship of multiple COS-7 recordings acquired at the whole-cell configuration. A. I-V curves (each colour represents a single cell) generated post-application of the voltage-clamp protocol in COS-7 cells (n=10) in gradient solutions provided by Nanion. All curves had a voltage-dependence at positive voltage steps and a reversal potential close to -60 mV **B.** Mean± SEM was calculated resulting in a mean I-V curve with a maximal current amplitude of 2500 pA at +80 mV and a strong outward rectification between +20 and +80 mV. A weak inward rectification could be observed between -65 and -100 mV and the overall curve slope was voltage-dependent at positive voltage-steps.

Finally, series or membrane (Rm) resistances along with Cm recorded in PatchControl were compared to published planar or conventional patch-clamp studies focusing in K^+ channels (Table 6.1) to identify if alignment can be achieved between the outputs of this study and earlier findings. In 2003, a group of researchers studied hERG channel in Chinese hamster ovary cells (CHO) at the whole-cell configuration on QPatch, a highly automated parallel-operating patch-clamp system (Kutchinsky, Friis et al. 2003). In 2005, Dubin, Nasser et al, characterised hERG channel at the whole-cell configuration both by planar (PatchXpress) and conventional patch-clamping in human embryonic kidney (HEK293) cells (Dubin, Nasser et al. 2005). In 2009, another study adopting the planar-patch clamp system Patchliner studied in HEK293 cells the Ca^{2+}-activated K^+ channel subunit 1.1 (KCa1.1) (Milligan, Li et al. 2009). These studies had comparable research interests as K^+ channels were characterised at the whole-cell configuration in HEK293 (analogous size with COS-7; ~20 μm diameter) or CHO cells. During planar patch studies, chip resistances ranged between 1.5-4 MOhm, which were similar to the ones used on the port-a-patch and suction pulses between -50 and -200 mBar for HEK293 cells and up to -600 mBar for CHO cells (Fertig, Blick et al. 2002, Kutchinsky, Friis et al. 2003, Li, Lu et al. 2017). Moreover, these experiments were performed in gradient solutions with 110-140 mM and 4-5 mM K^+ ions in internal and external recording solutions accordingly.

Rm acquired on planar systems had comparable values reaching 1.5-3.5 GOhm and revealing that the whole-cell configuration was established (Table 6.1). Rs values in the current study on the other hand were marginally lower than other planar or conventional published studies, suggesting that resistance between the chip and ground did not particularly interfere with currents elicited within cell membranes. Low R_s is considered as an advantage as, less electrical noise affected by the geometry of the pipette or air bubbles, poorly conducting solution and debris in the bath that would block the pipette tip, will contaminate acquired results. Cm values were also in close accordance with published studies, indicating that ions can cross COS-7 membranes faster than HEK293 cells and that the port-a-patch can effectively detect cell surface areas of the samples studied. Comparison of R_m, R_s and C_m values with published planar or conventional studies provided a seal of approval on acquired results as it showed that the whole-cell configuration could be established in COS-7 cells due to strong similarities in resistance and capacitance values.

Planar				
Cell type	**R_m (MOhm)**	**R_s (MOhm)**	**C_m (pF)**	**n**
COS-7 (TASK-5)	2-3500	2.76± 0.68	11.8± 0.45	82
CHO (hERG)	2-3000	<10	-	18
HEK293 ($K_{Ca1.1}$)	2000 ± 0.4	6.7 ± 0.5	12.3 ± 1.2	109
HEK293 (hERG)	710 ± 40	14 ± 1	17.4 ± 1.3	133
Conventional				
HEK293 (hERG)	1590 ± 80	8 ± 03	-	81

Table 6. 1 Comparison of membrane resistance (R_m), series resistance (R_s) and membrane capacitance (C_m) values between planar or conventional patch-clamp studies and results acquired within the study. Within each cell line TASK-5, the human *ether-a-go-go-* (hERG) potassium channel or the Ca^{2+}-activated K^+ channel subunit 1.1 (KCa1.1) were over-expressed and studied accordingly. All values are reported as Mean±SEM. Dashes represent absent C_m values that were not provided during the studies.

6.3 Establishment of the whole-mitochondrial configuration on the planar patch-clamp system

Electrophysiological characterisation of non-transfected mitochondrial currents was performed to establish control conditions that would subsequently be compared to currents recorded from organelles over-expressing TASK-5. These sets of control results allowed the determination of variations in current amplitudes/I-V relationship between organelles endogenously expressing TASK-5 and those over-expressing the channel.

To identify parameters that would lead to the whole-mitochondrial configuration in PatchControl, primary experiments were performed in recording solutions that were more applicable to cells (Table 3.3). This allowed to determine optimal pre-set parameters leading to the whole-mitochondrial configuration while designing the ionic composition of organelle recording solutions for the characterisation of mitoK^+ channels (Table 3.4). Preliminary patch-clamp trials revealed that pre-set parameters applied to COS-7 cells were not suitable for isolated mitochondria in suspension. In fact, forming and maintaining a gigaohm seal was challenging as suction pulses seemed to damage mitochondrial membranes and interrupt the software. Therefore, longer but lower in amplitude suction pulses were applied to attract the organelles towards the chip aperture. The following software parameters were thus optimised and presented as (light red: R<20 MOhm; 20mB), adjust pipette offset (dark red: -30mB), wait for cell (orange: R>20 MOhm; -40 to -60mB with 5mB increments), wait for seal (yellow: R>100 MOhm; -50 to -80mB with 10mB increments), improve seal 1 (dark green: R>500 MOhm; -60 to -90mB with 10mB increments), improve seal 2 (light green: R>1 GOhm; -120mB), maintain

whole-cell (blue: Cs>4 pF and Rs<40 MOhm; -100 to – 120mB with 5mB increments) leading to stable whole-mitochondrial configurations (Figure 6.5A).

Once optimal parameters were defined, it was important to repeat the experiments in symmetrical K^+ solutions (150mM) established according to published conventional patch-clamp studies that characterised K^+ channels in mitoplasts as previously described in Chapter 4 (section 4.6) (Rusznak, Bakondi et al. 2008, Kajma and Szewczyk 2012, Toczylowska-Maminska, Olszewska et al. 2014). Removal of F^- ions from the internal conventional recording solution prevented the gigaohm seal resistance establishment on the port-a-patch. Hence, stepwise substitution of Cl^- with F^- ions allowed to reach the gigaohm seal resistance and subsequently the whole-mitochondrial configuration. Corresponding I-V curves of mitochondrial currents elicited in Nanion (gradient) or symmetrical K^+ solutions are presented in Figure 6.5B. Stronger outward rectification is observed at positive voltage steps (between +20 and +80 mV) in gradient (60mM KF internal solution; round marker) compared to symmetric solutions. The electrochemical imbalance generated in gradient solution induced a larger movement of K^+ ions from the mitochondrial matrix to the external solution, resulting in a maximal current generation of ~1 nA at +80 mV. Reduced overall [K^+] (120mM) in symmetrical solution with 80mM KF internally and 40mM KCl externally, resulted in the generation of smaller outward currents (~200 nA) compared to mitochondria bathed in 150mM K^+ solutions (~600 nA) at +80 mV (Figure 6.5B). Complete substitution of Cl^- with F^- ions did not induce significant current amplitude or I-V relationship alteration. As current amplitudes and I-V curve relationships recorded between symmetrical K^+ solutions either containing 150 or 80mM KF internally were comparable, a decision to opt for an internal solution containing lower [KF] was taken to minimise any effect on mitochondrial physiology and ionic transports.

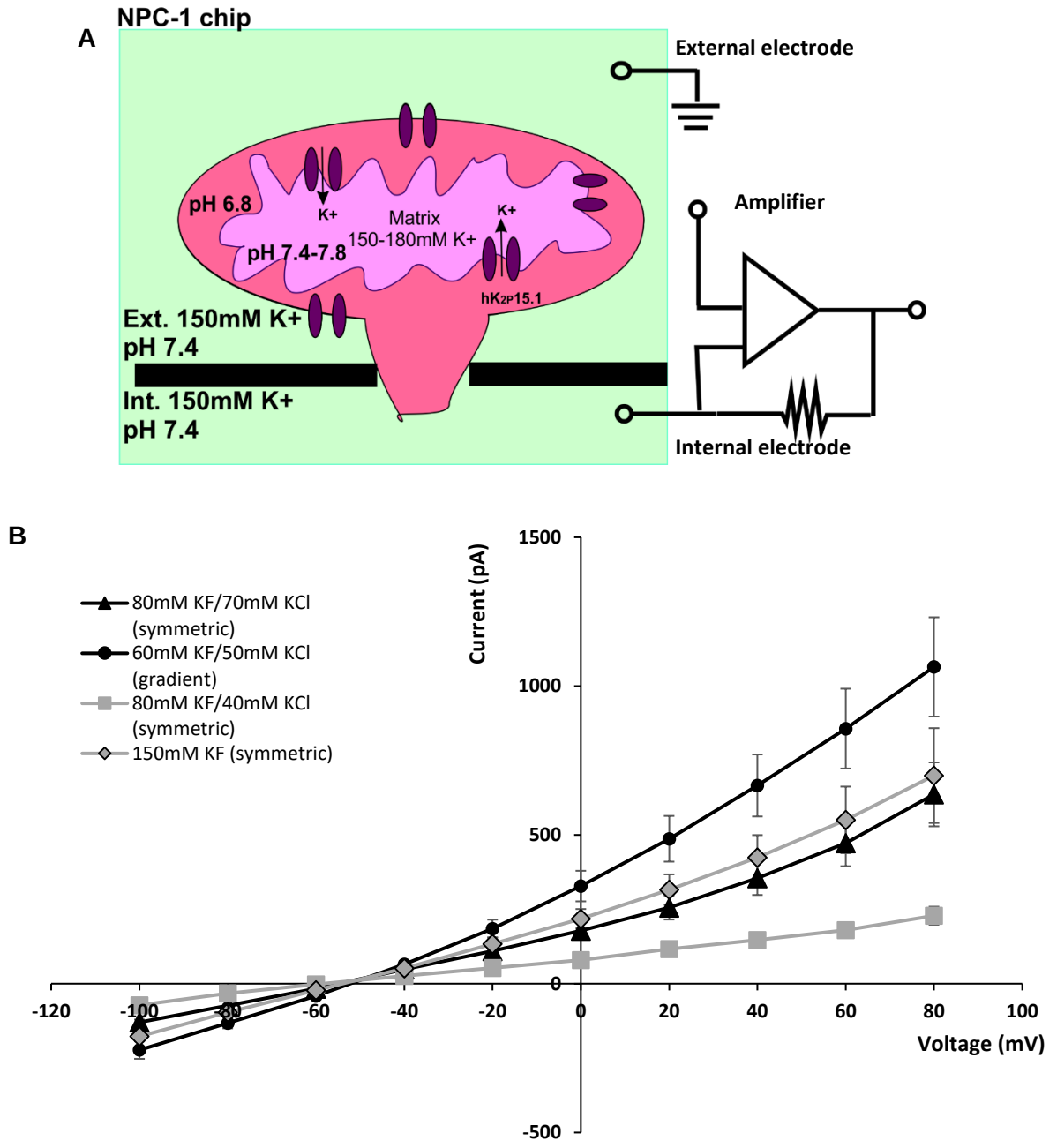

Figure 6. 5 Mitochondrial current recordings on the port-a-patch. A. Illustration of a single mitochondrion bathed in symmetrical K^+ solutions with its suggested whole-mitochondrial configuration establishment on a NPC-1 chip. Progressive application of negative pressure by the suction unit would induce mitochondrial migration towards the chip aperture. Short pulses of negative pressure would then rupture the OMM (dark pink) and result in the whole-mitochondrial configuration. Mitochondrial matrix (light pink) [K^+] and pH were reported to range between 150-180mM and pH7.4-7.8 accordingly, in comparison to the inter-membrane space which is more acid (pH 6.8). Ion or K^+ channels are illustrated on the outer or inner MM in purple, demonstrating the direction of K^+ ion movement. **B.** Comparison of I-V relationship and current amplitudes of mitochondrial recordings isolated from HeLa cells and bathed symmetric (diamond marker) or gradient solutions as shown in the legend. All values are reported as Mean±SEM for n=5-12 organelles.

Mitochondrial current traces elicited during each voltage stimulation step were recorded in optimal symmetrical solutions and illustrated in Figure 6.6A. Compared to whole-cell recordings, inward rectification between -100 and -50 mV was more pronounced while the outward current was 3-4 times lower in magnitude (1-1.5 nA). Current to voltage curves

recorded from multiple whole-mitochondrial seals are shown in Figure 6.6B, together with their respective mean I-V curve (Figure 6.6C). What is more, steepness of the I-V curve was less important compared to whole-cells suggesting that OM membranes express fewer voltage-dependent ion channels. Stronger inward rectification during negative voltages (~250 pA) on the other hand, indicated that Ca^{2+} uptake could have occurred upon administration of seal enhancer solution as, mitochondria act as Ca^{2+} buffers when external [Ca^{2+}] rises (Williams, Boyman et al. 2013).

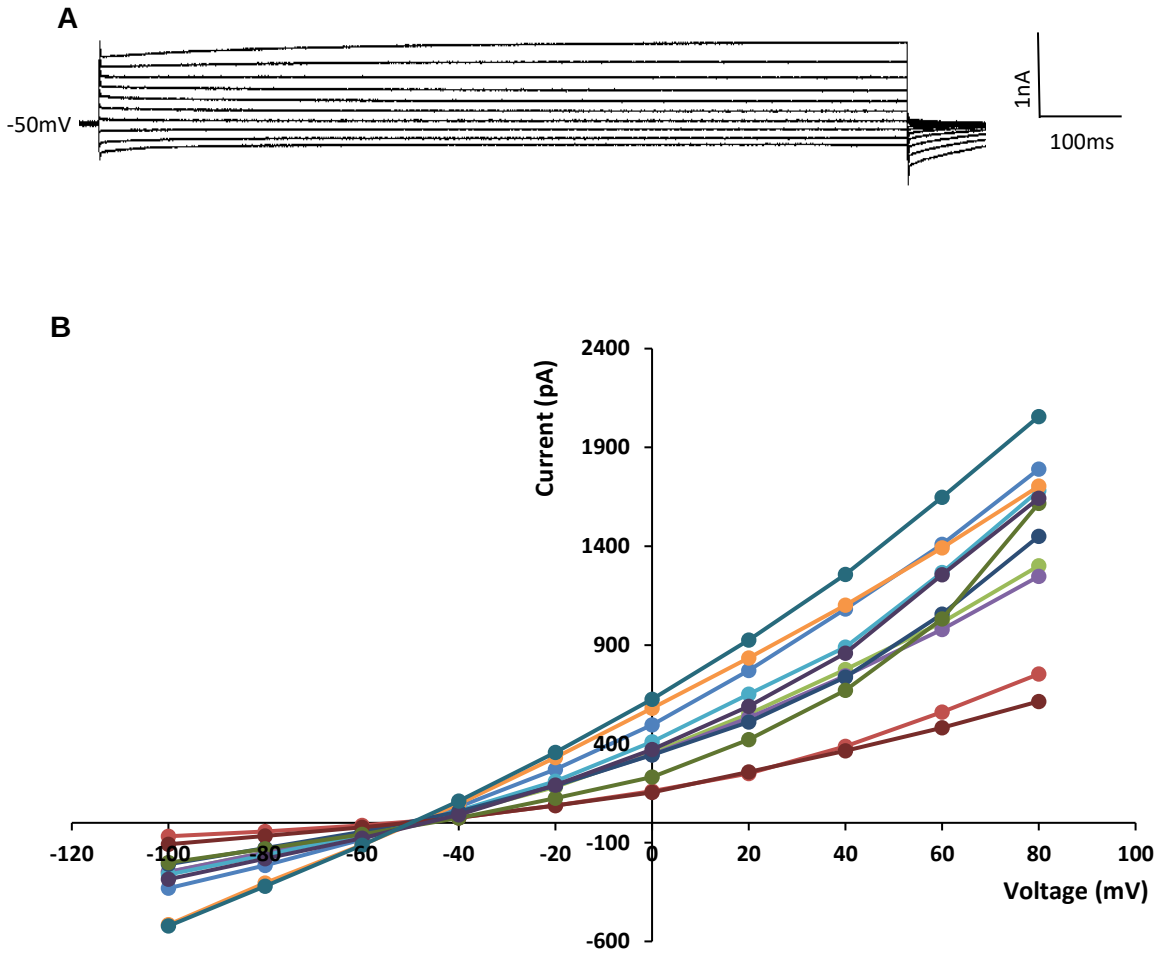

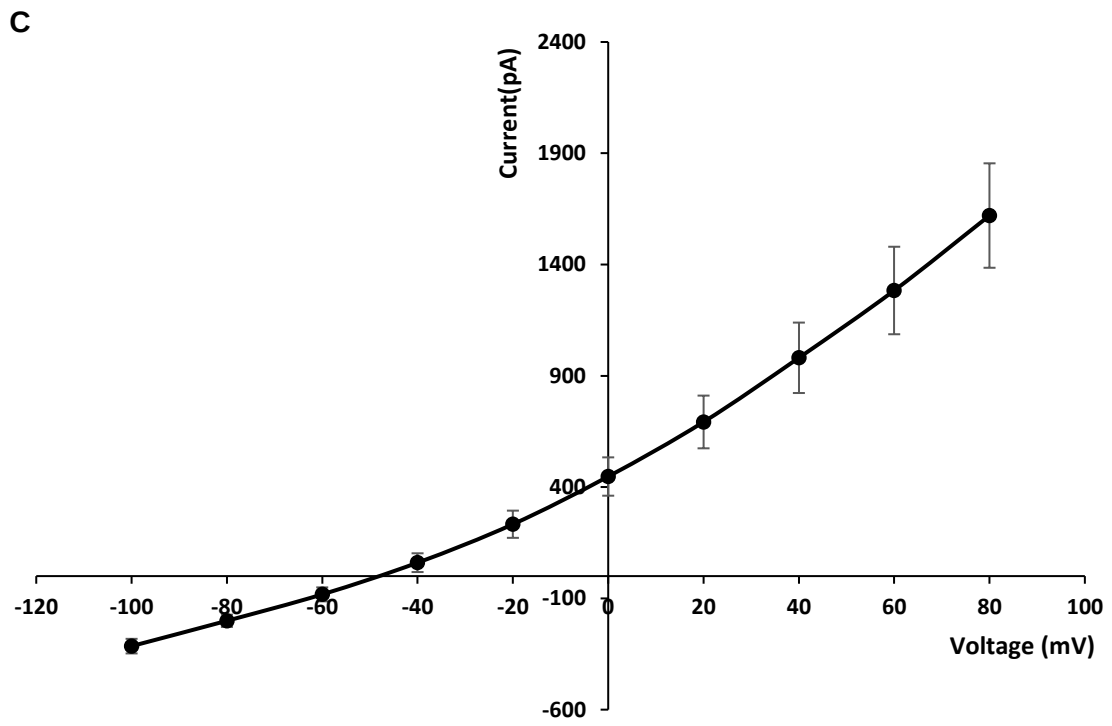

Figure 6. 6 Whole-mitochondrial recordings in symmetrical K^+ solutions (150mM) with their corresponding I-V curves. A. Current traces recorded in a single mitochondrion isolated from HeLa cells in symmetrical solutions post-application of the voltage-clamp protocol. Membrane potential was set at -50 mV and maximal outward current reached 1 nA at +80 mV. **B.** Current to voltage curves recorded from n=11 mitochondria isolated from HeLa cells. Reversal potential was observed at -50 mV with variable outward rectifying currents ranging from 400 pA to 2000 pA. **C.** Mean I-V curve of recordings shown in B denotes a small voltage-dependence and a higher inward rectification compared to whole-cell recordings. All values are reported as Mean±SEM.

Another key experimental output to assess and evaluate is V_{rev}. In theory, V_{rev} in symmetrical K^+ solutions should be 0 mV and according to the GHK equation equal to -5 mV. Remarkably, during experiments in optimal solutions I-V curves drift towards higher (negative) values, with V_{rev} = -45 mV. A possible explanation could be that the highly hyperpolarised mitochondrial matrix at rest ($\Delta\psi_m$ between -180 and -200 mV) would have been depolarised at more positive voltage steps hence becoming more positive (Perry, Norman et al. 2011). This would result in a more positively charged mitochondrial matrix that will tend to drive $\Delta\psi_m$ back to its negatively charged state by expulsing positively charged ions from matrix or collecting negatively charged ions. Moreover the V_{rev} shift could be linked to a fluoride and chloride ion concentration imbalance. Despite demonstrating that F^- ions did not affect hERG V_{rev} in HEK293 cells, the effect of halide ions on mitochondrial membranes remains to date elusive and could be considered as a potential curve shift factor (Zeng, Penniman et al. 2008).

Lastly, it was crucial to compare acquired with published conventional patch-clamp data in order to identify similarities, but also differences, in Rs and Cm between the two approaches. Published studies aiming to characterise OMM channels while establishing the whole-cell mitochondrial configuration are currently restricted as studies usually adopt single-channel

approaches or do not acknowledge seal resistances or capacitances within their manuscripts. For the time being, whole-mitochondrial seals established on the planar patch-clamp system during this study had R_m of 710 ± 40 MOhm (n = 140), R_s: 7 ± 1 MOhm (n = 132), Rseal: 1.9 GOhm and C_m: 3.4 ± 1.3 pF (n = 133).

6.4 Potassium currents elicited at the whole-mitoplast configuration

To study K^+ currents elicited from IMM channels, identical pre-set parameters together with 10-15 MOhm resistance chips were initially used on isolated mitoplasts. Preliminary experiments however revealed that the 'wait for seal' (yellow) step duration was problematic. More specifically, automatic termination of the experiment occurred due to failure to establish gigaseals on mitoplast membranes within the time lapse set up. The step duration was hence extended to 10 minutes. Apart from this modification, the remaining parameters were identical to those applied on mitochondria and indeed resulted to a whole-mitoplast formation (Figure 6.7A).

Current traces recorded post-stimulation with the voltage protocol had similar current amplitudes (Figure 6.7B) with those recorded in mitochondria, reaching a maximal outward current of 1 nA (at +80 mV) and a mean inward rectification of ~200 pA at -100 mV (Figure 6.7C). Similarly to mitochondrial currents, the presence of two current populations (up to 2 nA or less than 1 nA) was also observed during mitoplast recordings, reinforcing previous findings that larger mitochondria could have greater IMM surfaces and thus a larger expression of ion channels (Figure 6.7C).

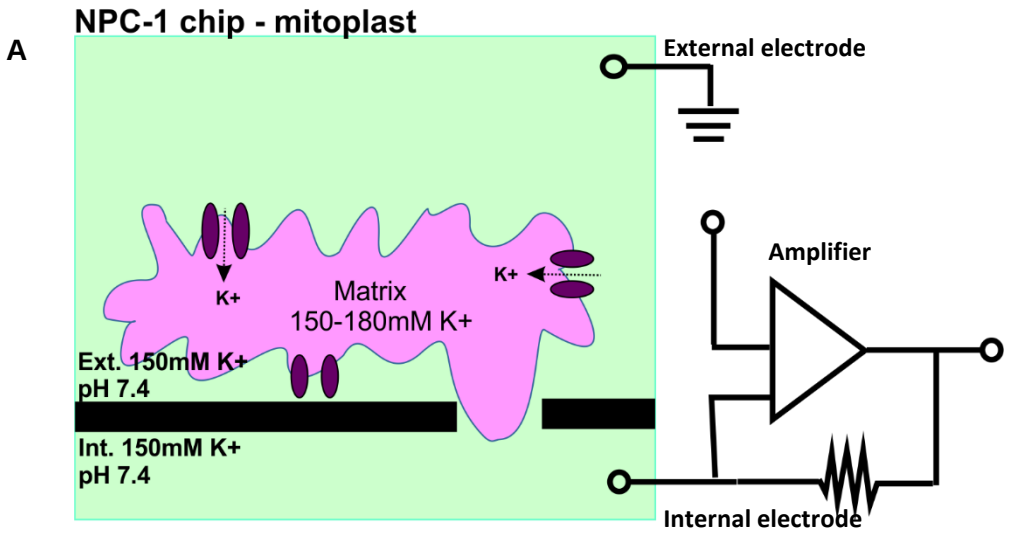

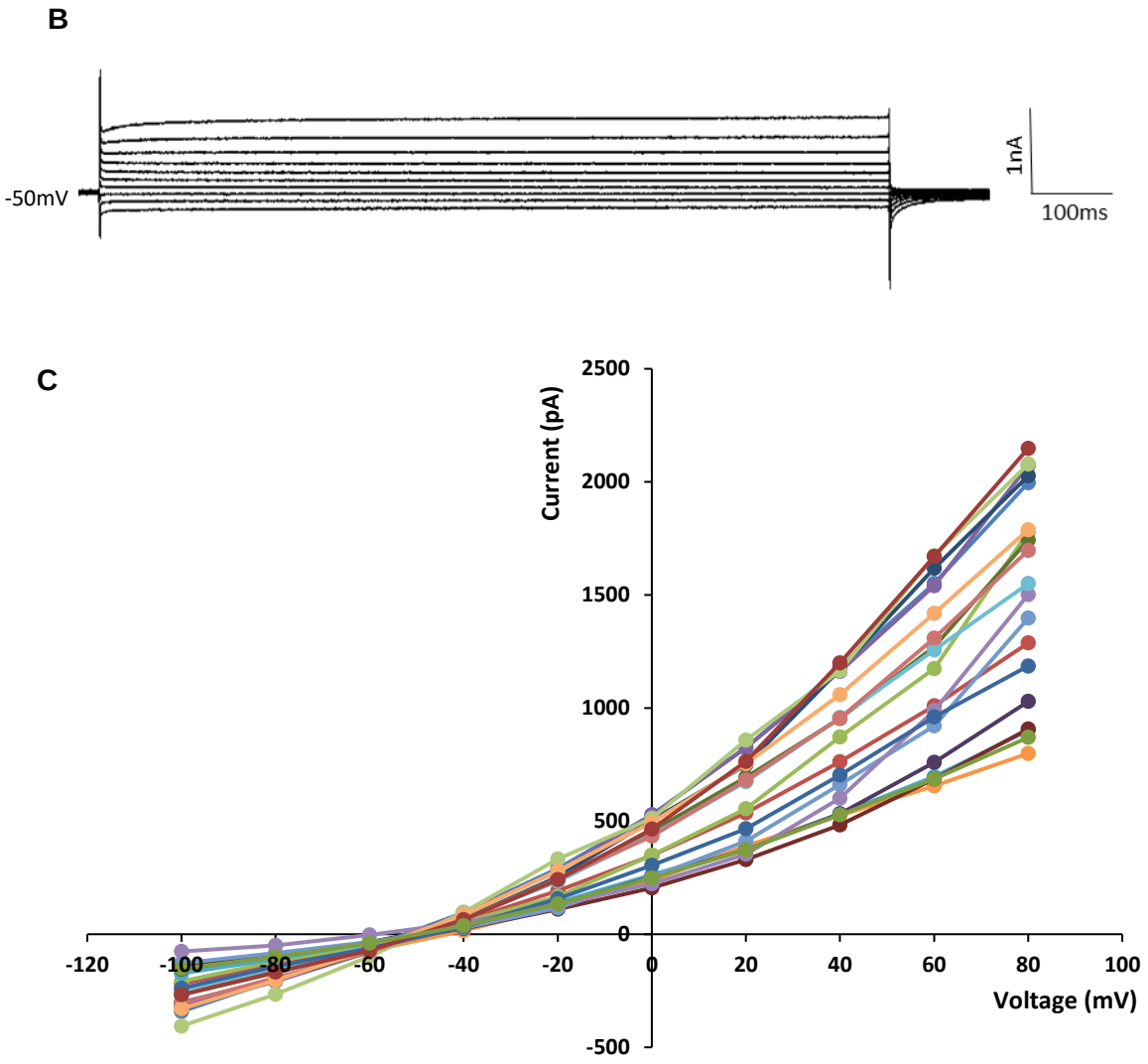

Figure 6. 7 Whole-mitoplast current recordings in symmetrical solutions. A. Illustration of a whole-mitoplast configuration established between the IMM and the chip aperture in symmetrical K^+ solutions. Matrix [K^+] along with the direction of K^+ transport across TASK-5 (purple) are indicated. **B.** Current traces generated post-voltage step stimulations reaching a maximal current value of ~1 nA at +80 mV. **C.** Individual mitoplast current to voltage curves (n=19) showed a voltage-dependence at positive voltage stimulations.

Mean I-V curves of several mitoplast currents presented in Figure 6.7C were calculated and compared to whole-mitochondria mean curve (Figure 6.8A). Outward current amplitudes recorded in mitoplasts are larger (by 70 pA) than mitochondria at +80 mV nevertheless, results are considered non-significant (p=0.93) due to an error bar overlap (Cumming, Fidler et al. 2007) that indicates that mitochondrial and mitoplast currents are in fact not statistically different. Another curve characteristic deduced from the I-V relationship was V_{rev} value (close to -45 mV) (Figure 6.7C and 6.8A), a shift to the curve that remains to date not characterised, but could be related to the presence of F^- ions in the internal solution and/or mitochondrial membrane depolarisation. Although expectations would be that mitoplast current amplitudes

would be lower than mitochondria due to OMM rupture a key question to address in this chapter is whether the experimental output supports that:

- the IMM is more electrochemically active than the OMM and thus, explains the similar amplitudes elicited from membranes, or
- currents were recorded from organelles with a larger surface area that generate stronger currents, or
- the OMM is partially stripped off and gigaseals are formed on outer membrane remainders instead of the IMM.

Mean I-V curve characteristics of whole-cell and whole-organelle such as current amplitudes, curve rectifications and V_{rev} values were compared (Figure 6.8B). Highest outward current elicited by COS-7 cells was 3-4 nA at +80 mV compared to organelles (1 nA). I-V relationship also indicates that plasma cell membranes are more voltage-dependent than organelles due to a more rectifying curve. In fact, current recordings in gradient solutions mainly stimulated K^+ channels due to its close V_{rev} value (-65 mV) to the hypothetical K^+ equilibrium (-80 mV). The slope of organelle curves exhibit a smaller voltage-dependency and interestingly, the curve shift towards more positive ($p<0.05$) (Figure 6.8 C) values suggests that mitochondrial $\Delta\psi_m$ was altered due to the reasons defined in section 6.3.

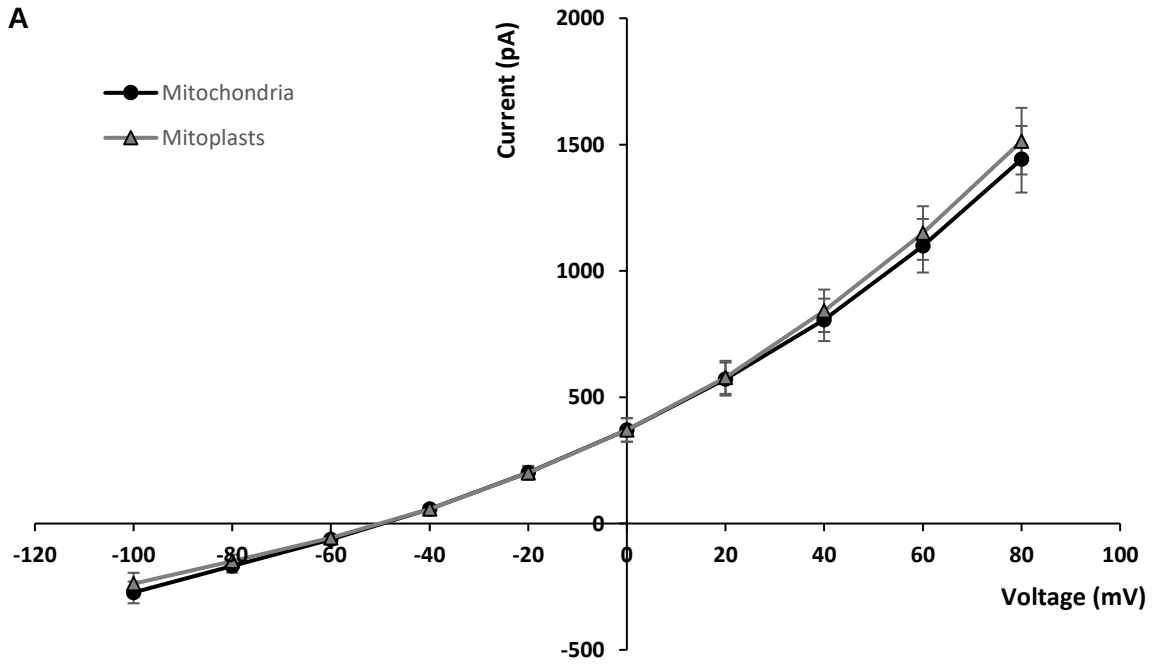

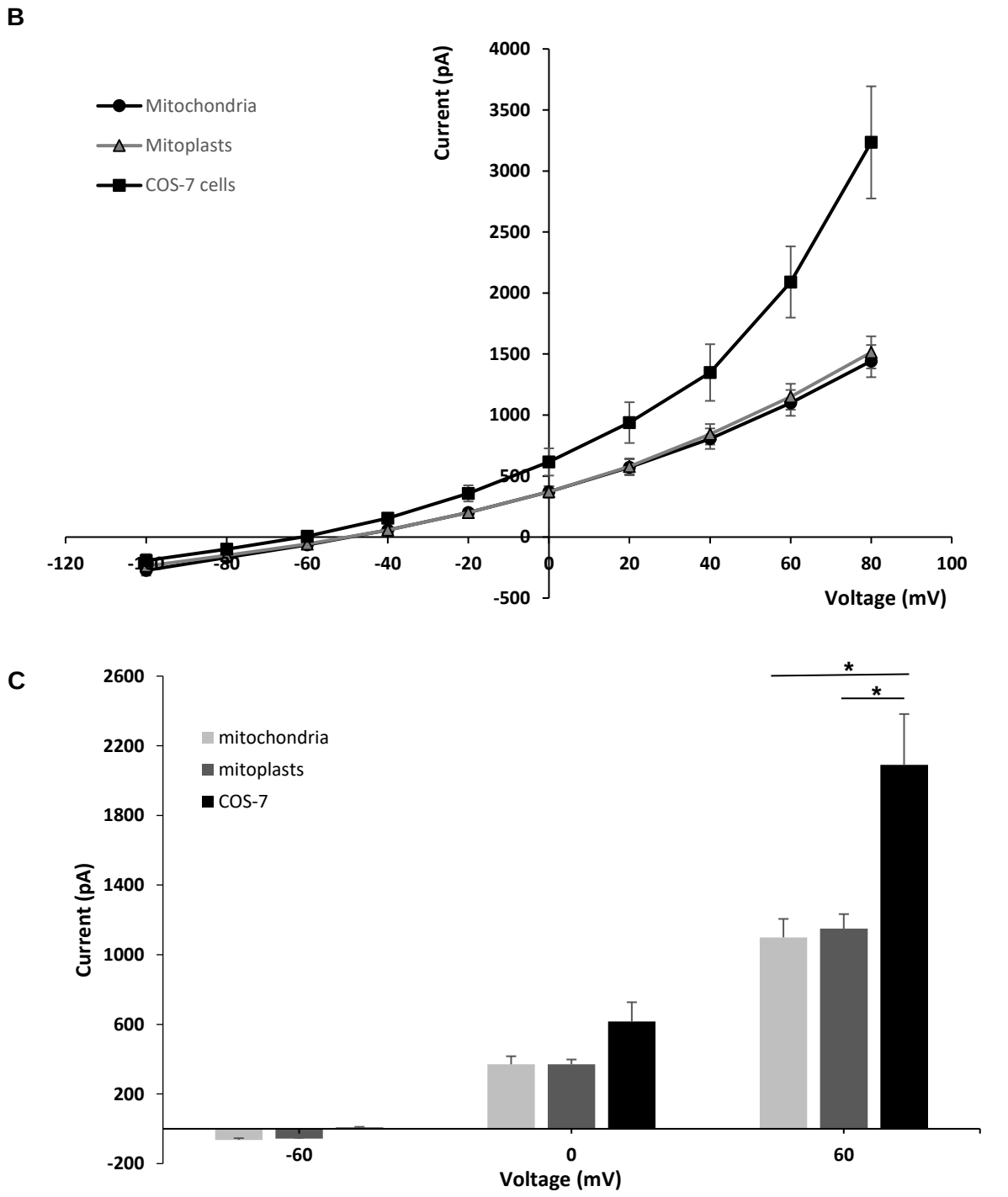

Figure 6. 8 Current to voltage curves acquired within COS7 cells and organelles isolated from HeLa cells. A. Mean current amplitude and curve kinetics had identical characteristics between isolated mitochondria (n=11) and mitoplasts (n=19) in symmetrical K^+ solutions. Reversal potential was close to -45 mV and outward currents reached a maximal value of 1500 pA at +80 mV. **B.** Comparison of mean currents acquired in COS-7 cells (n=9) and isolated organelles shown in A. **C.** COS-7 current amplitude was significantly ($p<0.05$) different at positive voltages (+60 mV) compared to organelles. All values are reported as Mean±SEM and significant differences obtained after 1-way ANOVA are indicated by asterisks with *$p<0.05$.

Lastly, Rs and Cm values of acquired data were compared to published conventional patch-clamp studies performed on mitoplasts isolated from COS-7, mouse or rat cardiomyocytes at the whole-mitochondria configuration with Rm>1 GOhm (Table 6.2) (Kirichok, Krapivinsky et al. 2004, Fieni, Lee et al. 2012, Joiner, Koval et al. 2012). Results suggest that Rs values extracted using the adopted methodology in this study, were lower than conventional patch-clamp studies. The difference could be attributed to higher pipettes resistances used during conventional experiments (25-50 MOhm) compared to NPC-1 chips but also to Rs threshold values defined in PatchControl. Membrane capacitance values were comparable to conventional studies. Results indicate that the membrane surface area and dielectric properties of mitoplast membranes could vary between 0.3 and 9 pF, correlating with previous findings that mitochondrial ultra-structure differs within samples/tissues (Kirichok, Krapivinsky et al. 2004, Fieni, Lee et al. 2012, Joiner, Koval et al. 2012).

Conventional		
Cell type	**R_s (MOhm)**	**C_m (pF)**
COS-7	30-60	0.6
Rodent	-	5-9
cardiomyocytes	40-80	0.36-1.31
Planar		
COS-7/ HeLa (n=74)	3.3 ± 0.42	7 ± 0.6

Table 6. 2 Series resistance (R_s) and membrane capacitance (C_m) values recorded during conventional and planar patch-clamp studies on isolated mitoplasts from COS-7 cells or mouse cardiomyocytes at the whole-mitoplast configuration. Dashes represent a unreported R_s values that were not provided during the study. Values are reported as Mean±SEM.

Comparison of R_s and C_m values between cells and organelles also reveals that reaching the whole-cell/organelle configuration on a port-a-patch generated lower R_s contamination especially during organelle current assessments, in comparison to conventional patch studies. This indicates that NPC-1 chips enclosed in a Faraday cage (Appendix 2) are better insulators of electromagnetic waves than classic glass pipettes demanding less R_s compensation. As expected, C_m values show that the surface area of COS-7 cells is larger than organelles. Notably, mitoplast C_m values are greater than mitochondria suggesting that currents were recorded from mainly large organelles but also because the IMM surface area is greater than the OMM due to its folding into cristae (Alberts 2014)

6.5 Conclusions

During the last 20 years the emergence of planar patch-clamp technology made automatic current recordings possible with stable gigaseal and whole-cell configuration establishment as well as solution exchange during pharmacological assays (Chen, Zhang et al. 2009). Characterisation of reconstituted ion channels in giant unilamellar vesicles (GUVs) is also feasible on the port-a-patch where suction pulses are highly controlled to avoid membrane rupture or noise contamination is monitored during single-channel recordings (Sondermann, George et al. 2006). Nevertheless, planar systems have also their limitations requiring comparison with conventional patch-clamp data. During electrophysiological characterisation of TASK5-eGFP for example, visualisation of transfected cells is not possible, making it difficult to interpret if the transfection efficiency is homogeneous or not. Therefore, such experiments are either performed on conventional patch-clamp rigs equipped with a microscope or fluorescent samples are sorted by FACS prior undergoing planar patch-clamp experiments.

6.5.1 Ionic currents elicited in COS-7 cells

In this study, planar patch-clamping was initially performed in COS-7 cells using PatchControl software and solutions provided by Nanion. A key objective of these preliminary trials was to identify ionic currents and more specifically K^+ currents elicited during the whole-cell configuration.

To reach the whole-cell configuration, pre-programmed parameters controlling the amplitude of pressure pulses, seal resistances and timing of the whole experiment in PatchControl were optimised. To confirm that the experimental procedure and pre-set parameters led to whole-cell configuration, acquired K^+ currents were compared to whole-cell conventional or other published planar results. Despite limited availability of published studies focusing on K^+ channel characteristics at the whole-cell configuration on planar rigs (PatchXPress or Patchliner being controlled by PatchControl software), several conventional studies were identified and compared to acquired data to investigate potential similarities. These studies focused on characterising hERG and KCa1.1 channels in CHO or HEK293 cells, which had comparable cell diameters (10-20µm) with COS-7 cells (Kutchinsky, Friis et al. 2003, Dubin, Nasser et al. 2005, Milligan, Li et al. 2009). Published results had analogous Rm, Rs and Cm values with ones extracted from experiments performed on the port-a-patch, endorsing the accountability of the approach. Current amplitudes were found to be similar to published reports at positive voltage steps (nA range) and V_{rev} value was in accordance with values predicted using the GHK equation for K^+ ions, demonstrating a preference for K^+ ion transport across COS-7 membranes when bathed in solutions provided by the manufacturer.

A key parameter of the experimental methodology was the removal of the seal enhancer solution prior to reaching the whole-cell configuration. The seal enhancer contains high [Ca^{2+}] and is suggested to enhance gigaohm seal formation during its interaction with F^- ions present in the internal solution. During the 'wait for seal' step, seal enhancer solution is added to the external solution; Ca^{2+} and F^- ions then form a highly insoluble precipitate between the cell membrane and the chip edges resulting in a quicker, tighter and more stable gigaseal formation with reduced current leakage. These remarks are in accordance to experiments presented in Chapter 4 as complete removal of KF from internal solution did not lead to successful gigaseal formation. Large extracellular [Ca^{2+}] however, can activate voltage-sensitive Ca^{2+} channels during voltage-clamp experiments. As cytoplasmic [Ca^{2+}] is usually lower (nanomolar scale) than the seal enhancer concentration (mM), the difference in [ion] could activate Ca^{2+}-activated channels if not replaced with external solution before reaching the whole-cell configuration (McDonough and Button 1989, Hardingham, Chawla et al. 1997). Ion channels with Ca^{2+}-dependent activation characteristics such as L-type channels are stimulated by strong extracellular [Ca^{2+}] or between -60 mV and +10 mV voltage steps (Lipscombe, Helton et al. 2004, Lacinova 2005). Blocking or limiting L-type or other Ca^{2+} channels with nifedipine or EGTA, a Ca^{2+} chelator could have been done if inward rectification was more significant. Notably, currents were recorded 5-10mins post-removal of seal enhancer solution, in order to ensure the closure of potentially stimulated Ca^{2+} channels. Nevertheless, the process does not totally exclude Ca^{2+} or Na^+ induced-current contamination, as the ions are present in the external solution of mitochondrial or cell solutions accordingly.

6.5.2 Mitochondrial currents

Initial experiments on isolated mitochondria were performed in recording solutions and pre-set parameters that were identical to COS-7 recordings. The elapsed time for the mitochondrial gigaseal formation was found to be longer than cells and applying suction pulses up to -200 mBar were found to induce mitochondrial membrane rupture. This was deduced from the dramatic seal resistance reduction and inability to re-attain the gigaohm seal configuration during recordings. Therefore, stepwise negative pressure reduction to -120 mBar is considered most appropriate to break through organelle membranes and maintain the whole-mitochondrial configuration for several minutes. The time-out session was also extended as the gigaseal formation required longer suction pulses to attract mitochondria in suspension towards the chip aperture.

Despite the strong generation of outward K^+ currents from mitochondria bathed in gradient solutions provided by the manufacturer, these conditions were considered hypotonic (4mM) compared to mitochondrial matrix [K^+] (150mM). Matrix swelling followed by loss of organelles ultra-structure was hence highly probable explaining perhaps, why previous

studies adopted symmetrical [K^+] solutions with mitochondrial matrix content. When the ion concentration is equal on both sides of a membrane, transport and current generation for that ion is expected to be null at rest. During a voltage clamp protocol however, voltage-sensitive ion channels are stimulated generating ionic currents even in symmetrical conditions. Leak currents, are also known to be constantly active (even at 0 mV) in order to maintain a stable resting Vm. Therefore, the symmetrical conditions in which the study was carried out, enabled the observation of ionic currents elicited by active K^+ channels. Nevertheless, other factors such as change in $\Delta\psi_m$, [H^+ or Ca^{2+}] and pH could also influence the activity of mitochondrial channels and hence the possibility that other types of ion channels were activated is not excluded.

To date, conventional patch-clamp studies adopting the whole-mitochondrial configuration are limited as most organelle ion channels are characterised at the single-channel level. This observation is primarily a result of the limited distance (~20nm) between outer and inner MM which thus increases the possibility of piercing the IMM while trying to reach the whole-mitochondrial configuration with a glass pipette (Kühlbrandt 2015). Despite a lack of information about whole-mitochondrial R_s or C_m values, plotting I-V curves aided to graphically interpret mitochondrial biophysical characteristics such as current amplitudes, voltage-dependences and determine which ions are primarily transported across organelle membranes by V_{rev}. Acquired data suggest that mitochondrial channels generate weaker (pA range) and less voltage-dependent currents than cells (nA range). Moreover, outward currents are mostly found to be generated as a result of mainly K^+ channels activation or other positively charged ions leaving the mitochondrial matrix as a result of voltage- channels' activation. K^+ ions can freely shuttle across the OMM through VDAC and up to two-thirds of the proton leak is attributable to the ANT where positively charged H^+ enter the matrix (Brand, Pakay et al. 2005).

Larger inward rectification compared to COS-7 cells at negative voltages conversely could be related to an increased Ca^{2+} uptake within the matrix followed by expulsion from transporters as mitochondria are recognised as Ca^{2+} 'suppliers' of the cell (Williams, Boyman et al. 2013). During brain and heart ischaemia for example, significant increase in cytoplasmic [Ca^{2+}] (mM range) induces mPTP activation and uptake of Ca^{2+} within the mitochondrial matrix, resulting in membrane potential depolarisation, cessation of ATP synthesis, inhibition of respiration and large production of reactive oxygen species (ROS) (Turrens 2003).

In addition, a shift of V_{rev} value which was significantly different from predicted GHK equation was observed. Under symmetrical K^+ solutions, predicted V_{rev} should be close to 0 mV. During experiments however, V_{rev} was found to converge to -45 mV, indicating that an

electrochemical force was driving K^+ equilibrium towards higher negative values. If Ca^{2+} was the only permeant ion transported across mitochondrial membranes, its calculated reversal potential would be positive (+60 mV). This further implies that positively charged Ca^{2+} ions would move down their concentration gradient towards mitochondrial matrix as, extra- and intra-mitochondrial [Ca^{2+}] were in the mM and nM ranges respectively. A parameter that could have affected V_{rev} could be the depolarisation of mitochondrial membrane upon application of more positively charged voltage steps compared to $\Delta\psi_m$ values at rest (-180 mV to -200 mV). Elevated Ca^{2+} uptake, ATP depletion and mitochondrial depolarisation are conditions that could have impaired organelles and promoted the opening of mPTP, VDAC leading to programmed necrosis (Webster 2012). Alternatively, the ionic imbalance concentration generated between F^- and Cl^- ions could be responsible for the curve shift. Despite not having identified a correlation between mitochondrial membrane depolarisation and F^- ions during planar patch studies in mammalian cells, the effect of halide ions remains unclear. Presence of F^- ions in internal solution could have enhanced membrane depolarisation by passing through VDAC and activating anion channels expressed in the IMM as Cl^- and F^- ions have similar atomic radius sizes allowing the later to pass through mitochondrial membranes (Clark 2015). Electrical characterisation of mitochondrial anion channels is currently limited (section 2.12.3), restricting our understanding in anion transport and physiological consequences during impaired conditions. Further lines of investigation associated to the physiological features of mitochondrial anion channels will aid to enlighten the effect of halide ions on organelles.

6.5.3 Mitoplasts currents

Mitoplast K^+ currents recorded in symmetrical K^+ conditions required pre-set parameters similar to ones used in mitochondrial experiments to reach the whole-mitoplast configuration. The only parameter that was in fact modified was to the 'wait for seal' step where its time-duration was extended to 10 minutes (compared to 5 minutes for mitochondria). This observation can be attributed to the marginally less dense structure of mitoplasts due to a partial loss of OMM (Fieni, Bae Lee et al. 2012) and thus anticipated longer time for mitoplasts to migrate towards the aperture upon suction application.

Plotting and comparing mean I-V curves between mitoplast and mitochondrial currents revealed that outer and inner MMs responded to voltage step stimuli in analogous ways. This observation may have two possible explanations; either the OMM was perforated during several mitochondrial experiments and ionic currents were recorded from channels expressed in the IMM or, the ionic transport in the OMM is limited and/or negligible compared to IMM metabolic and energy production processes. In fact, it has previously been proposed that most ion, electron and lipid transports, the Krebs cycle and ATP synthesis

(Zoratti, De Marchi et al. 2009) occurs within the IMM, suggesting that the second hypothesis could be more reasonable. During conventional patch-clamp experiments, OM residual membranes (caps) can be visualised and avoided. During planar approaches however, samples cannot be visualised and therefore based on Rm, Rs and Cm values seal characteristics are assessed and provide additional information on the whole-mitoplast configuration. Despite not having the advantage to observe patched mitoplasts, gigaseal formation on the IMM was considered successful as it is doubtful that high-resistance seals can be maintained on OMM remnants. Comparing Rs and Cm values between acquired and conventional published studies also allowed to demonstrate that acquired data were recorded on IMM and that the port-a-patch is a valuable system to study mitochondrial currents. Rs values recorded on the port-a-patch were lower than conventional studies. This difference may be related to the initial pipette resistances in conventional patch studies that had higher (25-50 MOhm) threshold resistances than NPC-1 chips (10-15 MOhm). Mitoplast Cm values conversely, were smaller than cells, demonstrating that intracellular organelle membranes with smaller surface areas were patched. Variations between mitoplast Cm values may be linked to the dynamic morphology of mitochondria undergoing highly co-ordinated processes such as fission (division of a single organelle into two or more independent structures) or fusion (the opposing reaction) resulting in surface alterations (Scott and Youle 2010). Therefore, wide Cm values, could suggest mitochondrial length alterations (shift between fission and fusion rates) that are influenced by metabolic and pathogenic conditions inside mitochondria or their external environment.

Interestingly, mitochondria and mitoplast inward current amplitudes and V_{rev} were analogous. Calcium uptake was initially considered to result from a single transport mechanism mediated by MCU as it was shown to be the dominant channel in the IMM (Williams, Boyman et al. 2013). As stated in section 2.12.2, Kirichok et al., proposed that MCU conductance saturated at high [Ca^{2+}] (millimolar range), was largely open when $\Delta\Psi_m$ = −200 mV and could be found at its closed state when $\Delta\Psi_m$ reached −80 mV (Kirichok, Krapivinsky et al. 2004). Isolated mitoplasts during planar experiments were bathed in solutions containing 100μM Ca^{2+} and were patched between -100 and +80 mV, suggesting that MCU channel might be at its closed and inactive state during the studies. Equally to MCU, the activity of the rapid mode uptake RaM channel could also have been compromised as it was shown that the channel was closed within [Ca^{2+}] larger than 100nM (Sparagna, Gunter et al. 1995). As external [Ca^{2+}] could reach the mM range when seal enhancer was added to the external solution, the probabilities of MCU and RaM closure increased. Therefore, other distinctive mitochondrial Ca^{2+} uptake pathways including the voltage dependent Ca^{2+} channels (mCa1 and mCa2) or RyR could be alternative ‘doors’ for Ca^{2+} uptake (section

2.12.2). These channels were active during voltage stimulations close to -100 mV for mCa1 and mCa2 or between -30 and +20 mV for RyR (Michels, Khan et al. 2009) (Altschafl, Beutner et al. 2007). Lastly, despite an enhancement of seal formation and maintenance of a gigaohm resistance due to an interaction between F^- with Ca^{2+} ions, the effect of halide ions on IMM channels conductance remains elusive and further research needs to be undertaken to clarify the curves shift.

To understand if OMM was stripped off the organelles and K^+ currents were characterised at the whole-mitoplast configuration, application of blockers targeting IMM channels helped to detect changes in current amplitudes between mitochondria and mitoplasts (Chapter 7). Even though, blockade of K^+ channels was mainly performed to study residual currents generated from background channels such as TASK-5; it also allowed to determine if IMM were patched.

Chapter 7

TASK-5, a functional mitochondrial channel

7.1 Introduction

Work to this point was to optimise conditions to enable the successful recording and analysis of TASK-5 current within the IMM using a planar patch-clamp system. This chapter presents data that validates both the characterisation process and the functionality of the channel. To focus on the channel of interest and determine if TASK-5 elicits K^+ currents at the whole-mitoplast configuration, it was imperative to identify conditions that would minimise current contamination from other IMM channel populations and most importantly, from TASK-3. Based on RT-PCR and immunocytochemistry experiments performed by members of the O'Kelly group, model cell systems in which TASK-3 was not endogenously expressed and therefore, not considered as a potential current contaminant, were identified. Within this study, the activity of several K^+, Ca^{2+} and anion channels along with ionic pumps were inhibited by applying five different channel blockers on isolated organelles. The selection of mitochondrial channel blockers was grounded on previously published studies where the IC_{50} and IC_{100} inhibitory concentration of each blocker was identified by patching isolated mitochondria or mitoplast membranes at the single-channel configuration on conventional patch-clamp systems (Rusznak, Bakondi et al. 2008, Kajma and Szewczyk 2012, Toczylowska-Maminska, Olszewska et al. 2014). K^+ current activity generated by mitochondrial voltage-gated K^+ channels was inhibited by two commonly used blockers 4-AP and TEA which were administrated to the external recording solution to constitute a 'cocktail' of channel blockers. In addition to these, the activity of mitochondrial Ca^{2+}-activated K^+ channels, Ca^{2+} and anion channels or ATP-sensitive K^+ channels was inhibited to further limit the endogenous current activity that was not associated to TASK-5. These blockers consisted of ChTx, RR and ATP respectively. As TASK-5 is a member of the K2P family and as such, is predicted to be active at a range of potentials that voltage sensitive channels are inactive, currents were analysed and compared at 0 mV to reduce contamination by other voltage gated channels (section 2.6) (Enyedi and Czirják 2010).

Here, three experimental phases were performed. During the first experimental phase each blocker with its corresponding IC_{50} and IC_{100} concentration was individually applied to isolated and non-transfected mitochondria in order to observe the inhibitory pattern or pharmacological effect of these blockers. These sets of experiments also tested the ability of the compounds to cross the OMM and inhibit the targeted IMM channels without inducing an outer membrane rupture. The second experimental phase consisted of designing and applying cocktails of 4 or 5 channel blockers to maximally reduce endogenous currents as control conditions. In the final phase, the H^+ composition of the external recording solution containing blockers was modified from neutral to basic or acidic pH.

To determine if TASK-5 drives a functional response when over-expressed within organelles, its electrical characteristics should follow several rationalised criteria based on the electrophysiological features of ideal TASK channels. These include the generation of larger current amplitudes which should be less-voltage dependent (background channel characteristic) and more K^+ selective (reversal potential close to E_{K+}) when TASK-5 is over-expressed. TASK-5 currents should also be more sensitive to acid conditions and potentially to RR as an E70 residue was identified in the extracellular M1–P1 linker of the channel conferring a sensitivity to the dye similar to TASK-3. Based on these predicted characteristics, current recordings will denote whether TASK-5 is a functional channel when transiently transfected in mitochondria.

7.2 Endogenous expression of TASK-3 in HeLa and COS-7 cells

TASK-3 has previously been identified as a functional K^+ channel in the IMM of isolated mitochondria within human keratinocyte cells and rat embryonic hippocampus neurons (Rusznak, Bakondi et al. 2008, Kajma and Szewczyk 2012, Toczylowska-Maminska, Olszewska et al. 2014). TASK-5 shares sequence similarities with TASK-3 with an anticipated sensitivity to protons (H90) and possibly RR (section 2.7) (Karschin, Wischmeyer et al. 2001). Based on the sequence homology of the K2P channels, it is possible that their co- expression in organelles could prevent the differentiation of TASK-5 from TASK-3 currents. To overcome this and better examine the channel of interest, this study sought to use cell lines lacking TASK-3 expression. RT-PCR experiments examining the mRNA expression of *KCNK9* (TASK-3) and *KCNK15* (TASK-5) in human cancer cell lines and two control lines (COS-7 and HEK293) (Roncoroni 2012, Williams 2013) found that *KCNK9* cDNA was absent from cervical (HeLa) and monkey derived fibroblasts (COS-7) while *KCNK15* cDNA products were present in HeLa (Figure 7.1 A and B) suggesting that these cell lines were potential models to study the electrophysiological characteristics of TASK-5 in mitochondria. To confirm these findings at the protein level but also demonstrate the specificity of the antibodies used or designed by the group, immunocytochemistry experiments on transfected HEK293 and COS-7 cells with TASK3-eGFP or TASK5-eGFP accordingly were undertaken. Selective targeting of TASK-3 antibody has previously been validated by the O'Kelly group (Williams 2013; unpublished data) where the corresponding GFP-tagged channels co-localised with the antibody in transfected HEK293 cells (Appendix 4). Similarly, the targeting efficiency of $_h$K2P15.1-LR antibody was demonstrated by both Western blotting (section 4.2.2) and immunocytochemistry. More precisely, immunocytochemistry of transfected COS-7 cells with TASK-5-eGFP were probed with the costum made antibody and co-localisation analysis demonstrated a strong co-expression confirming the targeting efficiency of the antibody (Appendix 5). The presence of TASK-5 proteins was also studied at the endogenous level using $_h$K2P15.1-LR in HEK293 cells (Appendix 6). Epifluorescence imaging of immunocytochemistry confirmed that HEK293 cells express TASK-3 proteins and that the antibody is not able to recognise TASK-5 within the cell line.

Using these powerful tools the endogenous expression of TASK-3 and TASK-5 was investigated in HeLa and COS-7 cells by confocal microscopy. Absence of red fluorescence linked to TASK-3 expression at the protein level confirms previously acquired RT-PCR findings and indicates that these cell lines do not endogenously express the channel. Converserly, endogenous TASK-5 proteins were detected in both HeLa and COS-7 cells (Figure 7.1 C). To investigate the intracellular distribution of TASK-5, images were enlarged

(Figure 7.1D) and compared to COX II staining previously performed in HeLa cells (Figure 5.2). Immunocytochemistry results demonstrate a strong cytoplasmic but also nucleic staining of TASK-5 in comparison to COX II where a more granular fluorescent staining can be observed. Despite a difference in intracellular staining pattern, both HeLa and COS-7 were considered suitable cell lines to electrophysiologically characterise TASK-5 ionic activity due to a lack of TASK-3 expression in mitoplasts. In fact, changes in residual current amplitudes during pharmacological assays or sensitivity to modified proton concentrations will directly be linked to TASK-5 activity.

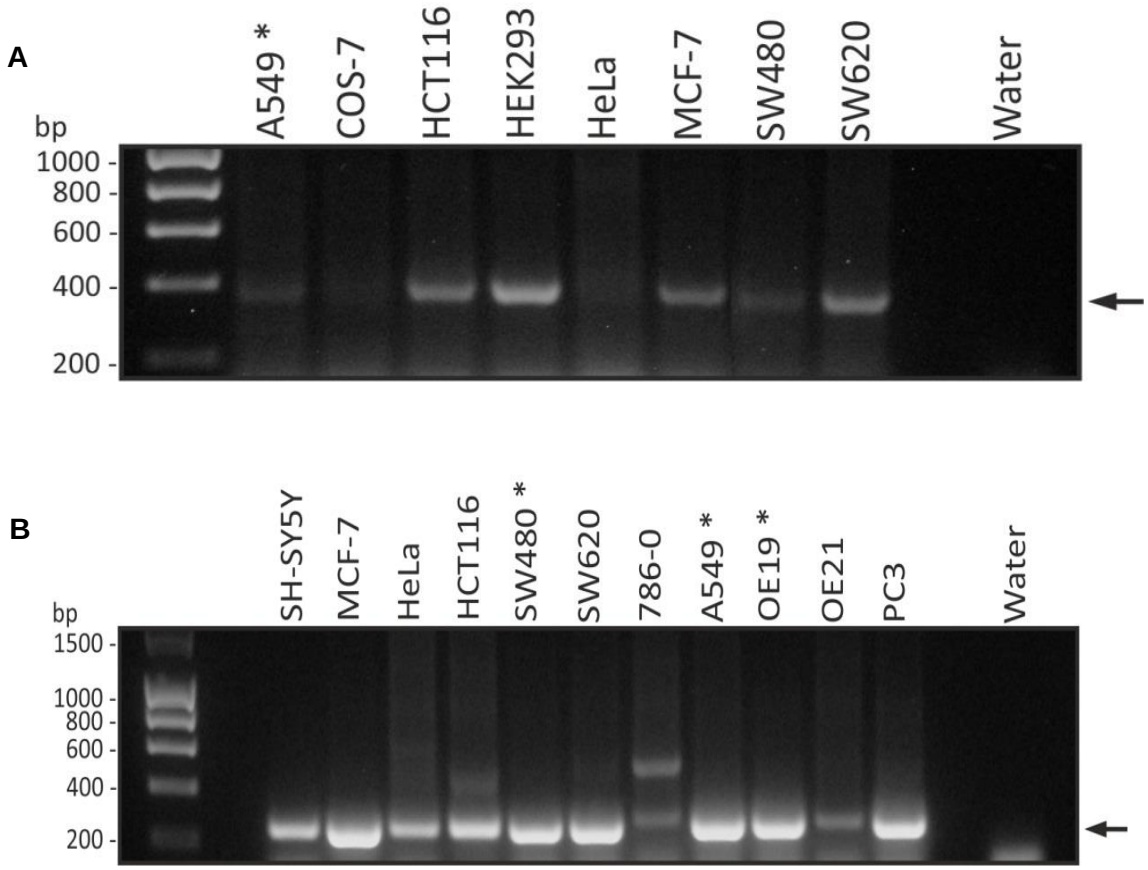

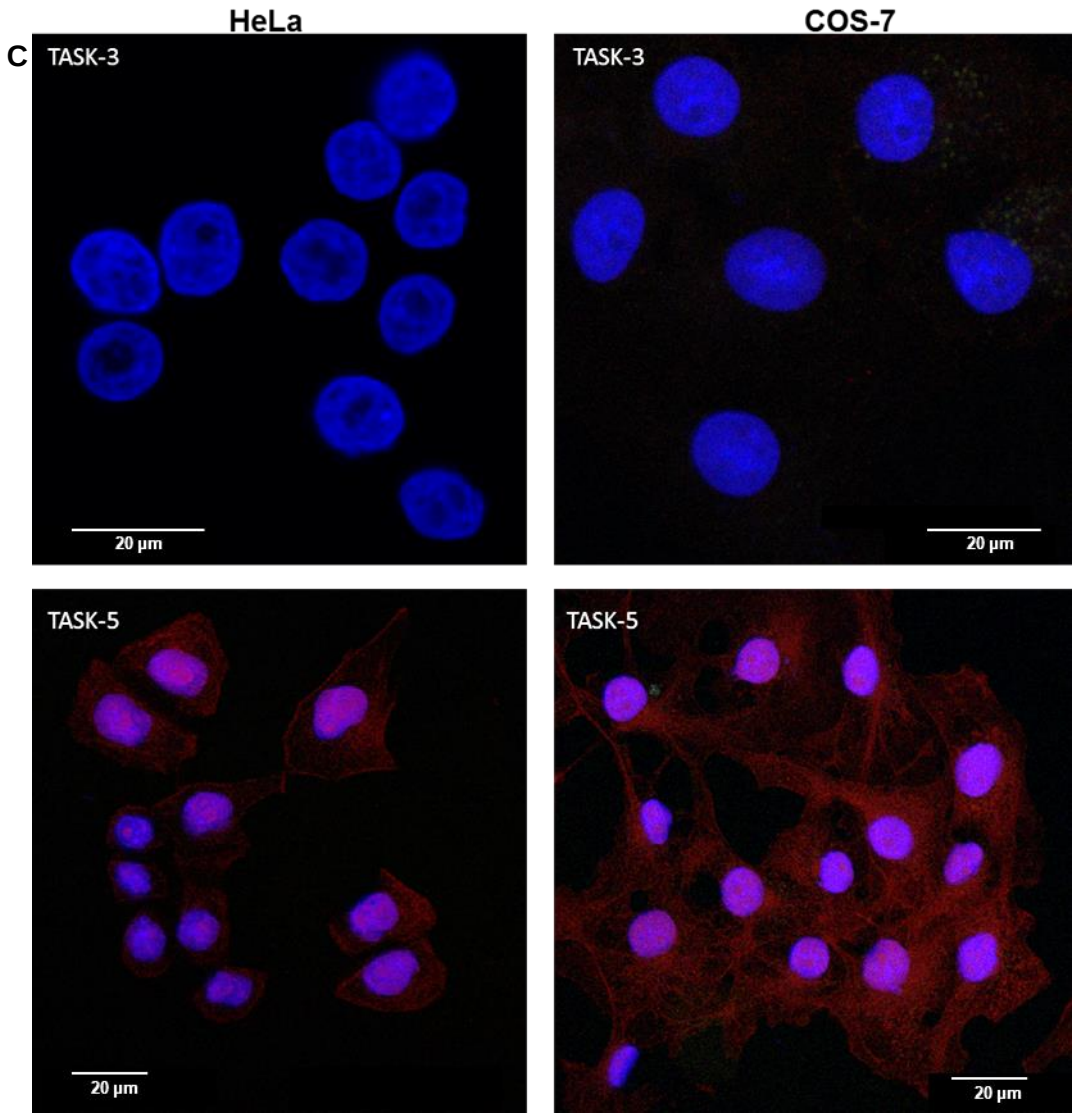
C
HeLa
COS-7
TASK-3
TASK-3
20 µm
20 µm
TASK-5
TASK-5
20 µm
20 µm

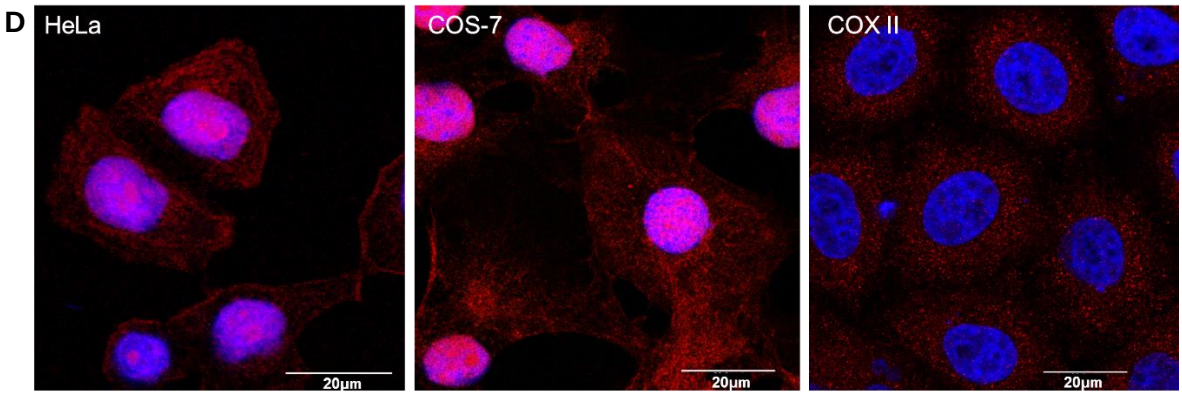

Figure 7. 1 Endogenous expression of TASK-3 and TASK-5 channels in HeLa or COS-7 at the mRNA and protein level. A. KCNK9 mRNA expression in human cancer cell lines. KCNK9 PCR product was amplified at the predicted size of 413 bp (indicated by an arrow) from A549, MCF-7, HCT116, SW480, SW620 and SH-SY5Y cancer cell line cDNA. No PCR products were detected in HeLa, 786-0, PC3 and OE19 and OE21 cancer cell lines, in addition to COS-7 cell line cDNA. Water was run as a no cDNA template control to ensure no PCR contamination. * indicates where the PCR product has been confirmed to be KCNK9 by DNA sequencing. Image adapted from Williams, 2012. **B.** KCNK15 mRNA expression in human cancer cell lines. KCNK15 PCR product was amplified, at the predicted size of 259 bp (indicated by an arrow), from breast (MCF-7), cervical (HeLa), colon (HCT116, SW480, and SW620), lung (A549), oesophageal (OE19), prostate (PC3), and neuroblastoma (SH-SY5Y) cancer cell line cDNA. No PCR products were detected at 259 bp in renal (786-0) and oesophageal (OE21) cancer cell lines. Water was run as a no cDNA template control to ensure no PCR contamination. * indicates where the PCR product has been confirmed to be KCNK15 by DNA sequencing. Image adapted from Williams, 2012. **C.** Confocal images of fluorescent immunocytochemistry was performed using primary antibodies against TASK-3, (20µg/ml) or $_{h}$K2P15.1-LR (1:50) coupled with anti-mouse (2ug/ml) and anti-rabbit (1:150) Texas red secondary antibodies. **D.** Enlarged sections of endogenous expression of TASK-5 or COX II in HeLa and COS-7 cells. DAPI staining was used to visualise the nuclei. Scale bars: 20µm.

7.3 Strategy employed to limit mitochondrial residual currents

All cells express an array of mitochondrial ion channels according to their physiological and functional needs. As the mitochondrial channel expression profile of HeLa or COS-7 cells has not been defined to date, it was hypothesised that any known mitochondrial channel referred within the literature could be expressed in these organelles. Based on this assumption, 5 different channel blockers with their corresponding IC_{50} and IC_{100} concentrations (Table 7.1) were selected according to their specificity in targeting several groups of mitochondrial channels expressed in the outer and/or inner MMs (Figure 7.2) (Grissmer, Nguyen et al. 1994, Jaburek, Yarov-Yarovoy et al. 1998, Xu, Liu et al. 2002, Kirichok, Krapivinsky et al. 2004, Szabo, Bock et al. 2005, Jiang, Ljubkovic et al. 2006, Fahanik-babaei, Eliassi et al. 2011). These compounds were individually applied to non-transfected mitochondria during the first phase of the study in order to test their potency in inhibiting the channels of interest, study the residual (i.e the remaining active) currents generated from non-targeted mitochondrial channels / pores / exchangers but also identify 'dominant' blockers that would more effectively inhibit these groups of channels.

Mitochondrial Channels	IC_{50}	IC_{100}
$MitoKB_{Ca}$/$MitoKI_{Ca}$	1.4nM ChTx	200nM ChTx
$MitoK_{ATP}$	0.5mM ATP	1mM ATP
$MitoKv_{1.3}$	2.6nM ChTx 10mM TEA 200µM 4-AP	100nM ChTx 20mM TEA 10mM 4-AP
VDAC	0.3µM RR	5µM RR
RyR	105nM RR	5µM RR
MCU	9nM RR	200nM RR
mPTP	-	5µM RR
mitoTASK-3	0.7µM RR	5-20µM RR

Table 7. 1 Summary of characterised mitochondrial ion channels with their corresponding half-maximal or total inhibitory blocker concentrations. Mitochondrial ion channels expressed in the outer or inner MM were partially (IC_{50}) or totally (IC_{100}) blocked with blockers listed accordingly. ChTx: Charybdotoxin, ATP: Adenosine triphosphate, TEA: Tetraethylammonium, 4-AP: 4-Aminopyridine, RR: Ruthenium red.

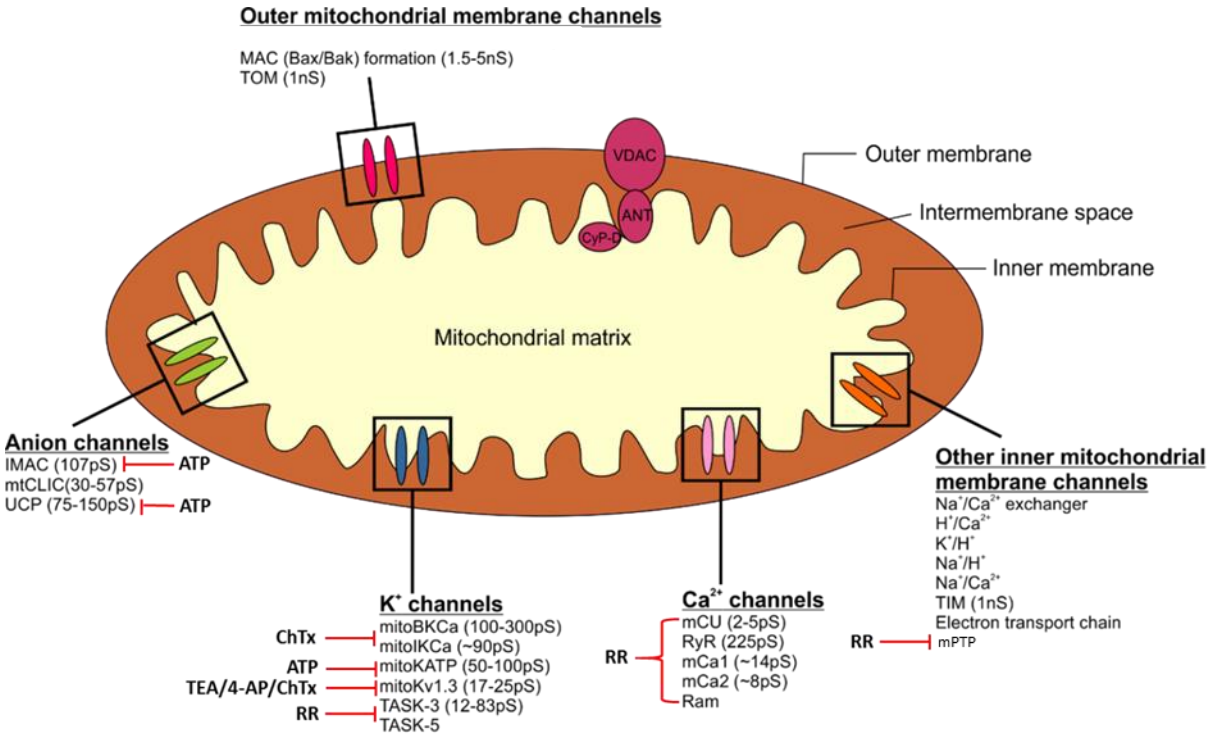

Figure 7. 2 Illustration of a single mitochondrion showing ion channels expressed in the outer and inner MMs with their corresponding blockers and conductances. Channel blockers specifically targeting and inhibiting mitochondrial channel populations such as K^+, Ca^{2+} and anion channels are shown with red lines. Mitochondrial permeability transition pore (mPTP) configuration with its corresponding proteins expressed either on the OMM (VDAC) or IMM (ANT) and matrix (CyP-D) are shown in dark pink**.**

7.3.1 Individual application of channel blockers to mitochondrial samples

During the first set of experiments, decision to study the electrical characteristics of TASK-5 channels in HeLa cells was taken as it was considered more valuable to first explore the organelle ionic properties of human cancer cells and subsequently of monkey derived fibroblasts. The IC_{50} or IC_{100} concentration of each blocker was subsequently applied at the whole–mitochondrial configuration in symmetrical K^+ conditions to abolish voltage- or Ca^{2+}-activated K^+ channels, Ca^{2+} or anion channels.

This approach allows the classification and precise quantification of the average current inhibition that several isolated mitochondria undergo post-application of the IC_{50} or IC_{100} concentrations of a blocker. Application of channel blockers decreases the activity of specifically targeted ion channel populations while the remaining residual current represents the collective response from all other active channels. The percentage of residual current elicited from several patched mitochondria post-application of each blocker is calculated according to Equation 1 defined in Methods 3.7.3. Controls in external recording solution are used as reference baseline where their percentage of residual current is set to 100% as these organelles have a conserved mitochondrial channel activity. Mean I-V curves (across the voltage range of –100 to + 80 mV) plotting total current or residual current (recorded 10-15 min post-application of each inhibitor) are presented in Figures 7.3-7.7. Additionally, percentages of residual currents are presented at 0mV as this condition minimised current contamination from potential voltage-sensitive mitochondrial channels. Differences in current amplitude are also compared within the positive (+80 mV) and negative (-100 mV) voltage range to provide additional insight on the inhibitory effect of voltage-gated channels.

Application of low concentrations of 4-AP reveals a noticeable impact on the recorded mitochondrial channel currents. In fact, current traces recorded from single mitochondria 10 min post-application of 200 μM 4-AP showed an increased current amplitude at positive voltages with 1077 ± 133 pA compared to 780 ± 117 pA (pre-exposure, n=5) at +80 mV (Figure 7.3 A,B). In contrast, the administration of 10 mM 4-AP reduced whole-mitochondrial current to ~460±55 pA at +80 mV (p=0.06, n=5). A minor inward rectification reduction at negative voltage steps is also observed following application of 10 mM 4-AP (Figure 7.3 A, B).

The inhibitory effect of 4-AP was next represented and compared to control conditions assigned to a total (100%) channel activity at 0 mV(Figure 7.3C). Results show that at low micromolar concentrations 4-AP potentiated the activity of mitochondrial channels by 39%, reaching a mean current of 139±4%. Application of higher [4-AP] in contrast inhibited the

mitochondrial channel activity by 32±4% indicating that the blocker can still target ion channels that are active and not active (voltage-insensitive) at 0 mV, resulting to a 68±6% residual current activity (p=0.03).

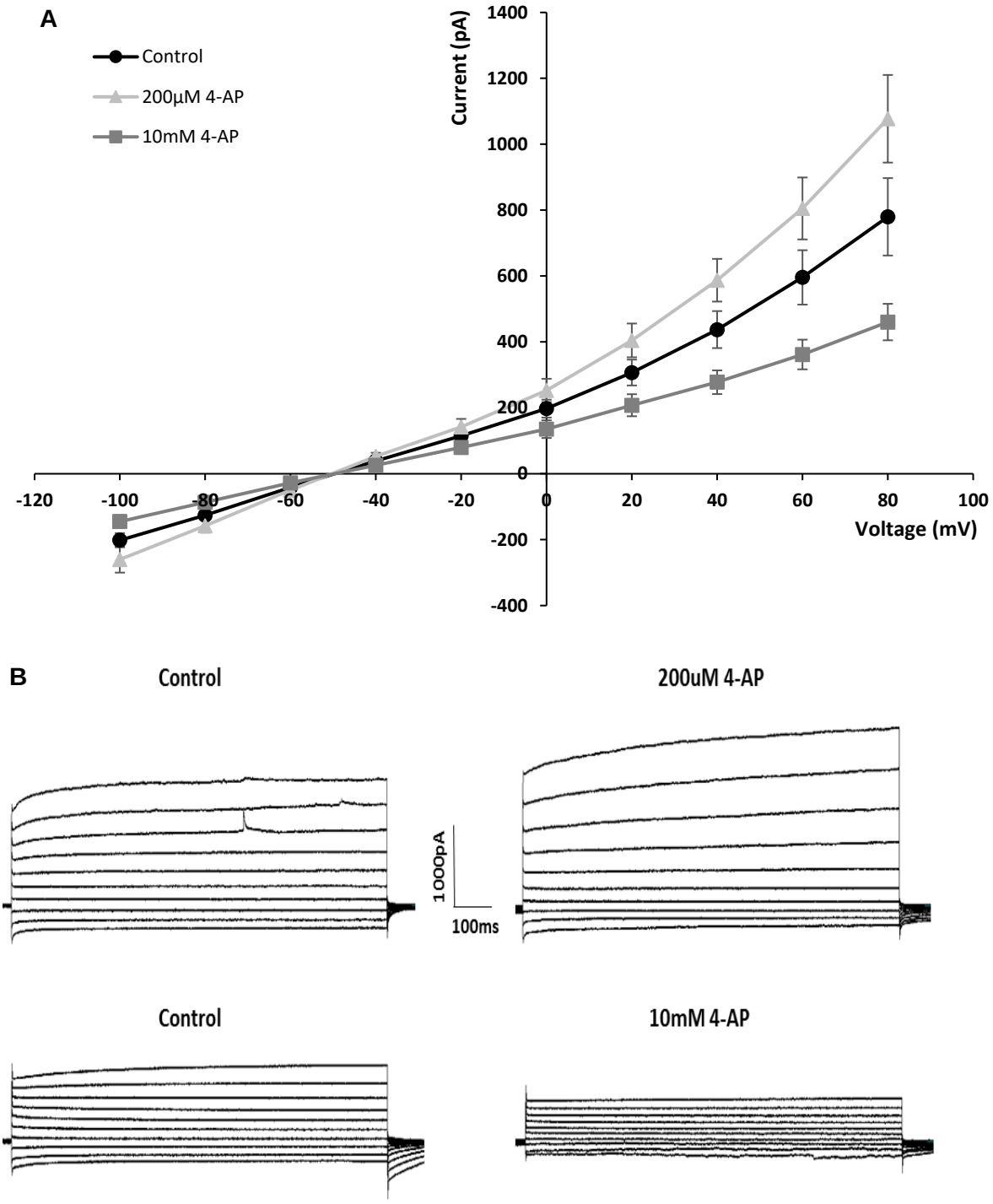

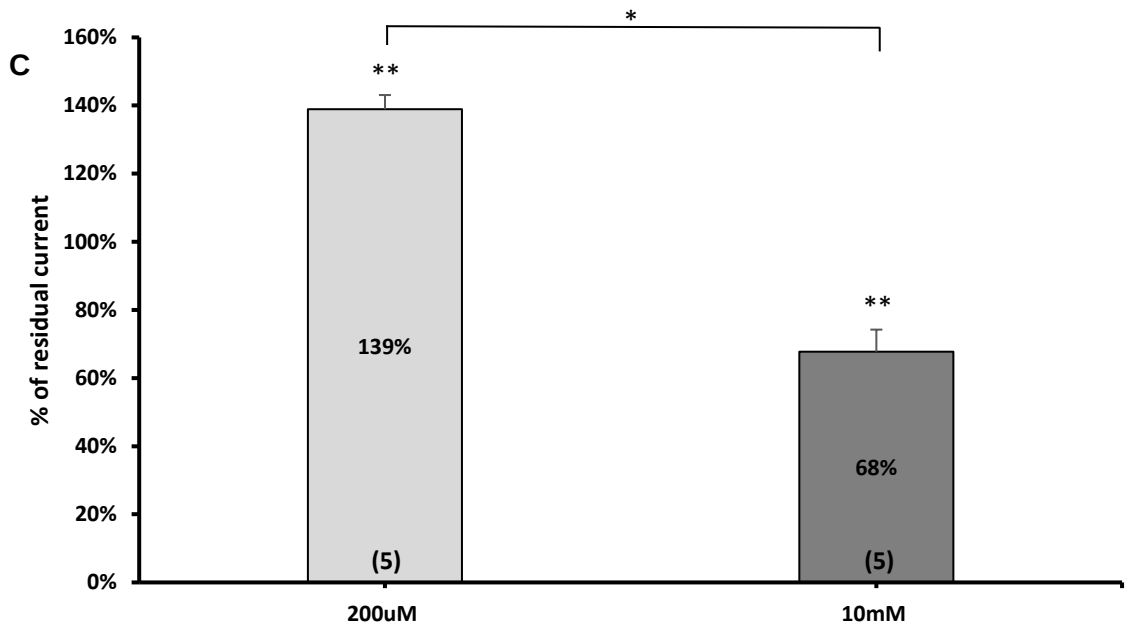

Figure 7. 3 Ionic current modulation post-administration of 4-AP to isolated mitochondria from non-transfected HeLa cells. A. Current-voltage relationship of isolated mitochondria bathed in symmetrical recording solution (control) or in response to 200µM or 10mM 4-AP (n=5; from 2 preparations). **B.** Example family of traces recorded from isolated mitochondria in control conditions or following exposure to 4-AP. Voltage was stepped from -100 to +80mV in 20mV increments with a holding potential of -50mV (solid line). **C.** Percentage of mean mitochondrial current potentiation or inhibition following application of 4-AP at 0mV. Each column was compared to its corresponding control condition recorded in symmetrical recording solution (without 4-AP) representing 100% current activity n=5 (column not shown). Data are Mean ± SEM and significant differences obtained after paired or unpaired t-test are indicated by asterisks with **p<0.01.

The effect of TEA was then examined in isolated mitochondria. Mean I-V curves (Figure 7.4 A) and current traces (Figure 7.4 B) recorded after voltage-stimulations show that both [TEA] reduce current amplitudes from 677±110 pA to 346±49 pA (10mM, p=0.06, n=8) and 390± 143 pA (20mM, p=0.2, n=5) accordingly at +80mV (Figure 7.4 A). Studying the difference in residual currents between both [TEA] at a positive voltage stimulation (+80mV) reveals a more substantial reduction difference; where 62±4% and 48±7% of the total channel activity remained active post-application of the IC_{50} and IC_{100} concentrations (p=0.6). Results also denote that voltage-sensitive K^+ channels gating was altered in symmetrical K^+ solutions and during voltage-clamp application. More specifically, the activation potential of these channels shifted towards more negative values (-50 mV) compared to the hypothetical V_{rev} value (0 mV) usually observed under such conditions (Rusznak, Bakondi et al. 2008, Kajma and Szewczyk 2012, Toczylowska-Maminska, Olszewska et al. 2014) . Despite this reversal current change, application of TEA reduced the K^+ gating of the channels without further modifying their activation potential.

Mean residual current percentages were also measured at 0 mV, denoting a quasi-identical current amplitude reaching 90±15 and 106±34 pA (57 and 55± 5 % residual currents) post-

application of 10 or 20 mM TEA, indicating that despite a two-fold blocker concentration increase, mitochondrial channel activity was not further affected.

Even though K_v channels such as mitoKv1.3 and perhaps other uncharacterised channels were suggested to not be active at 0 mV and thus, not inhibited by the blockers, 32 ± 6 % and 45±5 % (IC_{100}, n=5) of the total mitochondrial ion channel population was targeted at 0mV by 4-AP and TEA.

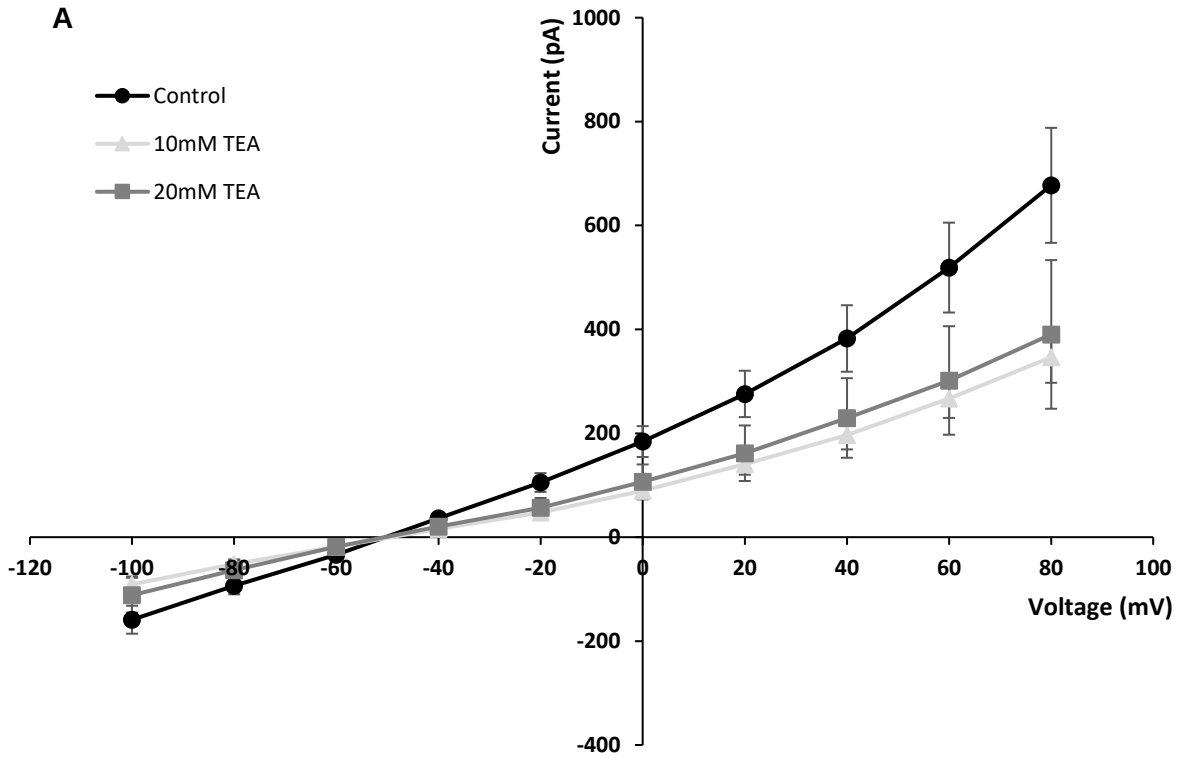

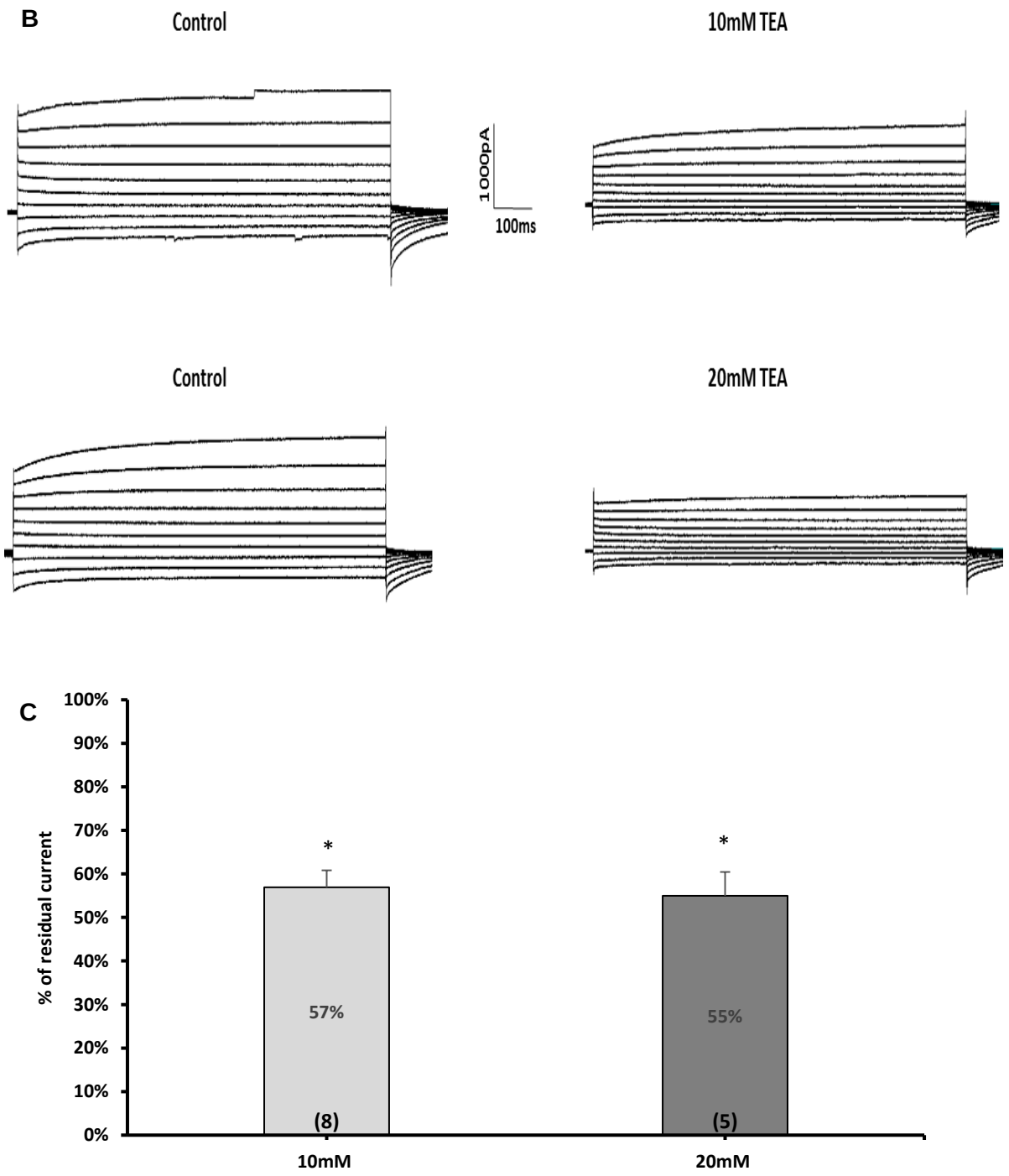

Figure 7. 4 Residual current reduction post-administration of TEA on isolated mitochondria from HeLa cells. A. Current-voltage relationship of isolated mitochondria bathed in symmetrical recording solution (control) or in response to 10mM (n=8) or 20mM (n=5; from 2 preparations) TEA. **B.** Example family of traces recorded from isolated mitochondria in control conditions or following exposure to TEA. Voltage was stepped from -100 to +80mV in 20mV increments with a holding potential of -50mV (solid line). **C.** Mitochondrial residual current following application of TEA at 0mV is presented as a percentage of control current where current recorded in symmetrical recording solution represents 100% current activity n=5-8 (column not shown). Data are Mean ± SEM and significant differences obtained after paired t-test are indicated by asterisks with *p<0.05.

Application of the IC_{50} or IC_{100} concentrations of ATP to isolated mitochondria induces stronger current reduction compared to TEA and 4-AP. Outward currents reduced from 1468±275 pA to 660± 170 pA (0.5mM ATP, $p<0.05$, n=9) and 488±146 pA (1mM ATP, $p<0.05$, n=9) at +80mV (Figure 7.5A). Current inhibition pattern in response to 0.5 and 1mM ATP and voltage step stimulations (from -100 to +80mV) is also demonstrated with the extracted current traces recorded in two separate mitochondria (Figure 7.5B).

To further validate the blocking efficiency of ATP the mean residual current post-administration of its IC_{50} and IC_{100} concentrations (Figure 7.5B) was measured at 0mV. The percentage of residual current was found to decrease by 48±5 % after the application of 0.5mM ATP ($p<0.01$) targeting almost half of the total mitochondrial channel population. In addition, mitochondrial channels bathed in 1mM ATP underwent significant channel blockade (62±4 %, $p<0.01$) leading to a weak 38±6 % residual current activity representing the remaining active and ATP-insensitive channels (p=0.7).

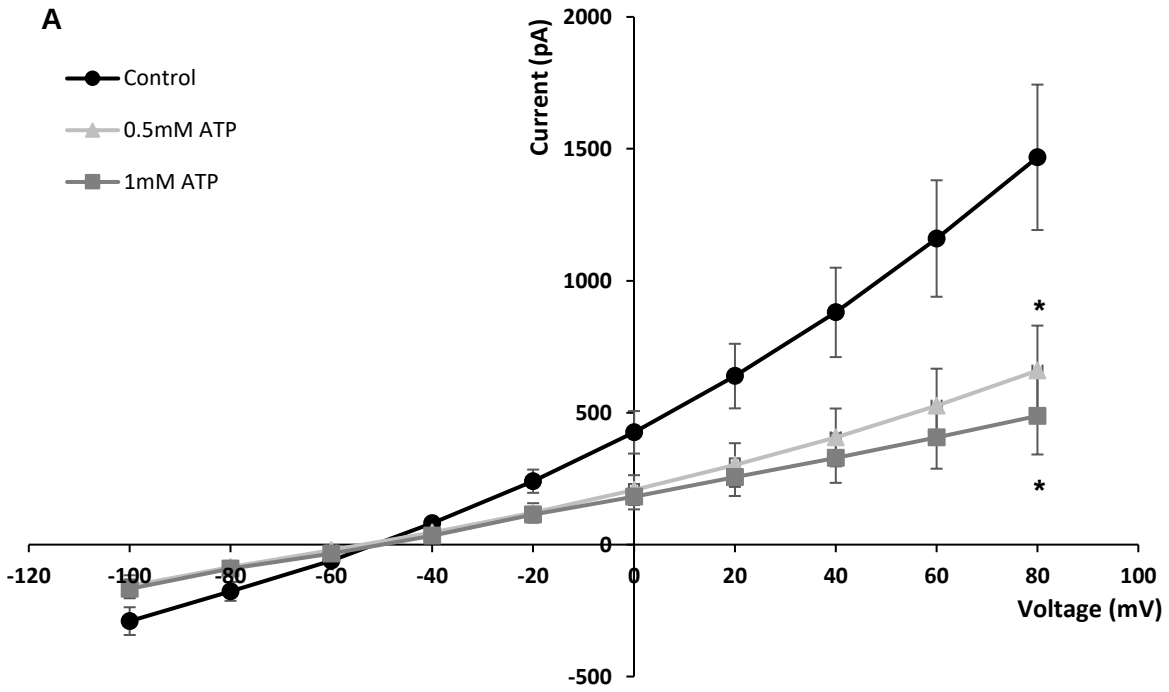

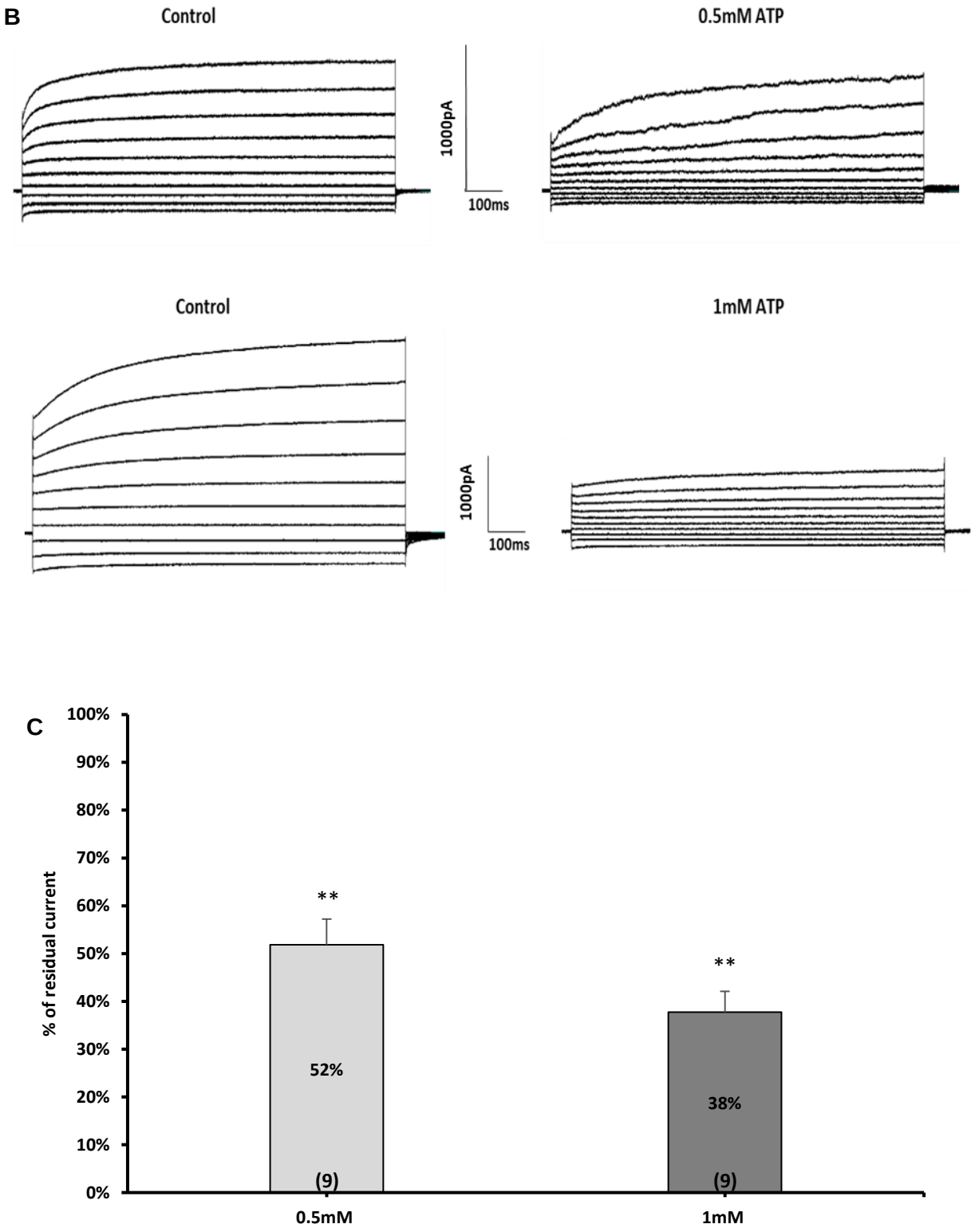

Figure 7. 5 Mitochondrial current inhibition post-administration of ATP on isolated organelles from HeLa cells. A. Current-voltage relationship of isolated mitochondria bathed in symmetrical recording solution (control) or in response to 0.5 mM (n=9) or 1 mM (n=9; from 3 preparations) ATP. **B.** Example family of traces recorded from isolated mitochondria in control conditions or following exposure to ATP. Voltage was stepped from -100 to +80mV in 20mV increments with a holding potential of -50mV (solid line). **C.** Mitochondrial residual current following application of ATP at 0mV is presented as a percentage of control current where current recorded in symmetrical recording solution represents 100% current activity n=9 (column not shown). Data are Mean ± SEM and significant differences obtained after paired t-test are indicated by asterisks with *p<0.05, **p<0.01.

To test the efficacy of ChTx on mitochondrial Ca^{2+} and voltage-sensitive K^+ channels the recommended IC_{50} and IC_{100} concentrations (Table 7.1) were applied to isolated mitochondria. The resulting I-V curves or current traces exhibit a maximal outward current of 1150±345 pA which reduced down to 408±112 pA (p=0.4, n=4) and 366±56 pA (p=0.2, n=7) upon application of 2nM and 200nM ChTx respectively at +80mV (Figure 7.6 A, B). Inward current inhibition followed a dose dependent reduction from -83±1.6 pA to -92±23 pA in response to 2nM and 200nM ChTx at -100 mV.

Additionally, by applying the IC_{50} and IC_{100} concentrations of ChTx an analogous inhibitory effect with ATP was observed at 0 mV. More specifically, the residual current activity post-application of 2nM or 200nM ChTx decreased to 58±8 % or 39±6 % (from 283±77 pA to 111±46 pA or 104±16 pA) (Figure 7.6C). The large current reduction post-application of 200nM ChTx (up to 60±6%, p=0.7) was linked to mitoBK$_{Ca}$ and mitoIK$_{Ca}$ inhibition and possibly other channels that remain to be characterised. In a similar manner to ATP, ChTx can be considered as a dominant channel blocker of the study due to its strong inhibitory current potential.

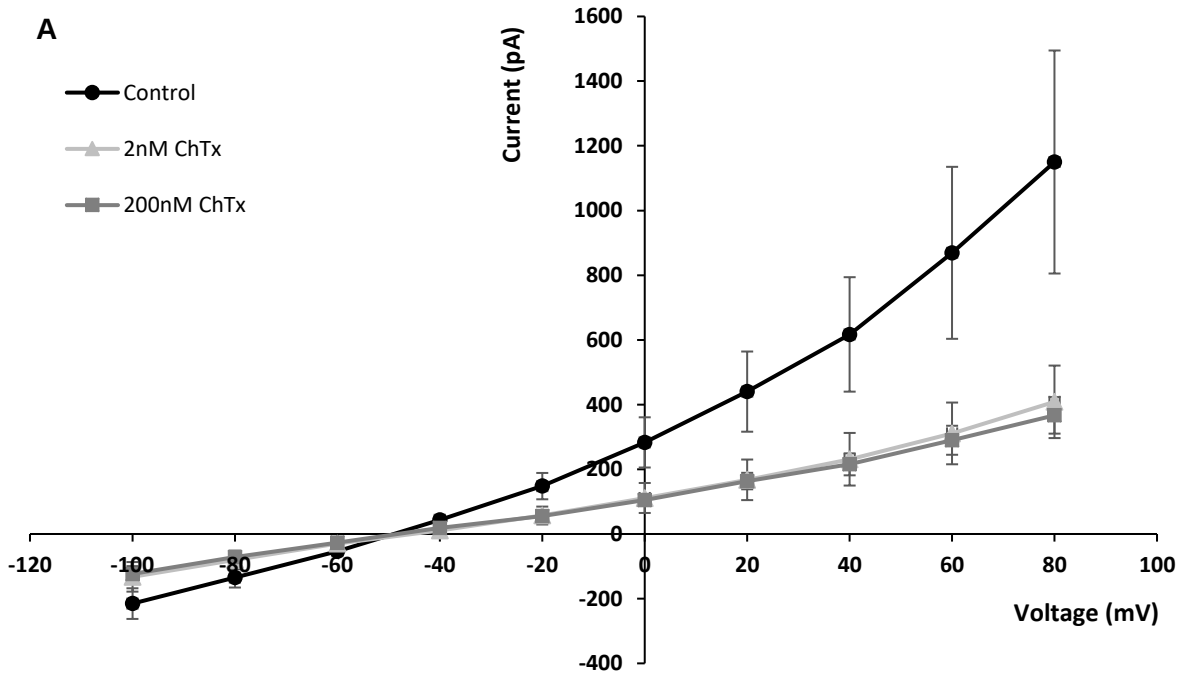

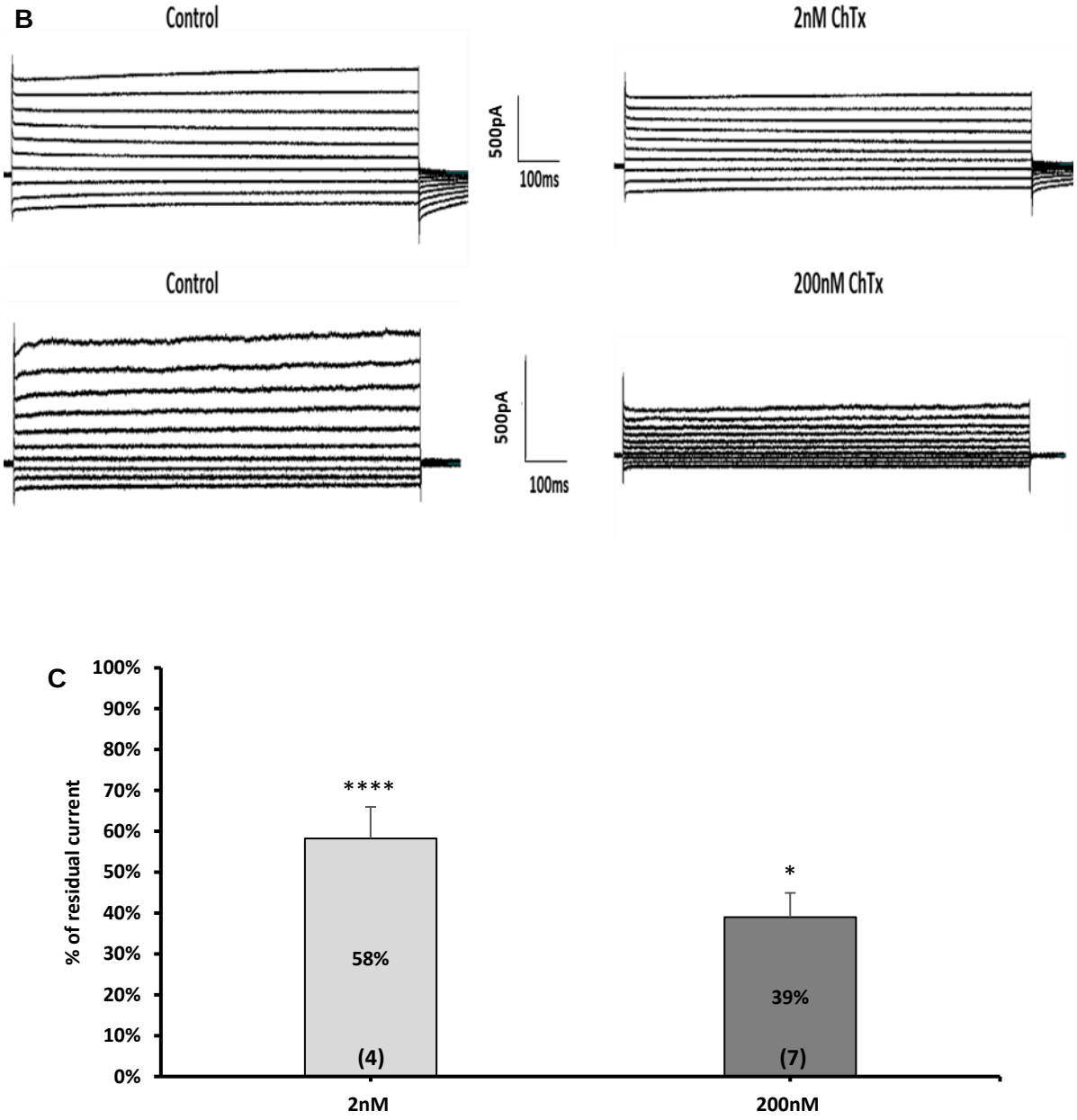

Figure 7. 6 Ionic current reduction post-administration of Charybdotoxin on isolated mitochondria from HeLa cells. A. Current-voltage relationship of isolated mitochondria bathed in symmetrical recording solution (control) or in response to 2 nM (n=4) or 200 nM (n=7; from 2 preparations) ChTx. **B.** Example family of traces recorded from isolated mitochondria in control conditions or following exposure to ChTx. Voltage was stepped from -100 to +80mV in 20mV increments with a holding potential of -50mV (solid line). **C.** Mitochondrial residual current following application of ChTx at 0mV is presented as a percentage of control current where current recorded in symmetrical recording solution represents 100% current activity n=4-7 (column not shown). Data are Mean ± SEM and significant differences obtained after paired t-test are indicated by asterisks with *p<0.05, ****p>0.0001.

The final inhibitor, RR, was used at a concentration of 10μM to target the ionic activity of Ca^{2+} channels (Figure 7.2). The concentration of the dye was nevertheless reduced or totally removed from the cocktails during the pharmacological assays performed within the following sections as it is also documented as a TASK channel inhibitor (section 2.6.2, Table 7.1).

When applied to isolated mitochondria, a current amplitude reduction was observed through the I-V curves and current traces in response to voltage step stimulations (Figure 7.7A, B). A mean outward current inhibition from 720 ±136 pA to 401±63 pA ($p<0.01$, n=7) at +80mV and -140±29 pA to 98±24 pA ($p<0.0001$) at -100mV was observed. Significant current reduction was also recorded (from 189± 30 pA to 118±19 pA) resulting to a 63±7% residual current ($p<0.05$) at 0 mV (Figure 7.8).

Synopsis of the blocking effect of each individually applied inhibitor with its IC_{100} concentration at 0 mV is shown in Figure 7.8 suggesting that targeted Ca^{2+}, possibly endogenous TASK-5 and an array of other channels/pores/exchangers may account for 40% of the total mitochondrial channel population while the remainder channels (60%) can be RR-insensitive K2P channels, ATP and/or ChTx sensitive and H^+ pumps of the ETC. While the activity of voltage-sensitive channels should be minimal at 0 mV, ~30-45 % of the total channel population is still blocked by 4-AP and TEA. This suggests that other types of channels such as ANT1 which confer voltage sensitivity to the mPT pore or members of the ETC (complex I) are sensitive to these blockers (Fontaine, Eriksson et al. 1998, Fontaine and Bernardi 1999, Doczi, Turiák et al. 2011, Doczi, Torocsik et al. 2016).

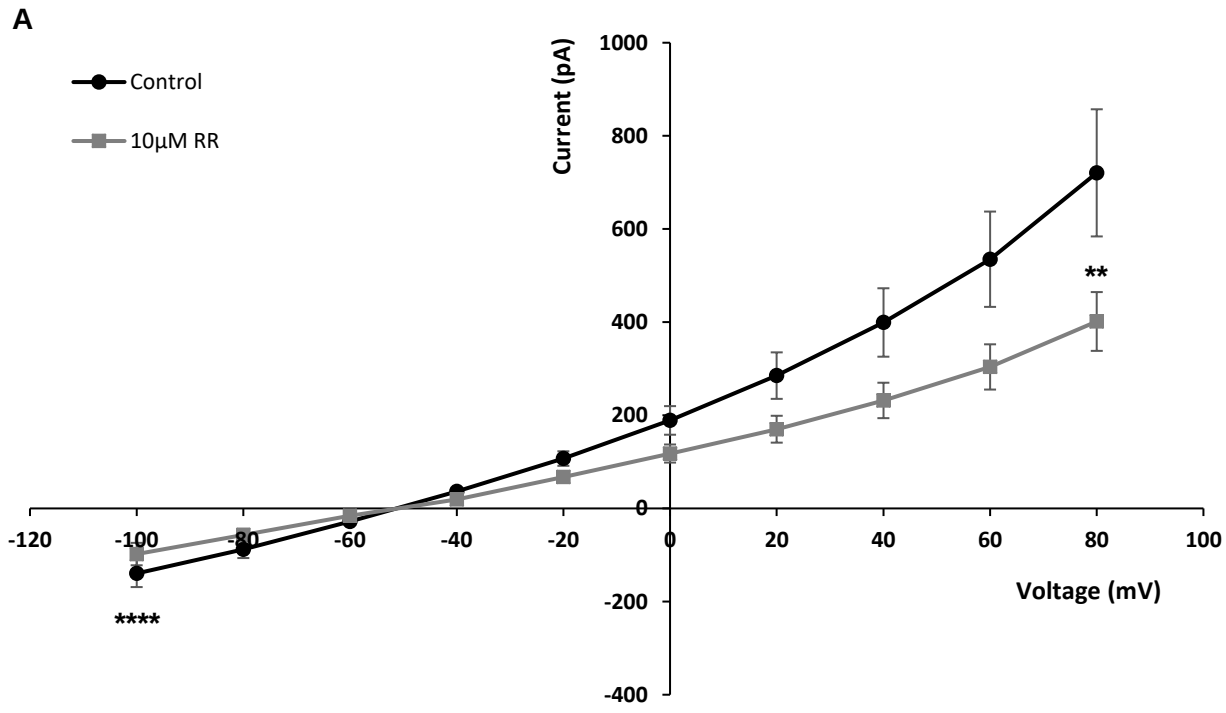

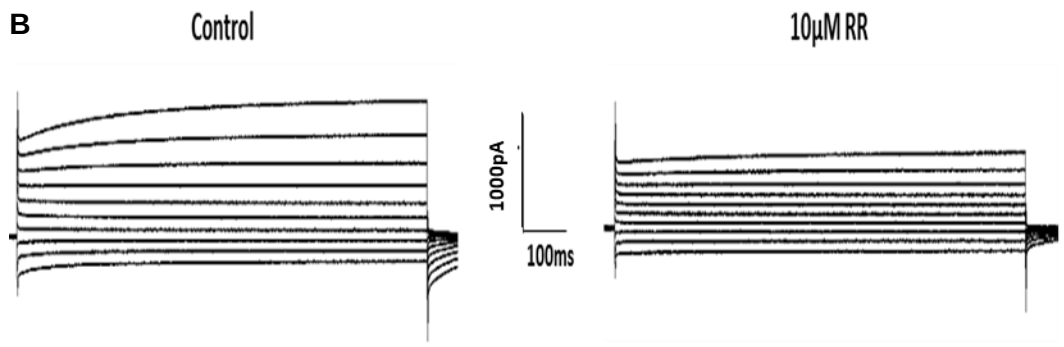

Figure 7. 7 Residual mitochondrial current post application of ruthenium red dye on isolated organelles from HeLa cells together with the summarised inhibitory effect of each blocker (IC_{100}). A. Current-voltage relationship of isolated mitochondria bathed in symmetrical recording solution (control) or in response to 10µM RR (n=7; from 2 preparations). **B.** Example family of traces recorded from isolated mitochondria in control conditions or following exposure to RR. Voltage was stepped from -100 to +80mV in 20mV increments with a holding potential of -50mV (solid line). Data are Mean ± SEM and significant differences obtained after paired t-test are indicated by asterisks with **p<0.01 and ****p<0.0001.

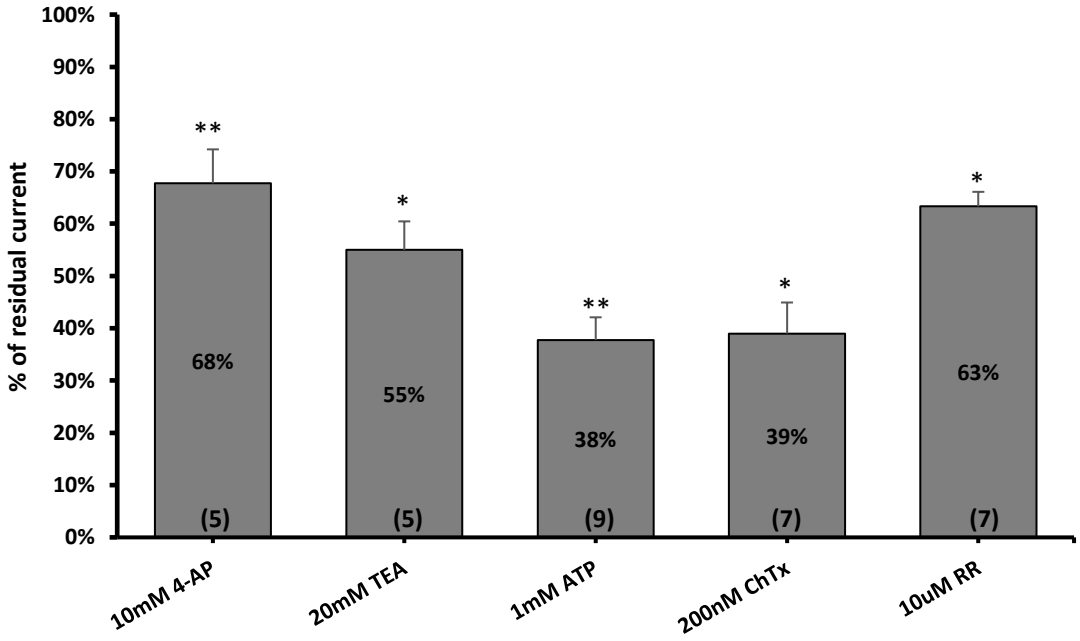

Figure 7. 8 Percentage of mitochondrial residual currents measured post-application of the IC100 concentration of each blocker at 0 mV. The total inhibitory effect of each blocker with its corresponding IC_{100} concentration on mitochondrial residual currents at rest (0mV). Each percentage of residual current was calculated and compared with its control (100%) condition. Data are Mean ± SEM and significant differences obtained after paired t-test are indicated by asterisks with *p<0.05 and **p<0.01.

It is lastly important to mention that the blocking effect of each individually applied blocker (IC_{100} concentration) on isolated mitochondria was reversible upon washout with external recording solution (Figure 7.9). More precisely, a time constant for recovery of ~10 minutes post-blocker removal was observed leading to half or less than the original whole-mitochondrial current conductance. Results also indicate that unbinding occurs more often at positive voltages where channels' opening is favoured. Additionally, the inhibitory effect

of 4-AP, TEA and ChTx was less reversible compared to ATP and RR where a stronger current recovery was detected. This suggests that either 4-AP, TEA and ChTx can be trapped in an internal cavity located between the channels' selectivity filter and/ or activation gate with a higher affinity; or require a longer period to washout. To unravel these possibilities, computational methods like *in silico* modeling, molecular docking and dynamic simulation could be particularly valuable in future studies.

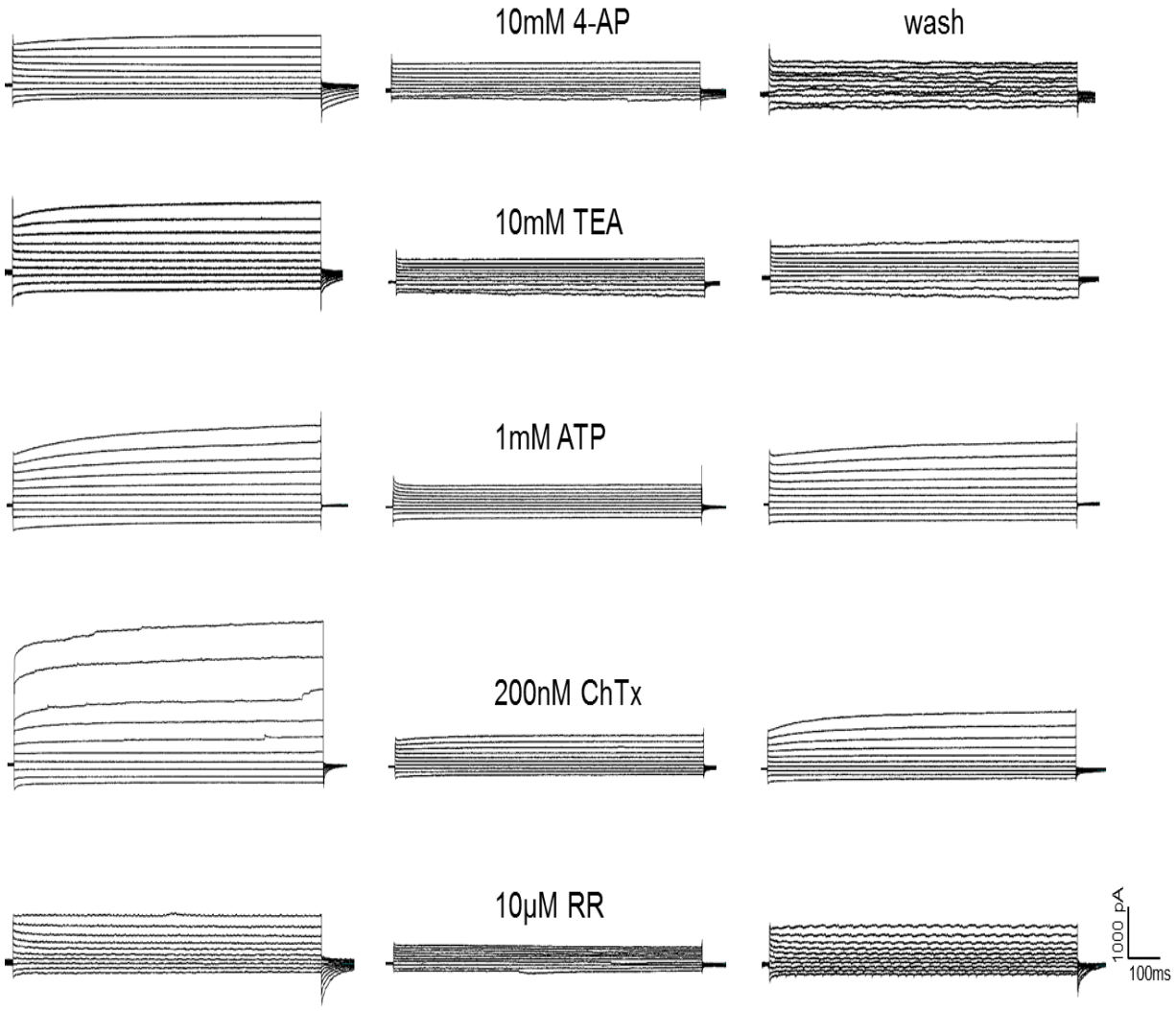

Figure 7. 9 Example family of traces recorded from isolated mitochondria in control conditions (without blockers) or following exposure to the IC_{100} concentrations of 4-AP, TEA, ATP, ChTx or RR. Blockers were washed away after 10mins of exposure using a perifusion system. Voltage was stepped from -100 to +80mV in 20mV increments with a holding potential of -50mV (solid line).

7.4 Residual current upon application of cocktails of channel blockers to non-transfected organelles

To investigate the residual current differences elicited between non- and transfected organelles it was first imperative to block residual currents in a synchronised manner in non-transfected organelles. These data were later used as control conditions against current recordings acquired within transfected mitochondria and/or mitoplasts as part of the research strategy. This way, comparison of current amplitude alterations between endogenous and organelles that over-expressed TASK-5 allowed to evaluate whether the channel of interest was functional or not. This was accomplished by designing and testing various cocktails of channel blockers that either contained the IC_{100} concentrations of 4 (without RR) or 5 blockers (with 5μM or 10μM RR; Figure 7.10 A, B). From these results I-V relationships, outward and inward current amplitudes along with V_{rev} values were extracted and compared in the presence or absence of blocker cocktails (Figure 7.10 A).

Mitochondrial and mitoplast currents acquired in absence (control) or presence of 4 blockers (IC_{100}) and in response to voltage steps from -100 to +80 mV were plotted (Figure 7.10 A). A strong reduction from 951±123 pA to 230±50 pA ($p<0.0001$, n=8) was observed in mitochondrial outward currents in comparison to a mitoplast current reduction from 697±147 pA to 260±65 pA ($p<0.01$, n=6) upon application of 4 blockers at +80mV (Figure 7.10 A). A large mitochondrial amplitude reduction that is mainly related to the higher current elicited within the organelles in absence of blockers (950±123 pA) in contrast to mitoplasts (697±147 pA, p=0.3). The overall inward rectification difference at -100mV was also less prominent in mitoplasts with a reduction from -148±33 pA to -80±16 pA versus -217±36 pA to -100±25 pA in mitochondria (p=0.5). These results imply that following swell induction, OMM removal and hence, mPTP absence may be linked to the stronger influx and efflux current reduction observed in mitochondria. In addition to the current amplitude reduction, the slope of the organelle I-V curves post blocker application adopted a more linear trend indicating that voltage-sensitive channels were inhibited by TEA and 4-AP. The more linear the I-V relationship is, the less voltage depend are the channels expressed on the membranes studied in response to voltage-clamp stimulation (Hille 2001). There was also no change in organelles' V_{rev} values upon addition of the blockers, which maintained a value close to -49±1 mV as previously observed in Chapter 6 (sections 6.3-6.4).

Addition of 10 μM RR to the cocktail of 4 blockers induced a stronger current reduction from 652±140 pA to 162± 27 pA (p=0.9, n=8) in mitoplasts and 673±83 pA to 252±46 pA (p=0.1, n=10) in mitochondria at +80 mV. The inward current also reduced from -117±16 pA to -70±13 pA in mitoplasts and from -126±9 pA to -75±7 pA in mitochondia (p=0.08) indicating

that RR does not considerably influence the ionic efflux post-OMM removal (reduction of -68.12±18 pA with 4 blockers versus -48.5±2 pA with 5 blockers, p=0.18). The mitochondrial ionic efflux on the other hand was affected, reducing down to -118±11 pA with 4 blockers versus -48.5±2 pA with 5 blockers (p=0.22) indicating that OMM channels/pores could have been targeted by RR. At 0 mV, mitochondrial currents reduced from 183±23 pA to 83±12 pA (n=10) and mitoplasts from 179±37 pA to 52±5 pA (n=8, p=0.3). Finally, mitoplast outward currents seemed to be marginally larger when 5 µM RR was administrated to the cocktail of 4 blockers in contrast to 10 µM as, the overall current amplitude reduced from 382±28 pA to 172±16 pA (n=6, p<0.001) compared to 10 µM (162± 27 pA, p=0.7) at +80 mV. The same observation was made at negative and 0 mV. In fact, current reduced from -126±9 pA to -75±7 pA at -100mV and from 183±23 pA to 83±12 pA at 0 mV (n=6) in the presence of lower [RR].

Another general observation was that the I-V slopes of the residual currents were more linear and hence, less voltage-dependent in the presence of blockers and in response to voltage stimulations which was mainlylinked to the presence of 4-AP and TEA inhibiting K_v channels. A non-significant (p>0.05) shift in V_{rev} from -49±1 mV to -52.23±1.21mV was also observed between organelles bathed in absence (4 blockers) and presence of RR (5-10 µM) which could be linked to the closure of Ca^{2+} channels or the depolarised state of the organelles.

The percentage of residual current post-application of the IC_{100} concentration of 4 blockers (without RR) was also measured at 0 mV. A stronger current reduction was observed in mitochondria resulting to a 37±5 % (from 227± 32 pA to 87±17 pA) residual current activity compared to 51±1 % (from 159± 29 pA to 81±16 pA; p=0.3) in mitoplasts (Figure 7.10 B). Conversely, mitoplast residual currents were weaker (from 179±37 pA to 67±11 pA; 43±5 %) in comparison to mitochondria (from 183±23 pA to 83±12 pA; 48±4 %; p=0.3) post-application of the IC_{100} concentrations of 5 blockers. In addition, by reducing [RR] to 5 µM in the cocktail of 4 blockers, mitoplast residual currents increased from 43±5 % (from 52±5 pA to 67±11 pA) in 10 µM RR to 51±4 % (p=0.2) indicating that RR-sensitive channels (excluding Ca^{2+} channels) were less targeted by the dye. In fact, at 5µM the dye will still target and totally abolish the activity of Ca^{2+} channels as shown in Table 7.1. Hence, 5µM instead of 10µM RR was administered to the cocktail of 4 channel blockers during the final sets of experiments on sorted organelles to reduce the likelihood of targeting and inhibiting channels such as TASK-5 (assuming that it is sensitive to the dye).

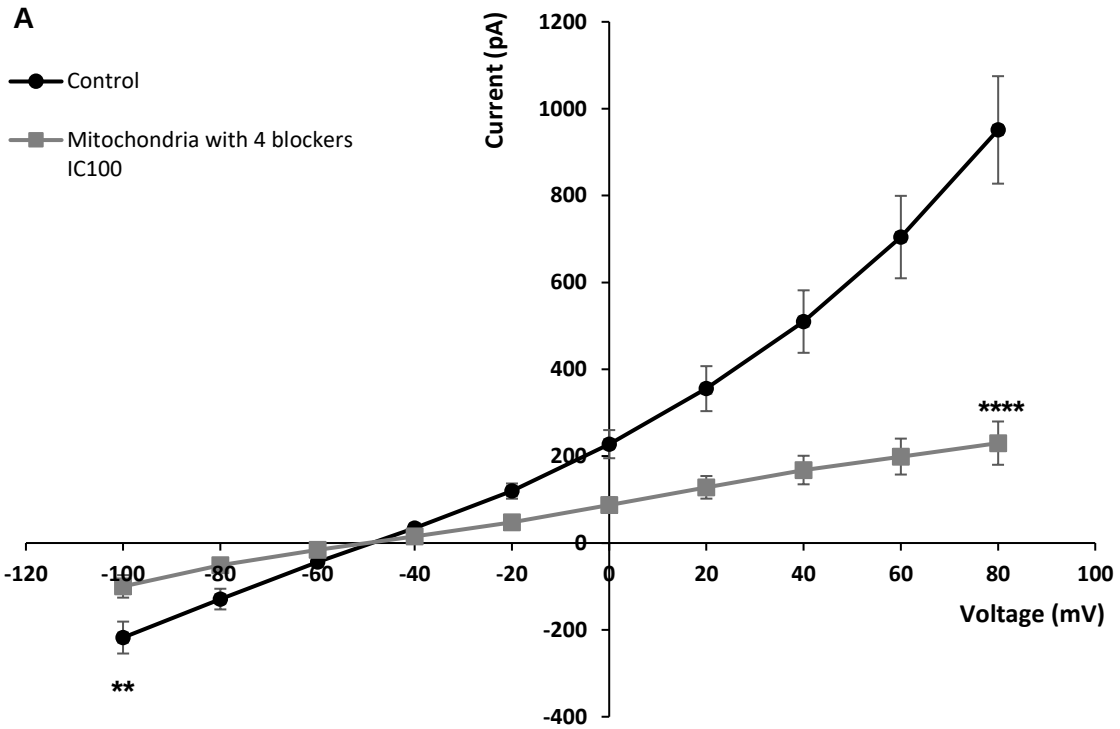
A
Control
Mitochondria with 4 blockers IC100
Current (pA)
1200
1000
800
600
400
200
0
-200
-400
-120
-100
-80
-60
-40
-20
0
20
40
60
80
100
Voltage (mV)
**
****

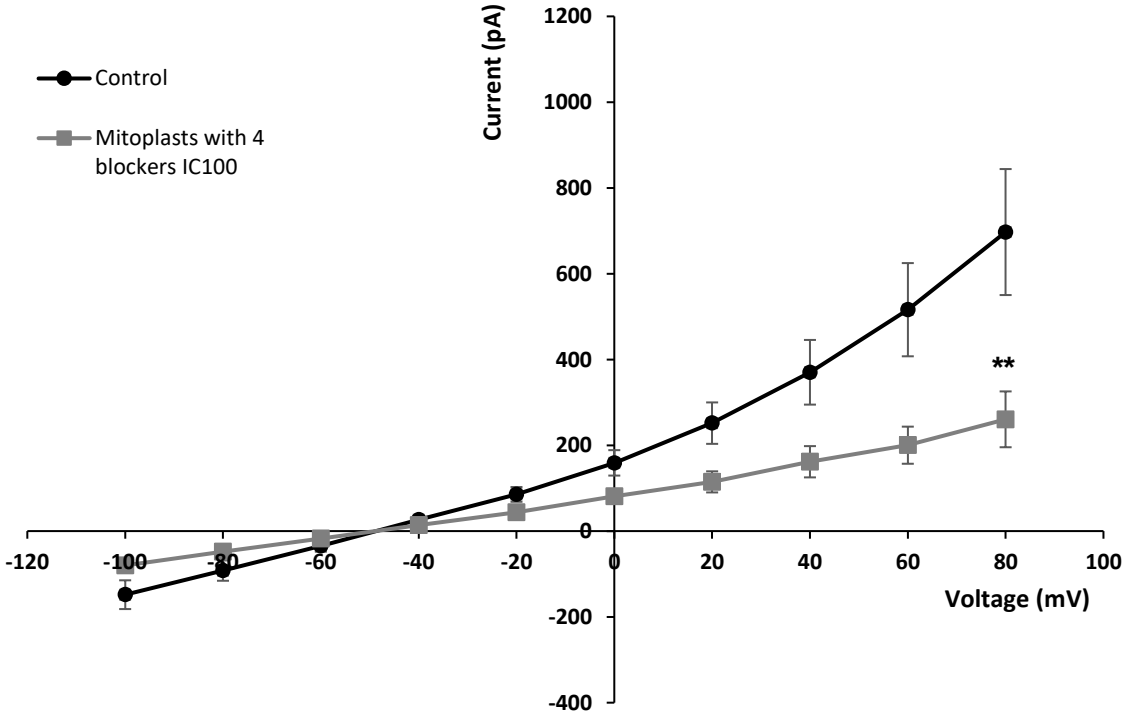
Control
Mitoplasts with 4 blockers IC100
Current (pA)
1200
1000
800
600
400
200
0
-200
-400
-120
-100
-80
-60
-40
-20
0
20
40
60
80
100
Voltage (mV)
**

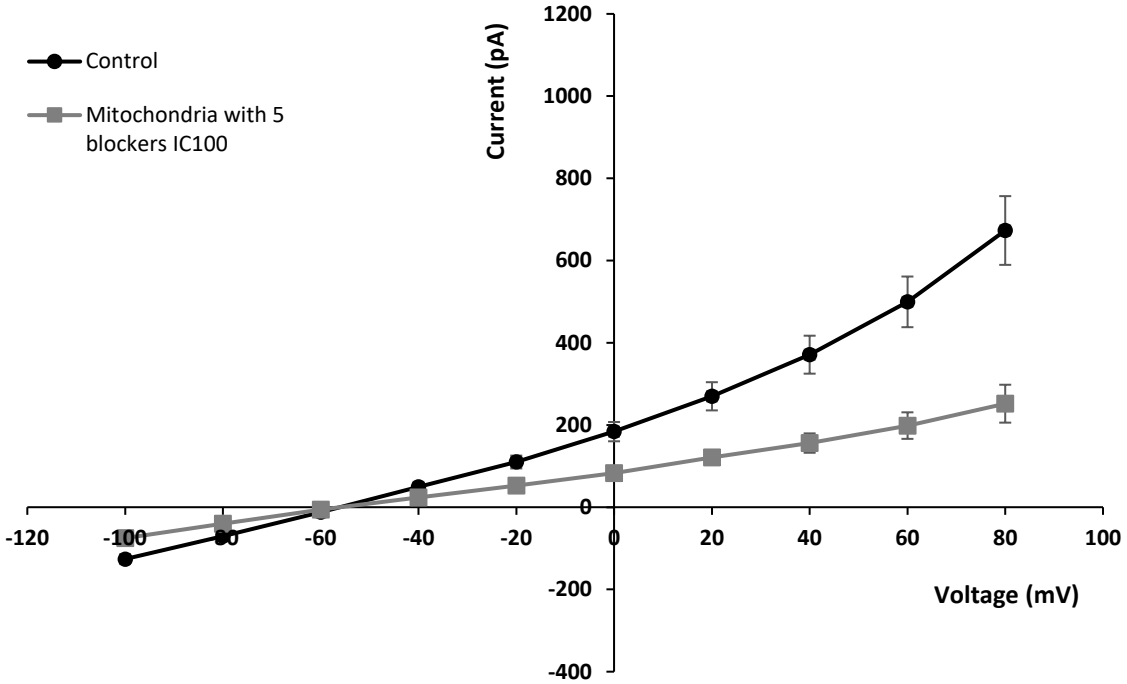
Control
Mitochondria with 5 blockers IC100
Current (pA)
1200
1000
800
600
400
200
0
-200
-400
-120
-100
-80
-60
-40
-20
0
20
40
60
80
100
Voltage (mV)

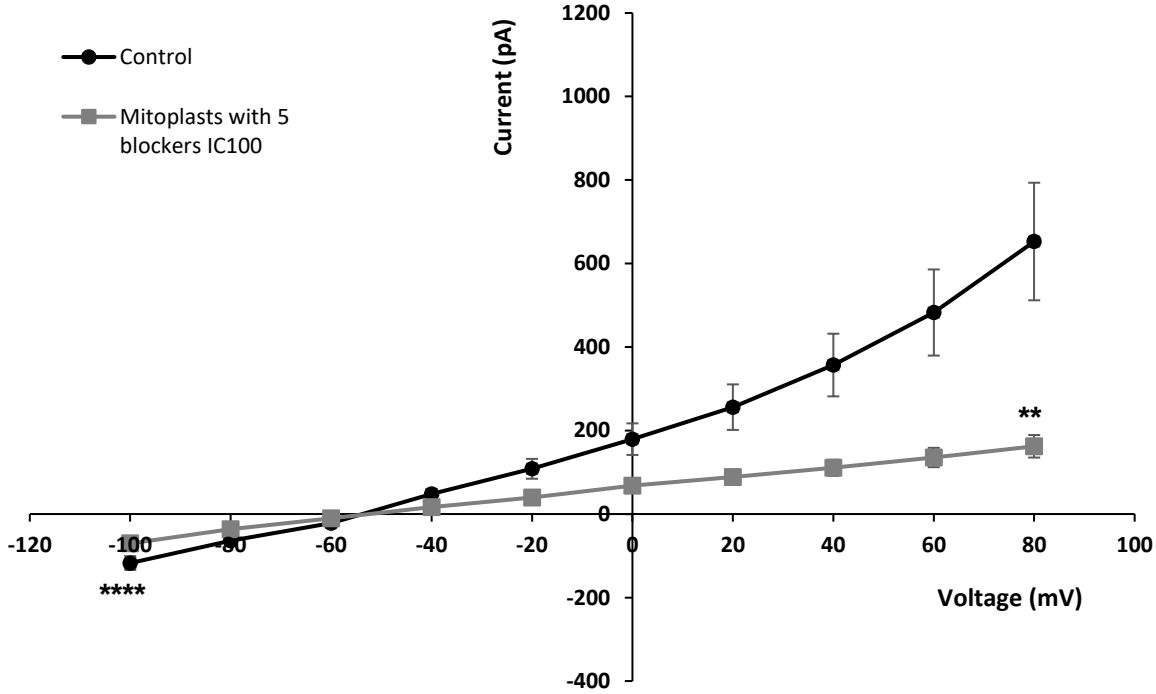
Control
Mitoplasts with 5 blockers IC100
Current (pA)
1200
1000
800
600
400
200
0
-200
-400
-120
-100
-80
-60
-40
-20
0
20
40
60
80
100
**
****
Voltage (mV)

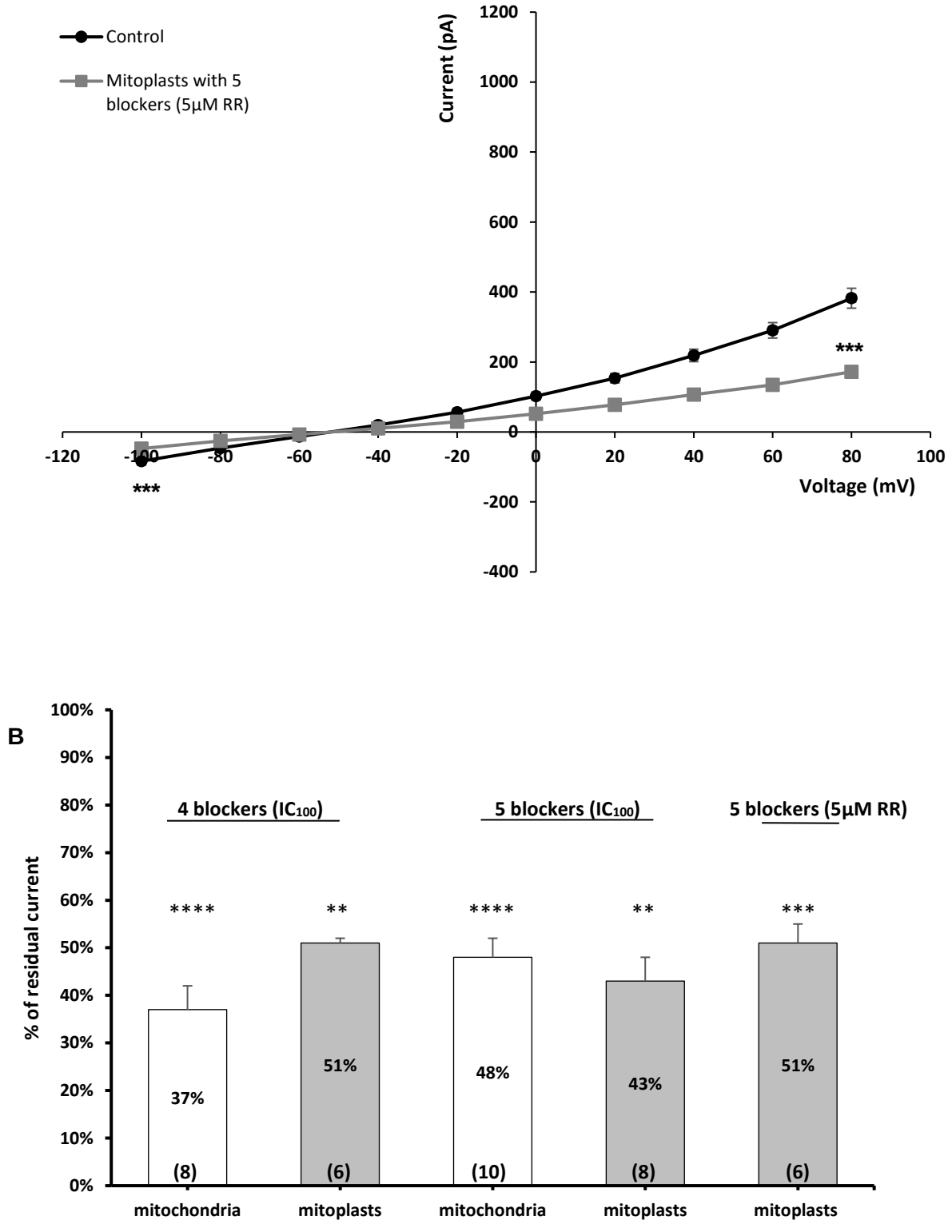

Figure 7. 10 Residual current reduction upon administration of channel blocker cocktails on isolated mitochondria or mitoplasts from HeLa cells. A. I-V relationship of organelle residual currents recorded in the presenceof a cocktail of 4 blockers (TEA, 4-AP, ATP, ChTx) excluding or including RR (5 or 10µM) and in response to voltage stimulations from -100 to +80 mV with 20 mV increments. **B.** Residual currents elicited in mitochondria or mitoplasts in response to cocktail blockers shown at 0 mV. All residual current values were calculated according to their control conditions (not shown) accounting for a total 100% mitochondrial current activity. n values for each recording sub-group is show in () in the graph. Data were collected from 2-3 preparations. Data are Mean ± SEM and significant differences obtained after paired t-test or 1-way Anova are indicated by asterisks with *p<0.05 and **p<0.01, ***p<0.001, ****p<0.0001.

This set of experimental trials also suggests that the combination of 5 channel blockers induced weaker current inhibition than ATP or ChTx alone (Figure 7.7). An observation that could be related to an osmolarity alteration of the external recording solution after combining the IC_{100} concentrations of 5 different compounds. More specifically, the combination of mainly 4-AP and TEA increased the solution osmolarity from 300 to 360mOsmol that can alter the mitochondrial matrix dynamics. To check whether such an osmolarity modification might have an impact on organelle membrane structure and response to blockers, the ionic composition of the external recording solution was reduced down to 300mOsmol in the presence of 5 blockers (IC_{100} concentrations). Isolated mitochondria were hence bathed in external recording solution with a reduced [KCl].

The response of mitochondrial channels as a function of voltage stimulations are plotted as shown in Figure 7.11 A. The graph exhibits how mitochondrial channels responded to blockers during different osmolarity conditions. Mean outward current amplitudes of both control (765±125 pA in 300mOsmol versus 636.17±107 pA in 360mOsmol) and blocked conditions (228.47±30 pA in 300mOsmol versus 261.15.17±64 pA in 360mOsmol) were found to have analogous (p=0.6) responses at +80 mV upon osmolarity modifications (n=10). No significant current amplitude change was observed at -100 mV between the two conditions (-45±3 pA in 300 mOsmol versus -53.3±2 pA in 360 mOsmol). The large error bars observed in Figure 7.11 within control samples is associated with the organelle size variability previously discussed in section 6.4, suggesting no significant difference between the samples (Cumming, Fidler et al. 2007). Mean residual current percentages measured at 0 mV also denoted a non-significant (p= 0.7) difference between conditions showing that 48±4 % (360 mOsmol) and 43±5 % (300 mOsmol) of mitochondrial currents are elicited from active channels (Figure 7.11 B). As the osmolarity modification was not found to have an effect on mitochondrial channel responses to blockers, experiments were performed in 150mM symmetrical K^+ solutions with an osmolarity of 360mOsmol in the presence of 5 blockers to reproduce the solute composition of published studies (Rusznak, Bakondi et al. 2008, Kajma and Szewczyk 2012, Toczylowska-Maminska, Olszewska et al. 2014).

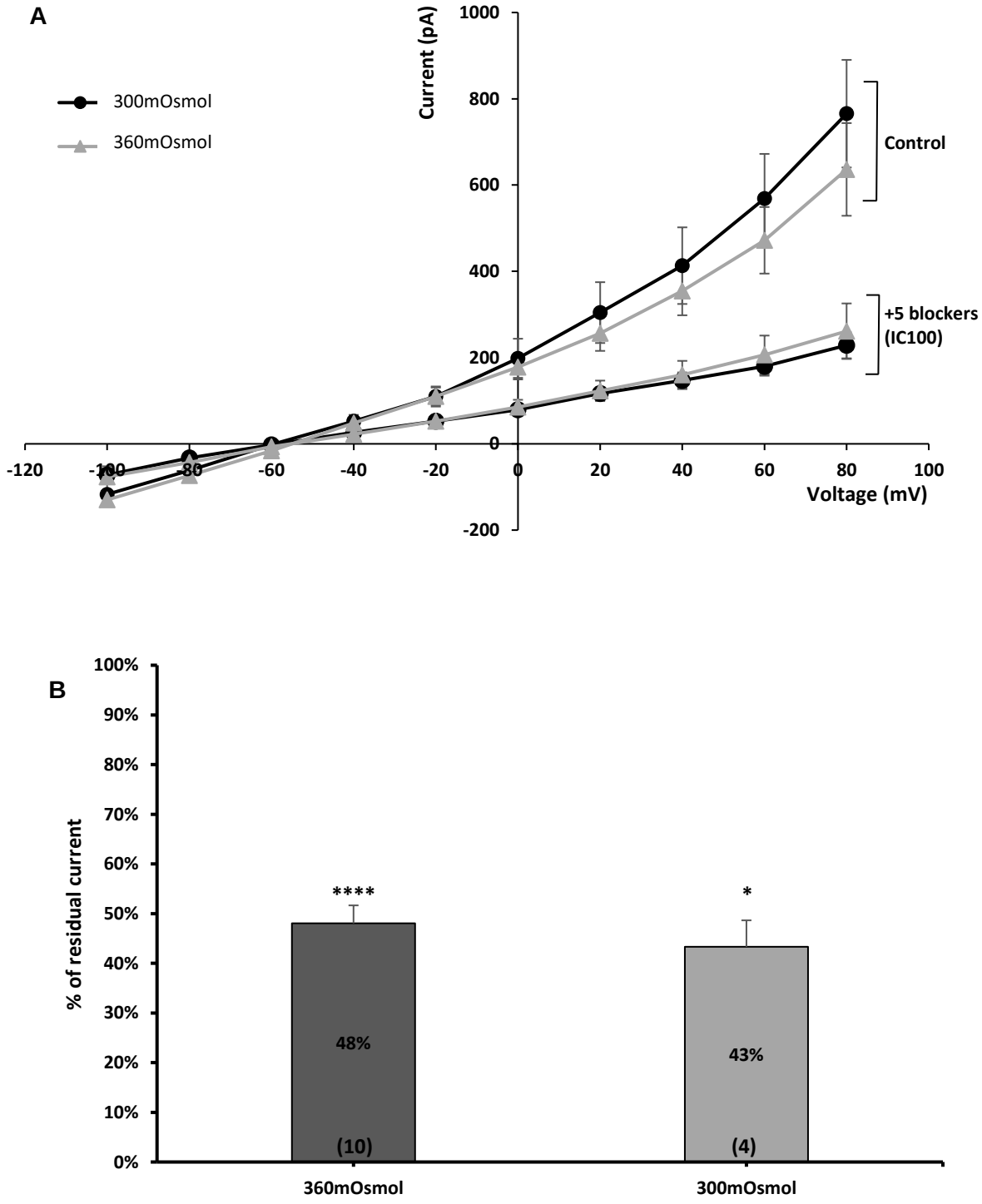

Figure 7. 11 External recording solution osmolarity modification and its effect on mitochondrial residual current post-administration of 5 blockers (IC_{100}). A. I-V relationship of mitochondria bathed in solutions of low (300mOsmol) or higher (360mOsmol) osmolarity and in response to voltage stimulations from -100 to +80 mV with 20 mV increments. **B.** Residual currents measured in response to 5 blockers (IC_{100}) are shown at 0 mV. All residual current values were calculated according to their control conditions (not shown) accounting for a total 100% mitochondrial current activity. n values for each recording sub-group is show in () in the graph. Data were collected from 2-3 preparations. Data are Mean ± SEM and significant differences obtained after paired or unpaired t-tests are indicated by asterisks with *p<0.05 and ****p<0.0001, n=4-10.

7.5 Is TASK-5 a functional mitochondrial channel?

The last step of the strategic approach includes the comparison of current amplitudes elicited in non-transfected (previously acquired in section 7.4) and transfected mitoplasts in the presence or absence of blockers. Currents were also recorded and compared in isolated mitochondria to investigate potential differences when the OMM is conserved.

Maximal current amplitude elicited from non-transfected mitochondria is greater (950±123 pA, n=7) than in mitochondria over-expressing TASK-5 (393±56 pA, n=4, $p<0.01$) at positive (+80 mV) voltage steps and in the absence of blockers (control condition; Figure 7.12 A). A first explanation for the two-fold difference in current amplitude is that TASK-5 over-expression could induce a physiological imbalance to the matrix of organelles resulting to $\Delta\psi_m$ modification (more positive) and matrix volume alteration due to a large pull of K^+ ions coupled with H_20 (section 2.12.1). Another hypothesis is that larger surface area and hence more channels expressed on the mitochondrial membranes of non-transfected mitochondria were patched during this set of experiments and generated larger currents. A possibility that could explain why the difference in current inhibition is more pronounced in non-transfected mitochondria (721±74 pA versus 210±49 pA, $p=0.2$) at +80 mV upon application of 4 blockers (IC_{100}) as, the likelihood of patching larger mitochondria was ~30% as shown by TEM (Figure 4.5). The inward current inhibition was also more pronounced in non-transfected mitochondria (from 217±36 pA to -100±25 pA, $p<0.01$) compared to transfected mitochondria (from -99±9 pA to -90±8 pA, $p=0.8$). Reversal potentials of non- (-49.71 mV) and transfected mitochondria (-48.89 mV) did not indicate a significant ($p>0.05$) alteration following TASK-5 transfection suggesting that the channel did not impact the resting membrane potential of the OMM.

In contrast, currents recorded in non-transfected mitoplasts have more comparable amplitudes with transfected mitoplasts both in the presence or absence of 4 blockers making it easier to identify potential changes linked to TASK-5 expression. A difference in current amplitude was detected at positive voltage steps and to a less extent at -100 mV between the two organelle groups. In fact, outward and inward currents are more noticeable in non-transfected mitoplasts (697±146 pA at +80 mV and -148±33 pA at -100 mV, n=6) in comparison to transfected organelles (496±133 pA and -99±19 pA, n=7). Application of 4 blockers reduced residual currents of non- and transfected mitoplasts down to 260±65 pA and 221±46 pA at +80 mV ($p<0.01$) respectively. Measuring and comparing V_{rev} values between the groups revealed that transfected mitoplast ionic equilibriums shifted towards more negative values (-57.74 mV) and closer to E_{K+} in the presence of 4 blockers in comparison to non-transfected conditions (-49.91 mV) which had a similar V_{rev} value with mitochondria (-49.71 mV) in absence of blockers.

Addition of 5 μM RR reduced outward currents from 410±70 pA to 141±40 pA in transfected versus 382±28 pA to 172±16 pA in non-transfected mitoplasts ($p<0.01$, n=6-7) at +80 mV. These results support the fact that despite a general reduction in mitoplast current amplitude in control conditions compared to currents acquired in the presence of 4 blockers, current inhibition was more noticeable in transfected organelles. Although no changes in inward current amplitude was detected between mitoplast groups bathed in 5 blockers, addition of RR reduced ionic efflux from -83±8 pA to -47±7 pA and from -81±13 pA to -37±8 pA ($p<0.01$) in non- and transfected mitoplasts respectively at -100 mV. V_{rev} values were also affected by RR as it induced a shift from -57.74 mV to -53.5 mV in transfected mitoplasts and from -49.91 mV to -52.57 mV in non-transfected organelles. Blocking Ca^{2+} channels with RR in addition to the previously targeted K^+, anion and voltage-sensitive channels seems to marginally affect the reversal potentials of organelles. Nonetheless, resting potential of transfected mitoplasts shifts towards less negative values and closer to non-transfected conditions in the presence of 5 μM RR. It is also important to note that transfected mitochondrial and mitoplast maximal outward current amplitudes were in the 400-500 pA range compared to organelles that did no over-express TASK-5 (400-950 pA) in absence of blockers. A difference in current amplitude that was taken into account as the strongest current inhibition observed in non-transfected organelle samples was, as previously mentioned, directly linked to their larger surface area and thus, stronger overall channel activity and not due to a more robust inhibitory efficiency of the blockers.

Residual currents elicited from both non- and transfected mitochondria/ mitoplasts were compared at 0 mV (Figure 7.12 B). Mean mitochondrial residual currents elicited after the application of 4 blockers revealed that 70±4% (from 92±8 pA to 73±2 pA) of the total channel activity remained active compared to 37±5% (from 227±32 pA to 87±17 pA) in non-transfected mitochondria (Figure 7.12 B). Application of 4 blockers to mitoplasts was then studied. Non-transfected mitoplasts had a mean residual current of 51±1% (from 159±29 pA to 81±16 pA) in comparison to transfected mitoplasts 57±2% (from 149±45 pA to 84±26 pA). A difference in channel activity ($p=0.1$) that may be linked to TASK-5 over-expression as no significant outward or inward alteration was detected within the I-V curves (Figure 7.12 A). Residual currents elicited from transfected mitochondria were more pronounced (70±4%) compared to mitoplasts (57±2%) at 0 mV. Application of 4 blockers to non-transfected mitochondria however, resulted to a stronger inhibition of mitochondrial residual currents compared to mitoplasts. Mitoplasts bathed in 4 blockers with 5μM RR resulted in 51±4% (from 102±8 pA to 52±5 pA) and 42±3% (from 95±22 pA to 41±11 pA) residual currents in non- and transfected mitoplasts accordingly. These data show that in the presence of RR the mitoplasts over-expressing TASK-5 were more effectively targeted (by 9%) than non-

transfected conditions by the blockers. Results also denote an additional residual current decrease accounting for 15% (p=0.07) between transfected mitoplasts in the presence of 4 or 5 blockers (from 84±26 pA to 41±11 pA) which is proposed to be related to TASK-5 inhibition.

Current traces acquired at 0 mV within non- or transfected mitoplasts in the presence of 4 or 5 blockers are shown in Figure 7.12 C. Traces demonstrate that transfected mitoplast current amplitudes are enhanced (~220 pA versus 100 pA) in comparison to non-transfected conditions and that in the presence of 5 blockers, transfected currents are more effectively inhibited. Addition of RR to the cocktail inhibits the channel activity of both mitoplast groups suggesting that despite having similar mean residual current values (51%) at 0 mV (as previously shown in Figure 7.12 B) IMM channels were still affected by RR.

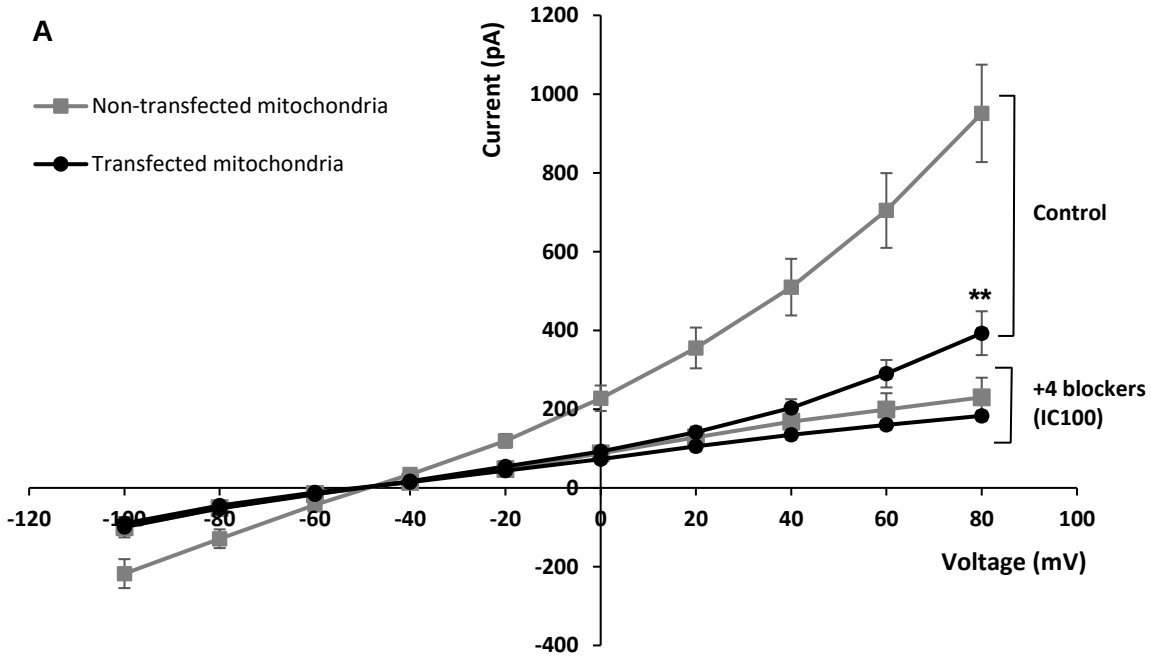

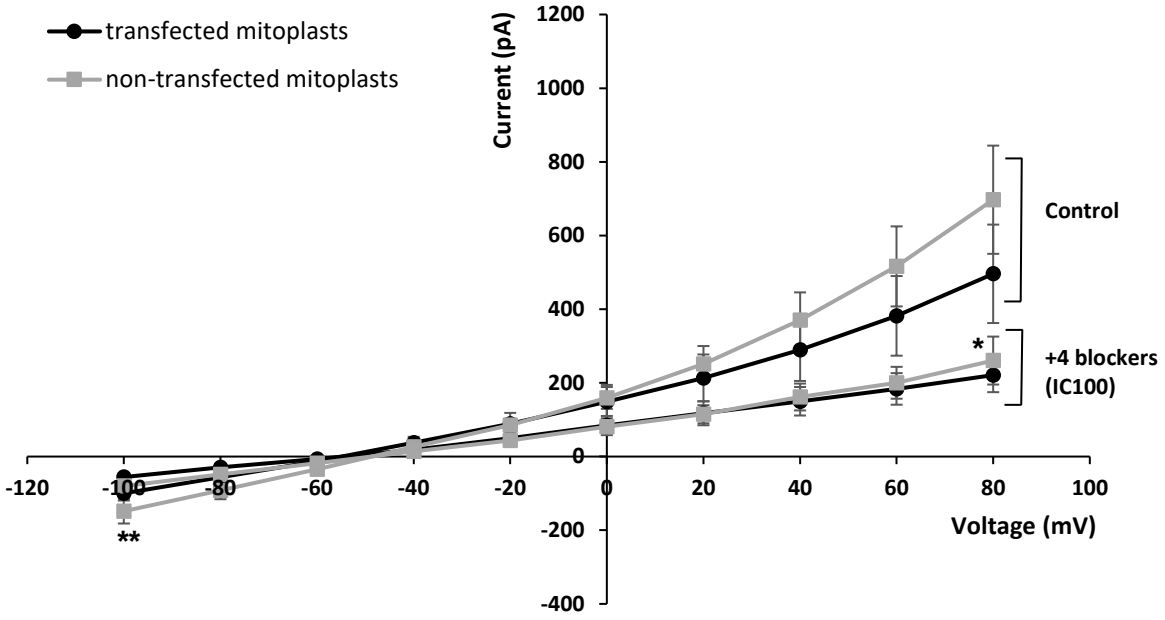
transfected mitoplasts
non-transfected mitoplasts
Current (pA)
1200
1000
800
600
400
200
0
-200
-400
-120
-100
-80
-60
-40
-20
0
20
40
60
80
100
Voltage (mV)
Control
+4 blockers
(IC100)
*
**

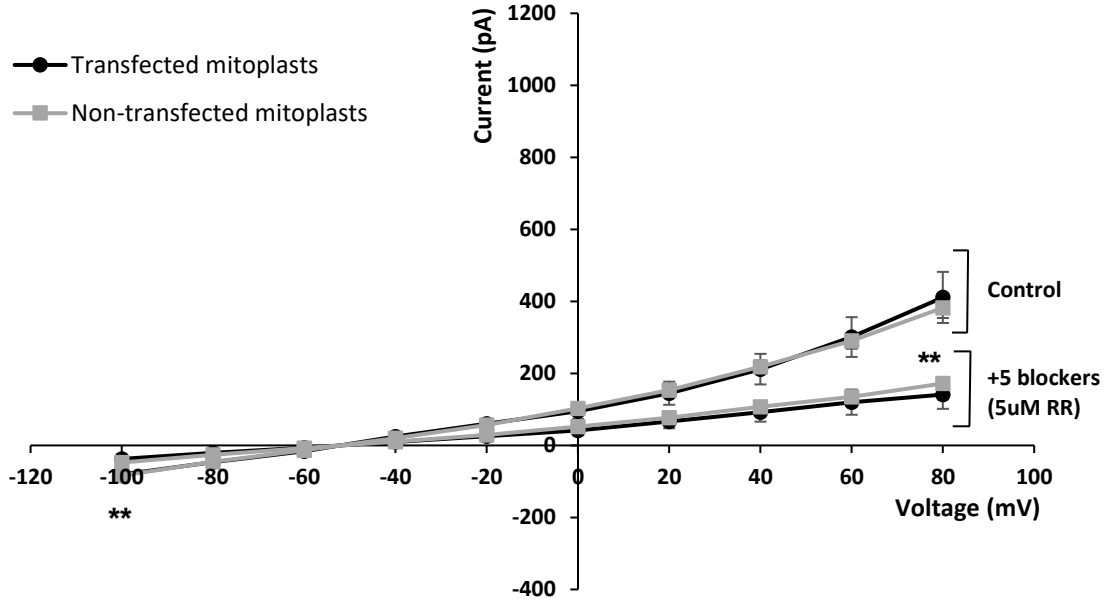
Transfected mitoplasts
Non-transfected mitoplasts
Current (pA)
1200
1000
800
600
400
200
0
-200
-400
-120
-100
-80
-60
-40
-20
0
20
40
60
80
100
Voltage (mV)
Control
+5 blockers
(5uM RR)
**
**

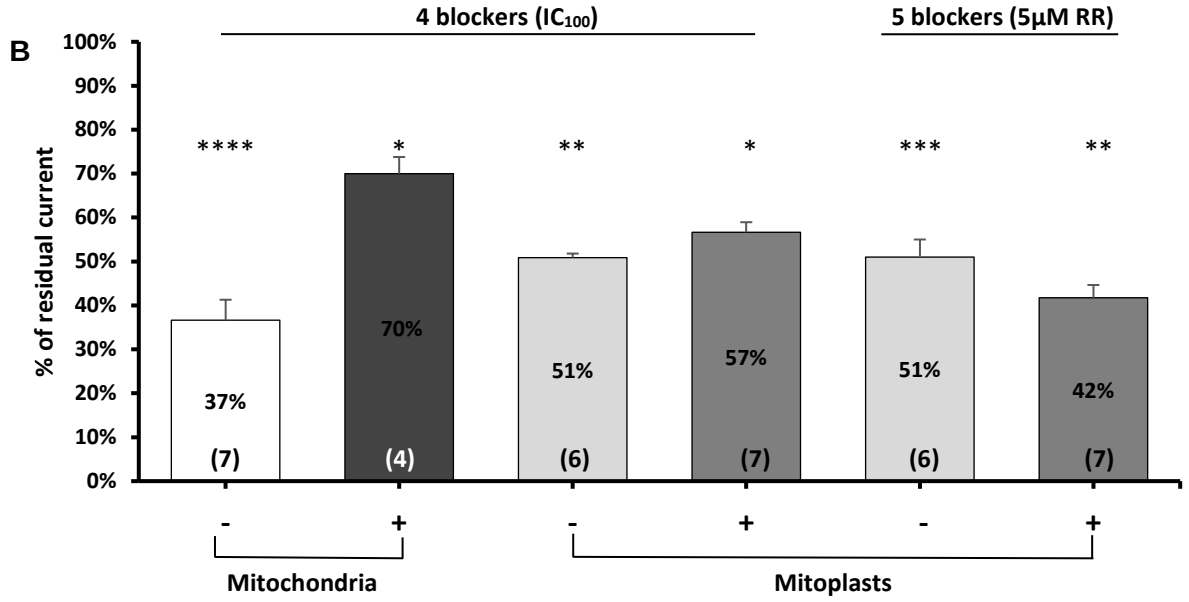

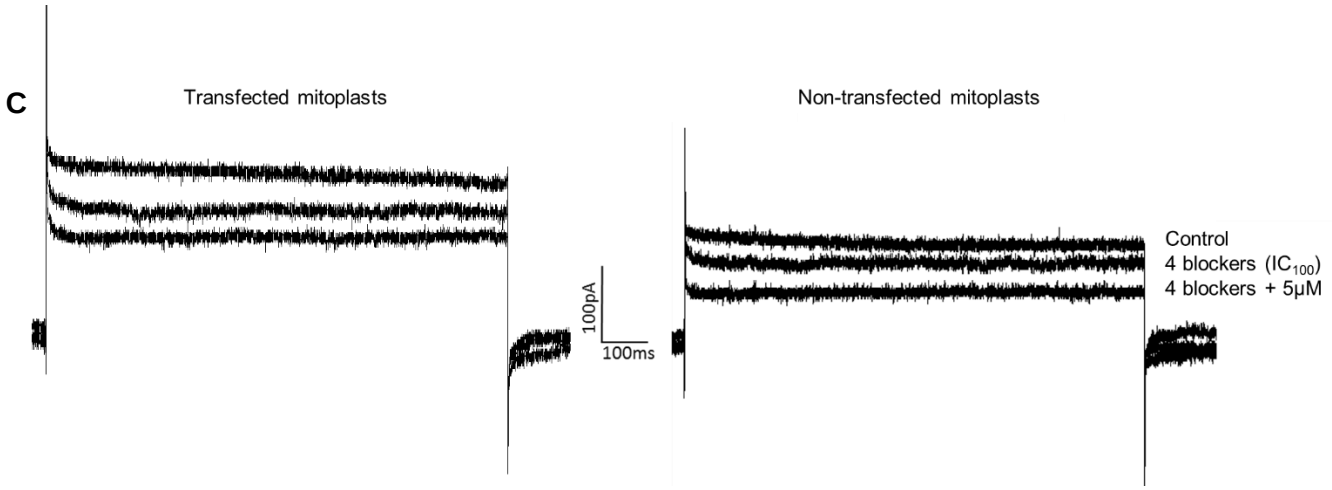

Figure 7. 12 Residual currents elicited post-application of 4 (IC_{100}) or 5 blockers (including 5µM RR) in non- and transfected organelles. A. I-V relationship of non- (-) and transfected (+) organelle residual currents recorded in the presence of a cocktail of 4 (IC_{100} concentration) or 5 blockers (5µM) and in response to voltage stimulations from -100 to +80 mV with 20 mV increments. **B.** Residual currents elicited in mitochondria or mitoplasts in response to cocktail blockers shown at 0 mV. All residual current values were calculated according to their control conditions (not shown) accounting for a total 100% mitochondrial current activity. **C.** Example family of traces recorded from isolated mitochondria or mitoplasts in control conditions or following exposure to 4 or 5 blockers. Voltage was stepped from -100 to +80 mV in 20 mV increments with a holding potential of -50 mV (solid line). Scale bar shows the current amplitude (pA) as a function of time in ms. n values for each recording sub-group is show in () in the graph. Data were collected from 2-3 preparations. Data are Mean ± SEM and significant differences obtained after paired t-test or 1-way Anova are indicated by asterisks with *p<0.05 and **p<0.01, ***p<0.001, ****p<0.0001.

7.6 Potential regulators of TASK-5

TASK channels are known to be sensitive to high [H^+] (section 2.7), a main characteristic of the sub-group that allows their discrimination from other K2P channels. TASK-5 has a conserved histidine residue at position 98 of the pore region responsible for its acid sensitivity, similarly to other TASK channels. Application of acid solution to transfected mitoplasts is hence hypothesised to induce larger current inhibition compared to non-transfected organelles, assuming that TASK-5 is a functional channel and that TASK-3 is not expressed in HeLa cells. To investigate whether the larger residual currents generated in transfected mitoplasts originate from TASK-5 channels electrophysiological experiments were performed in external recording solutions (with 4 blockers) of altered pH, ranging from acid (pH 6.2) to alkaline (pH 8.2) H^+ concentrations and compared to previously acquired data in neutral (7.4) pH (section 7.4-7.5). Control data in absence of blockers were averaged and individually compared to their blocked counterparts at 0 mV where voltage-gated channels were not active. RR was not used during these sets of experiments to avoid a possible targeting of TASK-5.

The percentage of residual currents recorded in transfected mitoplasts post-application of 4 blockers and at neutral pH were found to be higher (57±1%) than non-transfected organelles (51±2%, p=0.2) (Figure 7.13 A). Bathing mitoplasts in more alkaline solutions resulted to a 47±1% residual current in non-transfected mitoplasts which did not significantly differ (p>0.05) from data acquired in neutral pH. Alkaline conditions also seemed to induce an insignificant (p=0.4) but more pronounced blockade than neutral conditions in transfected (51±4%) organelles. Exposure of organelles to acid solutions reduced the residual current down to 39±5% in transfected organelles while non-transfected samples had a larger residual channel activity (51±6%). These data indicate that in the presence of 4 blockers the mitoplast channel activity was marginally larger in transfected compared to non-transfected organelles in neutral or alkaline solutions (p=0.2 and p<0.01). On the other hand, mitoplasts over-expressing TASK-5 were more efficiently inhibited in acid solution (p=0.2) compared to non-transfected organelles suggesting that the transfected mitoplast membranes express acid-sensitive channels that were targeted by an increase in [H^+].

Current traces extracted from a transfected mitoplast also demonstrate how K^+ current amplitudes decline during each pH modification of the external recording solution at 0 mV (Figure 7.13 B). Data show that under acid conditions the overall current amplitude is reduced in mitoplasts over-expressing TASK-5 and further endorse the fact that the channel of interest can be sensitive to increased [H^+]. More precisely currents reduced from ~60 pA in neutral pH to 55 pA in alkaline or 47 pA in acid solutions.

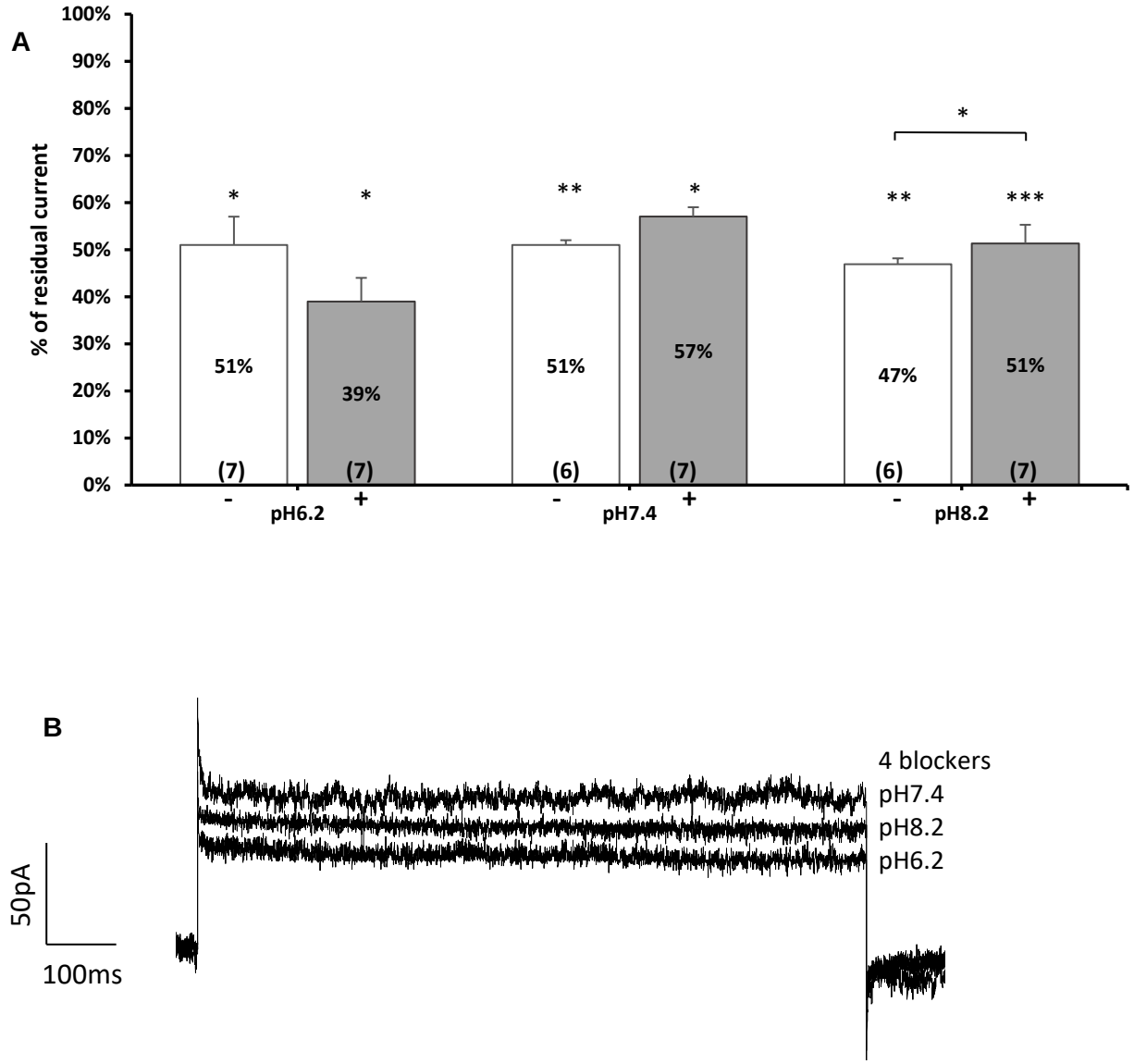

Figure 7. 13 Current inhibition of transfected mitoplasts by the administration of 4 blockers (IC_{100}) and pH modification of the external recording solution. A. Residual currents elicited in non- (-) and transfected (+) mitoplasts in response to 4 blockers and pH modification at 0 mV. All residual current values were calculated according to their control conditions (not shown) accounting for a total 100% mitochondrial current activity. n values for each recording sub-group is show in () in the graph. Data were collected from 2-3 preparations. **B.** Example family of traces recorded from isolated transfected mitoplasts following exposure to 4 blockers and different pH. Voltage was stepped at 0 mV with a holding potential of -50 mV (solid line). Scale bar shows the current amplitude (pA) as a function of time in ms. Data are Mean ± SEM and significant differences obtained after paired t-test are indicated by asterisks with *p<0.05 and **p<0.01, ***p<0.001.

To demonstrate that current inhibition in acid pH is mainly triggered by the over-expression of TASK-5 channels in comparison to non-transfected conditions, mitoplast residual currents recorded in the presence of 4 blockers and acid pH were subtracted from currents recorded in neutral pH and 4 blockers. Figure 7.14 A shows I-V curves recorded from transfected mitoplasts post-application of 4 blockers in neutral or acid pH. A reduction in outward currents was observed in the presence of 4 blockers and neutral pH from 697±147 pA (not shown) to 220±65 pA at +80 mV ($p<0.05$, $n=7$) whereas inward currents decreased from

148±33 pA (not shown) to -55±16 pA at -100 mV (p=0.2). Under these conditions, TASK-5 channels are hypothesised to be active while the 4 blockers target other residual K^+, Ca^{2+} and anion channels. Under acid conditions on the other hand, current reduced from 517±57 pA (not shown) to 165±50 pA at +80 mV (p=0.06) and from -128±36 pA (not shown) to -68±21 pA at -100 mV (p=0.08, n=7) demonstrating that by modifying the solutions pH, a stronger inhibitory effect was induced to transfected mitoplast channels at both positive and negative voltages. This observation was also made at 0 mV where residual currents significantly reduced from 84±26 pA at neutral pH to 61±18 pA (p=0.4) at acid pH.

By subtracting the currents recorded at pH 6.2 (at which TASK5 is predicted to be inhibited) away from the current at pH 7.4 (without TASK-5 inhibition) of transfected mitoplasts, a weak current was observed in comparison to non-transfected conditions where no current was detected (Figure 7.14 A). These results provide for the first time the evidence that over-expression of TASK-5 in the IMM was linked to an increased sensitivity to acid conditions. A mitoplast current reduction that can be linked to the closure of active TASK-5 channels expressed in the IMM.

TASK-5 current characteristics are summarised in Figure 7.14 B where a non-linear I-V curve with weak outwardly and inwardly rectifying properties, similarly to TASK-3, was observed (Kajma and Szewczyk 2012). The outward current reached 56±4 pA at +80 mV (p<0.01) and -12±11 pA at -100 mV. The residual current at 0 mV was 23±7 pA in comparison to 9±7 pA in non-transfected organelles with V_{rev} values of -52.5 mV and -45 mV accordingly.

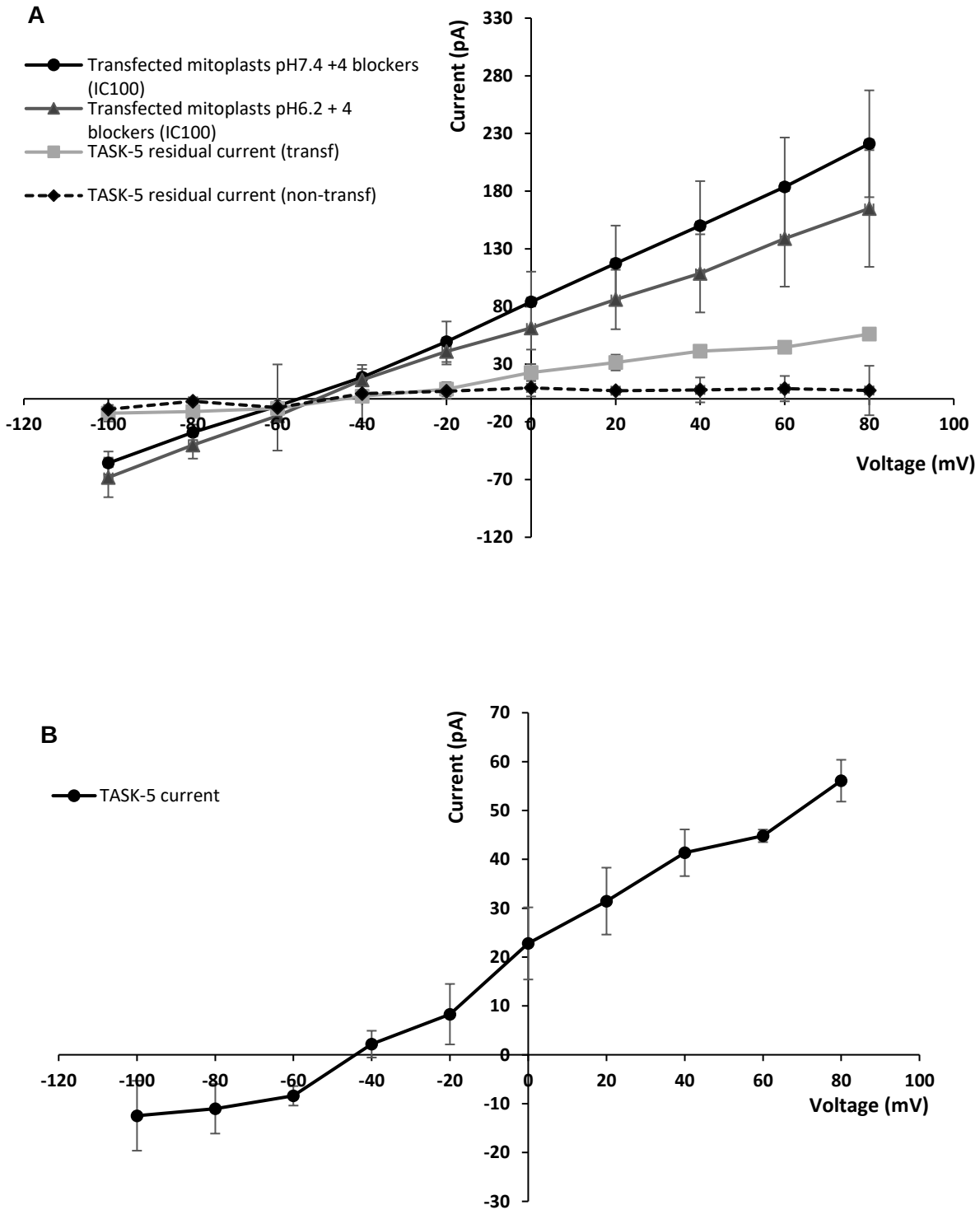

Figure 7. 14 Figure 7.13 Identification of TASK-5 currents in transfected mitoplasts. A. I-V relationship of transfected mitoplast residual currents recorded in the presence of 4 blockers and neutral pH or modified external H^+ concentration (pH 6.2). Currents were recorded in response to voltage stimulations from -100 to +80 mV with 20 mV increments. No particular channel activity was detected in non-transfected conditions (dashed line) (n=7-19). Data were collected from 3-5 preparations. **B.** I-V curve showing the current characteristics of TASK-5 channels when over-expressed in mitoplast inner membranes and blocked by acid pH. Data are Mean ± SEM.

7.6.1 TASK-5 is sensitive to ruthenium red

The final sets of experiments were designed to determine if TASK-5 channels were sensitive to RR, as predicted by TASK-5 sequence similarities to TASK-3. This was achieved by adding RR to the cocktail of blockers in neutral pH and comparing the inhibitory effect between solution acidification and RR application.

Previously acquired data in the presence of 5 or 4 blockers and acid pH (Figures 7.12 and 7.14) were merged in a single graph demonstrating that both RR and solution acidification can affect TASK-5 activity in a comparable manner (Figure 7.15 A). Application of 4 blockers in acid conditions inhibited outward currents from 517±125 pA to 165±50 pA (n=7) and from 411±114 pA to 141±40 pA (p=0.73, n=6-7) in the presence of 5 blockers at +80 mV. Inward currents recorded in the presence of 5 blockers were marginally weaker (from -81±22 pA to -37±8 pA) than mitoplasts bathed in acid conditions with 4 blockers (from -129±34 to -68±21 pA, p=0.67) which may be linked to an additional blockade of Ca^{2+} channels by RR. Moreover, the resting membrane potential of transfected mitoplasts bathed in the two different conditions was found to marginally different. In fact, in acid solution containing 4 blockers V_{rev} was -49 mV in contrast to –53.5 mV when organelles were bathed in 5 blockers (Figure 7.15 A).

Residual currents were then measured and compared at 0 mV where a reduction from 167± 25 pA to 61± 18 pA (39±5%) and from 95±21 pA to 41± 11 pA (42±3%, p=0.6) was induced by either an increase in $[H^+]$ or administration of RR in comparison to their corresponding control counterparts (51±3%) (Figure 7.15 B).

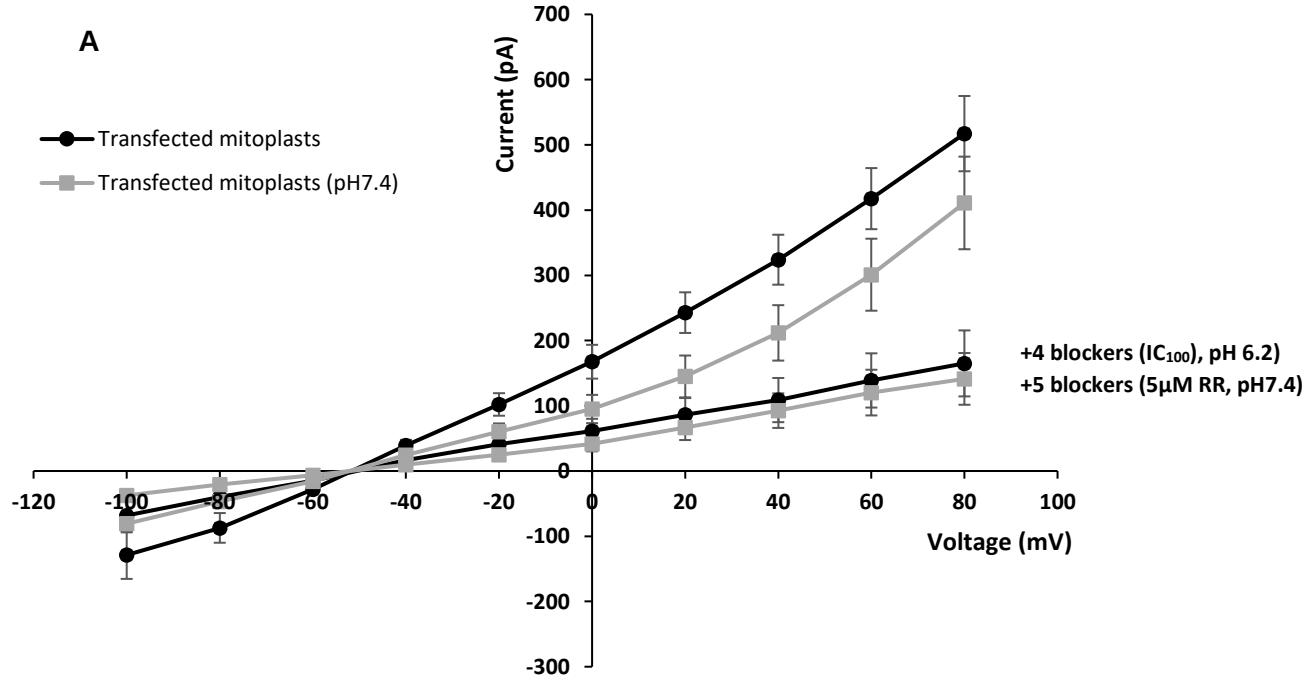

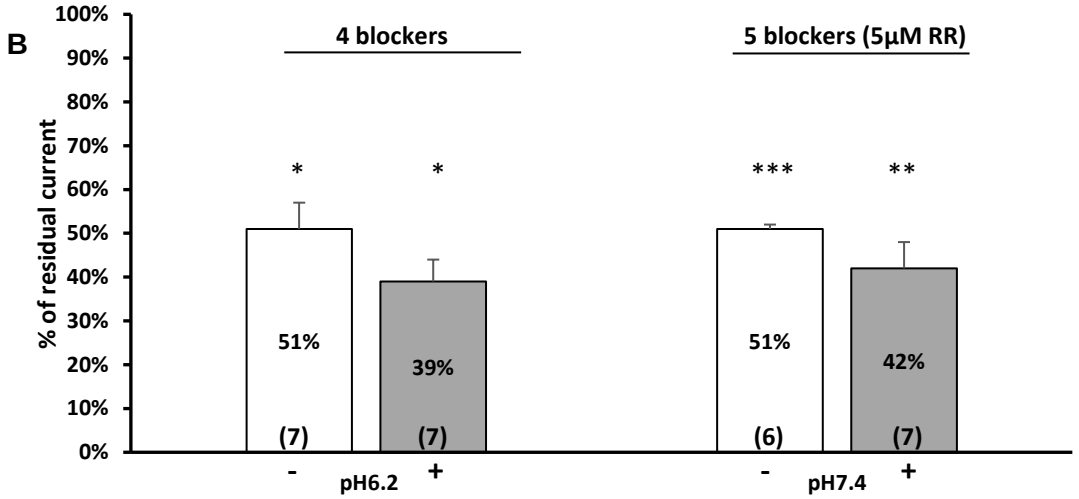

Figure 7. 15 Identification of potential inhibitors of TASK-5 channel within transfected mitoplasts, isolated from HeLa cells. A. I-V relationship of transfected mitoplasts bathed in acid or neutral external solutions in the presence of 4 or 5 blockers (5µM RR) accordingly and in response to voltage stimulations from -100 to +80 mV with 20 mV increments. **B.** Residual currents measured in response to 4 or 5 blockers at acid and neutral pH at 0 mV. All residual current values were calculated according to their control conditions (not shown) accounting for a total 100% mitochondrial current activity. n values for each recording sub-group is show in () in the graph. Data were collected from 2-3 preparations. Data are Mean ± SEM and significant differences obtained after paired t-test are indicated by asterisks with *p<0.05 and **p<0.01 and ***p<0.001.

As in Figure 7.14, the electrical characteristics of TASK-5 were assessed by subtracting the currents recorded post-RR application (where TASK5 was blocked) away from the current measured in the presence of 4 blockers and pH 7.4 (without TASK-5 inhibition) in transfected mitoplasts (Figure 7.16 A). Results show that the remaining active channels upon addition of 4 blockers are more sensitive to RR when TASK-5 is over-expressed compared to non-transfected conditions. Currents ranged between -18±2 pA at -100 mV and 80±6 pA at +80 mV when TASK-5 was over-expressed or from -32±9 pA at -100 mV to 28±28 pA at +80 mV in normal conditions (Figure 7.16 A). Additionally, the I-V curve characteristics of TASK-5 alone were comparable to Figure 7.14 B where a non-linear I-V curve with weak outwardly and inwardly rectifying properties was observed (Figure 7.16 B). Current amplitudes reached 42±14 pA compared to 9±10 pA at 0 mV in non-transfected conditions and reversal potentials of -60 mV and -41 mV accordingly.

Even though more experimental analyses should be performed in order to further study the electrophysiological, pharmacological and functional properties of TASK-5, this study provides a first piece of evidence that TASK-5 is a functional channel that can be sensitive to increased [H^+] and micromolar concentrations of RR within the IMM of HeLa cells.

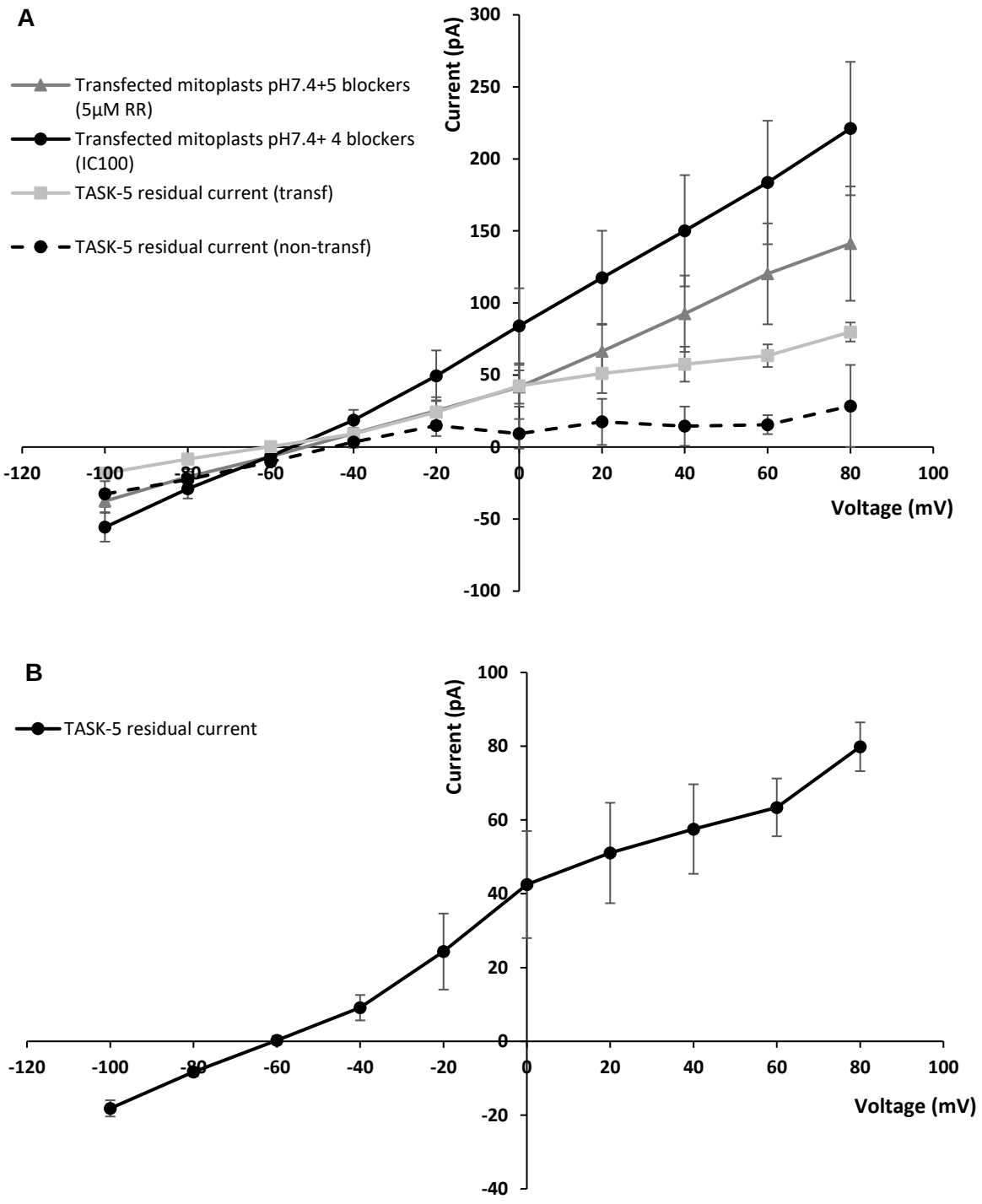

Figure 7. 16 TASK-5 channels are sensitive to RR. A. I-V relationship of transfected mitoplast residual currents recorded in the presence of 4 or 5 blockers at neutral pH and in response to voltage stimulations from -100 to +80 mV with 20 mV increments. No particular channel activity was detected in non-transfected conditions (dashed line) (n=7). Data were collected from 2-3 preparations. **B.** I-V curve showing the current characteristics of TASK-5 channels when over-expressed in mitoplast inner membranes and blocked by RR. Data are Mean ± SEM.

7.7 Conclusions

7.7.1 Identification of cell lines with an impaired TASK-3 endogenous expression

Previously acquired RT-PCR experiments studied the expression of *KCNK9* and *KCNK15* at the mRNA level in several cancer or healthy cell lines (Roncoroni 2012). The specificity of non- or commercially available antibodies in targeting TASK-3 and TASK-5 proteins was validated by immunocytochemistry on transiently transfected HEK293 or COS-7 cells (Roncoroni 2012). Based on these information, the endogenous expression of TASK-3 and TASK-5 was studied by immunocytochemistry on cell lines where the RT-PCR approach did not detect their mRNA products.

Inability to detect TASK-5 proteins in HEK293, where TASK-3 is endogenously expressed, was shown using the custom made antibody confirming the targeting efficacy of $_{h}$K2P15.1-LR. Conversely, TASK-5 protein was detectable and mainly located within the cytoplasm of COS-7 and HeLa cells confirming its subcellular localisation and inability to reach the plasma membrane. Endogenous TASK-3 was not detected both at the mRNA and protein level in these cells. Interestingly, the intracellular distribution staining of TASK-5 was not consistent with mitochondrial staining markers such as COX II. A reason explaining the different staining pattern could be the polyclonal origin of $_{h}$K2P15.1-LR recognising multiple TASK epitopes and increasing the potential for cross-reactivity compared to the monoclonal COX II antibody. Another plausible reason is the variable localisation of TASK-5 expressed within the nucleus, ER and endocytic vesicles in addition to the IMM and explaining the stronger cytoplasmic fluorescent staining pattern (Roncoroni 2012). Hence, results suggest that TASK-5 is intracellularly expressed with a putative mitochondrial localisation.

Using antibodies that have previously been validated provided an additional piece of evidence endorsing the lack of TASK-3 expression in COS-7 and HeLa. Even though positive and negative control cell lines should have been used to demonstrate endogenous TASK-3 or lack of TASK-5 expression in HEK293 or 786-0 cells for example; pharmacological experiments performed at later stages of the study confirmed the lack of TASK-3 expression in the cells tested and endorsed the targeting capability of the antibodies used. HeLa cells were thus considered appropriate for the particular study as the identification of TASK-5 currents elicited in transfected mitoplasts during pharmacological assays was facilitated. Isolation of organelles from COS-7 or HeLa was a direct and less invasive approach to circumvent current contamination generated from another acid-sensitive K2P channel while not having to silence TASK-3 with a siRNA construct.

7.7.2 Effect of 4-AP and TEA on mitochondrial channels

Administration of the IC_{100} concentrations of 4-AP and TEA, two inhibitors of voltage-sensitive channels, inhibited 32% and 45% of the total mitochondrial channel population at 0

mV. During these sets of experiments the probability that TASK-5 channels would be inhibited by these blockers was negligible as K2P channels are insensitive to classic K^+ channel blockers such as TEA^+, 4-AP, Ba^{2+} and Cs^+ (O'Connell, Morton et al. 2002, Patel, Jackson et al. 2013).

The large current potentiation (139%) induced by micromolar concentrations of 4-AP remains enigmatic as this is mostly attributed to the activation of voltage-activated Ca^{2+} channels (VACCs) expressed on the plasma membrane of excitable cells (Basavappa, Romano-Silva et al. 1994, Wu, Li et al. 2009, Li, Li et al. 2014). Between 1994 and 2014, several studies observed that application of micromolar or low millimolar concentrations of 4-AP indirectly stimulated VACCs during voltage-gated K^+ (K_v) channels targeting (Basavappa, Romano-Silva et al. 1994, Wu, Li et al. 2009, Li, Li et al. 2014). Basavappa, Romano-Silva et al., suggested that blockade of K^+ channels with 4-AP significantly increased intracellular ($[Ca^{2+}]i$) via activation of N-type plasma membrane Ca^{2+} channels in CHP-100 (Human neuroblastoma epidural tumour of spine) cells; while Wu and Li's studies performed in rodent neurons and HEK293 cells suggested that 4-AP also potentiated L-type Ca^{2+} channels between -90 and +50mV. These studies denote that high voltage-activated Ca^{2+} channels (HVACCs) are profoundly affected by 4-AP and several of its analogues independently of K_v channels.

Current traces recorded during the study were outwardly rectifying from -40mV indicating that positively charged ions could enter the mitochondrial matrix. To date, HVAC channels have not been identified in mitochondrial membranes but it is hypothesised that during administration of 4-AP at micromolar concentrations and the voltage clamp protocol applied activated HVACC. Large concentrations of Ca^{2+} ions might have thus entered the mitochondrial matrix disrupting the $\Delta\psi_m$. Even though this study focuses on studying residual TASK-5 currents post-application of a cocktail of channel blockers containing 10mM 4-AP, the electrophysiological and functional facet of 4-AP at the micromolar range should be further investigated in order to understand the mechanisms behind the current enhancement observed.

It is also important to note that both IC_{50} and IC_{100} concentration of TEA had a similar (55-57%) inhibitory efficiency to the mitochondrial channels at 0 mV and could be indicative of a saturated channel-compound binding level. However, residual current amplitudes greatly reduced with 20mM TEA at +80 mV showing that Kv channels were just inactive at 0 mV and thus, decision to use the IC_{100} concentration of the compound was taken.

Additionally, mitoKv1.3 is the only voltage-dependent K^+ channel that has been electrophysiologically characterised in mitochondria and shown to be sensitive to both TEA

and 4-AP (Szabo, Bock et al. 2005). The voltage clamp applied during the experimental recordings (0 mV) however was not in favour of activating voltage-dependent channels such as mitoKv1.3, which are known to be stimulated at +30 mV in symmetrical K^+ conditions (Szabo, Bock et al. 2005). The significant current reduction observed upon application of the blockers could hence either be linked to a) the inhibition of other voltage-sensitive channels together with their downstream signalling pathways such as TOM (+20-30 mV) or b) the prolonged (10-15 min) closed status of mitoKv1.3 at 0 mV which might have induced a $\Delta\psi_m$ depolarisation that affected the activity of other channels such as voltage-sensitive Ca^{2+} channels.

This study shows that application of millimolar concentrations of 4-AP and TEA can efficiently inhibit the activity of voltage-dependent K^+ and Ca^{2+} channels, significantly reduce current contamination from these channel sub-populations and facilitate TASK-5 characterisation. The fact that several mitochondrial channel populations have still not been fully characterised or even identified is another limitation of the study; as we assume that some ion channels such as HVAC are expressed in the organelles explaining the increase in current amplitude in response to 4-AP. It would be lastly important to understand which signalling pathways are involved in response to these blockers as mitochondria are highly excitable organelles, capable of generating and conveying electrical signals in response to stress indicating that several routes can be involved.

7.7.3 ATP, potentially a dominant mitochondrial channel blocker and its effect

Following 4-AP and TEA blockade, administration of ATP to the external recording solution was undertaken to block the activity of IMM channels such as mitoK_{ATP}, IMAC and UCPs.

Results showed that a significant and marginally stronger current reduction than that induced by 4-AP and TEA was induced by 1mM ATP as ~60% of the total mitochondrial residual current was blocked. These results suggest that ATP can be classified as a dominant blocker of the study due to its stronger inhibitory influence on mitochondrial channels. This blocking effect can have two interpretations; an assumption is that the endogenous expression of mitoK_{ATP}, IMAC and UCPs is more pronounced than other mitochondrial channels or alternatively, simultaneous blockade of stronger conducting (~100-150pS) channels (Figure 7.2), explains the stronger reduction in current amplitude.

Amongst the three targeted channels, mitoK_{ATP} has been more extensively characterised compared to anion channels. It is currently suggested that it participates in the regulation of mitochondrial ionic homeostasis and ischaemic preconditioning (IP) leading to cardio-protection by a yet unclear mechanism (Cohen, Baines et al. 2000). Reduction of K^+ and H^+ pumping following mitoK_{ATP} and UCP blockade is proposed to alter $\Delta\psi_m$ and hence increase

the superoxide production within the mitochondrial ETC, while inducing UCP-dependent proton leak activation (section 2.12.3) (Jarmuszkiewicz and Woyda-Ploszczyca 2008). Even though the exact functions and precise transport activities of UCPs are yet to be clarified, observations during this study there is a possible scenario that inhibition of anti-apoptotic channels together with UCPs affected the ATP synthesis machinery leading to the initiation of programmed mitochondrial death, explaining the sharp current reduction.

Another mitochondrial channel inhibited by the administration of ATP is IMAC; an anion channel that is activated during stress circumstances such as matrix alkalinisation due to ETC inactivity, Mg^{2+} depletion, $\Delta\psi_m$ depolarisation and increased oxidising conditions (Sorgato, Keller et al. 1987, Beavis 1992, Borecký, Ježek et al. 1997)**.** The functional role(s) of this channel remain in part to be clarified but it has been proposed to contribute to the oscillatory behaviour of $\Delta\psi_m$ and ROS production in cardiomyocytes subjected to oxidative stress and increased ROS production (O'Rourke, Cortassa et al. 2005, Aon, Cortassa et al. 2006, Zorov, Juhaszova et al. 2006, O'Rourke 2007). IMAC was also postulated to account for anion-selective mitochondrial swelling responses by cation and anion movements into the matrix compartment enabling them to restore their normal volume following pathological situations (Garlid and Beavis 1986). As IMAC is activated by ROS which exit the mitochondrial matrix once the superoxide levels are higher than physiological conditions; promoting its closure with ATP can potentially lead to ROS accumulation and ultimately induce organelles apoptosis.

The energy synthesis/release relationship was probably also affected post-ATP application as mitochondria were bathed in external recording solution devoid of ADP suggesting that ATP synthesis was not in favour as it would normally occur *in vivo*. A typical ATP molecule in the human body shuttles out of a mitochondrion and back into it (as ADP) for recharging more than once per minute, keeping [ATP] in the cytoplasm about 10 times higher than that of ADP (Alberts B 2002). During the study, the adopted experimental conditions were not in favour of maintaining the physiological milieu of the organelles. This was due to a $\Delta\psi_m$ depolarisation down to -50mV (instead of -200mV), an ADP deficiency and addition of ATP as a blocker in the external recording solution. Hence, the chances of promoting ATP hydrolysis within the IMM increased. Despite meeting the requirements of having lower [ATP] in the matrix compared to the external recording solution, $\Delta\psi_m$ depolarisation together with a prolonged stimulation of the ATPase (in reverse mode) may have led to organelle impairment during current recordings. This may explain the dramatic reduction in channel activity post-application of ATP.

In summary, administration of ATP to isolated organelles can reduce the activity of anti-apoptotic channels such as mitoK$_{ATP}$ but also, affect the electrochemical H^+ gradient due to an impairment of the F1F0 ATPase activity followed by energy depletion. Inhibition of mitoK$_{ATP}$, IMAC and UCP channels strongly reduces the residual current activity (by ~60%) and may be linked to the functionality/ultrastructure loss of the organelles when incubated for a prolonged time (more than 15 min) with ATP. Although continuous ATPase stimulation (in reverse) and its physiological effect on mitochondria has not been extensively studied to date, it is highly possible that ATP hydrolysis *ex vivo* is fatal for isolated mitochondria. These results should therefore take into consideration the conditions in which the organelles were patched, as absence of cytoplasmic factors that would contribute to the maintenance of their ultra-structure and viability *in vivo* have probably affected ion channel responses. Nevertheless, these conditions should not dramatically affect the characterisation of TASK-5 as planar patch-clamp recordings were performed within 10 min to avoid a potentially inducible mitotoxicity by the blockers. Examining isolated mitochondria in conditions that would mimic the cytoplasmic milieu is currently challenging but not impossible and would aid to better investigate the mitochondrial signalling pathways/mechanisms involved during ATP hydrolysis.

7.7.4 Application of Charybdotoxin on isolated organelles

Charybdotoxin was used to reduce residual currents elicited by mitoBK$_{Ca,}$ mitoIK$_{Ca}$ and mitoKv1.3. Application of the IC$_{100}$ concentration of ChTx inhibited ~60% of the total mitochondrial residual current. A blocking efficiency that also allowed to entitle ChTx as a dominant inhibitor.

mitoBK$_{Ca}$ plays a dual role both in modulating mitochondrial bioenergetics under physiological and Ca^{2+} overload conditions (Xu, Liu et al. 2002). In 2002, it was first suggested to protect cardiac tissues from ischemia and reperfusion using the BK$_{Ca}$ opener NS1619 (10–30 μM) (Xu, Liu et al. 2002). The role of mitoBK$_{Ca}$ in regulating ROS production has also been examined in guinea pig heart mitochondria. Results stated that ROS production was likely mediated by the inhibition of the channel (Heinen, Aldakkak et al. 2007). Therefore, inhibition of mitoBK$_{Ca}$ activity is proposed to consequently reduce the amount of K^+ transport necessary to depolarise mitochondrial membranes and increase cytochrome *c* release which is a landmark of mPTP opening and apoptosis (Cheng, Gu et al. 2008, Cheng, Gulbins et al. 2011).

In a recent study, IKCa expressed on the plasma membrane were shown to be inhibited by ChTx suggesting that their corresponding mitochondrial channels (mitoIKCa) could potentially be sensitive to the blocker (Guéguinou, Chantôme et al. 2014). It was also shown

that inhibition of mitoBKCa and mitoIKCa by ChTx induced a $\Delta\psi_m$ imbalance due to reduced K^+ transport across the IMM affecting the respiratory chain, ROS and energy production balance and matrix swelling following mPTP activation (Balderas, Zhang et al. 2015). Therefore, the strong current reduction observed post-application of ChTx may suggest that organelles started losing their physiological/structural characteristics leading to necrosis if patched for more than 15 minutes.

Inhibition of cyto-protective channels such as mitoKB$_{Ca}$, mitoKI$_{Ca}$ and mitoK$_{ATP}$ which are thought to be part of the main K^+ carriers (together with the K^+/H^+ exchanger) involved in the K^+ cycle across the IMM suggests that protection against ROS production, Ca^{2+} overload or mPTP opening can be impaired during recordings (Szabo, Leanza et al. 2012). Blocking these channels is expected to compromise mitochondrial functions due to the aforementioned simulated patho-physiological conditions which can lead to cell death as observed during neurodegenerative diseases or ischemia in heart (Ryu, Peixoto et al. 2010). Even though the long-term physiological consequences post-application of channel blockers were not of interest during the current study, residual currents should be studied up to 15 min post-application of the IC_{100} concentration of ChTx as organelles to properly interpret the blocking activity of this blockers. Finally, even though mitoKv1.3 is considered to be closed during planar recordings at 0 mV, bathing organelles with ChTx increase the chances of restricting its activity due to its sensitivity to the blocker (section 2.12.1).

7.7.5 Blocking effect of RR on mitochondrial channels

The activity of Ca^{2+} channels such as MCU, RyR, RAM, mCa1 and mCa2 (section 2.12.2) but also that of mPTP (section 2.11) was found to be sensitive to RR.

Administration of 10μM RR blocked ~40% of the total mitochondrial channel population representing Ca^{2+} (RaM, UP, Na^+/Ca^{2+} exchangers) channels and to a lesser extent endogenous TASK-5 channels. Conversely, the remaining channels (60%), mainly sensitive to ATP and ChTx accounted for K^+, anion, H^+ pumps of the ETC. Ca^{2+} signalling and uptake within the matrix is considered to be a fundamental characteristic of the organelles regulating intracellular trafficking, cell homeostasis and energy synthesis (section 2.12.2). In fact, when mitochondrial Ca^{2+} uptake is inhibited by the dye, $\Delta\Psi_m$ is suggested to collapse following ATP depletion, leading to increased ROS production, potentially opening of mPTP (Heinen, Camara et al. 2007) and explaining why nearly half of the residual current was affected. Moreover, reduction of Ca^{2+} signalling by RR may directly or indirectly affect the K^+ cycle involved in the volume regulation and prevention of matrix contraction, leading to an imbalance between energy supply and ATP consumption (Szabadkai, Simoni et al. 2006, Rizzuto, Marchi et al. 2009, Garcia-Perez, Schneider et al. 2011). Although the inter-

connection between the K^+ cycle and downstream signalling pathways, following Ca^{2+} channels blockade is currently unknown, application of RR for more than 15 minutes could damage the whole mitochondria channel/signalling machinery alike ChTx and ATP.

Additionally, it would be tempting to report that each blocker specifically targets a distinct ion channel group. However, signalling pathways downstream of each channel population may indirectly be linked to other ion channel regulatory cascades and therefore, residual current reductions should not be considered as absolute values representing a specific ion channel population. Residual ionic currents that might have not been affected by the 5 blockers are proposed to represent several complexes of the ETC (pumping H^+ outside the matrix), ion transporters, leak channels and possibly channels which have not been characterised yet.

Current reversibility upon blocker washout was also of great interest as it demonstrated that mitochondrial functionality and loss of membrane depolarisation can be recovered. Blockers that less inhibited organellar residual currents were 4-AP, TEA, ATP and RR which blocked voltage- and ATP-sensitive K^+ channels or Ca^{2+} channels. A current reversibility was anticipated for voltage-sensitive channels as voltage clamp stimulation should promote their opening in absence of blockers. ATP sensitive channels such as mitoK_{ATP} and considered anti-apoptotic were also shown to re-open as these are responsible for $\Delta\psi_m$ re-establishment, ROS production and PTP opening prevention. Moreover, as mitochondria act as Ca^{2+} buffers in response to increased external [Ca^{2+}], blocker removal was also expected to affect the opening of Ca^{2+} channels. In fact, the effect of RR was fully reversible indicating how important Ca^{2+} transport is important to maintain $\Delta\psi_m$ and synthesise ATP. The blocking recovery from ChTx on the other hand was less outstanding. Even though the reversibility efficiency of ChTx remains elusive to date a hypothesis would be that matrix [Ca^{2+}] restoration is prolonged under the effect of ChTx hence, the lower current amplitude recorded post 10 minutes of washout. To determine if this suggestion stands true, currents should be recorded after a longer period post-blocker removal.

All in all, these data demonstrate that blockers can be applied and studied on isolated organelles on a planar system and that they can inhibit IMM channels despite not having stripped off the OMM of isolated mitochondria. This suggests that either the blockers were able to cross the OMM by diffusion or through mPTP or; suction pulses applied by PatchControl did perforate the OMM resulting in patching the IMM. Even though the second hypothesis seems more credible, current amplitudes elicited from mitoplasts generated weaker currents than mitochondria annulling this suggestion.

7.7.6 Administration of cocktails of channel blockers on isolated organelles

To discriminate TASK-5 currents from K^+, Ca^{2+} or anion channels that were not of interest during the study, cocktails of channel blockers were designed and applied non- and transfected organelles so that these channels are inhibited in a synchronised manner. Any I-V curve or current amplitudes differences observed between endogenous or over-expressed TASK-5 would be hence due to the introduction of TASK5.

Application of the IC_{100} concentration of 4 blockers

To begin with, the IC_{100} concentration of 4 blockers was tested on organelles isolated from non-transfected HeLa cells. Currents were recorded from mitochondria to investigate potential current differences in response to blockers between organelles that had a conserved structure and those that were stripped off their OMM. This approach also allowed to confirm that blockers could cross the OMM suggesting that the induction of an osmotic shock to the organelles prior any pharmacological assay may be avoided.

Interestingly, both mitochondrial and mitoplast residual currents elicited from transfected cells were stronger than non-transfected conditions in the presence of 4 blockers at 0 mV. Even though mitochondrial residual current amplitudes were considerably different between non- (950±123 pA) and transfected (393±56 pA) mitochondria at +80 mV, residual currents measured at 0 mV had analogous amplitudes ($p>0.05$) indicating that the 4 blockers had an identical blocking effect to the remaining populations of channels. Mitoplast residual currents measured at 0 mV on the other hand were weaker in non- (81±16 pA) compared to transfected (84±26 pA) mitoplasts. Despite a non-significant difference ($p=0.1$) between the residual currents at 0 mV, there was a trend towards larger current differences at positive voltages ($p<0.05$). This is proposed to be linked to TASK-5 activity which might be lightly activated by positive voltage clamp stimulations. Results also denote that TASK-5 channels were not sensitive to any of the 4 blockers explaining the larger current amplitude observed in transfected organelles. The large difference in current amplitude between non- and transfected mitochondria is suggested to be mainly related to their difference in surface area stated in the following section. Additionally, V_{rev} values between organelle groups revealed that the ionic equilibrium of transfected mitoplasts shifted towards more negative values (-57.74 mV) and closer to E_{K+} in contrast to non-transfected conditions (-49.91 mV). A shift that was mainly linked to the over-expression of TASK-5 and thus, larger transport of K^+ ions across the IMM. Reversal potentials of non- (-49.71 mV) and transfected mitochondria (-48.89 mV) on the other hand did not significantly ($p>0.05$) differ following TASK-5 transfection. Results demonstrate that over-expression of TASK-5 in the IMM did not affect

the ionic activity of OMM channels but it also predicts that OMM can be patched on a planar patch-clamp system without rupturing it.

Addition of RR to the cocktail of 4 blockers

Non-transfected mitochondrial and mitoplast residual currents were studied in the presence of 5 blockers where the IC_{50} or IC_{100} concentrations of RR were administrated. According to previous studies where RR was used to totally abolish the activity of several mitochondrial Ca^{2+} channels, the most appropriate concentration to use for the current study was deduced to be 5 μM (Table 7.1). TASK channels are also reported to be sensitive to this dye at higher concentrations (Czirják and Enyedi 2002, Czirják and Enyedi 2003), therefore it was important to investigate whether a reduction in endogenous TASK-5 currents could be detected. Upon application of 10 μM RR, currents reduced from 183±23 pA to 83±12 pA in mitochondria and from 179±37 pA to 52±5 pA in mitoplasts ($p=0.3$) at 0 mV suggesting that RR targets and inhibits both OMM (VDAC) and IMM channels with a strong efficiency. Results also suggest that RR can potentially cross the outward membrane and block IMM channels confirming previous observations made within the study denoting that stripping off the OMM in order to study the current activity of IMM channels is important but not compulsory. Subsequently, by decreasing RR concentration to 5μM the residual channel activity increased from 52±5 pA (in 10 μM RR) to 67±11 pA ($p=0.2$) suggesting that the activity of endogenous channels such as TASK-5 may be sensitive to increased [RR]. Hence, decision to apply 5 μM RR to transfected organelles during the second phase of the study was taken to totally abolish the activity of Ca^{2+} channels while maintainig TASK-5 partially or totally active. Furthermore, it is interesting to note that addition of 5 or 10 μM RR reduced mitoplast residual currents down to ~170 pA and ~160 pA accordingly at +80 mV suggesting that RR and voltage-sensitive channels can generate up to 100 pA ($p<0.01$ and $p<0.001$) outward currents. These currents could be elicited from endogenous TASK-5 channels together with other channels or transporters that have not yet been reported as RR sensitive.

Transfected conditions

Current amplitudes were subsequently compared between non- and transfected conditions. Interestingly, transfected currents were reduced compared to non-transfected mitoplasts. An observation that was not in accordance with the hypothesis as over-expression of a functional channel should generate larger currents in comparison to endogenous conditions. In fact, these results may indicate that TASK-5 is instead not functional but several observations were made to contradict/explain this interpretation. A first possible explanation could be related to the additional manipulations that transfected organelles underwent. It is

important to keep in mind that transfected organelles were sorted by FACS, collected for ultra-centrifugation and bathed in hypotonic solution which may have affected their viability in comparison to their non-transfected counterparts. To investigate whether such conditions or TASK-5 over-expression caused current reduction, a mock control with GFP-transfected organelles should have been performed in parallel to these experiments. This approach would have allowed the treatment of GFP-tagged organelles similarly to TASK5-eGFP tagged mitoplasts, comparing their residual currents with non-transfected mitoplasts and determining whether the experimental procedure or TASK-5 over-expression could have triggered a down-regulation of other IMM channels.

Another observation was that a link between mitochondrial membrane surface area and current amplitude may exist. In fact, we hypothesise that the larger the organelle membranes, the more ion channels can be expressed and hence, generate larger currents. During organelle patch-clamp experiments, current amplitudes varied indicating that two populations of outward currents existed. This observation was confirmed during current analyses where a first set of I-V curves had a maximal outward current of ~500 pA while the second elicited stronger currents (up to 1.5 nA) at +80 mV (Figure 6.6B and 6.7C).

The surface area to current amplitude relationship was supported by comparing currents recorded from non-transfected mitochondria (Figure 7.11 A) which were significantly larger than transfected mitochondria. During pharmacological experiments, capacitance measurements of non-transfected mitochondria bathed in 4 blockers had an overall larger capacitance (indicative of surface area: ~5-6 pF) than transfected conditions (~2-3pF) and possibly explaining the stronger current difference observed. To further confirm this statement TEM images acquired in Chapter 4 (Figure 4.5) demonstrated that the size of several organelles can be larger than others. This finding provides a key interpretation to current recordings as it confirms the theory that the smaller the organelle, the less activity will occur due to a reduced surface area and hence, less ion channels expressed within membranes. Inability to visualise the samples studied on the planar patch-clamp system is considered to be a main limitation of the system as it prevents the observation of structure but also the size of patched organelles. Selecting organelles according to their membrane capacitance and comparing current amplitudes elicited from analogous organelle sizes would help in comparative channel. Membrane capacitance of non- and transfected mitoplasts conversely were within the same conductance (~6pF) range as observed in Chapter 6 (Table 6.2) and was more appropriate for residual current comparisons. K^+ currents elicited from transfected mitoplasts of the same surface area however, generated weaker currents than non-transfected organelles ($p>0.05$) suggesting that over-expression of TASK-5 may be linked to the inhibition/down-regulation of other channels.

Current to voltage relationship along with curve kinetics were compared between non- and transfected conditions. I-V curves plotted from non- and transfected organelles had similar curve kinetics (in absence of blockers) with a stronger rectification at positive voltage steps indicating that the activity of voltage-dependent channels was not impaired upon TASK-5 transfection. The non-linear current–voltage characteristics which did not follow the ideal background characteristics and was observed upon over-expression of TASK-5 could be due to a weak voltage dependence of the channel, similarly to TASK-3. In fact, the open probability of TASK-3 channels was shown to be voltage-dependent in symmetric 150/150 mM KCl isotonic solution with currents rectifying at both positive (+ 20 mV and + 80 mV) and negative (− 80 mV and − 20 mV) holding potentials in the inner mitochondrial membrane of isolated embryonic rat hippocampal cells (Kajma and Szewczyk 2012).

Additionally, during pharmacological experiments addition of 5μM RR to the cocktail of 4 blockers reduced transfected residual currents down to 41±11 pA in comparison to non-transfected (52±5 pA) conditions at 0 mV suggesting that sensitivity of the current to RR reveals the active expression of TASK-5. The difference in residual current amplitudes was more striking when transfected mitoplast currents were recorded in the presence of 4 blockers (84±26 pA) and compared to those bathed in 5 blockers with RR (41±11 pA). In fact, addition of RR reduced residual currents by 43 pA proposing that TASK-5 is targeted by the dye due to an E70 residue on its M1-P1 linker. Application of 5μM RR also induced a shift from -57.74 mV (in the presence of 4 blockers) to -53.5 mV in transfected mitoplasts and from -49.91 mV to -52.57 mV in non-transfected organelles. Data implying that in addition to K^+ and anion channel blockade, Ca^{2+} channels and endogenous TASK-5 inhibition by RR induced a small V_{rev} shift towards more negative values due to a reduced influx of positively charged ions. Inhibition of over-expressed TASK-5 channels on the other hand induced a shift towards less negative values which was far from E_{K+} demonstrating a reduction in K^+ transport and a strong indication that the channel of interest can be functional.

Finally, another crucial observation was that the total organelle residual currents were expected to have strongly reduced post-administration of the cocktails in comparison to individually applied blockers at 0 mV. Instead residual currents generated post application of cocktails were greater than ATP or ChTx alone. The osmolarity difference between mitochondrial matrix and the solute composition of the external recording solution did not significantly alter the channel sensitivity to the 5 blockers. Results indicate that organelles ultra-structure can be highly conserved as it is known that mitochondria can undergo rapid and considerable size/morphology changes during fission and fusion or stress conditions without losing their plasticity (Vincent, Ng et al. 2016). To date, it remains elusive why the

blocking efficiency of a single blocker is stronger than a cocktail of channel inhibitors and further studies need to be undertaken to investigate how these blockers interact or affect the binding sites of each targeted channel.

7.7.7 Identification of TASK-5 resembling currents

To examine if the current amplification observed in transfected organelles was linked to TASK-5 over-expression, the [H^+] of the external recording solution containing 4 blockers was modified and compared to currents acquired from non-transfected mitoplasts.

Bathing mitoplasts in alkaline solution significantly affected the sensitivity of transfected IMM channels in comparison to neutral conditions which resulted in the generation of stronger residual currents. Despite a non-significant current reduction in acid solution and in the presence of 4 blockers at 0 mV, results imply that there is a trend towards stronger channel inhibition at pH 6.2 when TASK-5 is over-expressed. These data do not directly demonstrate that over-expression of TASK-5 is associated to a stronger sensitivity to increased [H^+] but there is good evidence that the channel of interest is sensitive to acid pH. A possible reason could be that TASK-5 is partially inhibited at pH 6.2 and requires higher [H^+] to be totally blocked.

The current characteristics of TASK-5 were subsequently studied by subtracting residual currents measured in the presence of 4 blockers and neutral pH away from residual currents recorded in acid pH and 4 blockers. The same approach was adopted for currents measured within transfected mitoplasts bathed in 5 blockers with RR as it was observed that transfected currents were more sensitive to the dye upon addition of RR compared to their non-transfected counterparts. Single I-V curves were plotted in order to denote the current characteristics of TASK-5 in response to acid solution or RR. It is important to note that these currents do not exclusively represent TASK-5, over-expression of these channels may up- or down-regulate other signalling or functional pathways. Nevertheless, subtracted currents from transfected conditions were clearly larger than non-transfected ones both in response to acid pH and RR demonstrating that over-expression of TASK-5 can be responsible for the additional sensitivities to altered [H^+] and the dye.

Both subtracted TASK-5 I-V curves had similar current characteristics, rectifying at both negative and positive voltages suggesting that the channels may be to some extent voltage dependent similar to TASK-3. Results also endorse immunocytochemistry results showing that TASK-3 was not expressed in mitochondria of HeLa cells as subtraction of non-transfected currents during the pharmacological experiments with RR did not reveal another active channel group that would be sensitive to the dye.

Moreover, data showed that acid sensitive TASK-5 currents were smaller than RR-sensitive currents at both positive and negative voltage stimulations. This observation was also made at 0 mV where currents accounted for 23±7 pA in acid conditions compared to 42±14 pA measured in the presence of RR. Information indicating that RR may block the activity of other IMM (in addition to Ca^{2+}) channels that have not been characterised to date and function in conjunction with TASK-5. To further investigate this observation and identify the maximal blocking efficiency of RR, single channel recordings should be undertaken either by planar or automated patch-clamping on transfected organelles.

Reversal potentials also differed between TASK-5 currents, where acid sensitive ones reached equilibrium at -52.5 mV and RR-sensitive at -65 mV. V_{rev} values were nonetheless more negative than their non-transfected control counterparts (-41 to -45 mV), indicating that transfected mitoplast membranes are more K^+ selective (closer to E_{K+}) than non-transfected organelles. The explanation for why the RR-sensitive currents are closer to E_{K+} than acid-sensitive ones remains elusive but it could suggest that TASK-5 are partially active at pH6.2 and require higher $[H^+]$ to be totally inactive. More single channel recordings should be performed in external recording solutions of larger pH ranges to confirm this hypothesis.

Based on rationalised criteria (section 7.1) and data acquired during pharmacological experiments on non- and transfected mitoplasts it became clear that the significance of signature differences defined by the aforementioned criteria is equivocal. Results to this point only denote a putative mitochondrial expression of TASK-5 and a sensitivity to acid and RR when studied at the whole-mitoplast configuration on a planar patch-clamp system. Even though, there are still many lines of investigation and hypotheses to study or demonstrate (Chapter 8) in terms of functionality, metabolic or signalling processes, this work can be used as a proof of concept for future studies.

Chapter 8

Discussion

8.1 Thesis findings and novelties

This study is the first, as far as we know, to demonstrate that TASK-5 can be an active channel when expressed in the IMM of isolated organelles that have been electrophysiologically characterised on a planar patch-clamp system. This section summarises the novel technological but also ion channel characterisation approaches adopted during the study.

1. The putative mitochondrial localisation of TASK-5 channel in the IMM, previously demonstrated by the O'Kelly group (Laura et al., 2012; unpublished), was endorsed using immunofluorescence methods here. Even though the targeting efficiency of the antibody against TASK-5 does not seem absolute due to its polyclonal origin, it can still be used as a reliable tool to identify the channel within mammalian cells. To date, there are no commercially available antibodies able to detect TASK-5 by immunocytochemistry and thus, the usage of a custom made antibody able to identify the channel at the protein level is novel.

2. During the study, technically challenging techniques were optimised to enable the characterisation of mitochondrial IMM channels.
Techniques such as mitochondrial isolation and OMM removal were optimised to expose IMM channels. To confirm the immunopositivity of GFP-tagged organelles and that their ultrastructure was preserved following swell induction, flow cytometry and TEM were found to be suitable approaches to study mitochondria/mitoplasts in suspension. Both flow cytometry and TEM on isolated mitochondria were optimised to maintain mitochondrial ultra-structure and allow detection of their microscopic sizes as previous published studies did not provide sufficient technical information (Kirichok, Krapivinsky et al. 2004, Fahanik-babaei, Eliassi et al. 2011, Bednarczyk, Wieckowski et al. 2013). Hence, by performing TEM, optimal incubation periods in hypotonic conditions were identified in order to rupture the OMM of mitochondria and expose IMM channels and perform pharmacological assays.

3. Planar patch-clamp experiments on isolated and sorted TASK-5-eGFP positive mitoplasts have never been reported in the past and provide proof of principle that mitochondrial K^+ channels can be electrophysiologically characterised on such platform.
In fact, recording of ion currents elicited from intra-cellular membranes on a planar patch-clamp system has only been undertaken for mitochondrial Ca^{2+} or lysosomal Cl^- channels (Schieder, Rötzer et al. 2010). In the last 3 years several planar patch-clamp studies have been published on mitochondrial channels such as VDAC, respiratory chain complexes, ANT, mitoBK$_{Ca}$ or mitochondrial transporters at the single-channel level (Barthmes, et al.

2015, Briones, Weichbrodt et al. 2016, Barthmes, et al. 2017). More precisely, channels were isolated and reconstituted in giant unimaller vesicles (GUVs) and characterised on a port-a-patch or SynchroPatch 384. Ion channels that were studied using this approach were the A/M2 a proton channel essential for influenza virus replication (Balannik, Obrdlik et al. 2010), Nicotinic acetylcholine receptors (Niessen, Muschik et al. 2016) and neuronal purinoceptor 2 ($P2X_2$) (Schulz, Dueck et al. 2009). As these channels were characterised at the single-channel configuration in GUVs, characterisation of TASK-5 at the whole-mitochondrial configuration in isolated organelles is considered novel to date.

Moreover, the symmetrical recording solutions in which organelles were bathed were designed *de novo* for the study allowing to maintain stable seals and characterise mitochondrial K^+ channels. The presence of F^- ions was found to be vital during planar recordings as complete abolishment of these ions failed to form mitochondrial membrane gigaseals. Another aspect that was fundamental was to identify optimal recording parameters on PatchControl software as this information was not reported in any published study. Such parameters included the negative or positive pressures applied by the suction unit, setting up seal resistance thresholds and time periods. Future studies interested in investigating the channel activity of mitochondrial K^+ channels can follow this technological approach as this study not only states optimal recording solutions suitable for the platform, but it also presents detailed recording parameters allowing to achieve the whole-mitochondrial and mitoplast configuration.

4. Characterisation of TASK-5 currents was carried out in mitochondria isolated from HeLa cells which were shown to not endogenously express TASK-3 and thus, avoid current contamination from another K2P channel. By applying a cocktail of channel blockers designed for the particular study and modifying the $[H^+]$ of the external recording solution this study is the first, to our knowledge, to demonstrate that TASK-5 channels may be functional when over-expressed in the IMM. This observation is partially in accordance with previous findings stating that TASK-5 channels are not functional on the plasma membrane; this sub-group of channels is preferentially expressed and probably active intracellularly.

Even though the single-channel biophysical characteristics of TASK-5 were not investigated during this study, it provides the first evidence that the channel of interest may be functional when adopting a series of optimal experimental approaches and a planar patch-clamp system.

8.2 Proposed physiological role of TASK-5 in mitochondria

Endogenous expression of TASK-5 is proposed to have a physiological role in human tissues where its cDNA product was detected (Roncoroni, 2012). *KCNK15* mRNA was

previously shown to be expressed in a broad range of human adult and fetal tissues and in certain human cancer cell lines (Roncoroni, 2012, Williams, 2011). TASK-5 showed concomitant expression with either TASK-1 or TASK-3 in several tissues including heart, lung, kidney, pancreas and brain for TASK-1 and pancreas and brain for TASK-3. The expression of TASK-5 in the same tissues with TASK-1 or TASK-3 together with previous evidence of heterodimerisation between TASK-1 and TASK-3 (Czirjak and Enyedi 2002, Berg, Talley et al. 2004, Clarke, Veale et al. 2004, Kang, Han et al. 2004, Enyedi and Czirják 2010) gives ground to hypothesise that potential heterodimerisation between TASK-5 and another TASK channel may also occur in mitochondria. This potential hetero-dimerisation may have regulatory effects on TASK-5 or TASK-1 and TASK-3 as shown for other K^+ channel subunits. Nevertheless, absence of TASK-3 expression in COS-7 and HeLa denotes that TASK-5 does not necessarily require to hetero-dimerise with another channel to properly operate in these particular cell lines and thus, disproving the channel dimerisation hypothesis.

The possible significance of TASK-5 within mitochondrial function is supported by several pieces of evidences summarised in Figure 8.1. Briefly, by controlling $\Delta\psi_m$, TASK-5 could impact the activity of voltage-gated K^+ and Ca^{2+} channels, which are known to regulate nitric oxide (NO) signalling pathways or $[Ca^{2+}]$ homeostasis within the mitochondrial matrix respectively (Figure 8.1A). Mitochondrial Ca^{2+} signalling is involved in the inhibition of ROS generation which together with NO-driven pathways are suggested to suppress apoptosis. Additionally, the inner mitochondrial membrane has a high permeability to water, which allows an osmotic equilibrium between mitochondrial matrix and its environment (Das, Parker et al. 2003, Garlid and Paucek 2003, Bednarczyk, Barker et al. 2008). TASK-5 could participate in the control of the mitochondrial K^+ concentration (ΔK^+), influence osmotic movements and hence mitochondrial matrix volume by regulating H_2O entrance (Figure 8.1B). Concurrently, increased K^+ within mitochondrial matrix is known to enhance the activity of K^+/H^+ exchangers with consequent mitochondrial matrix acidification. Protons within the mitochondrial matrix are transported into the intermembrane space (Bednarczyk 2009), conferring a double importance to the K^+/H^+ exchange in avoiding excess matrix swelling and increasing the proton gradient across the mitochondrial inner membrane which is essential to ATP generation. In this context, the presence of TASK-5 within mitochondrial membranes may be of particular interest as it may inhibit TASK-5 activity through the channel pH sensor and hence result in a feedback control mechanism to regulate mitochondrial membrane potential. The second hypothetical role of TASK-5 seems more plausible as, during stress conditions where matrix swelling and acidification occurs; TASK-5 closure would alter $\Delta\psi_m$ and promote activation of mitoBK_{Ca} and mitoK_{ATP} as a rescue

mechanism. Restoration of matrix pH would subsequently trigger TASK-5 in a feedback activation loop. Furthermore, co-localisation of TASK-5 with two components of the respiratory mitochondrial chain cytochrome bc1 and COX II suggests that it could also be involved in the biochemical generation of ATP. By controlling $\Delta\psi_m$ and levels of H^+ pumped within the ETC, TASK-5 may be involved in procedures requiring high energy supply such as cell signalling, hormone and neurotransmitter release, muscle contraction and cell excitability.

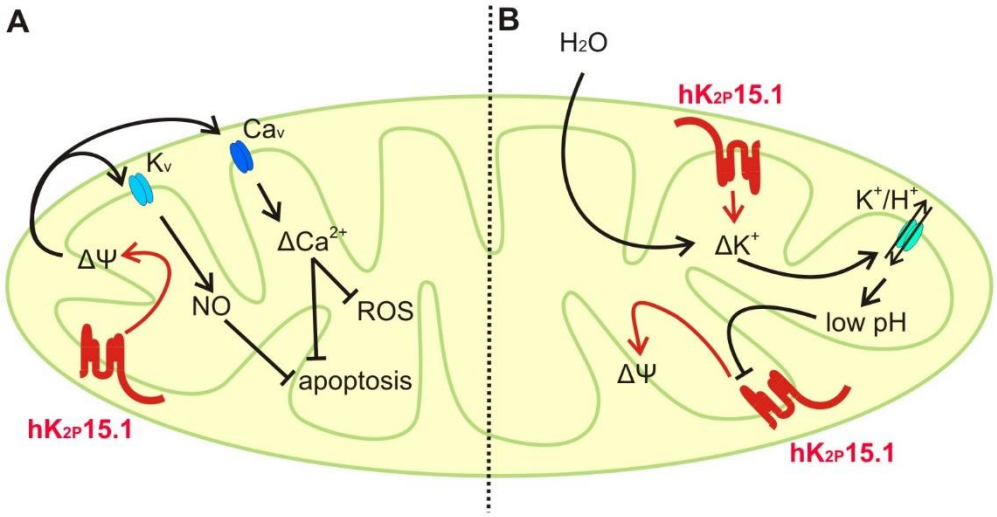

Figure 8. 1 Two proposed roles for TASK-5 in mitochondrial function. Diagram showing two potential roles for TASK-5 (red) within mitochondria. Other mitochondrial membrane proteins including a K_v channel (pale blue), a $Ca^{2+}{}_v$ channel (blue) and a K^+/H^+ exchanger are indicated. Red lines indicated direct consequences of TASK-5 activity, while black lines indicate subsequent implications of these. **A.** By controlling mitochondrial membrane potential (ΔΨm) TASK-5 may directly influence voltage-gated K^+ (K_v) and Ca^{2+} channels (Ca_v). K_v and Ca_v activity would influence NO pathway and mitochondrial Ca^{2+} signalling and result in the regulation of ROS production and mitochondrial-driven apoptosis. **B.** By controlling the influx of K^+ into the mitochondrial matrix (ΔK^+) TASK-5 may influence H_2O osmotic entrance into mitochondria and hence regulate mitochondrial volume. Increased ΔK^+ would then stimulate K^+/H^+ exchanger activity leading to mitochondrial matrix acidification. This may inhibit TASK-5 activity through predicted channel pH sensitivity. TASK-5 inhibition would then affect ΔΨ in a feedback regulatory mechanism to control both mitochondrial swelling and acidification. Image adapted from Roncoroni, 2012.

Altered mitochondrial activity of TASK channels in cancer cells

K^+ channels play fundamental roles in cell behaviours linked to cancer progression including regulation of cell proliferation, migration, apoptosis and angiogenesis (Lang, Föller et al. 2005, Hanahan and Weinberg 2011, Schwab, Fabian et al. 2012). Increased or decreased expression of these channels has previously been shown to induce membrane hyperpolarisation or depolarisation respectively resulting in altered cell functioning (Duprat et al., 1997; Enyedi and Czirják, 2010; Goldstein et al., 2001; Lesage and Lazdunski, 2000; Meadows and Randall, 2001). In fact, cell membrane potential (driven by K^+ channel activity) plays an important regulatory role in cell cycle progression, proliferation and apoptosis with

highly proliferating cells displaying a more positive membrane potential than quiescent cells (A, L et al. 1995, Pardo 2004, Wang 2004). As K_{2P} channels directly affect cellular membrane potential at rest, their ability to impact the function of other ion channels and their sensitivity to environmental stimuli (O2, pH, glucose, stretch) known to change in the cancer microenvironment may be impaired in cancer cells and provide these the ability to survive. To date, the precise regulatory mechanisms adopted by TASK-5 channels are unknown but evidence supports two hypotheses. The first proposes that changes in membrane potential due to K^+ channel activity modulates voltage-gated Ca^{2+} channels impacting Ca^{2+} influx and downstream signalling (Pardo 2004, Felipe, Vicente et al. 2006). The alternative hypothesis proposes that the changes in cell volume seen during proliferation and apoptosis (cell shrinkage or swelling) may be regulated by K^+ channel activity (Waldegger, Steuer et al. 1998, Wang 2004, Bortner and Cidlowski 2007). In a similar manner, K^+ channel control of membrane potential has been shown to impact cell migration through regulation of cell volume, pH and intracellular Ca^{2+} concentration. Therefore, changes in TASK channel activity in cancer cells could have physiological consequences, either by directly regulating cancer hallmark functions or by altering the activity of other ion channels.

Of the fifteen K2P channels only TREK-1 and TASK-3 have been well described as differentially expressed in cancer (Mu, Chen et al. 2003, Voloshyna, Besana et al. 2008). More recently, two other K2P channels (TASK-1 and TASK-5) have been identified in cancer cell lines without being physiologically characterised (Williams, Bateman et al. 2013).

Hypermethylation of gene promoters was shown to repress binding of transcription factors to DNA resulting in gene silencing (Berdasco and Esteller 2010). In cancer, hypermethylation of ion channel promoters (Ca^{2+} channel; CACNAIG and Na^+ channel; SLC5A8) is thought to have a role in tumour suppression (Shu, Jelinek et al. 2006). The promoter of *KCNK15* which encodes TASK-5 has been found to be hypermethylated in colorectal and leukaemia cancer cell lines (Shu, Jelinek et al. 2006). The functional implications of altered *KCNK15* expression are yet unknown but could be linked to membrane potential changes involved in cell apoptosis and migration. Hence, TASK-5 hypermethylation could be used as a process to avoid cancer cell survival, suppress tumourigenesis or cancerous cell differentiation. In fact, early apoptotic pathways involve enhanced K^+ efflux from the mitochondrial matrix which results to a first hyperpolarisation of the membrane potential, followed by Ca^{2+} overload, cytochrome *c* release and ROS production (Yu 2003, Lehen'kyi, Shapovalov et al. 2011).

Additionally, to resist apoptosis some cancer cells downregulate specific K^+ channels (decreased mitochondrial KV1.5 expression is detected in lung and glioblastoma cancer cell

lines), or upregulate certain transporters to restore intracellular [K^+] (such as Na^+/K^+ ATPase; Bonnet et al., 2007; Lehen'kyi et al., 2011; Yu, 2003). TASK-5 could be involved in this procedure by upregulating the activity of these channels. TASK-3 channels expressed within the mitochondrial membranes of melanoma cells (WM35) are suggested to support mitochondrial activity, ATP production and enhance cell survival (Kosztka, Rusznak et al. 2011). Knockdown of TASK-3 in melanoma cells was shown to reduce their proliferative abilities and impair the mitochondrial functions (Rusznak et al., 2008). Assuming that TASK-5 has similar functional characteristics with TASK-3, inhibition of TASK-5 could instead be detrimental to mitochondria and cells, suggesting that the channel may have a pro- and/or anti-apoptotic roles in cancer.

Neuronal and cardiac expression of TASK channels

K2P channels are widely expressed in the central nervous system and periphery with different but often overlapping expression patterns. In neurons, they have a major role in determining not only the membrane potential but also membrane input resistance which is a primary factor in the magnitude and kinetics of synaptic responses (Bayliss and Barrett 2008). Despite their widespread expression and contributions to crucial cell properties, K2P gene deletion has proved remarkably benign in unstressed mice (Bayliss and Barrett 2008). Under physiological or behavioural challenges however, TASK and TREK-1 knockout mice for example, revealed to have key contributions to several important functions. In fact, TREK-1 channels were activated by intracellular acidification and by PUFAs known to provide neuroprotection from cerebral ischaemic stress (Honore 2007). By knocking out TREK-1, mice displayed a lower incidence of behaviours representative of helplessness and depression.

Knockdown of TASK-3 in late-born cortical neurons by RNAi resulted in migration defects as the channel was shown to play an important role in neuronal migration in the developing cerebral cortex (Barel, Shalev et al. 2008, Bando, Hirano et al. 2014). Additionally, electrophysiological experiments showed that knockdown of TASK-3 depolarised resting membrane potential and increased the frequency of spontaneous Ca^{2+} transients (Barel, Shalev et al. 2008). These studies suggest that dysfunction of TASK-3 impairs migration of cortical excitatory neurons in an activity-dependent mechanism. In male mice deleted for both TASK-1 and TASK-3 subunits ($TASK^{-/-}$), the membrane potential of zona glomerulosa (ZG) cells expressed in the adrenal cortex was significantly depolarised (Davies, Hu et al. 2008). Characteristics of $TASK^{-/-}$ mice that were similar to those of patients with idiopathic primary hyperaldosteronism (Wisgerhof, Carpenter et al. 1978, Wisgerhof, Brown et al. 1981, Young 2007), indicating that TASK channels have an important role in regulating ZG

cell-membrane potential and limiting aldosterone production. To lower aldosterone levels and improve target-organ damage produced by aldosterone excess, drugs that increase TASK-channel activity were suggested to represent a new therapeutic avenue (Rajagopalan and Pitt 2003, Calhoun 2006, Young 2007).

Neurons critically depend on mitochondrial function to establish membrane excitability and to execute the complex processes of neurotransmission and plasticity. The central nervous system (CNS) has a high metabolic demand as neurons are highly differentiated cells that need large amounts of ATP for maintenance of ionic gradients across the cell membranes and for neurotransmission (Silver and Erecinska 1998). Since most neuronal ATP is generated by oxidative metabolism, neurons critically depend on mitochondrial function and oxygen supply (Mayevsky and Chance 1975, Ames 2000, Collins, Berridge et al. 2002) and are very sensitive to mitochondrial dysfunction (Fiskum, Murphy et al. 1999, Brookes, Yoon et al. 2004). Pathological neuronal activity for example induces mitochondrial dysfunction and ROS production in the early phase of seizure activity (occurring in epileptic patients) which contributes to neuronal cell death (Bengzon, Mohapel et al. 2002).

TASK-5 can have several functions in neurons. As with other K2P channels, TASK-5 could monitor the membrane potential and excitability of neurons in response to external stimuli under normal but also stress conditions. It can also serve as a molecular substrate for chemoreception (regulation of acid-base balance during respiration) similarly to TASK-1 and TASK-3 K^+ currents identified in raphe neurons (Washburn, Sirois et al. 2002, Talley, Sirois et al. 2003, Mulkey, Stornetta et al. 2004, Putnam, Filosa et al. 2004). During a study in 2007, pH sensitivity was abolished in raphe cells of the brainstem of TASK-1 and TASK-3 knockout mice but interestingly, CO_2-induced ventilatory responses were preserved (Mulkey, Talley et al. 2007). Data indicated that the expression of TASK channels in the plasma membrane of respiratory-related brainstem neurons was not necessary for ventilatory responses to CO_2. Nevertheless, pH regulation by TASK-3 and/or TASK-5 channels in the mitochondrial matrix may be more essential for the preservation of neuronal functions/structure/excitability. In fact, knocking-down or inhibiting TASK-5 in the organelles could be detrimental for the brain cells as the matrix pH balance will be impaired, directly affecting $\Delta\psi_m$ due to an ionic imbalance linked to K^+ and Ca^{2+} transport but also other processes such as ATP or ROS production. Such compromised conditions were shown to occur in the early phase of epilepsy seizure activity which contribute to neuronal cell death (Bengzon, Mohapel et al. 2002). Hence, TASK-5 channels can be important for the maintenance of the mitochondrial oxidative and/or glycolytic energy metabolism in neurons. It is finally important to take into consideration that by knocking down TASK-5 channel, TASK-3 may take over and compensate for the loss of its functions and vice versa. To avoid

a potential lack of phenotype and investigate the neuronal consequences post ablation, both channel sub-types should be silenced.

Alternatively, enhancement of TASK activity with inhalational anaesthetics such as halothane was shown to cause membrane hyperpolarisation and decreased excitability of neuronal preparations (Nicoll and Madison 1982). Even though, it is unknown if TASK-5 channels are sensitive to halothane, further exploration of the roles of anaesthetic-activated K2P channels will provide a better understanding of the enigmatic behavioural effects of anaesthetics in neurons.

K^+ channel-dependent mitochondrial cardio-cytoprotection against oxidative stress and ischaemia has also been demonstrated (Mattson and Kroemer 2003, Busija, Lacza et al. 2004, O'Rourke 2004). Indeed, K^+ channel activation was shown to be involved in NO-mediated cell protection after ischaemic injury and in cardiac myocytes death reduction (Cole, McPherson et al. 1991, Shinbo and Iijima 1997, Liu, Sato et al. 1998, Ockaili, Emani et al. 1999, Garlid and Paucek 2003, Mattson and Kroemer 2003). Cytoprotection is hypothesised to be influenced by an increased activation of mitochondrial K^+ channels during reperfusion which results in mitochondrial membrane depolarisation and reduction of ROS production (Ozcan, Bienengraeber et al. 2002). Increased activation of mitochondrial K^+ channels after ischaemia improves energy production (Ozcan, Bienengraeber et al. 2002, O'Rourke 2004), causes mitochondrial membrane depolarisation and reduces Ca^{2+} accumulation within the matrix. Reduced Ca^{2+}-dependent mitochondrial permeability consequently results to a reduced production of pro-apoptotic factors such as ROS and cytochrome *c* and dissipates the proton gradient producing sufficient levels of energy (Holmuhamedov, Wang et al. 1999, Korge, Honda et al. 2002). Despite several lines of evidence supporting this hypothesis, the mechanisms of mitochondrial K^+ channel dependent cytoprotection remain controversial and still to be fully characterised as these channels are anti-apoptotic (Mattson and Kroemer 2003, Busija, Lacza et al. 2004). Based on these evidence, TASK-5 may be involved in the protection of cardiac cells by maintaining the mitochondrial membrane potential and a balance between ROS and cytochrome *c* release.

8.3 Future lines of investigation

The results of this study suggest that elements of this work may be benefited from further experimental work to enable further assessment of the biophysical, pharmacological and functional characterisation of TASK-5 in both isolated mitochondria and the whole-cell configuration.

During immunocytochemistry experiments (section 5.2.2) the fluorescence intensity of COX II antibody was relatively weak. To endorse the mitochondrial co-expression between TASK-5 and COX II, future work consists of performing Western blot analysis on mitochondrial protein lysates isolated from cells over-expressing the channel. More precisely, co-localisation with TASK-5 can be assessed by stripping off hK_{2P}15.1-LR antibody from the nitrocellulose membrane and re-probing it with COX II. Detection of identical band sizes would hence indicate that hK_{2P}15.1-LR and COX II antibodies are expressed in the IMM. An alternative but more time consuming approach would be to perform immuno-EM on transiently transfected and isolated mitochondria using secondary antibodies against COX II and hK_{2P}15.1-LR previously conjugated with gold particles that will enable to visualise if the channel co-localises with the ETC complex (Yao, McHedlishvili et al. 2017).

Another fundamental trial would be to compare mitochondrial $\Delta\Psi_m$ between non- and transfected organelles using TMRE, a permeant and positively-charged dye that readily accumulates in active and healthy mitochondria which usually have a negatively charged matrix. This approach will allow to determine to which extent over-expression of TASK-5 alters $\Delta\Psi_m$ of organelles as V_{rev} was shown to be shifted towards more positive values during current recordings. Alternatively, it will help to understand whether external factors such as presence of F^- ions in the internal recording solution or the voltage protocol adopted during the study did affect V_{rev}. Finally, it would be interesting to assess the mitochondrial gigaseal formation strength/ability and anion channel conductivity/selectivity by substituting F^- with bromide (Br^-) ions in the internal recording solution. This will help to determine if other halide ions can be used to maintain a stable gigaOhm seal on a planar patch-clamp system and how V_{rev} is potentially affected during ion composition modifications.

Application of ATP or ChTx resulted to a significant ($p<0.01$ or $p<0.1$) and stronger current reduction when individually applied on non-transfected mitochondria compared to cocktails of channel blockers (sections 7.4-7.5). An observation that led to the hypothetical conclusion that closure of cyto/mito protective channels (mitoKATP and mitoBKCa) together with an excess of external [ATP] leading to ATP hydrolysis (sections 7.7.3-7.7.4) might have influenced mitochondrial survival pathways. Measurement of pro-apoptotic factors such as cytochrome *c* release, caspase activation and ROS production will hence allow to determine if the strong current reduction was linked to an efficient channel closure by ATP or ChTx or, due to mitochondria entering apoptosis. Moreover, as apoptotic cell death is characterised by its unique morphological features during which mitochondrial membrane permeabilisation occurs; investigation of the mitochondrial morphology and $\Delta\Psi_m$ of transfected organelles can be undertaken in the presence of channel blockers by live cell fluorescence imaging using Mitotracker red and TMRE. MitoSOX probes could also be used to measure the levels of

ROS production. Allowing to determine whether TASK-5 over-expression can endorse or rescue $\Delta\Psi_m$ impairment and/or cytochrome c release and ROS generation triggered by the blockers.

To identify the IC_{50} and IC_{100} blocking concentrations of RR over TASK-5, electrophysiological recordings should be performed on transfected mitochondrial membranes at the single-channel configuration. This will be the most direct method available for obtaining detailed and precise information about the kinetic behaviour of TASK-5 channels in response to the blocker. The single-channel configuration can be used to study TASK-5's conductance and identify specific activators or blockers. As TASK-1 and TASK-3 channels are known to be generally sensitive to sub-micromolar concentrations of volatile (halothane, isoflurane) or local (anandamide) anaesthetics; anandamide and halothane can be tested at the single channel configuration as potential inhibitors and activators of TASK-5 (Maingret, Patel et al. 2001). Alternatively, the single-channel configuration can be adopted on giant unilamellar vesicles post-incorporation of immuno-precipitated TASK-5 proteins in the synthetic lipid bilayers. Another suggestion would be to patch sub-mitochondrial vesicles (SMVs) isolated from mouse tissues over-expressing TASK-5. The advantage of using SMVs is their ability to retain the structural and functional integrity of the channel of interest as shown in (Alavian, Li et al. 2011, Sacchetti, Alavian et al. 2013) with the F1F0 ATPase and were free of contamination by other subcellular organelles. Even though the aforementioned approaches are less straight forward than studying TASK-5 currents on mitochondrial membranes isolated from cells; data can be used as a supplemental standard of comparison of TASK-5 electrophysiological characteristics when expressed in synthetic lipid bilayers or SMVs derived from animal tissues.

Once channel-specific activators and inhibitors are identified, it would be central to study the biophysical, structural, proliferative and physiological responses of organelles in both healthy and cancer cells. This could be achieved by either administrating pharmacological reagents or performing genetic modifications to the model cells studied. Knocking-down the channel with a siRNA construct for example will aid to evaluate if other channels, regulatory or signalling pathways can substitute and take over the functional roles of TASK-5 by observing physiological and functional changes at the single or whole-cell configuration and structural alterations at the mitochondrial level. In addition, TASK-5 currents can be studied under conditions of cellular stress such as hypoxia or deprived nutrients affecting the Krebs cycle occurring in mitochondria such as low glucose, amino acid and fatty acid levels. This will provide a better understanding of the energy consumption, signalling and regulatory role of TASK-5 under modified conditions.

Endogenous, over-expressed or down-regulated expression of TASK-5 can also be investigated and compared between normal (HEK293) or cancer human cells such as MCF-7, SH-SY5Y, SW480/620. This will enable to examine if the channel has a biophysical, structural or electrophysiological role in cancer cell survival or death by interacting with pro- or anti-apoptotic proteins or, is involved in signalling cascades that trigger or inhibit tumourigenesis (section 8.2). This could be performed using standard molecular approaches such as immunocytochemistry, Western blotting and measurement of apoptotic factors by FACS or in-*vitro* binding assays followed by mass spectrometry as in (Roncoroni, 2012).

It would be finally important to understand why some cell lines such as human lung adenocarcinoma (A549) express both TASK-3 and TASK-5 suggesting that these maybe require their heterodimerisation to function, while HeLa only express TASK-5 to control the mitochondrial resting membrane potential. In previous studies, TASK-1 and TASK-3 were shown to constitute functional heterodimers in *Xenopus* systems which inherited their features (RR and pH sensitivities) asymmetrically from the two parent subunits (Czirják and Enyedi 2002). These heterodimers were shown to display regulatory features that were distinct from their parent subunits, showing how diverse their functionalities could be from other K^+ channel proteins. Additionally, heterodimerisation between TASK-1 with TALK-2, two different channel subfamilies was reported in HEK293 cells and was shown to provide cells with the ability to make multiple responses to a variety of physiological and pharmacological stimuli (Suzuki, Tsutsumi et al. 2017). TASK1-TALK2 heterodimer showed intermediate pH sensitivity to a wider range of pH changes (from pH 5.4 to pH 9.4), alike TASK1-TASK3 heterodimer where their homodimers where highly sensitive to either acid or alkaline pH (Czirják and Enyedi 2002, Berg, Talley et al. 2004). Similar responses have been observed when isoflurane was applied to HEK293 cells expressing TASK1 (weakly inhibited), TASK3 (largely increased) or TASK1-TASK3 heterodimers (moderately increased) (Berg, Talley et al. 2004). These studies suggest that heterodimerisation provides unique characteristics that are distinct from their homodimer counterparts and allow them to sense much larger variations of physiological stimuli. Therefore in A549 cells, TASK3-TASK5 heterodimers may alter the intracellular trafficking pathway and exhibit different properties from TASK-5 homodimers expressed in HeLa or HEK293 cells. To further investigate this, the electrical and functional characteristics of hetero-dimers could be studied at the single-channel and whole-organelle configuration and compared to homo-dimers during pharmacological studies.

Appendices

Appendix 1. Amino acid sequence of the eGFP-tagged C-terminal TASK-5 GYG channel cloned into pEGFP-N1.

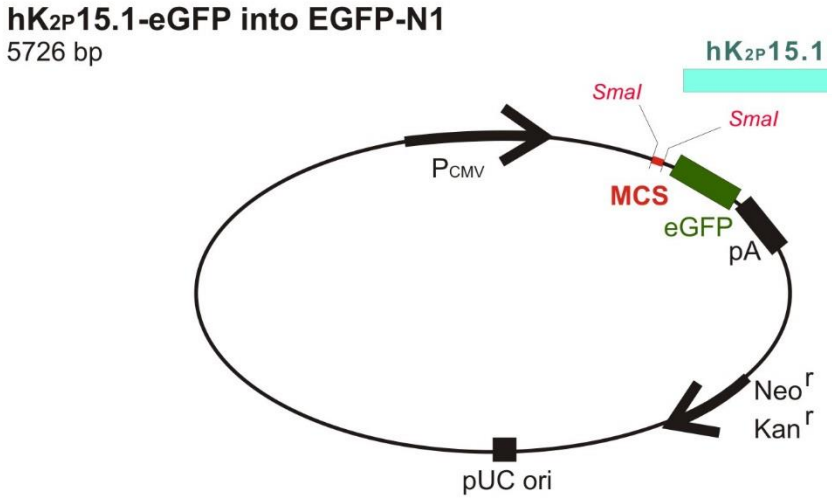

TAGTTATTAATAGTAATCAATTACGGGGTCATTAGTTCATAGCCCATATATGGAGTTC
CGCGTTACATAACTTACGGTAAATGGCCCGCCTGGCTGACCGCCCAACGACCCCCGCC
CATTGACGTCAATAATGACGTATGTTCCCATAGTAACGCCAATAGGGACTTTCCATTG
ACGTCAATGGGTGGAGTATTTACGGTAAACTGCCCACTTGGCAGTACATCAAGTGTAT
CATATGCCAAGTACGCCCCCTATTGACGTCAATGACGGTAAATGGCCCGCCTGGCATT
ATGCCCAGTACATGACCTTATGGGACTTTCCTACTTGGCAGTACATCTACGTATTAGT
CATCGCTATTACCATGGTGATGCGGTTTTGGCAGTACATCAATGGGCGTGGATAGCGG
TTTGACTCACGGGGATTTCCAAGTCTCCACCCCATTGACGTCAATGGGAGTTTGTTTT
GGCACCAAAATCAACGGGACTTTCCAAAATGTCGTAACAACTCCGCCCCATTGACGCA
AATGGGCGGTAGGCGTGTACGGTGGGAGGTCTATATAAGCAGAGCTGGTTTAGTGAAC
CGTCAGATCCGCTAGCGCTACCGGACTCAGATCTCGAGCTCAAGCTTCGAATTCTGCA
GTCGACGGTACCGCGGGCCCCCATGCGGAGGCCGAGCGTGCGCGCGGCCGGGCTGGTC
CTGTGCACCCTGTGTTACCTGCTGGTGGGCGCTGCTGTCTTCGACGCGCTCGAGTCCG
AGGCGGAAAGCGGCCGCCAGCGACTGCTGGTCCAGAAGCGGGGCGCTCTCCGGAGGAA
GTTCGGCTTCTCGGCCGAGGACTACCGCGAGCTGGAGCGCCTGGCGCTCCAGGCTGAG
CCCCACCGCGCCGGCCGCCAGTGGAAGTTCCCCGGCTCCTTCTACTTCGCCATCACCG
TCATCACTACCATCGGGTACGGCCACGCCGCGCCGGGTACGGACTCCGGCAAGGTCTT
CTGCATGTTCTACGCGCTCCTGGGCATCCCGCTGACGCTGGTCACTTTCCAGAGCCTG
GGCGAACGGCTGAACGCGGTGGTGCGGCGCCTCCTGTTGGCGGCCAAGTGCTGCCTGG
GCCTGCGGTGGACGTGCGTGTCCACGGAGAACCTGGTGGTGGCCGGGCTGCTGGCGTG
TGCCGCCACCCTGGCCCTCGGGGCCGTCGCCTTCTCGCACTTCGAGGGCTGGACCTTC
TTCCACGCCTACTACTACTGCTTCATCACCCTCACCACCATCGGCTTCGGCGACTTCG
TGGCACTGCAGAGCGGCGAGGCGCTGCAGAGGAAGCTCCCCTACGTGGCCTTCAGCTT
CCTCTACATCCTCCTGGGGCTCACGGTCATTGGCGCCTTCCTCAACCTGGTGGTCCTG
CGCTTCCTCGTTGCCAGCGCCGACTGGCCCGAGCGCGCTGCCCGCCCCCCCAGCCCGC
GCCCCCCGGGGGCGCCCGAGAGCCGTGGCCTCTGGCTGCCCCGCCGCCCGGCCCGCTC
CGTGGGCTCCGCCTCTGTCTTCTGCCACGTGCACAAGCTGGAGAGGTGCGCCCGCGAC
AACCTGGGCTTTTCGCCCCCCTCGAGCCCGGGGGTCGTGCGTGGCGGGCAGGCTCCCA
GGCCTGGGGCCCGGTGGAAGTCCATCGGGGATCCACCGGTCGCCACCATGGTGAGCAA
GGGCGAGGAGCTGTTCACCGGGGTGGTGCCCATCCTGGTCGAGCTGGACGGCGACGTA
AACGGCCACAAGTTCAGCGTGTCCGGCGAGGGCGAGGGCGATGCCACCTACGGCAAGC
TGACCCTGAAGTTCATCTGCACCACCGGCAAGCTGCCCGTGCCCTGGCCCACCCTCGT

GACCACCCTGACCTACGGCGTGCAGTGCTTCAGCCGCTACCCCGACCACATGAAGCAG
CACGACTTCTTCAAGTCCGCCATGCCCGAAGGCTACGTCCAGGAGCGCACCATCTTCT
TCAAGGACGACGGCAACTACAAGACCCGCGCCGAGGTGAAGTTCGAGGGCGACACCCT
GGTGAACCGCATCGAGCTGAAGGGCATCGACTTCAAGGAGGACGGCAACATCCTGGGG
CACAAGCTGGAGTACAACTACAACAGCCACAACGTCTATATCATGGCCGACAAGCAGA
AGAACGGCATCAAGGTGAACTTCAAGATCCGCCACAACATCGAGGACGGCAGCGTGCA
GCTCGCCGACCACTACCAGCAGAACACCCCCATCGGCGACGGCCCCGTGCTGCTGCCC
GACAACCACTACCTGAGCACCCAGTCCGCCCTGAGCAAAGACCCCAACGAGAAGCGCG
ATCACATGGTCCTGCTGGAGTTCGTGACCGCCGCCGGGATCACTCTCGGCATGGACGA
GCTGTACAAGTAAAGCGGCCGCGACTCTAGATCATAATCAGCCATACCACATTTGTAG
AGGTTTTACTTGCTTTAAAAAACCTCCCACACCTCCCCCTGAACCTGAAACATAAAAT
GAATGCAATTGTTGTTGTTAACTTGTTTATTGCAGCTTATAATGGTTACAAATAAAGC
AATAGCATCACAAATTTCACAAATAAAGCATTTTTTTCACTGCATTCTAGTTGTGGTT
TGTCCAAACTCATCAATGTATCTTAAGGCGTAAATTGTAAGCGTTAATATTTTGTTAA
AATTCGCGTTAAATTTTTGTTAAATCAGCTCATTTTTTAACCAATAGGCCGAAATCGG
CAAAATCCCTTATAAATCAAAAGAATAGACCGAGATAGGGTTGAGTGTTGTTCCAGTT
TGGAACAAGAGTCCACTATTAAAGAACGTGGACTCCAACGTCAAAGGGCGAAAAACCG
TCTATCAGGGCGATGGCCCACTACGTGAACCATCACCCTAATCAAGTTTTTTGGGGTC
GAGGTGCCGTAAAGCACTAAATCGGAACCCTAAAGGGAGCCCCCGATTTAGAGCTTGA
CGGGGAAAGCCGGCGAACGTGGCGAGAAAGGAAGGGAAGAAAGCGAAAGGAGCGGGCG
CTAGGGCGCTGGCAAGTGTAGCGGTCACGCTGCGCGTAACCACCACACCCGCCGCGCT
TAATGCGCCGCTACAGGGCGCGTCAGGTGGCACTTTTCGGGGAAATGTGCGCGGAACC
CCTATTTGTTTATTTTTCTAAATACATTCAAATATGTATCCGCTCATGAGACAATAAC
CCTGATAAATGCTTCAATAATATTGAAAAAGGAAGAGTCCTGAGGCGGAAAGAACCAG
CTGTGGAATGTGTGTCAGTTAGGGTGTGGAAAGTCCCCAGGCTCCCCAGCAGGCAGAA
GTATGCAAAGCATGCATCTCAATTAGTCAGCAACCAGGTGTGGAAAGTCCCCAGGCTC
CCCAGCAGGCAGAAGTATGCAAAGCATGCATCTCAATTAGTCAGCAACCATAGTCCCG
CCCCTAACTCCGCCCATCCCGCCCCTAACTCCGCCCAGTTCCGCCCATTCTCCGCCCC
ATGGCTGACTAATTTTTTTTATTTATGCAGAGGCCGAGGCCGCCTCGGCCTCTGAGCT
ATTCCAGAAGTAGTGAGGAGGCTTTTTTGGAGGCCTAGGCTTTTGCAAAGATCGATCA
AGAGACAGGATGAGGATCGTTTCGCATGATTGAACAAGATGGATTGCACGCAGGTTCT
CCGGCCGCTTGGGTGGAGAGGCTATTCGGCTATGACTGGGCACAACAGACAATCGGCT
GCTCTGATGCCGCCGTGTTCCGGCTGTCAGCGCAGGGGCGCCCGGTTCTTTTTGTCAA
GACCGACCTGTCCGGTGCCCTGAATGAACTGCAAGACGAGGCAGCGCGGCTATCGTGG
CTGGCCACGACGGGCGTTCCTTGCGCAGCTGTGCTCGACGTTGTCACTGAAGCGGGAA
GGGACTGGCTGCTATTGGGCGAAGTGCCGGGGCAGGATCTCCTGTCATCTCACCTTGC
TCCTGCCGAGAAAGTATCCATCATGGCTGATGCAATGCGGCGGCTGCATACGCTTGAT
CCGGCTACCTGCCCATTCGACCACCAAGCGAAACATCGCATCGAGCGAGCACGTACTC
GGATGGAAGCCGGTCTTGTCGATCAGGATGATCTGGACGAAGAGCATCAGGGGCTCGC
GCCAGCCGAACTGTTCGCCAGGCTCAAGGCGAGCATGCCCGACGGCGAGGATCTCGTC
GTGACCCATGGCGATGCCTGCTTGCCGAATATCATGGTGGAAAATGGCCGCTTTTCTG
GATTCATCGACTGTGGCCGGCTGGGTGTGGCGGACCGCTATCAGGACATAGCGTTGGC
TACCCGTGATATTGCTGAAGAGCTTGGCGGCGAATGGGCTGACCGCTTCCTCGTGCTT
TACGGTATCGCCGCTCCCGATTCGCAGCGCATCGCCTTCTATCGCCTTCTTGACGAGT
TCTTCTGAGCGGGACTCTGGGGTTCGAAATGACCGACCAAGCGACGCCCAACCTGCCA
TCACGAGATTTCGATTCCACCGCCGCCTTCTATGAAAGGTTGGGCTTCGGAATCGTTT
TCCGGGACGCCGGCTGGATGATCCTCCAGCGCGGGGATCTCATGCTGGAGTTCTTCGC

CCACCCTAGGGGGAGGCTAACTGAAACACGGAAGGAGACAATACCGGAAGGAACCCGC
GCTATGACGGCAATAAAAAGACAGAATAAAACGCACGGTGTTGGGTCGTTTGTTCATA
AACGCGGGGTTCGGTCCCAGGGCTGGCACTCTGTCGATACCCCACCGAGACCCCATTG
GGGCCAATACGCCCGCGTTTCTTCCTTTTCCCCACCCCACCCCCCAAGTTCGGGTGAA
GGCCCAGGGCTCGCAGCCAACGTCGGGGCGGCAGGCCCTGCCATAGCCTCAGGTTACT
CATATATACTTTAGATTGATTTAAAACTTCATTTTTAATTTAAAAGGATCTAGGTGAA
GATCCTTTTTGATAATCTCATGACCAAAATCCCTTAACGTGAGTTTTCGTTCCACTGA
GCGTCAGACCCCGTAGAAAAGATCAAAGGATCTTCTTGAGATCCTTTTTTTCTGCGCG
TAATCTGCTGCTTGCAAACAAAAAAACCACCGCTACCAGCGGTGGTTTGTTTGCCGGA
TCAAGAGCTACCAACTCTTTTTCCGAAGGTAACTGGCTTCAGCAGAGCGCAGATACCA
AATACTGTCCTTCTAGTGTAGCCGTAGTTAGGCCACCACTTCAAGAACTCTGTAGCAC
CGCCTACATACCTCGCTCTGCTAATCCTGTTACCAGTGGCTGCTGCCAGTGGCGATAA
GTCGTGTCTTACCGGGTTGGACTCAAGACGATAGTTACCGGATAAGGCGCAGCGGTCG
GGCTGAACGGGGGGTTCGTGCACACAGCCCAGCTTGGAGCGAACGACCTACACCGAAC
TGAGATACCTACAGCGTGAGCTATGAGAAAGCGCCACGCTTCCCGAAGGGAGAAAGGC
GGACAGGTATCCGGTAAGCGGCAGGGTCGGAACAGGAGAGCGCACGAGGGAGCTTCCA
GGGGGAAACGCCTGGTATCTTTATAGTCCTGTCGGGTTTCGCCACCTCTGACTTGAGC
GTCGATTTTTGTGATGCTCGTCAGGGGGGCGGAGCCTATGGAAAAACGCCAGCAACGC
GGCCTTTTTACGGTTCCTGGCCTTTTGCTGGCCTTTTGCTCACATGTTCTTTCCTGCG
TTATCCCCTGATTCTGTGGATAACCGTATTACCGCCATGCAT

Diagram of pGEGFP-N1 vector (4733bp) showing the site of insertion (multiple cloning site (MCS)) of PCR product corresponding to $hK_{2P}15.1C$ (993bp) (GYG) (blue) into SmaI sites (CCC-GGG, pink). EGFP (720bp) sequence is denoted in green. Final plasmid DNA construct size was 5726bp with a resistance to Kanamycin and Neomycin.

Appendix 2. Planar planar patch-clamp connected to the external perfusion system.

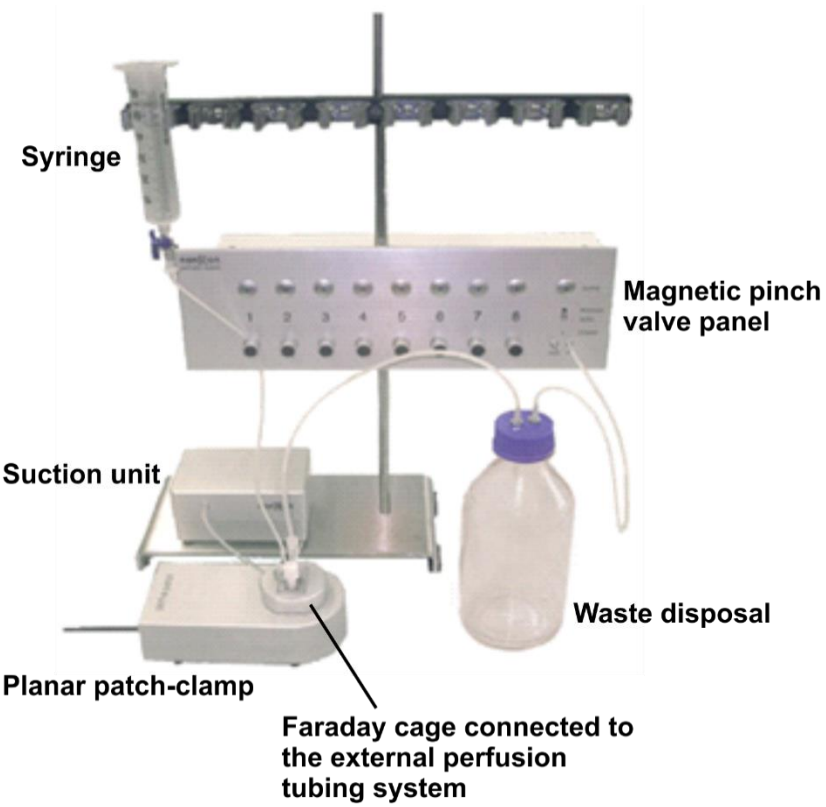

The planar patch-clamp system is connected to a detachable Faraday cage joined to an external perfusion system with a waste disposal and a suction unit applying positive or negative pressure. NPC-1 chips are screwed under the Faraday cage and the external solution is placed in portable syringes attached to a magnetic pinch.

Appendix 3. Co-localisation between endogenous TASK-5 and Mitotracker red in COS-7 cells.

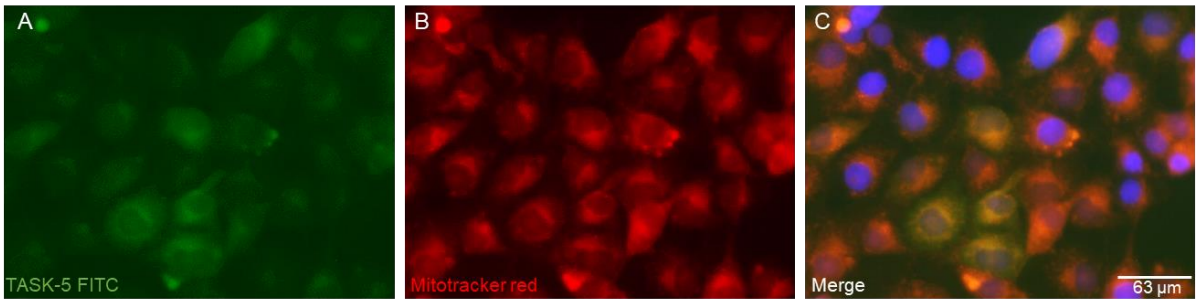

Epifluorescence microscopy of immunocytochemistry of non-transfected COS-7 cells stained with Mitotracker red. A. Endogenous TASK-5 channels were detected with hK_{2P}15.1-LR and a secondary FITC antibody. **B.** Mitochondrial localisation was determined using 25nM Mitotracker red and **C.** Merged image showing co-localisation of FITC and Mitotracker red fluorophores in yellow. Scale bar: 63µm.

Appendix 4. Co-localisation between TASK-3-eGFP and hK_{2P}9.1 antibody in HEK293 cells.

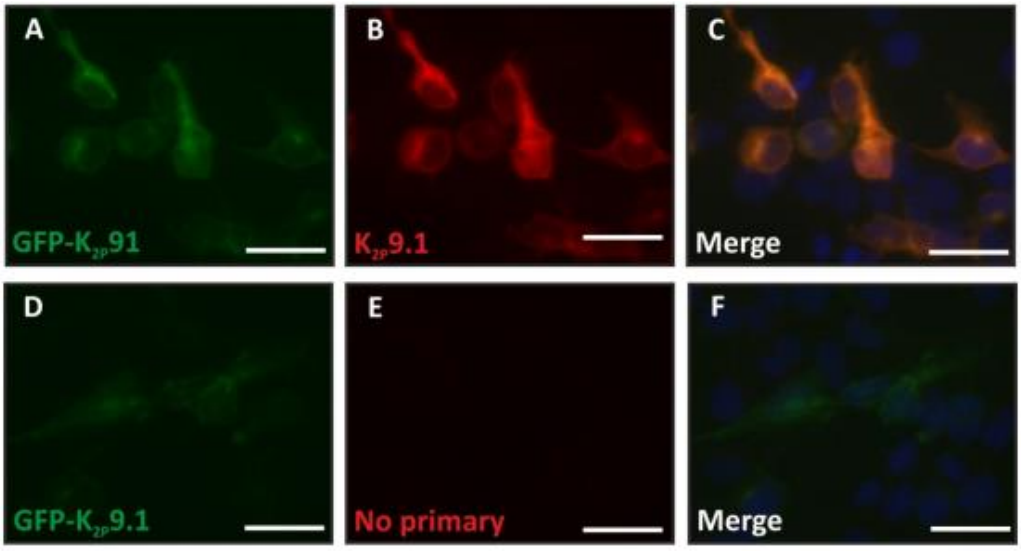

HEK293 cells transiently expressing N-terminally GFP tagged TASK-3. A, D. Transfected channel was detected by GFP fluorescence signal during confocal microscopy. **B.** Immunolabelling for TASK-3 using an anti-K_{2P}9.1 antibody (2ug/ml). **E.** No primary antibody incubation control. **C, F.** Overlapped fluorescence signals including nuclear stain (DAPI). Scale bars: 30 µm. Image adopted from Williams et al., 2013, unpublished.

Appendix 5. Co-localisation between TASK-5-eGFP and hK$_{2P}$15.1-LR antibody in COS-7 cells.

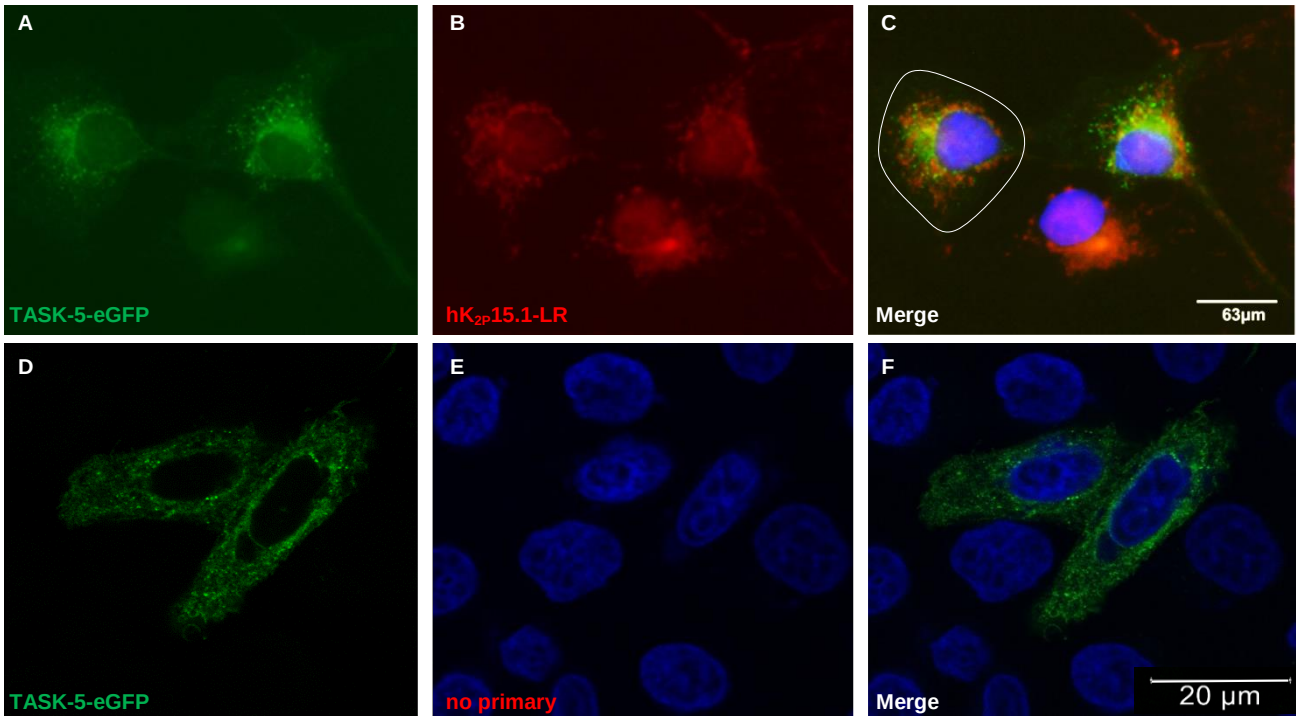

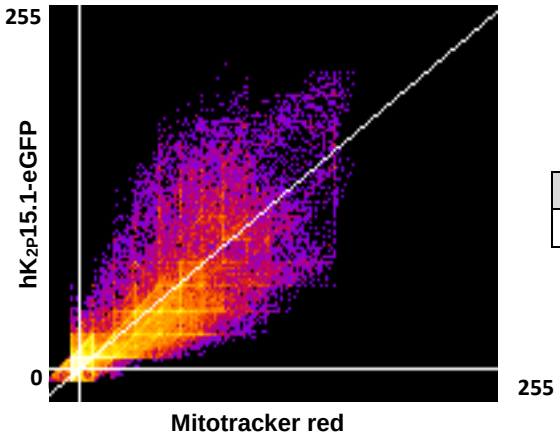

R(obs)	R(rand) mean±SD
0.743	0.034±0.004

Epifluorescence and confocal microscopy of transiently transfected COS-7 cells with TASK-5-eGFP. A. Transfected cells expressing TASK5-eGFP (green fluorescence) were probed against **B.** hK$_{2P}$15.1-LR antibody (Texas red fluorescence). **C.** Overlapped fluorescence signals including nuclear stain (DAPI). Co-localising pixels emit a yellow fluorescence. Following co-localisation analysis within the ROI selected in C, a scatter plot with co-localising pixels (yellow) clustering along the diagonal was generated. The colour components of individual pixels are measured in the range between 0 and 255. Coste's and Pearson correlation analysis resulted to an elevated R(obs) value after 200 iterations while R(rand) was close to 0. **D, E.** Transfected COS-7 cells were not probed against hK$_{2P}$15.1-LR as an incubation control. **F.** Merged fluorescence signals including nuclear stain (DAPI). Scaler bars: 20 and 63 µm.

Appendix 6. Co-localisation between endogenous TASK-3 and $hK_{2P}15.1$-LR antibody in HEK293 cells.

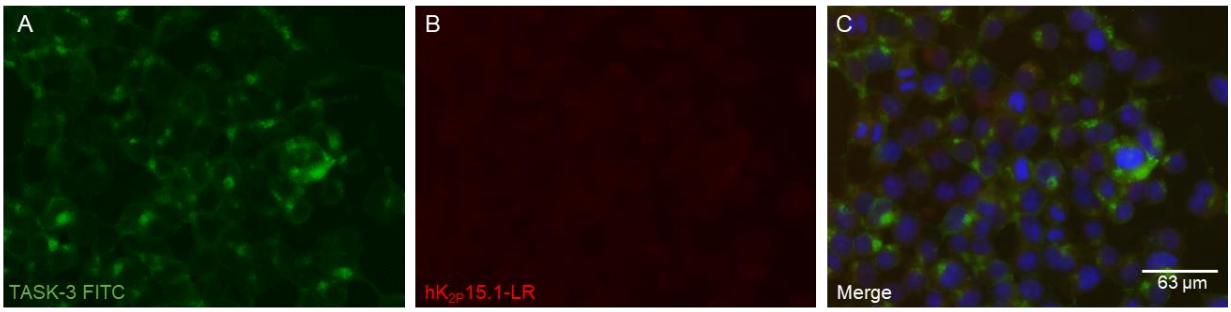

Epifluorescence microscopy of HEK293 cells endogenously expressing TASK-3. A. HEK293 cells were probed against TASK-3 and a secondary FITC antibody to visualise the endogenous expression of the channel. **B.** $hK_{2P}15.1$-LR antibody did not detect any TASK-5 proteins. **C.** Merged fluorescence signals including nuclear stain (DAPI) does not show any co-localisation. Scaler bars: 63 µm.

References

A, A., B. L, B. A, F. L, C. M, M. E, O. M and W. E (1995). "A novel inward ‐ rectifying K+ current with a cell ‐ cycle dependence governs the resting potential of mammalian neuroblastoma cells." The Journal of Physiology **489**(2): 455-471.
Adams, J. M. and S. Cory (2007). "The Bcl-2 apoptotic switch in cancer development and therapy." Oncogene **26**(9): 1324-1337.
Ahmad, T., K. Aggarwal, B. Pattnaik, S. Mukherjee, T. Sethi, B. K. Tiwari, M. Kumar, A. Micheal, U. Mabalirajan, B. Ghosh, S. Sinha Roy and A. Agrawal (2013). "Computational classification of mitochondrial shapes reflects stress and redox state." Cell Death Dis **4**: e461.
Akao, M., A. Ohler, B. O'Rourke and E. Marban (2001). "Mitochondrial ATP-sensitive potassium channels inhibit apoptosis induced by oxidative stress in cardiac cells." Circ Res **88**(12): 1267-1275.
Alavian, K. N., H. Li, L. Collis, L. Bonanni, L. Zeng, S. Sacchetti, E. Lazrove, P. Nabili, B. Flaherty, M. Graham, Y. Chen, S. Messerli, M. A. Mariggio, C. Rahner, E. McNay, G. Shore, P. J. S. Smith, J. M. Hardwick and E. A. Jonas (2011). "Bcl-x(L) regulates metabolic efficiency of neurons through interaction with the mitochondrial F(1)F(O) ATP synthase." Nature cell biology **13**(10): 1224-1233.
Alberts, B. (2014). Molecular biology of the cell.
Alberts B, J. A., Lewis J, et al. (2002). Molecular Biology of the Cell, 4th edition. The Mitochondrion. .
Altmann, R. (1890). The elementary organisms and their relationships to the cells. Germany, Veit&Co.
Altschafl, B. A., G. Beutner, V. K. Sharma, S.-S. Sheu and H. H. Valdivia (2007). "The mitochondrial ryanodine receptor in rat heart: A pharmaco-kinetic profile." Biochimica et Biophysica Acta (BBA) - Biomembranes **1768**(7): 1784-1795.
Altschafl, B. A., G. Beutner, V. K. Sharma, S. S. Sheu and H. H. Valdivia (2007). "The mitochondrial ryanodine receptor in rat heart: a pharmaco-kinetic profile." Biochim Biophys Acta **1768**(7): 1784-1795.
Ames, A., 3rd (2000). "CNS energy metabolism as related to function." Brain Res Brain Res Rev **34**(1-2): 42-68.
Amiry-Moghaddam, M., H. Lindland, S. Zelenin, B. A. Roberg, B. B. Gundersen, P. Petersen, E. Rinvik, I. A. Torgner and O. P. Ottersen (2005). "Brain mitochondria contain aquaporin water channels: evidence for the expression of a short AQP9 isoform in the inner mitochondrial membrane." Faseb j **19**(11): 1459-1467.
Antonsson, B., S. Montessuit, S. Lauper, R. Eskes and J. C. Martinou (2000). "Bax oligomerization is required for channel-forming activity in liposomes and to trigger cytochrome c release from mitochondria." Biochem J **345 Pt 2**: 271-278.
Aon, M. A., S. Cortassa, F. G. Akar and B. O'Rourke (2006). "Mitochondrial criticality: A new concept at the turning point of life or death." Biochimica et Biophysica Acta (BBA) - Molecular Basis of Disease **1762**(2): 232-240.
Aon, M. A., S. Cortassa, A. C. Wei, M. Grunnet and B. O'Rourke (2010). "Energetic performance is improved by specific activation of K+ fluxes through K(Ca) channels in heart mitochondria." Biochim Biophys Acta **1797**(1): 71-80.
Arakel, E. C. and B. Schwappach (2018). "Formation of COPI-coated vesicles at a glance." Journal of Cell Science **131**(5).
Ashmole, I., P. Goodwin and P. Stanfield (2001). "TASK-5, a novel member of the tandem pore K + channel family." Pfl&#xfffd;gers Archiv European Journal of Physiology **442**(6): 828-833.
Ashmole, I., P. A. Goodwin and P. R. Stanfield (2001). "TASK-5, a novel member of the tandem pore K+ channel family." Pflugers Arch **442**(6): 828-833.
Balaban, R. S. (2009). "The role of Ca(2+) signaling in the coordination of mitochondrial ATP production with cardiac work." Biochim Biophys Acta **1787**(11): 1334-1341.

Balannik, V., P. Obrdlik, S. Inayat, C. Steensen, J. Wang, J. M. Rausch, W. F. DeGrado, B. Kelety and L. H. Pinto (2010). "Solid-supported membrane technology for the investigation of the influenza A virus M2 channel activity." Pflügers Archiv - European Journal of Physiology **459**(4): 593-605.
Balderas, E., J. Zhang, E. Stefani and L. Toro (2015). "Mitochondrial BK(Ca) channel." Frontiers in Physiology **6**: 104.
Ballarin, C. and M. C. Sorgato (1995). "An electrophysiological study of yeast mitochondria. Evidence for two inner membrane anion channels sensitive to ATP." J Biol Chem **270**(33): 19262-19268.
Bando, Y., T. Hirano and Y. Tagawa (2014). "Dysfunction of KCNK Potassium Channels Impairs Neuronal Migration in the Developing Mouse Cerebral Cortex." Cerebral Cortex **24**(4): 1017-1029.
Barbour, B. (2014). Electronics for electrophysiologists.
Barel, O., S. A. Shalev, R. Ofir, A. Cohen, J. Zlotogora, Z. Shorer, G. Mazor, G. Finer, S. Khateeb, N. Zilberberg and O. S. Birk (2008). "Maternally inherited Birk Barel mental retardation dysmorphism syndrome caused by a mutation in the genomically imprinted potassium channel KCNK9." Am J Hum Genet **83**(2): 193-199.
Barthmes, M., A. B. , S. H. , N. F. , M. G. and A. B. (2017). High throughput real-time measurement of electrogenic membrane

transport driven by the SLC transporters PepT1 and OcT2.
Barthmes, M., T. A. G. , S. H. , M. G. , C. P. , R. B. , T. S. , M. V. , J. S. , A. B. , M. George and N. F. (2015). Organellar Transporters and Ion Channels -

How to access their electrophysiology by using the

SURFE2R technology and Planar Patch Clamp.
Basavappa, S., M. A. Romano-Silva, A. W. Mangel, D. Laro, I. Campbell and M. Brammer (1994). "Inhibition of K+ channel activity by 4-AP stimulates N-type Ca2+ channels in CHP-100 cells." Neuroreport **5**(10): 1256-1258.
Basso, E., L. Fante, J. Fowlkes, V. Petronilli, M. A. Forte and P. Bernardi (2005). "Properties of the Permeability Transition Pore in Mitochondria Devoid of Cyclophilin D." Journal of Biological Chemistry **280**(19): 18558-18561.
Bayliss, D. A. and P. Q. Barrett (2008). "Emerging roles for two-pore-domain potassium channels and their potential therapeutic impact." Trends in pharmacological sciences **29**(11): 566-575.
Beavis, A. D. (1992). "Properties of the inner membrane anion channel in intact mitochondria." J Bioenerg Biomembr **24**(1): 77-90.
Bednarczyk, P. (2009). "Potassium channels in brain mitochondria." Acta Biochim Pol **56**(3): 385-392.
Bednarczyk, P., G. D. Barker and A. P. Halestrap (2008). "Determination of the rate of K(+) movement through potassium channels in isolated rat heart and liver mitochondria." Biochim Biophys Acta **1777**(6): 540-548.
Bednarczyk, P., G. D. Barker and A. P. Halestrap (2008). "Determination of the rate of K+ movement through potassium channels in isolated rat heart and liver mitochondria." Biochimica et Biophysica Acta (BBA) - Bioenergetics **1777**(6): 540-548.
Bednarczyk, P., K. Dolowy and A. Szewczyk (2005). "Matrix Mg2+ regulates mitochondrial ATP-dependent potassium channel from heart." FEBS Lett **579**(7): 1625-1632.
Bednarczyk, P., A. Kicinska, V. Kominkova, K. Ondrias, K. Dolowy and A. Szewczyk (2004). "Quinine inhibits mitochondrial ATP-regulated potassium channel from bovine heart." J Membr Biol **199**(2): 63-72.
Bednarczyk, P., J. E. Kowalczyk, M. Beresewicz, K. Dolowy, A. Szewczyk and B. Zablocka (2010). "Identification of a voltage-gated potassium channel in gerbil hippocampal mitochondria." Biochem Biophys Res Commun **397**(3): 614-620.
Bednarczyk, P., M. R. Wieckowski, M. Broszkiewicz, K. Skowronek, D. Siemen and A. Szewczyk (2013). "Putative Structural and Functional Coupling of the Mitochondrial BKCa Channel to the Respiratory Chain." PLOS ONE **8**(6): e68125.

Beeton, C., H. Wulff, J. Barbaria, O. Clot-Faybesse, M. Pennington, D. Bernard, M. D. Cahalan, K. G. Chandy and E. Béraud (2001). "Selective blockade of T lymphocyte K(+) channels ameliorates experimental autoimmune encephalomyelitis, a model for multiple sclerosis." Proceedings of the National Academy of Sciences of the United States of America **98**(24): 13942-13947.
Bengzon, J., P. Mohapel, C. T. Ekdahl and O. Lindvall (2002). "Neuronal apoptosis after brief and prolonged seizures." Prog Brain Res **135**: 111-119.
Bentzen, B. H., O. Osadchii, T. Jespersen, R. S. Hansen, S. P. Olesen and M. Grunnet (2009). "Activation of big conductance Ca(2+)-activated K (+) channels (BK) protects the heart against ischemia-reperfusion injury." Pflugers Arch **457**(5): 979-988.
Berdasco, M. and M. Esteller (2010). "Aberrant Epigenetic Landscape in Cancer: How Cellular Identity Goes Awry." Developmental Cell **19**(5): 698-711.
Berg, A. P., E. M. Talley, J. P. Manger and D. A. Bayliss (2004). "Motoneurons express heteromeric TWIK-related acid-sensitive K+ (TASK) channels containing TASK-1 (KCNK3) and TASK-3 (KCNK9) subunits." J Neurosci **24**(30): 6693-6702.
Bernardi, P. (1999). "Mitochondrial transport of cations: Channels, exchangers, and permeability transition." Physiological Reviews **79**(4): 1127-1155.
Bernardi, P. (1999). "Mitochondrial transport of cations: channels, exchangers, and permeability transition." Physiol Rev **79**(4): 1127-1155.
Bers, D. M. (2008). "Calcium cycling and signaling in cardiac myocytes." Annu Rev Physiol **70**: 23-49.
Beutner, G., A. Ruck, B. Riede and D. Brdiczka (1998). "Complexes between porin, hexokinase, mitochondrial creatine kinase and adenylate translocator display properties of the permeability transition pore. Implication for regulation of permeability transition by the kinases." Biochim Biophys Acta **1368**(1): 7-18.
Beutner, G., A. Ruck, B. Riede, W. Welte and D. Brdiczka (1996). "Complexes between kinases, mitochondrial porin and adenylate translocator in rat brain resemble the permeability transition pore." FEBS Lett **396**(2-3): 189-195.
Beutner, G., V. K. Sharma, D. R. Giovannucci, D. I. Yule and S.-S. Sheu (2001). "Identification of a Ryanodine Receptor in Rat Heart Mitochondria." Journal of Biological Chemistry **276**(24): 21482-21488.
Beutner, G., V. K. Sharma, L. Lin, S. Y. Ryu, R. T. Dirksen and S. S. Sheu (2005). "Type 1 ryanodine receptor in cardiac mitochondria: transducer of excitation-metabolism coupling." Biochim Biophys Acta **1717**(1): 1-10.
Bichet, D., S. Blin, S. Feliciangeli, F. C. Chatelain, N. Bobak and F. Lesage (2015). "Silent but not dumb: how cellular trafficking and pore gating modulate expression of TWIK1 and THIK2." Pflugers Arch **467**(5): 1121-1131.
Bittner, S., T. Budde, H. Wiendl and S. G. Meuth (2010). "From the background to the spotlight: TASK channels in pathological conditions." Brain Pathology **20**(6): 999-1009.
Borchert, G. H., C. Yang and F. Kolar (2011). "Mitochondrial BKCa channels contribute to protection of cardiomyocytes isolated from chronically hypoxic rats." Am J Physiol Heart Circ Physiol **300**(2): H507-513.
Borecky, J., P. Jezek and D. Siemen (1997). "108-pS channel in brown fat mitochondria might Be identical to the inner membrane anion channel." J Biol Chem **272**(31): 19282-19289.
Borecký, J., P. Ježek and D. Siemen (1997). "108-pS Channel in Brown Fat Mitochondria Might Be Identical to the Inner Membrane Anion Channel." Journal of Biological Chemistry **272**(31): 19282-19289.
Bortner, C. D. and J. A. Cidlowski (2007). "Cell shrinkage and monovalent cation fluxes: Role in apoptosis." Archives of Biochemistry and Biophysics **462**(2): 176-188.
Brand, M. D., J. L. Pakay, A. Ocloo, J. Kokoszka, D. C. Wallace, P. S. Brookes and E. J. Cornwall (2005). "The basal proton conductance of mitochondria depends on adenine nucleotide translocase content." Biochem J **392**(Pt 2): 353-362.

Briones, R., C. Weichbrodt, L. Paltrinieri, I. Mey, S. Villinger, K. Giller, A. Lange, M. Zweckstetter, C. Griesinger, S. Becker, C. Steinem and Bert L. de Groot (2016). "Voltage Dependence of Conformational Dynamics and Subconducting States of VDAC-1." Biophysical Journal **111**(6): 1223-1234.
Brookes, P. S., Y. Yoon, J. L. Robotham, M. W. Anders and S.-S. Sheu (2004). "Calcium, ATP, and ROS: a mitochondrial love-hate triangle." American Journal of Physiology-Cell Physiology **287**(4): C817-C833.
Brookes, P. S., Y. Yoon, J. L. Robotham, M. W. Anders and S. S. Sheu (2004). "Calcium, ATP, and ROS: a mitochondrial love-hate triangle." Am J Physiol Cell Physiol **287**(4): C817-833.
Buntinas, L., K. K. Gunter, G. C. Sparagna and T. E. Gunter (2001). "The rapid mode of calcium uptake into heart mitochondria (RaM): comparison to RaM in liver mitochondria." Biochim Biophys Acta **1504**(2-3): 248-261.
Busija, D. W., T. Gaspar, F. Domoki, P. V. Katakam and F. Bari (2008). "Mitochondrial-mediated suppression of ROS production upon exposure of neurons to lethal stress: mitochondrial targeted preconditioning." Adv Drug Deliv Rev **60**(13-14): 1471-1477.
Busija, D. W., Z. Lacza, N. Rajapakse, K. Shimizu, B. Kis, F. Bari, F. Domoki and T. Horiguchi (2004). "Targeting mitochondrial ATP-sensitive potassium channels--a novel approach to neuroprotection." Brain Res Brain Res Rev **46**(3): 282-294.
Cahalan, M. D., K. G. Chandy, T. E. DeCoursey and S. Gupta (1985). "A voltage-gated potassium channel in human T lymphocytes." J Physiol **358**: 197-237.
Calhoun, D. A. (2006). "Use of aldosterone antagonists in resistant hypertension." Prog Cardiovasc Dis **48**(6): 387-396.
Capaldi, R. A., F. Malatesta and V. M. Darley-Usmar (1983). "Structure of cytochrome c oxidase." Biochim Biophys Acta **726**(2): 135-148.
Chandy, K. G., H. Wulff, C. Beeton, M. Pennington, G. A. Gutman and M. D. Cahalan (2004). "K+ channels as targets for specific immunomodulation." Trends Pharmacol Sci **25**(5): 280-289.
Chatelain, F. C., D. Bichet, S. Feliciangeli, M. M. Larroque, V. M. Braud, D. Douguet and F. Lesage (2013). "Silencing of the tandem pore domain halothane-inhibited K+ channel 2 (THIK2) relies on combined intracellular retention and low intrinsic activity at the plasma membrane." J Biol Chem **288**(49): 35081-35092.
Chavez, R. A., A. T. Gray, B. B. Zhao, C. H. Kindler, M. J. Mazurek, Y. Mehta, J. R. Forsayeth and C. S. Yost (1999). "TWIK-2, a new weak inward rectifying member of the tandem pore domain potassium channel family." J Biol Chem **274**(12): 7887-7892.
Chen, P., W. Zhang, J. Zhou, P. Wang, L. Xiao and M. Yang (2009). "Development of planar patch clamp technology and its application in the analysis of cellular electrophysiology." Progress in Natural Science **19**(2): 153-160.
Cheng, Y., X. Q. Gu, P. Bednarczyk, F. R. Wiedemann, G. G. Haddad and D. Siemen (2008). "Hypoxia increases activity of the BK-channel in the inner mitochondrial membrane and reduces activity of the permeability transition pore." Cell Physiol Biochem **22**(1-4): 127-136.
Cheng, Y., E. Gulbins and D. Siemen (2011). "Activation of the permeability transition pore by Bax via inhibition of the mitochondrial BK channel." Cell Physiol Biochem **27**(3-4): 191-200.
Cheng, Y., E. Gulbins and D. Siemen (2011). "Activation of the Permeability Transition Pore by Bax via Inhibition of the Mitochondrial BK Channel." Cellular Physiology and Biochemistry **27**(3-4): 191-200.
Chesler, M. and K. Kaila (1992). "Modulation of pH by neuronal activity." Trends Neurosci **15**(10): 396-402.
Clark, J. (2015). "ATOMIC AND PHYSICAL PROPERTIES OF THE GROUP 7 ELEMENTS (THE HALOGENS)." from https://www.chemguide.co.uk/inorganic/group7/properties.html.
Clarke, C. E., E. L. Veale, P. J. Green, H. J. Meadows and A. Mathie (2004). "Selective block of the human 2-P domain potassium channel, TASK-3, and the native leak potassium current, IKSO, by zinc." J Physiol **560**(Pt 1): 51-62.

Clarke, C. E., E. L. Veale, K. Wyse, J. I. Vandenberg and A. Mathie (2008). "The M1P1 loop of TASK3 K2P channels apposes the selectivity filter and influences channel function." J Biol Chem **283**(25): 16985-16992.
Cohen, M. V., C. P. Baines and J. M. Downey (2000). "Ischemic preconditioning: from adenosine receptor to KATP channel." Annu Rev Physiol **62**: 79-109.
Cole, W. C., C. D. McPherson and D. Sontag (1991). "ATP-regulated K+ channels protect the myocardium against ischemia/reperfusion damage." Circ Res **69**(3): 571-581.
Collins, T. J., M. J. Berridge, P. Lipp and M. D. Bootman (2002). "Mitochondria are morphologically and functionally heterogeneous within cells." Embo j **21**(7): 1616-1627.
Costes, S. V., D. Daelemans, E. H. Cho, Z. Dobbin, G. Pavlakis and S. Lockett (2004). "Automatic and quantitative measurement of protein-protein colocalization in live cells." Biophysical journal **86**(6): 3993-4003.
Crofts, A. R. (2004). "The cytochrome bc1 complex: function in the context of structure." Annu Rev Physiol **66**: 689-733.
Crompton, M. (1999). "The mitochondrial permeability transition pore and its role in cell death." Biochem J **341 (Pt 2)**: 233-249.
Cui, Y., A. G. Holt, C. A. Lomax and R. A. Altschuler (2007). "Deafness associated changes in two-pore domain potassium channels in the rat inferior colliculus." Neuroscience **149**(2): 421-433.
Cumming, G., F. Fidler and D. L. Vaux (2007). "Error bars in experimental biology." The Journal of Cell Biology **177**(1): 7-11.
Czirjak, G. and P. Enyedi (2002). "Formation of functional heterodimers between the TASK-1 and TASK-3 two-pore domain potassium channel subunits." J Biol Chem **277**(7): 5426-5432.
Czirják, G. and P. Enyedi (2002). "Formation of Functional Heterodimers between the TASK-1 and TASK-3 Two-pore Domain Potassium Channel Subunits." Journal of Biological Chemistry **277**(7): 5426-5432.
Czirják, G. and P. Enyedi (2003). "Ruthenium red inhibits TASK-3 potassium channel by interconnecting glutamate 70 of the two subunits." Molecular pharmacology **63**(3): 646-652.
Dahlem, Y. A., T. F. W. Horn, L. Buntinas, T. Gonoi, G. Wolf and D. Siemen (2004). "The human mitochondrial KATP channel is modulated by calcium and nitric oxide: a patch-clamp approach." Biochimica et Biophysica Acta (BBA) - Bioenergetics **1656**(1): 46-56.
Das, M., J. E. Parker and A. P. Halestrap (2003). "Matrix volume measurements challenge the existence of diazoxide/glibencamide-sensitive KATP channels in rat mitochondria." J Physiol **547**(Pt 3): 893-902.
Davies, L. A., C. Hu, N. A. Guagliardo, N. Sen, X. Chen, E. M. Talley, R. M. Carey, D. A. Bayliss and P. Q. Barrett (2008). "TASK channel deletion in mice causes primary hyperaldosteronism." Proc Natl Acad Sci U S A **105**(6): 2203-2208.
De Marchi, U., N. Sassi, B. Fioretti, L. Catacuzzeno, G. M. Cereghetti, I. Szabo and M. Zoratti (2009). "Intermediate conductance Ca2+-activated potassium channel (KCa3.1) in the inner mitochondrial membrane of human colon cancer cells." Cell Calcium **45**(5): 509-516.
Dębska, G., R. May, A. Kicińska, A. Szewczyk, C. E. Elger and W. S. Kunz (2001). "Potassium channel openers depolarize hippocampal mitochondria." Brain Research **892**(1): 42-50.
Dejean, L. M., S. Martinez-Caballero, L. Guo, C. Hughes, O. Teijido, T. Ducret, F. Ichas, S. J. Korsmeyer, B. Antonsson, E. A. Jonas and K. W. Kinnally (2005). "Oligomeric Bax is a component of the putative cytochrome c release channel MAC, mitochondrial apoptosis-induced channel." Mol Biol Cell **16**(5): 2424-2432.
Dejean, L. M., S. Martinez-Caballero, S. Manon and K. W. Kinnally (2006). "Regulation of the mitochondrial apoptosis-induced channel, MAC, by BCL-2 family proteins." Biochim Biophys Acta **1762**(2): 191-201.
Doczi, J., B. Torocsik, A. Echaniz-Laguna, B. Mousson de Camaret, A. Starkov, N. Starkova, A. Gál, M. J. Molnár, H. Kawamata, G. Manfredi, V. Adam-Vizi and C. Chinopoulos (2016). "Alterations in

voltage-sensing of the mitochondrial permeability transition pore in ANT1-deficient cells." Scientific Reports **6**: 26700.
Doczi, J., L. Turiák, S. Vajda, M. Mándi, B. Töröcsik, A. A. Gerencser, G. Kiss, C. Konràd, V. Adam-Vizi and C. Chinopoulos (2011). "Complex Contribution of Cyclophilin D to Ca2+-induced Permeability Transition in Brain Mitochondria, with Relation to the Bioenergetic State." Journal of Biological Chemistry **286**(8): 6345-6353.
Dookeran, K. A., W. Zhang, L. Stayner and M. Argos (2017). "Associations of two-pore domain potassium channels and triple negative breast cancer subtype in The Cancer Genome Atlas: systematic evaluation of gene expression and methylation." BMC Research Notes **10**: 475.
Dos Santos, P., A. J. Kowaltowski, M. N. Laclau, S. Seetharaman, P. Paucek, S. Boudina, J. B. Thambo, L. Tariosse and K. D. Garlid (2002). "Mechanisms by which opening the mitochondrial ATP- sensitive K(+) channel protects the ischemic heart." Am J Physiol Heart Circ Physiol **283**(1): H284-295.
Doyle, D. A., J. Morais Cabral, R. A. Pfuetzner, A. Kuo, J. M. Gulbis, S. L. Cohen, B. T. Chait and R. MacKinnon (1998). "The structure of the potassium channel: molecular basis of K+ conduction and selectivity." Science **280**(5360): 69-77.
Dubin, A. E., N. Nasser, J. Rohrbacher, A. N. Hermans, R. Marrannes, C. Grantham, K. Van Rossem, M. Cik, S. R. Chaplan, D. Gallacher, J. Xu, A. Guia, N. G. Byrne and C. Mathes (2005). "Identifying Modulators of hERG Channel Activity Using the PatchXpress® Planar Patch Clamp." Journal of Biomolecular Screening **10**(2): 168-181.
Dudek, J., P. Rehling and M. van der Laan (2013). "Mitochondrial protein import: Common principles and physiological networks." Biochimica et Biophysica Acta (BBA) - Molecular Cell Research **1833**(2): 274-285.
Dunn, K. W., M. M. Kamocka and J. H. McDonald (2011). "A practical guide to evaluating colocalization in biological microscopy." American Journal of Physiology - Cell Physiology **300**(4): C723-C742.
Dunne, M. J. (1994). "Phorbol myristate acetate and ATP-sensitive potassium channels in insulin-secreting cells." Am J Physiol **267**(2 Pt 1): C501-506.
Duprat, F., C. Girard, G. Jarretou and M. Lazdunski (2005). "Pancreatic two P domain K+ channels TALK-1 and TALK-2 are activated by nitric oxide and reactive oxygen species." J Physiol **562**(Pt 1): 235-244.
Duprat, F., F. Lesage, M. Fink, R. Reyes, C. Heurteaux and M. Lazdunski (1997). "TASK, a human background K+ channel to sense external pH variations near physiological pH." The EMBO Journal **16**(17): 5464-5471.
Enyedi, P. and G. Czirjak (2010). "Molecular background of leak K+ currents: two-pore domain potassium channels." Physiol Rev **90**(2): 559-605.
Enyedi, P. and G. Czirják (2010). "Molecular Background of Leak K+ Currents: Two-Pore Domain Potassium Channels." Physiol Rev **90**(2): 559-605.
Enyedi, P. and G. Czirják (2010). "Molecular background of leak K+ currents: two-pore domain potassium channels." Physiological reviews **90**(2): 559-605.
Fahanik-babaei, J., A. Eliassi, A. Jafari, R. Sauve, S. Salari and R. Saghiri (2011). "Electro-pharmacological profile of a mitochondrial inner membrane big-potassium channel from rat brain." Biochimica et Biophysica Acta (BBA) - Biomembranes **1808**(1): 454-460.
Feissner, R. F., J. Skalska, W. E. Gaum and S. S. Sheu (2009). "Crosstalk signaling between mitochondrial Ca2+ and ROS." Front Biosci (Landmark Ed) **14**: 1197-1218.
Felipe, A., R. Vicente, N. Villalonga, M. Roura-Ferrer, R. Martínez-Mármol, L. Solé, J. C. Ferreres and E. Condom (2006). "Potassium channels: New targets in cancer therapy." Cancer Detection and Prevention **30**(4): 375-385.
Fernandez-Salas, E., M. Sagar, C. Cheng, S. H. Yuspa and W. C. Weinberg (1999). "p53 and tumor necrosis factor alpha regulate the expression of a mitochondrial chloride channel protein." J Biol Chem **274**(51): 36488-36497.

Fernandez-Salas, E., K. S. Suh, V. V. Speransky, W. L. Bowers, J. M. Levy, T. Adams, K. R. Pathak, L. E. Edwards, D. D. Hayes, C. Cheng, A. C. Steven, W. C. Weinberg and S. H. Yuspa (2002). "mtCLIC/CLIC4, an organellular chloride channel protein, is increased by DNA damage and participates in the apoptotic response to p53." Mol Cell Biol **22**(11): 3610-3620.
Fernández-Salas, E., K. S. Suh, V. V. Speransky, W. L. Bowers, J. M. Levy, T. Adams, K. R. Pathak, L. E. Edwards, D. D. Hayes, C. Cheng, A. C. Steven, W. C. Weinberg and S. H. Yuspa (2002). "mtCLIC/CLIC4, an Organellular Chloride Channel Protein, Is Increased by DNA Damage and Participates in the Apoptotic Response to p53." Molecular and Cellular Biology **22**(11): 3610-3620.
Fertig, N., R. H. Blick and J. C. Behrends (2002). "Whole Cell Patch Clamp Recording Performed on a Planar Glass Chip." Biophysical Journal **82**(6): 3056-3062.
Fieni, F., S. Bae Lee, Y. N. Jan and Y. Kirichok (2012). "Activity of the mitochondrial calcium uniporter varies greatly between tissues." Nature Communications **3**: 1317.
Fieni, F., S. B. Lee, Y. N. Jan and Y. Kirichok (2012). "Activity of the mitochondrial calcium uniporter varies greatly between tissues." Nat Commun **3**: 1317.
Fink, M., F. Duprat, F. Lesage, R. Reyes, G. Romey, C. Heurteaux and M. Lazdunski (1996). "Cloning, functional expression and brain localization of a novel unconventional outward rectifier K+ channel." Embo j **15**(24): 6854-6862.
Fiskum, G., A. N. Murphy and M. F. Beal (1999). "Mitochondria in neurodegeneration: acute ischemia and chronic neurodegenerative diseases." J Cereb Blood Flow Metab **19**(4): 351-369.
Fontaine, E. and P. Bernardi (1999). "Progress on the mitochondrial permeability transition pore: regulation by complex I and ubiquinone analogs." J Bioenerg Biomembr **31**(4): 335-345.
Fontaine, E., O. Eriksson, F. Ichas and P. Bernardi (1998). "Regulation of the permeability transition pore in skeletal muscle mitochondria. Modulation By electron flow through the respiratory chain complex i." J Biol Chem **273**(20): 12662-12668.
Friedman, J. R. and J. Nunnari (2014). "Mitochondrial form and function." Nature **505**(7483): 335-343.
Fryer, R. M., A. K. Hsu, J. T. Eells, H. Nagase and G. J. Gross (1999). "Opioid-induced second window of cardioprotection: potential role of mitochondrial KATP channels." Circ Res **84**(7): 846-851.
Garcia-Perez, C., T. G. Schneider, G. Hajnoczky and G. Csordas (2011). "Alignment of sarcoplasmic reticulum-mitochondrial junctions with mitochondrial contact points." Am J Physiol Heart Circ Physiol **301**(5): H1907-1915.
Garcia-Rodriguez, L. J., A. C. Gay and L. A. Pon (2007). "Puf3p, a Pumilio family RNA binding protein, localizes to mitochondria and regulates mitochondrial biogenesis and motility in budding yeast." J Cell Biol **176**(2): 197-207.
Garcia, M., X. Darzacq, T. Delaveau, L. Jourdren, R. H. Singer and C. Jacq (2007). "Mitochondria-associated yeast mRNAs and the biogenesis of molecular complexes." Mol Biol Cell **18**(2): 362-368.
Garlid, K. (1988). Integration of Mitochondrial Function: 257-276.
Garlid, K. D. (1996). "Cation transport in mitochondria—the potassium cycle." Biochimica et Biophysica Acta (BBA)-Bioenergetics **1275**(1): 123-126.
Garlid, K. D. and A. D. Beavis (1986). "Evidence for the existence of an inner membrane anion channel in mitochondria." Biochim Biophys Acta **853**(3-4): 187-204.
Garlid, K. D. and P. Paucek (2003). "Mitochondrial potassium transport: the K(+) cycle." Biochim Biophys Acta **1606**(1-3): 23-41.
Garlid, K. D. and P. Paucek (2003). "Mitochondrial potassium transport: the K+ cycle." Biochimica et Biophysica Acta (BBA) - Bioenergetics **1606**(1): 23-41.
Garlid, K. D., P. Paucek, V. Yarov-Yarovoy, H. N. Murray, R. B. Darbenzio, A. J. D'Alonzo, N. J. Lodge, M. A. Smith and G. J. Grover (1997). "Cardioprotective effect of diazoxide and its interaction with mitochondrial ATP-sensitive K+ channels. Possible mechanism of cardioprotection." Circ Res **81**(6): 1072-1082.

Gaspar, T., J. A. Snipes, A. R. Busija, B. Kis, F. Domoki, F. Bari and D. W. Busija (2008). "ROS-independent preconditioning in neurons via activation of mitoK(ATP) channels by BMS-191095." J Cereb Blood Flow Metab **28**(6): 1090-1103.
Gazula, V. R., J. G. Strumbos, X. Mei, H. Chen, C. Rahner and L. K. Kaczmarek (2010). "Localization of Kv1.3 channels in presynaptic terminals of brainstem auditory neurons." J Comp Neurol **518**(16): 3205-3220.
Gincel, D., H. Zaid and V. Shoshan-barmatz (2001). "Calcium binding and translocation by the voltage-dependent anion channel: a possible regulatory mechanism in mitochondrial function." Biochemical Journal **358**(1): 147-155.
Girard, C., F. Duprat, C. Terrenoire, N. Tinel, M. Fosset, G. Romey, M. Lazdunski and F. Lesage (2001). "Genomic and functional characteristics of novel human pancreatic 2P domain K(+) channels." Biochem Biophys Res Commun **282**(1): 249-256.
Gogvadze, V., J. D. Robertson, M. Enoksson, B. Zhivotovsky and S. Orrenius (2004). "Mitochondrial cytochrome c release may occur by volume-dependent mechanisms not involving permeability transition." Biochem J **378**(Pt 1): 213-217.
Green, D. R. and G. Kroemer (2004). "The pathophysiology of mitochondrial cell death." Science **305**(5684): 626-629.
Grigoriev, S. M., C. Muro, L. M. Dejean, M. L. Campo, S. Martinez-Caballero and K. W. Kinnally (2004). "Electrophysiological approaches to the study of protein translocation in mitochondria." Int Rev Cytol **238**: 227-274.
Grissmer, S., A. N. Nguyen, J. Aiyar, D. C. Hanson, R. J. Mather, G. A. Gutman, M. J. Karmilowicz, D. D. Auperin and K. G. Chandy (1994). "Pharmacological characterization of five cloned voltage-gated K+ channels, types Kv1.1, 1.2, 1.3, 1.5, and 3.1, stably expressed in mammalian cell lines." Mol Pharmacol **45**(6): 1227-1234.
Grunnet, M., H. B. Rasmussen, A. Hay-Schmidt and D. A. Klaerke (2003). "The voltage-gated potassium channel subunit, Kv1.3, is expressed in epithelia." Biochim Biophys Acta **1616**(1): 85-94.
Guéguinou, M., A. Chantôme, G. Fromont, P. Bougnoux, C. Vandier and M. Potier-Cartereau (2014). "KCa and Ca2 + channels: The complex thought." Biochimica et Biophysica Acta (BBA) - Molecular Cell Research **1843**(10): 2322-2333.
Gutman, G. A., K. G. Chandy, J. P. Adelman, J. Aiyar, D. A. Bayliss, D. E. Clapham, M. Covarriubias, G. V. Desir, K. Furuichi, B. Ganetzky, M. L. Garcia, S. Grissmer, L. Y. Jan, A. Karschin, D. Kim, S. Kuperschmidt, Y. Kurachi, M. Lazdunski, F. Lesage, H. A. Lester, D. McKinnon, C. G. Nichols, I. O'Kelly, J. Robbins, G. A. Robertson, B. Rudy, M. Sanguinetti, S. Seino, W. Stuehmer, M. M. Tamkun, C. A. Vandenberg, A. Wei, H. Wulff and R. S. Wymore (2003). "International Union of Pharmacology. XLI. Compendium of voltage-gated ion channels: potassium channels." Pharmacol Rev **55**(4): 583-586.
Hajnoczky, G., G. Csordas, S. Das, C. Garcia-Perez, M. Saotome, S. Sinha Roy and M. Yi (2006). "Mitochondrial calcium signalling and cell death: approaches for assessing the role of mitochondrial Ca2+ uptake in apoptosis." Cell Calcium **40**(5-6): 553-560.
Halestrap, A. P. (1987). "The regulation of the oxidation of fatty acids and other substrates in rat heart mitochondria by changes in the matrix volume induced by osmotic strength, valinomycin and Ca²⁺." Biochemical Journal **244**(1): 159-164.
Halestrap, A. P. (1989). "The regulation of the matrix volume of mammalian mitochondria in vivo and in vitro and its role in the control of mitochondrial metabolism." Biochim Biophys Acta **973**(3): 355-382.
Halestrap, A. P. (2009). "What is the mitochondrial permeability transition pore?" J Mol Cell Cardiol **46**(6): 821-831.
Halestrap, A. P. and C. Brenner (2003). "The adenine nucleotide translocase: a central component of the mitochondrial permeability transition pore and key player in cell death." Curr Med Chem **10**(16): 1507-1525.
Hanahan, D. and Robert A. Weinberg (2011). "Hallmarks of Cancer: The Next Generation." Cell **144**(5): 646-674.

Hansford, R. G., B. Hogue, A. Prokopczuk, E. Wasilewska and B. Lewartowski (1990). "Activation of pyruvate dehydrogenase by electrical stimulation, and low-Na+ perfusion of guinea-pig heart." Biochimica et Biophysica Acta (BBA) - Bioenergetics **1018**(2): 282-286.
Hardingham, G. E., S. Chawla, C. M. Johnson and H. Bading (1997). "Distinct functions of nuclear and cytoplasmic calcium in the control of gene expression." Nature **385**(6613): 260-265.
Hausenloy, D. J., D. M. Yellon, S. Mani-Babu and M. R. Duchen (2004). "Preconditioning protects by inhibiting the mitochondrial permeability transition." Am J Physiol Heart Circ Physiol **287**(2): H841-849.
Heinen, A., M. Aldakkak, D. F. Stowe, S. S. Rhodes, M. L. Riess, S. G. Varadarajan and A. K. Camara (2007). "Reverse electron flow-induced ROS production is attenuated by activation of mitochondrial Ca2+-sensitive K+ channels." Am J Physiol Heart Circ Physiol **293**(3): H1400-1407.
Heinen, A., A. K. Camara, M. Aldakkak, S. S. Rhodes, M. L. Riess and D. F. Stowe (2007). "Mitochondrial Ca2+-induced K+ influx increases respiration and enhances ROS production while maintaining membrane potential." Am J Physiol Cell Physiol **292**(1): C148-156.
Heurteaux, C., G. Lucas, N. Guy, M. El Yacoubi, S. Thummler, X. D. Peng, F. Noble, N. Blondeau, C. Widmann, M. Borsotto, G. Gobbi, J. M. Vaugeois, G. Debonnel and M. Lazdunski (2006). "Deletion of the background potassium channel TREK-1 results in a depression-resistant phenotype." Nat Neurosci **9**(9): 1134-1141.
Hidalgo, P. and R. MacKinnon (1995). "Revealing the architecture of a K+ channel pore through mutant cycles with a peptide inhibitor." Science **268**(5208): 307-310.
Hille, B. (2001). Ion channels of excitable membranes, Sinauer Sunderland, MA.
Holmuhamedov, E., L. Lewis, M. Bienengraeber, M. Holmuhamedova, A. Jahangir and A. Terzic (2002). "Suppression of human tumor cell proliferation through mitochondrial targeting." Faseb j **16**(9): 1010-1016.
Holmuhamedov, E. L., A. Jahangir, A. Oberlin, A. Komarov, M. Colombini and A. Terzic (2004). "Potassium channel openers are uncoupling protonophores: implication in cardioprotection." FEBS Lett **568**(1-3): 167-170.
Holmuhamedov, E. L., L. Wang and A. Terzic (1999). "ATP-sensitive K+ channel openers prevent Ca2+ overload in rat cardiac mitochondria." J Physiol **519 Pt 2**: 347-360.
Holt, A. G., M. Asako, R. K. Duncan, C. A. Lomax, J. M. Juiz and R. A. Altschuler (2006). "Deafness associated changes in expression of two-pore domain potassium channels in the rat cochlear nucleus." Hearing research **216**: 146-153.
Holt, J. R. and D. P. Corey (1999). "Ion channel defects in hereditary hearing loss." Neuron **22**(2): 217-219.
Honore, E. (2007). "The neuronal background K2P channels: focus on TREK1." Nat Rev Neurosci **8**(4): 251-261.
Honore, E., F. Maingret, M. Lazdunski and A. J. Patel (2002). "An intracellular proton sensor commands lipid- and mechano-gating of the K(+) channel TREK-1." Embo j **21**(12): 2968-2976.
Hoppe, U. C. (2010). "Mitochondrial calcium channels." FEBS Letters **584**(10): 1975-1981.
Huang, S. G. and M. Klingenberg (1996). "Chloride channel properties of the uncoupling protein from brown adipose tissue mitochondria: a patch-clamp study." Biochemistry **35**(51): 16806-16814.
Innamaa, A., L. Jackson, V. Asher, G. Van Shalkwyk, A. Warren, D. Hay, A. Bali, H. Sowter and R. Khan (2013). "Expression and prognostic significance of the oncogenic K2P potassium channel KCNK9 (TASK-3) in ovarian carcinoma." Anticancer Res **33**(4): 1401-1408.
Inoue, I., H. Nagase, K. Kishi and T. Higuti (1991). "ATP-sensitive K+ channel in the mitochondrial inner membrane." Nature **352**(6332): 244-247.
Jaburek, M., V. Yarov-Yarovoy, P. Paucek and K. D. Garlid (1998). "State-dependent inhibition of the mitochondrial KATP channel by glyburide and 5-hydroxydecanoate." J Biol Chem **273**(22): 13578-13582.
James N. Spencer, G. M. B., Lyman H. Rickard (2010). Chemistry: Structure and Dynamics.

Jarmuszkiewicz, W. and A. Woyda-Ploszczyca (2008). "[Mitochondrial uncoupling proteins: regulation and physiological role]." Postepy Biochem **54**(2): 179-187.
Jiang, M. T., M. Ljubkovic, Y. Nakae, Y. Shi, W. M. Kwok, D. F. Stowe and Z. J. Bosnjak (2006). "Characterization of human cardiac mitochondrial ATP-sensitive potassium channel and its regulation by phorbol ester in vitro." Am J Physiol Heart Circ Physiol **290**(5): H1770-1776.
Joiner, M.-l. A., O. M. Koval, L. Jingdong, B. J. He, C. Allamargot, Z. Gao, E. D. Luczak, D. D. Hall, B. D. Fink, B. Chen, J. Yang, S. A. Moore, T. D. Scholz, S. Strack, P. J. Mohler, W. I. Sivitz, L.-S. Song and M. E. Anderson (2012). "CaMKII determines mitochondrial stress responses in heart." Nature **491**(7423): 269-273.
Jouaville, L. S., P. Pinton, C. Bastianutto, G. A. Rutter and R. Rizzuto (1999). "Regulation of mitochondrial ATP synthesis by calcium: Evidence for a long-term metabolic priming." Proceedings of the National Academy of Sciences **96**(24): 13807-13812.
Juhaszova, M., D. B. Zorov, S. H. Kim, S. Pepe, Q. Fu, K. W. Fishbein, B. D. Ziman, S. Wang, K. Ytrehus, C. L. Antos, E. N. Olson and S. J. Sollott (2004). "Glycogen synthase kinase-3beta mediates convergence of protection signaling to inhibit the mitochondrial permeability transition pore." J Clin Invest **113**(11): 1535-1549.
Kaasik, A., D. Safiulina, A. Zharkovsky and V. Veksler (2007). "Regulation of mitochondrial matrix volume." American Journal of Physiology - Cell Physiology **292**(1): C157-C163.
Kajma, A. and A. Szewczyk (2012). "A new pH-sensitive rectifying potassium channel in mitochondria from the embryonic rat hippocampus." Biochimica et Biophysica Acta (BBA)-Bioenergetics **1817**(10): 1867-1878.
Kajma, A. and A. Szewczyk (2012). "A new pH-sensitive rectifying potassium channel in mitochondria from the embryonic rat hippocampus." Biochimica et Biophysica Acta (BBA) - Bioenergetics **1817**(10): 1867-1878.
Kane, D. A. and E. V. Pavlov (2013). "Calculation of ion currents across the inner membrane of functionally intact mitochondria." Channels **7**(6): 426-431.
Kang, D., J. Han, E. M. Talley, D. A. Bayliss and D. Kim (2004). "Functional expression of TASK-1/TASK-3 heteromers in cerebellar granule cells." J Physiol **554**(Pt 1): 64-77.
Kang, S. H., W. S. Park, N. Kim, J. B. Youm, M. Warda, J. H. Ko, E. A. Ko and J. Han (2007). "Mitochondrial Ca2+-activated K+ channels more efficiently reduce mitochondrial Ca2+ overload in rat ventricular myocytes." Am J Physiol Heart Circ Physiol **293**(1): H307-313.
Karschin, C., E. Wischmeyer, R. Preisig-Muller, S. Rajan, C. Derst, K. H. Grzeschik, J. Daut and A. Karschin (2001). "Expression pattern in brain of TASK-1, TASK-3, and a tandem pore domain K(+) channel subunit, TASK-5, associated with the central auditory nervous system." Mol Cell Neurosci **18**(6): 632-648.
Kim, D. (2005). "Physiology and pharmacology of two-pore domain potassium channels." Curr Pharm Des **11**(21): 2717-2736.
Kim, D. and C. Gnatenco (2001). "TASK-5, a new member of the tandem-pore K(+) channel family." Biochem Biophys Res Commun **284**(4): 923-930.
Kim, Y., H. Bang, C. Gnatenco and D. Kim (2001). "Synergistic interaction and the role of C-terminus in the activation of TRAAK K+ channels by pressure, free fatty acids and alkali." Pflugers Arch **442**(1): 64-72.
Kim, Y., H. Bang and D. Kim (1999). "TBAK-1 and TASK-1, two-pore K(+) channel subunits: kinetic properties and expression in rat heart." Am J Physiol **277**(5 Pt 2): H1669-1678.
Kim, Y., H. Bang and D. Kim (2000). "TASK-3, a new member of the tandem pore K(+) channel family." J Biol Chem **275**(13): 9340-9347.
Kim, Y., H. Bang and D. Kim (2000). "TASK-3, a New Member of the Tandem Pore K+ Channel Family." Journal of Biological Chemistry **275**(13): 9340-9347.
Kindler, C. H., C. Pietruck, C. S. Yost, E. R. Sampson and A. T. Gray (2000). "Localization of the tandem pore domain K+ channel TASK-1 in the rat central nervous system." Brain Res Mol Brain Res **80**(1): 99-108.

Kinnally, K. W. and B. Antonsson (2007). "A tale of two mitochondrial channels, MAC and PTP, in apoptosis." Apoptosis **12**(5): 857-868.
Kirichok, Y., G. Krapivinsky and D. E. Clapham (2004). "The mitochondrial calcium uniporter is a highly selective ion channel." Nature **427**(6972): 360-364.
Kirichok, Y., G. Krapivinsky and D. E. Clapham (2004). "The mitochondrial calcium uniporter is a highly selective ion channel." Nature **427**(6972): 360-364.
Kitamura, A., M. Nishizuka, K. Tominaga, T. Tsuchiya, T. Nishihara and M. Imagawa (2001). "Expression of p68 RNA helicase is closely related to the early stage of adipocyte differentiation of mouse 3T3-L1 cells." Biochem Biophys Res Commun **287**(2): 435-439.
Kominkova, V., L. Malekova, Z. Tomaskova, P. Slezak, A. Szewczyk and K. Ondrias (2010). "Modulation of intracellular chloride channels by ATP and Mg2+." Biochim Biophys Acta **1797**(6-7): 1300-1312.
Korge, P., H. M. Honda and J. N. Weiss (2002). "Protection of cardiac mitochondria by diazoxide and protein kinase C: Implications for ischemic preconditioning." Proceedings of the National Academy of Sciences of the United States of America **99**(5): 3312-3317.
Korge, P., H. M. Honda and J. N. Weiss (2002). "Protection of cardiac mitochondria by diazoxide and protein kinase C: implications for ischemic preconditioning." Proc Natl Acad Sci U S A **99**(5): 3312-3317.
Kostyuk, P. G., O. A. Krishtal and V. I. Pidoplichko (1975). "Effect of internal fluoride and phosphate on membrane currents during intracellular dialysis of nerve cells." Nature **257**(5528): 691-693.
Kosztka, L., Z. Rusznak, D. Nagy, Z. Nagy, J. Fodor, G. Szucs, A. Telek, M. Gonczi, O. Ruzsnavszky, N. Szentandrassy and L. Csernoch (2011). "Inhibition of TASK-3 (KCNK9) channel biosynthesis changes cell morphology and decreases both DNA content and mitochondrial function of melanoma cells maintained in cell culture." Melanoma Res **21**(4): 308-322.
Kosztka, L., Z. Rusznák, D. Nagy, Z. Nagy, J. Fodor, G. Szucs, A. Telek, M. Gönczi, O. Ruzsnavszky, N. Szentandrássy and L. Csernoch (2011). "Inhibition of TASK-3 (KCNK9) channel biosynthesis changes cell morphology and decreases both DNA content and mitochondrial function of melanoma cells maintained in cell culture." Melanoma Research **21**(4): 308-322.
Kowaltowski, A. J., R. G. Cosso, C. B. Campos and G. Fiskum (2002). "Effect of Bcl-2 overexpression on mitochondrial structure and function." Journal of Biological Chemistry **277**(45): 42802-42807.
Kowaltowski, A. J., E. S. Naia-da-Silva, R. F. Castilho and A. E. Vercesi (1998). "Ca2+-stimulated mitochondrial reactive oxygen species generation and permeability transition are inhibited by dibucaine or Mg2+." Arch Biochem Biophys **359**(1): 77-81.
Kozoriz, M. G., J. Church, M. A. Ozog, C. C. Naus and C. Krebs (2010). "Temporary sequestration of potassium by mitochondria in astrocytes." J Biol Chem **285**(41): 31107-31119.
Kubisch, C., B. C. Schroeder, T. Friedrich, B. Lutjohann, A. El-Amraoui, S. Marlin, C. Petit and T. J. Jentsch (1999). "KCNQ4, a novel potassium channel expressed in sensory outer hair cells, is mutated in dominant deafness." Cell **96**(3): 437-446.
Kühlbrandt, W. (2015). "Structure and function of mitochondrial membrane protein complexes." BMC Biology **13**: 89.
Kutchinsky, J., S. Friis, M. Asmild, R. Taboryski, S. Pedersen, R. K. Vestergaard, R. B. Jacobsen, K. Krzywkowski, R. L. Schroder, T. Ljungstrom, N. Helix, C. B. Sorensen, M. Bech and N. J. Willumsen (2003). "Characterization of potassium channel modulators with QPatch automated patch-clamp technology: system characteristics and performance." Assay Drug Dev Technol **1**(5): 685-693.
Lacinova, L. (2005). "Voltage-dependent calcium channels." General physiology and biophysics **24**.
Lang, F., M. Föller, K. S. Lang, P. A. Lang, M. Ritter, E. Gulbins, A. Vereninov and S. M. Huber (2005). "Ion Channels in Cell Proliferation and Apoptotic Cell Death." The Journal of Membrane Biology **205**(3): 147-157.
Lauritzen, I., M. Zanzouri, E. Honoré, F. Duprat, M. U. Ehrengruber, M. Lazdunski and A. J. Patel (2003). "K+-dependent Cerebellar Granule Neuron Apoptosis: ROLE OF TASK LEAK K+ CHANNELS." Journal of Biological Chemistry **278**(34): 32068-32076.

Lee, G. W., H. S. Park, E. J. Kim, Y. W. Cho, G. T. Kim, Y. J. Mun, E. J. Choi, J. S. Lee, J. Han and D. Kang (2012). "Reduction of breast cancer cell migration via up-regulation of TASK-3 two-pore domain K+ channel." Acta Physiol (Oxf) **204**(4): 513-524.
Lehen'kyi, V., G. Shapovalov, R. Skryma and N. Prevarskaya (2011). "Ion channnels and transporters in cancer. 5. Ion channels in control of cancer and cell apoptosis." Am J Physiol Cell Physiol **301**(6): C1281-1289.
Lemasters, J. J., T. P. Theruvath, Z. Zhong and A. L. Nieminen (2009). "Mitochondrial calcium and the permeability transition in cell death." Biochim Biophys Acta **1787**(11): 1395-1401.
Leonoudakis, D., A. T. Gray, B. D. Winegar, C. H. Kindler, M. Harada, D. M. Taylor, R. A. Chavez, J. R. Forsayeth and C. S. Yost (1998). "An open rectifier potassium channel with two pore domains in tandem cloned from rat cerebellum." J Neurosci **18**(3): 868-877.
Lesage, F. and J. Barhanin (2011). "Molecular physiology of pH-sensitive background K(2P) channels." Physiology (Bethesda) **26**(6): 424-437.
Lesage, F., E. Guillemare, M. Fink, F. Duprat, M. Lazdunski, G. Romey and J. Barhanin (1996). "TWIK-1, a ubiquitous human weakly inward rectifying K+ channel with a novel structure." Embo j **15**(5): 1004-1011.
Lesage, F. and M. Lazdunski (2000). "Molecular and functional properties of two-pore-domain potassium channels." Am J Physiol Renal Physiol **279**(5): F793-801.
Lesage, F., R. Reyes, M. Fink, F. Duprat, E. Guillemare and M. Lazdunski (1996). "Dimerization of TWIK-1 K+ channel subunits via a disulfide bridge." The EMBO Journal **15**(23): 6400.
Levadny, V., M. Colombini, X. X. Li and V. M. Aguilella (2002). "Electrostatics explains the shift in VDAC gating with salt activity gradient." Biophys J **82**(4): 1773-1783.
Li, L., D. P. Li, S. R. Chen, J. Chen, H. Hu and H. L. Pan (2014). "Potentiation of high voltage-activated calcium channels by 4-aminopyridine depends on subunit composition." Mol Pharmacol **86**(6): 760-772.
Li, T., G. Lu, E. Y. Chiang, T. Chernov-Rogan, J. L. Grogan and J. Chen (2017). "High-throughput electrophysiological assays for voltage gated ion channels using SyncroPatch 768PE." PLOS ONE **12**(7): e0180154.
Lim, K. H., S. A. Javadov, M. Das, S. J. Clarke, M. S. Suleiman and A. P. Halestrap (2002). "The effects of ischaemic preconditioning, diazoxide and 5-hydroxydecanoate on rat heart mitochondrial volume and respiration." J Physiol **545**(Pt 3): 961-974.
Lipscombe, D., T. D. Helton and W. Xu (2004). "L-Type Calcium Channels: The Low Down." Journal of Neurophysiology **92**(5): 2633-2641.
Litsky, M. L. and D. R. Pfeiffer (1997). "Regulation of the mitochondrial Ca2+ uniporter by external adenine nucleotides: the uniporter behaves like a gated channel which is regulated by nucleotides and divalent cations." Biochemistry **36**(23): 7071-7080.
Littler, D. R., N. N. Assaad, S. J. Harrop, L. J. Brown, G. J. Pankhurst, P. Luciani, M. I. Aguilar, M. Mazzanti, M. A. Berryman, S. N. Breit and P. M. Curmi (2005). "Crystal structure of the soluble form of the redox-regulated chloride ion channel protein CLIC4." Febs j **272**(19): 4996-5007.
Liu, C., J. F. Cotton, J. A. Schuyler, C. S. Fahlman, J. D. Au, P. E. Bickler and C. S. Yost (2005). "Protective effects of TASK-3 (KCNK9) and related 2P K channels during cellular stress." Brain Research **1031**(2): 164-173.
Liu, X. and G. Hajnoczky (2011). "Altered fusion dynamics underlie unique morphological changes in mitochondria during hypoxia-reoxygenation stress." Cell Death Differ **18**(10): 1561-1572.
Liu, Y., T. Sato, B. O'Rourke and E. Marban (1998). "Mitochondrial ATP-dependent potassium channels: novel effectors of cardioprotection?" Circulation **97**(24): 2463-2469.
Lodish, H. F. M. c. b. N. Y. S. A. B. I.-.-.-O. (2000). Molecular Cell Biology. . New York.
Logan, A., V. R. Pell, K. J. Shaffer, C. Evans, N. J. Stanley, E. L. Robb, T. A. Prime, E. T. Chouchani, H. M. Cocheme, I. M. Fearnley, S. Vidoni, A. M. James, C. M. Porteous, L. Partridge, T. Krieg, R. A. Smith and M. P. Murphy (2016). "Assessing the Mitochondrial Membrane Potential in Cells and In Vivo using Targeted Click Chemistry and Mass Spectrometry." Cell Metab **23**(2): 379-385.

Long, S. B., E. B. Campbell and R. Mackinnon (2005). "Crystal structure of a mammalian voltage-dependent Shaker family K+ channel." Science **309**(5736): 897-903.
Lotshaw, D. P. (2007). "Biophysical, pharmacological, and functional characteristics of cloned and native mammalian two-pore domain K+ channels." Cell biochemistry and biophysics **47**(2): 209-256.
Ma, L., X. Zhang and H. Chen (2011). "TWIK-1 Two-Pore Domain Potassium Channels Change Ion Selectivity and Conduct Inward Leak Sodium Currents in Hypokalemia." Sci. Signal. **4**(176): ra37-.
Ma, L., X. Zhang and H. Chen (2011). "TWIK-1 two-pore domain potassium channels change ion selectivity and conduct inward leak sodium currents in hypokalemia." Sci Signal **4**(176): ra37.
Ma, L., X. Zhang, M. Zhou and H. Chen (2012). "Acid-sensitive TWIK and TASK Two-pore Domain Potassium Channels Change Ion Selectivity and Become Permeable to Sodium in Extracellular Acidification." The Journal of Biological Chemistry **287**(44): 37145-37153.
Maeno, E., Y. Ishizaki, T. Kanaseki, A. Hazama and Y. Okada (2000). "Normotonic cell shrinkage because of disordered volume regulation is an early prerequisite to apoptosis." Proc Natl Acad Sci U S A **97**(17): 9487-9492.
Maingret, F., A. J. Patel, M. Lazdunski and E. Honoré (2001). "The endocannabinoid anandamide is a direct and selective blocker of the background K⁺ channel TASK‐1." The EMBO Journal **20**(1-2): 47-54.
Maingret, F., A. J. Patel, F. Lesage, M. Lazdunski and E. Honore (1999). "Mechano- or acid stimulation, two interactive modes of activation of the TREK-1 potassium channel." J Biol Chem **274**(38): 26691-26696.
Marc, P., A. Margeot, F. Devaux, C. Blugeon, M. Corral-Debrinski and C. Jacq (2002). "Genome-wide analysis of mRNAs targeted to yeast mitochondria." EMBO Rep **3**(2): 159-164.
Martinez-Caballero, S., L. M. Dejean, E. A. Jonas and K. W. Kinnally (2005). "The role of the mitochondrial apoptosis induced channel MAC in cytochrome c release." J Bioenerg Biomembr **37**(3): 155-164.
Mattson, M. P. and G. Kroemer (2003). "Mitochondria in cell death: novel targets for neuroprotection and cardioprotection." Trends Mol Med **9**(5): 196-205.
Mayevsky, A. and B. Chance (1975). "Metabolic responses of the awake cerebral cortex to anoxia hypoxia spreading depression and epileptiform activity." Brain Res **98**(1): 149-165.
McDonough, P. M. and D. C. Button (1989). "Measurement of cytoplasmic calcium concentration in cell suspensions: correction for extracellular Fura-2 through use of Mn2+ and probenecid." Cell Calcium **10**(3): 171-180.
Medhurst, A. D., G. Rennie, C. G. Chapman, H. Meadows, M. D. Duckworth, R. E. Kelsell, Gloger, II and M. N. Pangalos (2001). "Distribution analysis of human two pore domain potassium channels in tissues of the central nervous system and periphery." Brain Res Mol Brain Res **86**(1-2): 101-114.
Meuth, S. G., M. I. Aller, T. Munsch, T. Schuhmacher, T. Seidenbecher, P. Meuth, C. Kleinschnitz, H. C. Pape, H. Wiendl, W. Wisden and T. Budde (2006). "The contribution of TWIK-related acid-sensitive K+-containing channels to the function of dorsal lateral geniculate thalamocortical relay neurons." Mol Pharmacol **69**(4): 1468-1476.
Meuth, S. G., A. M. Herrmann, C. W. Ip, T. Kanyshkova, S. Bittner, A. Weishaupt, T. Budde and H. Wiendl (2008). "The two-pore domain potassium channel TASK3 functionally impacts glioma cell death." J Neurooncol **87**(3): 263-270.
Michels, G., I. F. Khan, J. Endres-Becker, D. Rottlaender, S. Herzig, A. Ruhparwar, T. Wahlers and U. C. Hoppe (2009). "Regulation of the human cardiac mitochondrial Ca2+ uptake by 2 different voltage-gated Ca2+ channels." Circulation **119**(18): 2435-2443.
Miller, A. N. and S. B. Long (2012). "Crystal Structure of the Human Two–Pore Domain Potassium Channel K2P1." Science **335**(6067): 432-436.
Milligan, C. J., J. Li, P. Sukumar, Y. Majeed, M. L. Dallas, A. English, P. Emery, K. E. Porter, A. M. Smith, I. McFadzean, D. Beccano-Kelly, Y. Bahnasi, A. Cheong, J. Naylor, F. Zeng, X. Liu, N. Gamper, L.-H. Jiang, H. A. Pearson, C. Peers, B. Robertson and D. J. Beech (2009). "Robotic multi-well planar patch-clamp for native and primary mammalian cells." Nature protocols **4**(2): 244-255.

Milligan, C. J., J. Li, P. Sukumar, Y. Majeed, M. L. Dallas, A. English, P. Emery, K. E. Porter, A. M. Smith, I. McFadzean, D. Beccano-Kelly, Y. Bahnasi, A. Cheong, J. Naylor, F. Zeng, X. Liu, N. Gamper, L. H. Jiang, H. A. Pearson, C. Peers, B. Robertson and D. J. Beech (2009). "Robotic multiwell planar patch-clamp for native and primary mammalian cells." Nat Protoc **4**(2): 244-255.
Mitchell, P. (1961). "Coupling of phosphorylation to electron and hydrogen transfer by a chemi-osmotic type of mechanism." Nature **191**: 144-148.
Morikawa, D., K. Kanematsu, T. Shibata, K. Haseda, N. Umeda and Y. Ohta (2014). "Detection of swelling of single isolated mitochondrion with optical microscopy." Biomedical Optics Express **5**(3): 848-857.
Mourre, C., M. N. Chernova, M.-F. Martin-Eauclaire, R. Bessone, G. Jacquet, M. Gola, S. L. Alper and M. Crest (1999). "Distribution in Rat Brain of Binding Sites of Kaliotoxin, a Blocker of Kv1.1 and Kv1.3 α-Subunits." Journal of Pharmacology and Experimental Therapeutics **291**(3): 943-952.
Mu, D., L. Chen, X. Zhang, L. H. See, C. M. Koch, C. Yen, J. J. Tong, L. Spiegel, K. C. Nguyen, A. Servoss, Y. Peng, L. Pei, J. R. Marks, S. Lowe, T. Hoey, L. Y. Jan, W. R. McCombie, M. H. Wigler and S. Powers (2003). "Genomic amplification and oncogenic properties of the KCNK9 potassium channel gene." Cancer Cell **3**(3): 297-302.
Mulkey, D. K., R. L. Stornetta, M. C. Weston, J. R. Simmons, A. Parker, D. A. Bayliss and P. G. Guyenet (2004). "Respiratory control by ventral surface chemoreceptor neurons in rats." Nature Neuroscience **7**: 1360.
Mulkey, D. K., E. M. Talley, R. L. Stornetta, A. R. Siegel, G. H. West, X. Chen, N. Sen, A. M. Mistry, P. G. Guyenet and D. A. Bayliss (2007). "TASK channels determine pH sensitivity in select respiratory neurons but do not contribute to central respiratory chemosensitivity." J Neurosci **27**(51): 14049-14058.
Nadeau, H., S. McKinney, D. J. Anderson and H. A. Lester (2000). "ROMK1 (Kir1.1) Causes Apoptosis and Chronic Silencing of Hippocampal Neurons." Journal of Neurophysiology **84**(2): 1062-1075.
Neher, E. and A. Marty (1982). "Discrete changes of cell membrane capacitance observed under conditions of enhanced secretion in bovine adrenal chromaffin cells." Proceedings of the National Academy of Sciences of the United States of America **79**(21): 6712-6716.
Newmeyer, D. D. and S. Ferguson-Miller (2003). "Mitochondria: releasing power for life and unleashing the machineries of death." Cell **112**(4): 481-490.
Nicoll, R. A. and D. V. Madison (1982). "General anesthetics hyperpolarize neurons in the vertebrate central nervous system." Science **217**(4564): 1055-1057.
Niemeyer, M. I., L. P. Cid, G. Peña-Münzenmayer and F. V. Sepúlveda (2010). "Separate gating mechanisms mediate the regulation of K2P potassium channel TASK-2 by intra-and extracellular pH." Journal of Biological Chemistry **285**(22): 16467-16475.
Niessen, K. V., S. Muschik, F. Langguth, S. Rappenglück, T. Seeger, H. Thiermann and F. Worek (2016). "Functional analysis of Torpedo californica nicotinic acetylcholine receptors in multiple activation states by SSM-based electrophysiology." Toxicology Letters **247**: 1-10.
Nishimura, N., S. Bannykh, S. Slabough, J. Matteson, Y. Altschuler, K. Hahn and W. E. Balch (1999). "A di-acidic (DXE) code directs concentration of cargo during export from the endoplasmic reticulum." J Biol Chem **274**(22): 15937-15946.
Nufer, O., S. Guldbrandsen, M. Degen, F. Kappeler, J. P. Paccaud, K. Tani and H. P. Hauri (2002). "Role of cytoplasmic C-terminal amino acids of membrane proteins in ER export." J Cell Sci **115**(Pt 3): 619-628.
O'Connell, A. D., M. J. Morton and M. Hunter (2002). "Two-pore domain K+ channels—molecular sensors." Biochimica et Biophysica Acta (BBA) - Biomembranes **1566**(1–2): 152-161.
O'Kelly, I., M. H. Butler, N. Zilberberg and S. A. Goldstein (2002). "Forward transport. 14-3-3 binding overcomes retention in endoplasmic reticulum by dibasic signals." Cell **111**(4): 577-588.
O'Rourke, B. (2004). "Evidence for mitochondrial K+ channels and their role in cardioprotection." Circ Res **94**(4): 420-432.

O'Rourke, B., S. Cortassa and M. A. Aon (2005). "Mitochondrial ion channels: gatekeepers of life and death." Physiology (Bethesda) **20**: 303-315.
O'Kelly, I. and S. A. N. Goldstein (2008). "Forward Transport of K2P3.1: Mediation by 14-3-3 and COPI, Modulation by p11." Traffic **9**(1): 72-78.
O'Rourke, B. (2007). "Mitochondrial Ion Channels." Annual review of physiology **69**: 19-49.
Ockaili, R., V. R. Emani, S. Okubo, M. Brown, K. Krottapalli and R. C. Kukreja (1999). "Opening of mitochondrial KATP channel induces early and delayed cardioprotective effect: role of nitric oxide." Am J Physiol **277**(6 Pt 2): H2425-2434.
Orci, L., R. Schekman and A. Perrelet (1996). "Interleaflet clear space is reduced in the membrane of COP I and COP II-coated buds/vesicles." Proc Natl Acad Sci U S A **93**(17): 8968-8970.
Orij, R., J. Postmus, A. Ter Beek, S. Brul and G. J. Smits (2009). "In vivo measurement of cytosolic and mitochondrial pH using a pH-sensitive GFP derivative in Saccharomyces cerevisiae reveals a relation between intracellular pH and growth." Microbiology **155**(Pt 1): 268-278.
Ozcan, C., M. Bienengraeber, P. P. Dzeja and A. Terzic (2002). "Potassium channel openers protect cardiac mitochondria by attenuating oxidant stress at reoxygenation." Am J Physiol Heart Circ Physiol **282**(2): H531-539.
Page, A. M., J. R. Lagnado, T. W. Ford and G. Place (1994). "Calcium alginate encapsulation of small specimens for transmission electron microscopy." Journal of Microscopy **175**(2): 166-170.
Pagliarini, D. J., S. E. Calvo, B. Chang, S. A. Sheth, S. B. Vafai, S. E. Ong, G. A. Walford, C. Sugiana, A. Boneh, W. K. Chen, D. E. Hill, M. Vidal, J. G. Evans, D. R. Thorburn, S. A. Carr and V. K. Mootha (2008). "A mitochondrial protein compendium elucidates complex I disease biology." Cell **134**(1): 112-123.
Pardo, L. A. (2004). "Voltage-Gated Potassium Channels in Cell Proliferation." Physiology **19**(5): 285-292.
Patel, S. K., L. Jackson, A. Y. Warren, P. Arya, R. W. Shaw and R. N. Khan (2013). "A role for two-pore potassium (K2P) channels in endometrial epithelial function." Journal of Cellular and Molecular Medicine **17**(1): 134-146.
Pathania, D., M. Millard and N. Neamati (2009). "Opportunities in discovery and delivery of anticancer drugs targeting mitochondria and cancer cell metabolism." Adv Drug Deliv Rev **61**(14): 1250-1275.
Paucek, P., G. Mironova, F. Mahdi, A. D. Beavis, G. Woldegiorgis and K. D. Garlid (1992). "Reconstitution and partial purification of the glibenclamide-sensitive, ATP-dependent K+ channel from rat liver and beef heart mitochondria." J Biol Chem **267**(36): 26062-26069.
Pavlov, E. V., M. Priault, D. Pietkiewicz, E. H. Cheng, B. Antonsson, S. Manon, S. J. Korsmeyer, C. A. Mannella and K. W. Kinnally (2001). "A novel, high conductance channel of mitochondria linked to apoptosis in mammalian cells and Bax expression in yeast." J Cell Biol **155**(5): 725-731.
Pei, L., O. Wiser, A. Slavin, D. Mu, S. Powers, L. Y. Jan and T. Hoey (2003). "Oncogenic potential of TASK3 (Kcnk9) depends on K+ channel function." Proceedings of the National Academy of Sciences **100**(13): 7803-7807.
Peixoto, P. M., J. K. Lue, S.-Y. Ryu, B. N. Wroble, J. C. Sible and K. W. Kinnally (2011). "Mitochondrial Apoptosis-Induced Channel (MAC) Function Triggers a Bax/Bak-Dependent Bystander Effect." The American Journal of Pathology **178**(1): 48-54.
Perry, S. W., J. P. Norman, J. Barbieri, E. B. Brown and H. A. Gelbard (2011). "Mitochondrial membrane potential probes and the proton gradient: a practical usage guide." BioTechniques **50**(2): 98-115.
Pocsai, K., L. Kosztka, G. Bakondi, M. Gonczi, J. Fodor, B. Dienes, P. Szentesi, I. Kovacs, R. Feniger-Barish, E. Kopf, D. Zharhary, G. Szucs, L. Csernoch and Z. Rusznak (2006). "Melanoma cells exhibit strong intracellular TASK-3-specific immunopositivity in both tissue sections and cell culture." Cell Mol Life Sci **63**(19-20): 2364-2376.
Powers, M. F., L. L. Smith and A. D. Beavis (1994). "On the relationship between the mitochondrial inner membrane anion channel and the adenine nucleotide translocase." J Biol Chem **269**(14): 10614-10620.

Putnam, R. W., J. A. Filosa and N. A. Ritucci (2004). "Cellular mechanisms involved in CO2 and acid signaling in chemosensitive neurons." American Journal of Physiology-Cell Physiology **287**(6): C1493-C1526.
Rajagopalan, S. and B. Pitt (2003). "Aldosterone as a target in congestive heart failure." Med Clin North Am **87**(2): 441-457.
Rajan, S., L. D. Plant, M. L. Rabin, M. H. Butler and S. A. Goldstein (2005). "Sumoylation silences the plasma membrane leak K+ channel K2P1." Cell **121**(1): 37-47.
Rajan, S., R. Preisig-Muller, E. Wischmeyer, R. Nehring, P. J. Hanley, V. Renigunta, B. Musset, G. Schlichthorl, C. Derst, A. Karschin and J. Daut (2002). "Interaction with 14-3-3 proteins promotes functional expression of the potassium channels TASK-1 and TASK-3." J Physiol **545**(1): 13-26.
Rajan, S., R. Preisig-Müller, E. Wischmeyer, R. Nehring, P. J. Hanley, V. Renigunta, B. Musset, G. Schlichthörl, C. Derst, A. Karschin and J. Daut (2002). "Interaction with 14-3-3 proteins promotes functional expression of the potassium channels TASK-1 and TASK-3." The Journal of Physiology **545**(Pt 1): 13-26.
Rajan, S., E. Wischmeyer, G. X. Liu, R. Preisig-Müller, J. Daut, A. Karschin and C. Derst (2000). "TASK-3, a novel tandem pore domain acid-sensitive K+ channel an extracellular histidine as pH sensor." Journal of Biological Chemistry **275**(22): 16650-16657.
Reinders, J., R. P. Zahedi, N. Pfanner, C. Meisinger and A. Sickmann (2006). "Toward the complete yeast mitochondrial proteome: multidimensional separation techniques for mitochondrial proteomics." J Proteome Res **5**(7): 1543-1554.
Reyes, R., F. Duprat, F. Lesage, M. Fink, M. Salinas, N. Farman and M. Lazdunski (1998). "Cloning and expression of a novel pH-sensitive two pore domain K+ channel from human kidney." J Biol Chem **273**(47): 30863-30869.
Rinné, S., A. K. Kiper, C. Schmidt, B. Ortiz-Bonnin, S. Zwiener, G. Seebohm and N. Decher (2017). "Stress-Kinase Regulation of TASK-1 and TASK-3." Cellular Physiology and Biochemistry **44**(3): 1024-1037.
Rizzuto, R., M. R. Duchen and T. Pozzan (2004). "Flirting in little space: the ER/mitochondria Ca2+ liaison." Sci STKE **2004**(215): re1.
Rizzuto, R., S. Marchi, M. Bonora, P. Aguiari, A. Bononi, D. De Stefani, C. Giorgi, S. Leo, A. Rimessi, R. Siviero, E. Zecchini and P. Pinton (2009). "Ca(2+) transfer from the ER to mitochondria: when, how and why." Biochim Biophys Acta **1787**(11): 1342-1351.
Roncoroni, L. (2012). Functional role of the background potassium channel K2P15.1. Doctor of Philosofy, University of Southampton.
Ronnov-Jessen, L., R. Villadsen, J. C. Edwards and O. W. Petersen (2002). "Differential expression of a chloride intracellular channel gene, CLIC4, in transforming growth factor-beta1-mediated conversion of fibroblasts to myofibroblasts." Am J Pathol **161**(2): 471-480.
Rostovtseva, T. K., W. Tan and M. Colombini (2005). "On the role of VDAC in apoptosis: fact and fiction." J Bioenerg Biomembr **37**(3): 129-142.
Rusznak, Z., G. Bakondi, L. Kosztka, K. Pocsai, B. Dienes, J. Fodor, A. Telek, M. Gonczi, G. Szucs and L. Csernoch (2008). "Mitochondrial expression of the two-pore domain TASK-3 channels in malignantly transformed and non-malignant human cells." Virchows Arch **452**(4): 415-426.
Ryu, S. Y., P. M. Peixoto, O. Teijido, L. M. Dejean and K. W. Kinnally (2010). "Role of mitochondrial ion channels in cell death." Biofactors **36**(4): 255-263.
Sacchetti, S., K. N. Alavian, E. Lazrove and E. A. Jonas (2013). "F(1)F(O) ATPase Vesicle Preparation and Technique for Performing Patch Clamp Recordings of Submitochondrial Vesicle Membranes." Journal of Visualized Experiments : JoVE(75): 4394.
Saint-Georges, Y., M. Garcia, T. Delaveau, L. Jourdren, S. Le Crom, S. Lemoine, V. Tanty, F. Devaux and C. Jacq (2008). "Yeast mitochondrial biogenesis: a role for the PUF RNA-binding protein Puf3p in mRNA localization." PLoS One **3**(6): e2293.

Salinas, M., R. Reyes, F. Lesage, M. Fosset, C. Heurteaux, G. Romey and M. Lazdunski (1999). "Cloning of a New Mouse Two-P Domain Channel Subunit and a Human Homologue with a Unique Pore Structure." Journal of Biological Chemistry **274**(17): 11751-11760.
Salnikov, V., Y. O. Lukyanenko, W. J. Lederer and V. Lukyanenko (2009). "Distribution of ryanodine receptors in rat ventricular myocytes." J Muscle Res Cell Motil **30**(3-4): 161-170.
Samavati, L., M. M. Monick, S. Sanlioglu, G. R. Buettner, L. W. Oberley and G. W. Hunninghake (2002). "Mitochondrial K(ATP) channel openers activate the ERK kinase by an oxidant-dependent mechanism." Am J Physiol Cell Physiol **283**(1): C273-281.
Sandoz, G., S. C. Bell and E. Y. Isacoff (2011). "Optical probing of a dynamic membrane interaction that regulates the TREK1 channel." Proceedings of the National Academy of Sciences **108**(6): 2605-2610.
Santo-Domingo, J. and N. Demaurex (2012). "The renaissance of mitochondrial pH." The Journal of general physiology **139**(6): 415-423.
Sassi, N., U. De Marchi, B. Fioretti, L. Biasutto, E. Gulbins, F. Franciolini, I. Szabo and M. Zoratti (2010). "An investigation of the occurrence and properties of the mitochondrial intermediate-conductance Ca2+-activated K+ channel mtKCa3.1." Biochim Biophys Acta **1797**(6-7): 1260-1267.
Sato, T., T. Saito, N. Saegusa and H. Nakaya (2005). "Mitochondrial Ca2+-activated K+ channels in cardiac myocytes: a mechanism of the cardioprotective effect and modulation by protein kinase A." Circulation **111**(2): 198-203.
Schieder, M., K. Rötzer, A. Brüggemann, M. Biel and C. Wahl-Schott (2010). "Planar Patch Clamp Approach to Characterize Ionic Currents from Intact Lysosomes." Science Signaling **3**(151): pl3-pl3.
Schilling, T., F. N. Quandt, V. V. Cherny, W. Zhou, U. Heinemann, T. E. Decoursey and C. Eder (2000). "Upregulation of Kv1.3 K⁺ channels in microglia deactivated by TGF-β." American Journal of Physiology - Cell Physiology **279**(4): C1123-C1134.
Schulz, P., B. Dueck, A. Mourot, L. Hatahet and K. Fendler (2009). "Measuring Ion Channels on Solid Supported Membranes." Biophysical Journal **97**(1): 388-396.
Schwab, A., A. Fabian, P. J. Hanley and C. Stock (2012). "Role of Ion Channels and Transporters in Cell Migration." Physiological Reviews **92**(4): 1865-1913.
Scott, I. and R. J. Youle (2010). "Mitochondrial fission and fusion." Essays in biochemistry **47**: 85-98.
Sepúlveda, F. V., L. Pablo Cid, J. Teulon and M. I. Niemeyer (2015). "Molecular Aspects of Structure, Gating, and Physiology of pH-Sensitive Background K(2P) and Kir K(+)-Transport Channels." Physiological Reviews **95**(1): 179-217.
Shinbo, A. and T. Iijima (1997). "Potentiation by nitric oxide of the ATP-sensitive K+ current induced by K+ channel openers in guinea-pig ventricular cells." Br J Pharmacol **120**(8): 1568-1574.
Shu, J., J. Jelinek, H. Chang, L. Shen, T. Qin, W. Chung, Y. Oki and J. P. Issa (2006). "Silencing of bidirectional promoters by DNA methylation in tumorigenesis." Cancer Res **66**(10): 5077-5084.
Sickmann, A., J. Reinders, Y. Wagner, C. Joppich, R. Zahedi, H. E. Meyer, B. Schönfisch, I. Perschil, A. Chacinska, B. Guiard, P. Rehling, N. Pfanner and C. Meisinger (2003). "The proteome of Saccharomyces cerevisiae mitochondria." Proceedings of the National Academy of Sciences **100**(23): 13207-13212.
Siemen, D., C. Loupatatzis, J. Borecky, E. Gulbins and F. Lang (1999). "Ca2+-activated K channel of the BK-type in the inner mitochondrial membrane of a human glioma cell line." Biochem Biophys Res Commun **257**(2): 549-554.
Silver, I. and M. Erecinska (1998). "Oxygen and ion concentrations in normoxic and hypoxic brain cells." Adv Exp Med Biol **454**: 7-16.
Sirois, J. E., Q. Lei, E. M. Talley, C. Lynch, 3rd and D. A. Bayliss (2000). "The TASK-1 two-pore domain K+ channel is a molecular substrate for neuronal effects of inhalation anesthetics." J Neurosci **20**(17): 6347-6354.
Skaar, D., M. Gould, R. Jirtle and V. Seewaldt (2014). "Abstract CN02-03: Altered imprinted gene DMR regulatory methylation in breast cancer." Cancer Epidemiology Biomarkers & Prevention **23**(11 Supplement): CN02-03-CN02-03.

Skalska, J., P. Bednarczyk, M. Piwonska, B. Kulawiak, G. Wilczynski, K. Dolowy, A. P. Kudin, W. S. Kunz and A. Szewczyk (2009). "Calcium ions regulate K(+) uptake into brain mitochondria: the evidence for a novel potassium channel." Int J Mol Sci **10**(3): 1104-1120.
Skalska, J., M. Piwonska, E. Wyroba, L. Surmacz, R. Wieczorek, I. Koszela-Piotrowska, J. Zielinska, P. Bednarczyk, K. Dolowy, G. M. Wilczynski, A. Szewczyk and W. S. Kunz (2008). "A novel potassium channel in skeletal muscle mitochondria." Biochim Biophys Acta **1777**(7-8): 651-659.
Sondermann, M., M. George, N. Fertig and J. C. Behrends (2006). "High-resolution electrophysiology on a chip: Transient dynamics of alamethicin channel formation." Biochimica et Biophysica Acta (BBA) - Biomembranes **1758**(4): 545-551.
Sorgato, M. C., B. U. Keller and W. Stuhmer (1987). "Patch-clamping of the inner mitochondrial membrane reveals a voltage-dependent ion channel." Nature **330**(6147): 498-500.
Sparagna, G. C., K. K. Gunter, S.-S. Sheu and T. E. Gunter (1995). "Mitochondrial Calcium Uptake from Physiological-type Pulses of Calcium: A DESCRIPTION OF THE RAPID UPTAKE MODE." Journal of Biological Chemistry **270**(46): 27510-27515.
Speechly-Dick, M. E., G. J. Grover and D. M. Yellon (1995). "Does ischemic preconditioning in the human involve protein kinase C and the ATP-dependent K+ channel? Studies of contractile function after simulated ischemia in an atrial in vitro model." Circ Res **77**(5): 1030-1035.
Stojanovski, D., M. Bohnert, N. Pfanner and M. van der Laan (2012). "Mechanisms of protein sorting in mitochondria." Cold Spring Harb Perspect Biol **4**(10).
Streit, J. and H. D. Lux (1987). "Voltage dependent calcium currents in PC12 growth cones and cells during NGF-induced cell growth." Pflugers Arch **408**(6): 634-641.
Suzuki, Y., K. Tsutsumi, T. Miyamoto, H. Yamamura and Y. Imaizumi (2017). "Heterodimerization of two pore domain K+ channel TASK1 and TALK2 in living heterologous expression systems." PLOS ONE **12**(10): e0186252.
Szabadkai, G., A. M. Simoni, K. Bianchi, D. De Stefani, S. Leo, M. R. Wieckowski and R. Rizzuto (2006). "Mitochondrial dynamics and Ca2+ signaling." Biochim Biophys Acta **1763**(5-6): 442-449.
Szabo, I., J. Bock, H. Grassme, M. Soddemann, B. Wilker, F. Lang, M. Zoratti and E. Gulbins (2008). "Mitochondrial potassium channel Kv1.3 mediates Bax-induced apoptosis in lymphocytes." Proc Natl Acad Sci U S A **105**(39): 14861-14866.
Szabo, I., J. Bock, A. Jekle, M. Soddemann, C. Adams, F. Lang, M. Zoratti and E. Gulbins (2005). "A novel potassium channel in lymphocyte mitochondria." J Biol Chem **280**(13): 12790-12798.
Szabo, I., L. Leanza, E. Gulbins and M. Zoratti (2012). "Physiology of potassium channels in the inner membrane of mitochondria." Pflugers Arch **463**(2): 231-246.
Szewczyk, A., W. Jarmuszkiewicz and W. S. Kunz (2009). "Mitochondrial potassium channels." IUBMB Life **61**(2): 134-143.
Szewczyk, A., A. Kajma, D. Malinska, A. Wrzosek, P. Bednarczyk, B. Zablocka and K. Dolowy (2010). "Pharmacology of mitochondrial potassium channels: dark side of the field." FEBS Lett **584**(10): 2063-2069.
Talley, E. M., J. E. Sirois, Q. Lei and D. A. Bayliss (2003). "Two-Pore-Domain (Kcnk) Potassium Channels: Dynamic Roles in Neuronal Function." The Neuroscientist **9**(1): 46-56.
Tarasov, A. I., E. J. Griffiths and G. A. Rutter (2012). "Regulation of ATP production by mitochondrial Ca(2+)." Cell Calcium **52**(1): 28-35.
Territo, P. R., V. K. Mootha, S. A. French and R. S. Balaban (2000). "Ca(2+) activation of heart mitochondrial oxidative phosphorylation: role of the F(0)/F(1)-ATPase." Am J Physiol Cell Physiol **278**(2): C423-435.
Toczylowska-Maminska, R., A. Olszewska, M. Laskowski, P. Bednarczyk, K. Skowronek and A. Szewczyk (2014). "Potassium channel in the mitochondria of human keratinocytes." J Invest Dermatol **134**(3): 764-772.
Toczyłowska-Mamińska, R., A. Olszewska, M. Laskowski, P. Bednarczyk, K. Skowronek and A. Szewczyk (2014). "Potassium Channel in the Mitochondria of Human Keratinocytes." Journal of Investigative Dermatology **134**(3): 764-772.

Tomaskova, Z., J. Gaburjakova, A. Brezova and M. Gaburjakova (2007). "Inhibition of anion channels derived from mitochondrial membranes of the rat heart by stilbene disulfonate—DIDS." Journal of Bioenergetics and Biomembranes **39**(4): 301-311.
Tomaskova, Z. and K. Ondrias (2010). "Mitochondrial chloride channels--What are they for?" FEBS Lett **584**(10): 2085-2092.
Trapp, S., S. J. Tucker and F. M. Ashcroft (1997). "Activation and inhibition of K-ATP currents by guanine nucleotides is mediated by different channel subunits." Proceedings of the National Academy of Sciences **94**(16): 8872-8877.
Turrens, J. F. (2003). "Mitochondrial formation of reactive oxygen species." The Journal of physiology **552**(2): 335-344.
Uribe-Carvajal, S., L. A. Luévano-Martínez, S. Guerrero-Castillo, A. Cabrera-Orefice, N. A. Corona-de-la-Peña and M. Gutiérrez-Aguilar (2011). "Mitochondrial Unselective Channels throughout the eukaryotic domain." Mitochondrion **11**(3): 382-390.
Vicente, R., A. Escalada, N. Villalonga, L. Texido, M. Roura-Ferrer, M. Martin-Satue, C. Lopez-Iglesias, C. Soler, C. Solsona, M. M. Tamkun and A. Felipe (2006). "Association of Kv1.5 and Kv1.3 contributes to the major voltage-dependent K+ channel in macrophages." J Biol Chem **281**(49): 37675-37685.
Vincent, A. E., Y. S. Ng, K. White, T. Davey, C. Mannella, G. Falkous, C. Feeney, A. M. Schaefer, R. McFarland, G. S. Gorman, R. W. Taylor, D. M. Turnbull and M. Picard (2016). "The Spectrum of Mitochondrial Ultrastructural Defects in Mitochondrial Myopathy." Sci Rep **6**: 30610.
Voloshyna, I., A. Besana, M. Castillo, T. Matos, I. B. Weinstein, M. Mansukhani, R. B. Robinson, C. Cordon-Cardo and S. J. Feinmark (2008). "TREK-1 is a novel molecular target in prostate cancer." Cancer Res **68**(4): 1197-1203.
Vu, M. T., G. Du, D. A. Bayliss and R. L. Horner (2015). "TASK Channels on Basal Forebrain Cholinergic Neurons Modulate Electrocortical Signatures of Arousal by Histamine." J Neurosci **35**(40): 13555-13567.
Waizenegger, T., S. Schmitt, J. Zivkovic, W. Neupert and D. Rapaport (2005). "Mim1, a protein required for the assembly of the TOM complex of mitochondria." EMBO Rep **6**(1): 57-62.
Waldegger, S., S. Steuer, T. Risler, A. Heidland, G. Capasso, S. Massry and F. Lang (1998). "Mechanisms and clinical significance of cell volume regulation." Nephrology Dialysis Transplantation **13**(4): 867-874.
Wang, X., C. Yin, L. Xi and R. C. Kukreja (2004). "Opening of Ca2+-activated K+ channels triggers early and delayed preconditioning against I/R injury independent of NOS in mice." Am J Physiol Heart Circ Physiol **287**(5): H2070-2077.
Wang, Y., K. Hirai and M. Ashraf (1999). "Activation of Mitochondrial ATP-Sensitive K⁺ Channel for Cardiac Protection Against Ischemic Injury Is Dependent on Protein Kinase C Activity." Circulation Research **85**(8): 731-741.
Wang, Y., E. Takashi, M. Xu, A. Ayub and M. Ashraf (2001). "Downregulation of protein kinase C inhibits activation of mitochondrial K(ATP) channels by diazoxide." Circulation **104**(1): 85-90.
Wang, Z. (2004). "Roles of K+ channels in regulating tumour cell proliferation and apoptosis." Pflügers Archiv **448**(3): 274-286.
Washburn, C. P., J. E. Sirois, E. M. Talley, P. G. Guyenet and D. A. Bayliss (2002). "Serotonergic raphe neurons express TASK channel transcripts and a TASK-like pH- and halothane-sensitive K+ conductance." J Neurosci **22**(4): 1256-1265.
Watanabe, M., K. Katsura, I. Ohsawa, G. Mizukoshi, K. Takahashi, S. Asoh, S. Ohta and Y. Katayama (2008). "Involvement of mitoKATP channel in protective mechanisms of cerebral ischemic tolerance." Brain Res **1238**: 199-207.
Webster, K. A. (2012). "Mitochondrial membrane permeabilization and cell death during myocardial infarction: roles of calcium and reactive oxygen species." Future cardiology **8**(6): 863-884.
Wickenden, A. (2002). "K(+) channels as therapeutic drug targets." Pharmacol Ther **94**(1-2): 157-182.
Wickens, M., D. S. Bernstein, J. Kimble and R. Parker (2002). "A PUF family portrait: 3'UTR regulation as a way of life." Trends Genet **18**(3): 150-157.

Wieckowski, M. R., C. Giorgi, M. Lebiedzinska, J. Duszynski and P. Pinton (2009). "Isolation of mitochondria-associated membranes and mitochondria from animal tissues and cells." Nat. Protocols **4**(11): 1582-1590.
Wiedemann, N., A. E. Frazier and N. Pfanner (2004). "The Protein Import Machinery of Mitochondria." Journal of Biological Chemistry **279**(15): 14473-14476.
Williams, G. S. B., L. Boyman, A. C. Chikando, R. J. Khairallah and W. J. Lederer (2013). "Mitochondrial calcium uptake." Proceedings of the National Academy of Sciences **110**(26): 10479-10486.
Williams, S. (2013). Role of acid-sensitive two-pore domain potassium channels in cancer. Doctor of Philosophy, University of Southampton.
Williams, S., A. Bateman and I. O'Kelly (2013). "Altered Expression of Two-Pore Domain Potassium (K(2P)) Channels in Cancer." PLoS ONE **8**(10): e74589.
Wisgerhof, M., R. D. Brown, M. J. Hogan, P. C. Carpenter and A. J. Edis (1981). "The plasma aldosterone response to angiotensin II infusion in aldosterone-producing adenoma and idiopathic hyperaldosteronism." J Clin Endocrinol Metab **52**(2): 195-198.
Wisgerhof, M., P. C. Carpenter and R. D. Brown (1978). "Increased adrenal sensitivity to angiotensin II in idiopathic hyperaldosteronism." J Clin Endocrinol Metab **47**(5): 938-943.
Wu, Z. Z., D. P. Li, S. R. Chen and H. L. Pan (2009). "Aminopyridines potentiate synaptic and neuromuscular transmission by targeting the voltage-activated calcium channel beta subunit." J Biol Chem **284**(52): 36453-36461.
Xu, W., Y. Liu, S. Wang, T. McDonald, J. E. Van Eyk, A. Sidor and B. O'Rourke (2002). "Cytoprotective role of Ca2+- activated K+ channels in the cardiac inner mitochondrial membrane." Science **298**(5595): 1029-1033.
Yano, M., K. Terada and M. Mori (2003). "AIP is a mitochondrial import mediator that binds to both import receptor Tom20 and preproteins." J Cell Biol **163**(1): 45-56.
Yao, J., D. McHedlishvili, W. E. McIntire, N. A. Guagliardo, A. Erisir, C. A. Coburn, V. P. Santarelli, D. A. Bayliss and P. Q. Barrett (2017). "Functional TASK-3–Like Channels in Mitochondria of Aldosterone-Producing Zona Glomerulosa CellsNovelty and Significance." Hypertension **70**(2): 347-356.
Yao, X., A. Y. Chang, E. L. Boulpaep, A. S. Segal and G. V. Desir (1996). "Molecular cloning of a glibenclamide-sensitive, voltage-gated potassium channel expressed in rabbit kidney." Journal of Clinical Investigation **97**(11): 2525-2533.
Yatani, A. and A. M. Brown (1991). "Mechanism of fluoride activation of G protein-gated muscarinic atrial K+ channels." J Biol Chem **266**(34): 22872-22877.
Yi, M., D. Weaver and G. Hajnoczky (2004). "Control of mitochondrial motility and distribution by the calcium signal: a homeostatic circuit." J Cell Biol **167**(4): 661-672.
Yost, C. S., I. Oh, E. I. Eger and J. M. Sonner (2008). "Knockout of the gene encoding the K(2P) channel KCNK7 does not alter volatile anesthetic sensitivity." Behavioural brain research **193**(2): 192-196.
Young, J. C., N. J. Hoogenraad and F. U. Hartl (2003). "Molecular chaperones Hsp90 and Hsp70 deliver preproteins to the mitochondrial import receptor Tom70." Cell **112**(1): 41-50.
Young, W. F. (2007). "Primary aldosteronism: renaissance of a syndrome." Clin Endocrinol (Oxf) **66**(5): 607-618.
Yu, S. P. (2003). "Regulation and critical role of potassium homeostasis in apoptosis." Prog Neurobiol **70**(4): 363-386.
Zamore, P. D., J. R. Williamson and R. Lehmann (1997). "The Pumilio protein binds RNA through a conserved domain that defines a new class of RNA-binding proteins." Rna **3**(12): 1421-1433.
Zara, V., A. Ferramosca, P. Robitaille-Foucher, F. Palmieri and J. C. Young (2009). "Mitochondrial carrier protein biogenesis: role of the chaperones Hsc70 and Hsp90." Biochem J **419**(2): 369-375.

Zeng, H., B. Balasubramanian, J. R. Penniman, F. Kinose, J. J. Salata and A. Lagrutta (2013). "Halide ion effects on human Ether-a-go-go related gene potassium channel properties." Assay Drug Dev Technol **11**(9-10): 544-550.
Zeng, H., J. R. Penniman, F. Kinose, D. Kim, E. S. Trepakova, M. G. Malik, S. J. Dech, B. Balasubramanian and J. J. Salata (2008). "Improved throughput of PatchXpress hERG assay using intracellular potassium fluoride." Assay Drug Dev Technol **6**(2): 235-241.
Zhang, D. X., Y. F. Chen, W. B. Campbell, A. P. Zou, G. J. Gross and P. L. Li (2001). "Characteristics and superoxide-induced activation of reconstituted myocardial mitochondrial ATP-sensitive potassium channels." Circ Res **89**(12): 1177-1183.
Zoratti, M., U. De Marchi, E. Gulbins and I. Szabò (2009). "Novel channels of the inner mitochondrial membrane." Biochimica et Biophysica Acta (BBA) - Bioenergetics **1787**(5): 351-363.
Zorov, D. B., M. Juhaszova and S. J. Sollott (2006). "Mitochondrial ROS-induced ROS release: An update and review." Biochimica et Biophysica Acta (BBA) - Bioenergetics **1757**(5): 509-517.
Zuzarte, M., K. Heusser, V. Renigunta, G. Schlichthorl, S. Rinne, E. Wischmeyer, J. Daut, B. Schwappach and R. Preisig-Muller (2009). "Intracellular traffic of the K+ channels TASK-1 and TASK-3: role of N- and C-terminal sorting signals and interaction with 14-3-3 proteins." J Physiol **587**(Pt 5): 929-952.
Zuzarte, M., S. Rinne, G. Schlichthorl, A. Schubert, J. Daut and R. Preisig-Muller (2007). "A di-acidic sequence motif enhances the surface expression of the potassium channel TASK-3." Traffic **8**(8): 1093-1100.